Credit: Rene Reyes

Species Status Assessment for the San Francisco Bay-Delta Distinct Population Segment of the Longfin Smelt

SSA Core Team

Ernest Chen[1]
Vanessa Tobias[2]
Michael Eakin[3]
James Hobbs[4]
Arnold Roessler[1]

Editors

Steven Detwiler[5]
Matt Nobriga[5]

[1]U.S. Fish and Wildlife Service, Region 8 Regional Office
[2]U.S. Fish and Wildlife Service, Lodi Fish and Wildlife Office
[3]California Department of Fish and Wildlife, Water Branch
[4]California Department of Fish and Wildlife, Bay-Delta Region
[5]U.S. Fish and Wildlife Service, San Francisco Bay-Delta Fish and Wildlife Office

Contents

Acknowledgements

Drafting of this SSA would not have been possible without the analytical support provided by Noah Knowles, Marissa Wulff, and Brock Huntsman with the U.S. Geological Survey, and Bryan Matthias, Carissa Long, and Craig Anderson with the U.S. Fish and Wildlife Service. In addition, we are grateful for the expert survey input afforded by Jilian Burns and Kathy Hieb with the California Department of Fish and Wildlife. Special thanks to Service Directorate Fellow Joseph Miller of the University of Central Arkansas for his 11-week dedicated support for data analysis and compilation. We appreciate the many peer and partner reviewer's time and constructive comments to improve the final document. We want to also thank Leo Polansky for providing additional assistance finalizing the SSA following peer review.

Recommended Citation

U.S. Fish and Wildlife Service. 2022. Species Status Assessment for the San Francisco Bay-Delta Distinct Population Segment of the Longfin Smelt. U.S. Fish and Wildlife Service. San Francisco Bay-Delta Fish and Wildlife Office, Sacramento, California. XX pp. + Appendices A–G.

Chapter 1 - Introduction and Analytical Approach

This report summarizes the results of a Species Status Assessment (SSA) conducted for the San Francisco Bay-Delta Distinct Population Segment of the longfin smelt (*Spirinchus thaleichthys*) (Bay-Delta DPS). The longfin smelt belongs to the northern smelt family Osmeridae and is one of three extant (currently existing) species in the genus *Spirinchus*. The Bay-Delta DPS is considered a candidate species for listing by the U.S. Fish and Wildlife Service (Service). The longfin smelt has been listed as a threatened species throughout its range in California by the California Department of Fish and Wildlife (CDFW) since 2009, under the California Endangered Species Act (CESA).

In the literature, several different terms to describe the various portions of the San Francisco Bay-Sacramento/San Joaquin River Delta are used. In this document, we refer to these areas, as follows: the "Delta" represents the legal delta, as defined by the Delta Protection Act of 1992, encompassing all waters east of Chipps Island. The "Bay" encompasses all waters west of Chipps Island where the legal delta ends. The "Bay-Delta" and "San Francisco Bay-Delta" and "San Francisco Estuary" are synonymous and encompass both the Bay and the Delta.

In this SSA Report, we focus on the biological information and threats facing the Bay-Delta DPS. The reader is referred to the 2012 12-month finding (77 Federal Register [FR] 19756) for information on the status of the species range-wide. The SSA framework (Service 2016, entire) is intended to support an in-depth review of the species' biology, current and future threats, an evaluation of its biological status, and an assessment of the resources and conditions needed to maintain long-term viability. The intent is for the SSA Report to be easily updated as new information becomes available and to support all functions of the Service's Endangered Species Program from candidate assessment, listing, consultations, and recovery actions. As such, the SSA Report will be a living document upon which other documents would be based, such as listing rules, recovery plans, 5-year reviews, and Endangered Species Act §7 or §10 actions.

Ultimately, this SSA Report for the longfin smelt Bay-Delta DPS will provide the biological support for the decision on whether or not to propose to list the species as threatened or endangered and, if so, where to propose designating critical habitat. Importantly, the SSA Report does not result in a decision by the Service on whether this species should be proposed for listing as a threatened or endangered species under the Act. Instead, this SSA Report provides a review of the available information strictly related to the biological status of the longfin smelt. The listing decision will be made by the Service after reviewing this document and all relevant laws, regulations, and policies, and the results of a proposed decision will be announced in the *Federal Register*, with opportunities for public input as appropriate.

To assess the ability of the Bay-Delta DPS to maintain self-sustaining populations over time, we applied the conservation biology principles of resiliency, representation, and redundancy (Shaffer and Stein 2000, pp. 308–311). As described more fully below, resiliency is the species capacity to withstand environmental and demographic stochasticity and disturbances; redundancy is the species capacity to withstand catastrophes; and representation is the species capacity to withstand novel changes in its

biological and physical environment. A species with a high degree of resiliency, representation, and redundancy (the 3Rs) is better able to adapt to novel changes and to tolerate environmental stochasticity and catastrophes. In general, species viability will increase with increases in resiliency, redundancy, and representation (Smith *et al.* 2018, p. 306).

The 3Rs framework is specifically defined and utilized herein, as:

Resiliency is the ability of a species to withstand environmental stochasticity (normal, year-to-year variations in environmental conditions such as temperature, rainfall), periodic disturbances within the normal range of variation (fire, floods, storms), and demographic stochasticity (normal variation in demographic rates such as mortality and fecundity) (Redford *et al.* 2011, p. 40). Simply stated, resiliency is the ability to sustain populations through the natural range of favorable and unfavorable conditions. We can best gauge resiliency by evaluating population level characteristics such as: demography (abundance and the components of population growth rate—survival, reproduction, and migration), genetic health (effective population size and heterozygosity), connectivity (gene flow and population rescue), in context with habitat quantity, quality, configuration, and heterogeneity. For species prone to spatial synchrony (regionally correlated fluctuations among populations), distance between populations and degree of spatial heterogeneity (diversity of habitat types or microclimates) are also important considerations.

Redundancy is the ability of a species to withstand catastrophes. Catastrophes are stochastic events that are expected to lead to population collapse regardless of population heath and for which adaptation is unlikely (Mangal and Tier 1993, p. 1083). We can best gauge redundancy by analyzing the number and distribution of populations relative to the scale of anticipated species-relevant catastrophic events. The analysis entails assessing the cumulative risk of catastrophes occurring over time. Redundancy can be analyzed at a population or regional scale, or for narrow-ranged species, at the species level.

Representation is the ability of a species to adapt to both near-term and long-term changes in its physical (climate conditions, habitat conditions, habitat structure, etc.) and biological (pathogens, competitors, predators, etc.) environments. This ability to adapt to new environments—referred to as adaptive capacity—is essential for viability, as species need to continually adapt to their continuously changing environments (Nicotra *et al.* 2015, p. 1269). Species adapt to novel changes in their environment by either [1] moving to new, suitable environments or [2] by altering their physical or behavioral traits (phenotypes) to match the new environmental conditions through either plasticity or genetic change (Beever *et al.* 2016, p. 132; Nicotra *et al.* 2015, p. 1270). We can best gauge representation by examining the breadth of genetic, phenotypic, and ecological diversity found within a species and its ability to disperse and colonize new areas.

This SSA Report provides a thorough assessment of biology and natural history and assesses demographic risks, stressors, and limiting factors in the context of determining the viability and risks of extinction for the Bay-Delta DPS. We are required to use the best scientific and commercial data

available to guide us in our listing determinations. As mentioned above, this document is strictly intended to utilize the best available scientific information in evaluating the status of the Bay-Delta DPS. In some cases, information that is pertinent to aspects of the species' biology, life history, ecology, etc., may include primary peer-reviewed literature, 'gray' literature from resource agency reports, information gleaned from professional presentations (e.g., solicited presentations from experts at our Expert Elicitation workshops in late summer 2021), unpublished data, and sometimes personal communications from species experts. For our own novel analyses to support our understanding of the status and trend related to current and future condition of the DPS, our methods are presented below in detail within our technical appendices.

This document reflects an extensive peer and partner review that included 21 invited peer and partner review participants, of which 10 replied with over 962 general and specific comments, and this feedback was incorporated into improvements to the final SSA herein. The format for this SSA Report includes: the Bay-Delta DPS' life history, biological and ecological needs (Chapter 2); the Bay-Delta DPS' current condition, including factors affecting the population (Chapter 3); and the Bay-Delta DPS' anticipated future condition, including changes that could affect the Bay-Delta DPS and analytical population modeling factoring in our best available risk profile for the future trajectory of the DPS (Chapter 4). This document is a compilation of the best available scientific and commercial information and a description of past, present, and likely future risk factors to the Bay-Delta DPS.

Chapter 2 – Species Needs, Life History, and Biology

In this chapter, we provide an overview of biological information available for the longfin smelt Bay-Delta DPS, including its taxonomic history, genetics, morphological description, and known life history traits. We then outline the resource needs of individuals and populations of longfin smelt. Here, we report those aspects of the life history of the Bay-Delta DPS that are important to our analysis. Because information and research related to the longfin smelt most often applies to the species as a whole, any references to longfin smelt below also apply to the Bay-Delta DPS unless specifically described otherwise.

2.1. Species Description and Taxonomy

Adult longfin smelt average 9–11 centimeters (cm) (3.5–4.3 inches (in)) standard length, although some individuals as long as 15 cm (5.9 in) have been observed. The sides and lining of the gut cavity appear translucent silver (see Figure 2.1), the back is olive in color with an iridescent purple hue, and mature males are usually darker in color than females. Longfin smelt can be distinguished from other osmerids by their long pectoral fins (extending past the start of the pelvic fins), weak or absent striations on their opercular (covering the gills) bones, incomplete lateral line, low numbers of scales in the lateral series (54 to 65), long maxillary (jaw) bones (in adults, these bones extend past the middle of the eye), and lower jaw extending anterior of the upper jaw (McAllister 1963, p. 10; Miller and Lea 1972, pp. 158–160; Moyle 2002, pp. 234–236).

Figure 2.1: Longfin smelt (*Spirinchus* thaleichthys)

The longfin smelt belongs to the northern smelt family Osmeridae and is one of three extant (currently existing) species in the *Spirinchus* genus; the night smelt (*Spirinchus starksi*) also occurs in California, and the shishamo (*Spirinchus lanceolatus*) occurs in northern Japan (McAllister 1963, pp. 10, 15). The longfin smelt range extends scattered through bays, and both small and large estuaries from northern California through Alaska. These include: San Francisco Bay-Delta, Humboldt Bay, Russian River, Mad River, and the Klamath River in northern California (Garwood 2017, p. 98); northward through Yaquina and Coos Bays in Oregon; the lower Columbia River; Skagit Bay, Grays Harbor, and Willapa Bay in Washington; Harrison Lake in British Columbia; to Prince William Sound in Alaska (Moyle, 2002, p. 236), along with a

land-locked population in Lake Washington (a freshwater lake east of the City of Seattle in the State of Washington).

Because of its distinctive physical characteristics, the Bay-Delta population of longfin smelt was once described as a species separate from more northern populations, which were formerly identified as *Spirinchus dilatus* (Moyle 2002, p. 235). McAllister (1963, p. 12) merged the two species *S. thaleichthys* and *S. dilatus* because the difference in morphological characteristics represented a gradual change along the north-south distribution rather than discretely identifiable ones. Stanley *et al*. (1995, p. 395) concluded that longfin smelt from Lake Washington and the Bay-Delta are conspecific (of the same species) despite the large geographic separation but recommended that this isolation indicates that protection and management of this population as a discrete, genetically-independent entity would be best conservation biology practice. Israel and May (2010, p. 230) found moderate levels of differentiation between polymorphic microsatellite markers in the Lake Washington and Bay-Delta population, supporting the conclusion that geographic isolation of these populations has conferred distinctiveness. In our 12-month finding in 2012, we determined that the San Francisco Bay-Delta population of the longfin smelt is a valid DPS, due to discreteness and significance (**77 FR 19756**). More complete genetic analyses, published recently, found high genetic structure between major estuaries, with southern estuaries (north to Columbia River) showing evidence for unidirectional (northward) gene flow, suggesting the SFE population is genetically distinct from the northern populations and an important source population to maintain nearby northern estuarine populations (Saglam *et al.* 2021, p. 1793).

2.2. Distinct Population Segment Range and Distribution

Longfin smelt have been collected throughout the Bay-Delta (see Figure 2.2) and occasionally even upstream of the Delta in some of its tributary river systems. Longfin smelt have been observed in their winter and spring spawning period as far upstream as Colusa State Park in the Sacramento River, the City of Lathrop in the San Joaquin River system, Hog Slough off the South-Fork Mokelumne River, and in the South Delta near Old River south of Indian Slough (Radtke 1966, pp. 115–119; CDFG 2009a, p. 7; Baxter *et al.* 2010, p. 7; Merz *et al.* 2013, p. 132). They have been detected as far upstream on the San Joaquin River as the confluence with the Tuolumne River (Rosenfield 2010, p. 6) and also in the Napa and Petaluma Rivers (Merz *et al*. 2013, p. 136), especially during wet winters (Rosenfield 2010, p. 6; Grimaldo *et al.* 2020, pp. 11–12) In recent surveys, longfin smelt were captured in many major and tributary sloughs within the Alviso Marsh Complex salt pond restoration area in the South Bay (Lewis *et al.* 2019, p. 1). Longfin smelt migrate out into the ocean at least as far as the Gulf of the Farallones. Longfin smelt have been detected as far south as Monterey Bay (Garwood 2017, p. 117), which represents the southern-most extent of their range (Eschmeyer and Herald 1983, p. 82), although these detections are generally believed to represent very rare dispersal events.

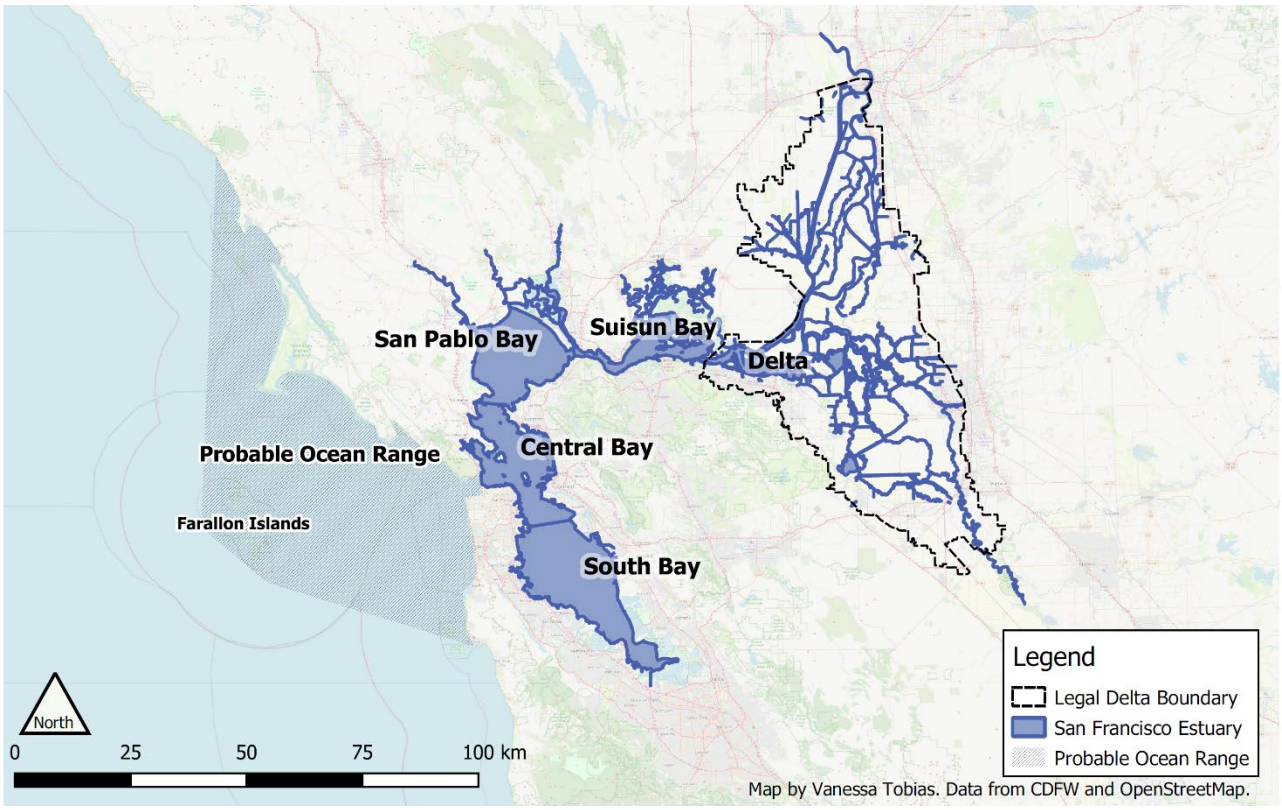

Figure 2.2: Range of the San Francisco Bay-Delta DPS of longfin smelt

2.3. Ecological Setting

The Bay-Delta is one of the largest estuaries on the West Coast of the continental United States (Sommer *et al*. 2007, p. 271). The modern Bay-Delta bears only a superficial resemblance to the historical Bay-Delta (Whipple *et al.* 2012, pp. 1–28). The region supports an estuary covering approximately 1,235 square kilometers (km^2) (477 square miles (mi^2)) (Rosenfield and Baxter 2007, p. 1577), receiving almost half of California's freshwater runoff (Lehman 2004, p. 313). The historical island marshes surrounded by low natural levees of the delta are now protected by large, humanmade and rock-reinforced levees, and the islands themselves are intensively farmed (Moyle 2002, p. 32). The watershed, which drains approximately 40 percent of the land area of California, has been heavily altered by multiple dams and water diversions. In the upper Sacramento/San Joaquin estuary, nonnative species now dominate the fish assemblages, both in terms of numbers of species and numbers of individuals (Matern *et al.* 2002, p. 807; Nobriga *et al.* 2005, p. 781; Feyrer and Healy 2003, p. 126). The Bay Institute has estimated that intertidal wetlands in the Delta have been diked and leveed so extensively that approximately 95 percent of the 141,640 ha (350,000 ac) of tidal wetlands that existed in 1850 are gone (The Bay Institute 1998, pp. 4–17).

Broadly, the Bay-Delta consists of several bays and the Delta (Figure 2.2). The San Francisco Bay consists of the San Pablo Bay in the north that receives freshwater input from the Sacramento-San Joaquin system (with additional inputs from the Napa, Sonoma, and Petaluma Rivers), the Central Bay, and the South Bay in the south that receives little freshwater input (e.g., Alviso Slough) (Largier 1996, p. 69).

Dominant fish species in the San Francisco Bay (including San Pablo and South bays) are highly salt-tolerant and include forage fishes such as northern anchovy and Pacific herring. There are also abundant recreationally important fish, including striped bass, white sturgeon, California halibut, leopard shark, and surf perches. In the estuary east of San Pablo Bay, major habitat types include lower salinity embayments, riverine and tidal wetlands, mud flats, and tidal marshes, with substantial areas of diked wetlands managed for waterfowl hunting in Suisun Marsh.

Everywhere freshwater flow enters the San Francisco Estuary, it can generate low-salinity habitats for plants and animals that are adapted to brackish water conditions. Inflow into the Delta represents an average of 90% of the estuary's freshwater and as such, it has the largest influence on estuarine habitat conditions (Jassby *et al.* 1995 p. 275, and Fig. 4, p. 279; Monismith *et al*. 2002, Fig. 7, p. 3010). The southern part of San Francisco Bay, which has very limited freshwater inputs is generally characterized as a lagoonal system, whereas the northern reaches function as a tidal river estuary due to the much larger freshwater flow inputs from the Delta (Kimmerer 2004, p. 7). However, the small tributaries can have important localized effects; for instance, supporting reproduction of longfin smelt during periods of high discharge (Lewis *et al.* 2019, p. 3). For a summary of flow data contributed by various tributaries to the Estuary, see Figure 2.3.

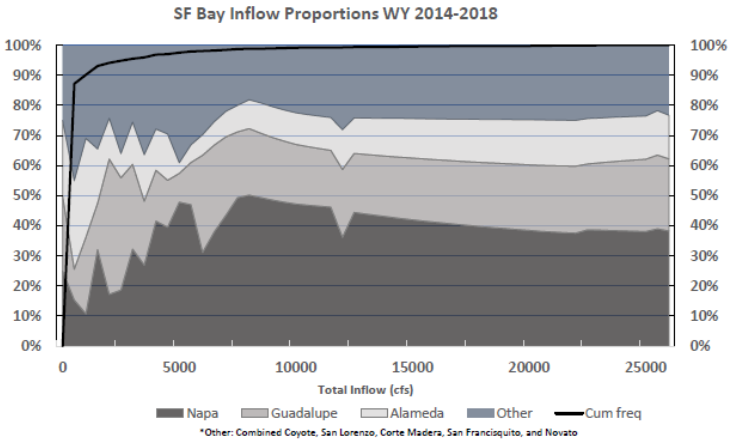

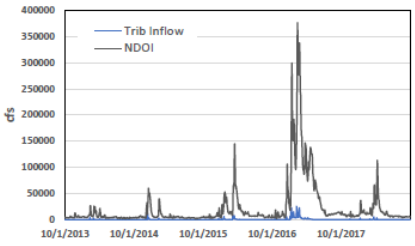

NAME	AGENCY	ID	DRAINAGE AREA (mi²)	Q annual var POR (ac-ft)	% Inflow '14-18
NAPA R NR NAPA CA	USGS	11458000	218	157600	33.7
GUADALUPE R ABV HWY 101 A SAN JOSE CA	USGS	11169025	160	51000	22.6
ALAMEDA C NR FREMONT CA	USGS	11179100	638	21700	16.5
COYOTE C AB HWY 237 A MILPITAS CA	USGS	11172175	319	31900	12.3
SAN LORENZO C A SAN LORENZO CA	USGS	11181040	45	15800	4.7
CORTE MADERA C A ROSS CA	USGS	11460000	18	19700	4.6
SAN FRANCISQUITO C A STANFORD UNIVERSITY CA	USGS	11164500	37	15200	3.9
NOVATO C A NOVATO CA	USGS	11459500	17	8900	1.7

Figure 2.3. Summaries of flow data from gauged tributaries to San Francisco Bay for water years 2014–2018 (see map inset for locations). The upper left panel shows the relative contribution as a function of increasing wetness in a format borrowed from Kimmerer (2004, Fig. 5, p. 16). The lower left panel is a tabular data summary. The upper right panel is a flow time series showing the peak wet year flows in water year 2017 for the net Delta outflow index (black) and the combined Bay Area tributary flow (blue).

Tidal flows that enter the estuary from the Pacific Ocean, and inflowing river water, present opposing forces because these two sources of water have inherent differences in density; saltwater is denser than fresh water. The ocean delivers more force during spring tides than neap tides, and the rivers deliver more force when they run high than when they run low. These opposing hydraulic forces interact with the estuary's bathymetry to create extremely variable and complex hydrodynamic mixing of fresh- and saltwater. Where saltwater and freshwater come into contact, vertical and lateral mixing currents are intermittently generated (Stacey *et al*. 2001, pp. 17026–17035). During periods of high outflow, salinity can be very different at the water surface than at the bottom due to freshwater flowing over the top of saltier water (MacWilliams *et al*. 2015, Fig. 8, p. 20). This stronger vertical salinity gradient when Delta outflow is elevated creates more surface area for mixing of fresh and brackish water and can result in water near the bottom having a net flow landward while overlying water has a net flow toward the ocean (Monismith *et al.* 2002, Fig. 15, p. 3014).

The changes to the bathymetry of the estuary that occurred between 1850 and circa 2008 (marsh reclamation, channel dredging, extensive leveeing) have collectively made the estuary deeper and less hydrodynamically-connected to the surrounding landscape (Andrews *et al.* 2017, Fig 5, p. 64). The deeper waterways create more space for the tides to bring salt landward. Specifically, landscape changes since 1850 are estimated to have resulted in an average landward shift of X2 of 3.23 km (Andrews *et al.* 2017, p. 68). In contrast, the changed freshwater flow hydrograph (discussed in the following paragraph) has caused a winter-spring landward shift of X2 on the order of 10–20 km. Changes to the estuary's landscape also have caused the tide to reach further into Old and Middle rivers (Andrews *et al.* 2017, p. 66) which, as discussed below, is necessary to support water exports from the Delta.

Most wetland conversion had occurred by about 1920 (Whipple *et al*. 2012, Fig 1.16, p. 24). Most large water storage projects were developed from 1910-1970, with the pace of development being especially rapid from 1945–1970 (Cloern and Jassby 2012, Fig 5, p. 6). By the early 1960s, there was more reservoir storage capacity in the estuary's watersheds than the historical average annual runoff from those watersheds. From the 1940s on, most of the larger reservoirs were serving the Federal Central Valley Project (CVP) or California State Water Project (SWP), with some exceptions such as on the Yuba, Merced, and Tuolumne rivers. The CVP and SWP annually decrement (reduce) an average of about 5 million acre-feet (MAF) of Delta outflow whereas non-project reservoirs and diverters annually decrement about 8 MAF of potential Delta outflow (Hutton *et al.* 2017, Fig 4, p. 8). The cumulative development of this annual average of about 13 MAF of surface water supplies has resulted in a long-term decline in Delta outflow during February-June relative to estimates of what flows would have been absent water development (Gross *et al.* 2018, Fig. 6, p. 12; Reis *et al*. 2019, Fig. 3, p. 12). This in turn has increased the frequency of very low outflows that prior to water development would have been very rare and associated only with extreme drought (Reis *et al.* 2019, Fig. 3, p. 12).

Taken together, the landscape changes discussed above, and changes to the estuary's flow regime have changed how mixing processes function, and thus altered ecological opportunities for the estuary's biota to potentially exploit. Studies of suspended sediment concentrations have confirmed the pattern mentioned above--that water mixing is influenced by the bathymetric 'shape' of the estuary, the spring-neap tidal cycle, and wind and wave action over shallower areas (Schoellhamer 2000, Fig. 3, p. 349; Ruhl

et al. 2001, Fig. 7, p. 808; Bever *et al.* 2018, Tables 6–7, p. 1960). These forces all work to aggregate (and disaggregate) sinking particles like sediment and phytoplankton.

A common metric of estuarine mixing and other habitat conditions in the low-salinity zone is X2, the distance in kilometers from the Golden Gate to the place where salinity near the bottom of the water column is 2 practical salinity units (PSU; also parts per thousand, Jassby *et al.* 1995, pp. 274–275). The 2 PSU isohaline was chosen in part because it represents the approximate upstream limit of where surface and bottom salinity diverge, and because historical turbidity and plankton aggregations were broadly associated with it. Estuarine pelagic fishes, including the Bay-Delta DPS, are also associated with this location (Dege and Brown, 2004, Fig 3, p. 57).

The X2 isohaline is always moving, reflecting changes in the size, shape, and ecological function of the low-salinity zone (Mac Williams *et al*. 2015, Figs. 11–12, p. 22). Tidal flows affect X2 most strongly over short time scales (hours to weeks; Kimmerer 2004, Fig. 2, p. 12). Over longer time scales, Delta outflow has the dominant influence on X2 (Jassby *et al.* 1995 p. 275, and Fig. 4, p. 279; Monismith *et al.* 2002, Fig. 7, p. 3010). The surface area of the low salinity zone increases very rapidly as it begins to include a large part of San Pablo Bay (X2 ≤ 55 km), resulting in peak low salinity zone areas of 150 to 250 square kilometers (Mac Williams *et al.* 2015, Fig. 12, p. 22). In the contemporary estuary, X2 moves seaward of 55 km only very rarely (Gross *et al.* 2018, Fig. 6, p. 12). However, in the pre-development estuary, Gross *et al.* (2018, Fig 6, p. 12) estimated that X2 reached monthly averages from February through May of ≤ 55 km in about half of all years. As described in more detail in section 3.1.1 of this SSA, Delta outflow, X2, and other co-linear indicators of wet versus dry conditions during the winter and spring have been statistically associated with first year recruitment and survival of longfin smelt.

Isohalines are lines (or contours) that join points of equal salinity in an aquatic system. Isohaline position refers to the distance (kilometers) of a near-bottom isohaline (usually 2 ppt) from the mouth of a coastal waterway (Figure 1).

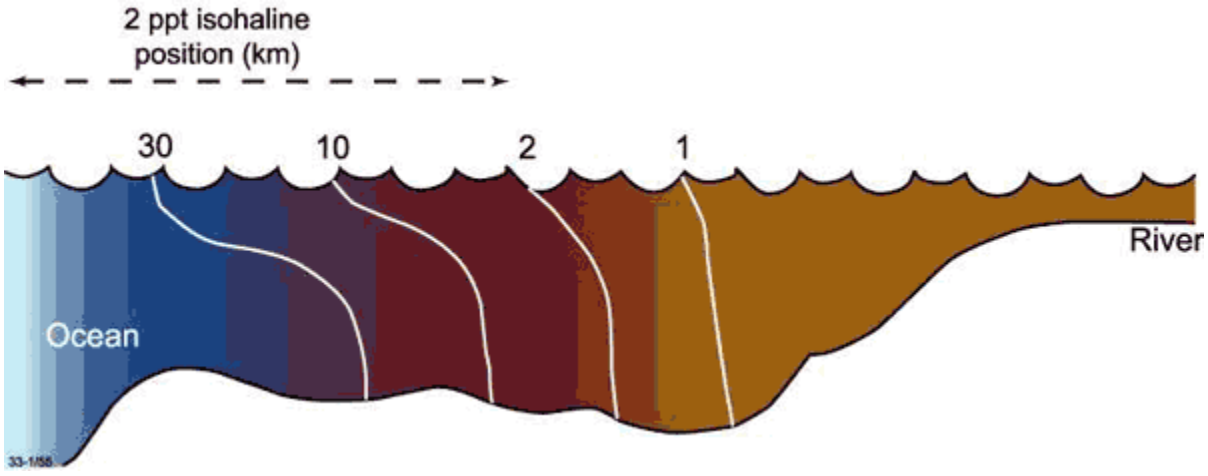

Figure 1. Schematic illustration showing the 30, 10, 2 and 1 ppt isohalines in vertical section and how the 2 ppt isohaline position is measured. (Source: https://ozcoasts.org.au/indicators/biophysical-indicators/isohaline_position/).

In the San Francisco Estuary, the 2 ppth near-bottom isohaline (*X2*) is related to important base-components of food-web (*i.e.* the amount of phytoplankton and particulate organic carbon); the abundance of zooplankton consumers and benthic macroinvertebrates; and often occurs near the location of the turbidity maximum. By this mechanism, it is also related to the abundance and survival of planktivorous, piscivorous, and demersal fish assemblages.

2.4. Life History and Biology

Longfin smelt in the Bay-Delta are pelagic (most frequently occurring in open water habitats) forage fish that exhibit a facultatively anadromous life history whereby migration to sea is not required to complete the lifecycle (Moyle 2002, p. 236). Longfin smelt are generally adapted to cold- and cool-water habitats so elements of their facultatively anadromous life cycle within the SFE are influenced by seasonal water temperature variation (e.g., Jeffries *et al.* 2016, p. 1712; Yanagitsuru *et al.* 2021, Fig. 1). The adults reproduce in low-salinity to freshwater habitats beginning in early winter and extending into the spring as water temperature allows. The larvae rear during the spring in locations near where they were spawned. As water temperatures warm each spring into early summer, the young fish move seaward and many individuals move into the Pacific Ocean during the summer months. It is speculated that some of these fish may spend extended periods of time at sea, but many individuals return to the estuary beginning in the fall and continuing into the early winter. These returning fish appear to be a combination of fish getting ready to spawn and younger individuals that are unlikely to do so.

2.4.1. Spawning

The longfin smelt life cycle is at least two years in duration (Rosenfield and Baxter 2007, Fig 6). It is believed that spawning is semelparous (occurring only once). Although some individuals may spawn as 1- or 3-year-old fish before dying (Moyle 2002, p. 236), this has not been confirmed in the San Francisco Estuary based on age-validated individuals. Longfin smelt migrate from the ocean and bay habitats to low-salinity habitats beginning in the fall, and spawn in fresh and low-salinity water in the winter and spring. Longfin smelt spawn negatively buoyant (demersal), adhesive eggs that are about 1-mm in diameter (Dryfoos 1965, p. 42; Chigbu and Sibley 1994, p. 6; Wang 2007, pp. 38–39), which is similar to other stream spawning members of family Osmeridae (Hay and McCarter 2000, p. 18; Martin and Swiderski 2001, p. 529). While eggs have not been observed in the SFE, observations of yolk-sac staged larvae suggest spawning habitat extends from the tidal reaches of the Sacramento and San Joaquin Rivers to Suisun Bay and Suisun Marsh (Grimaldo *et al.* 2017, p. 6; CDFG 2009a, p. 16; Meng and Matern 2001, p. 755; Wang 1986, p. 6–10). There has been recent confirmation of persistent and occasionally dense aggregations of adult longfin smelt in the sloughs of Coyote Creek in the South Bay, although recruitment success was confirmed during wet years only (Lewis *et al*. 2020, p. 1).

The spawning period of longfin smelt in the Bay-Delta may begin as early as November and historically lasted until as late as June, although spawning more typically occurs from January to April (CDFG 2009a, p. 10; Moyle 2002, p. 236). Observations from studies of longfin smelt in the San Francisco Estuary identify the longfin smelt spawning period as December through April based on ripe females (Radtke 1966, p. 116), and November through April based on a roughly month-long incubation time period

combined with when the presence of yolk-sac larvae have been observed in the environment (Hieb and Baxter 1993, p. 110). Using incubation duration information and monthly densities of newly hatched yolk-sac larvae, Baxter (2021, pers. comm.) estimates infrequent spawning in November, increasing and regular spawning in December, a peak in January or February followed by a sharp decline through April. Within the Bay-Delta, adult longfin smelt spawning starts when water temperature drops below ~14° C (57.2° F) and becomes consistent when water temperatures remain below 13° C (55.4° F) (CDFG 2009a, p. 11). However, recent studies indicate successful spawning may require temperatures of 13° C (55.4° F) or lower (Baxter 2016, pers. comm.). A minimum spawning temperature of 5.6° C (41° F) was reported in lab studies (Wang 1986, pp. 6–9). This lengthy spawning period may confer a degree of ecological resilience, as it may allow the Bay-Delta DPS to spread reproductive effort across the winter and into the spring, particularly during wet years.

Spawning areas have been inferred based on collection of recently hatched yolk-sac larvae (Grimaldo *et al*. 2017, Fig 9; Lewis *et al*. 2019, p. 3). They are believed to vary from year to year, depending primarily on the distribution of fresh and low-salinity water at the time of spawning (Grimaldo *et al.* 2020, p. 11–12) and likely on where and how long the adult fish can find suitable salinity water in a temperature range conducive to egg survival (Yanagitsuru *et al.* 2021, Fig 1).

While the spawning behavior of longfin smelt has not been observed in the SFE, it has been hypothesized that they make short runs upstream into fresh water and low salinity < 2 psu habitats, possibly at night (CDFG 2009a, p. 12; Rosenfield 2010, p. 8). This pattern is similar to documented spawning behavior for the Lake Washington population, in which spawners make overnight runs into tributaries of the lake then return to the lake before dawn (Dryfoos 1965, 61; Moulton 1974, p. 49-50). Catch patterns of mature longfin smelt in Coyote Creek, in the South San Francisco Bay, have suggested that maturing fish stage downstream in brackish waters, males move upstream before females, likely to prepare spawning substrates and await ripe females to make spawning runs upstream (Lewis *et al.* 2019, p. 101). Longfin smelt spawn negatively buoyant (demersal), adhesive eggs that are about 1 mm in diameter (Dryfoos 1965, p. 42; Chigbu and Sibley 1994, p. 12; Wang 2007, p. 39). The specific spawning substrates selected by longfin smelt in the San Francisco Estuary remain unknown.

2.4.2. Larval Hatching, Development, and Behavior

In the San Francisco Estuary, longfin smelt larvae hatch between December and May, with rare observations outside this range (Baxter 1999, p. 180). Peaks in abundance of recently hatched yolk-sac larvae occurred most commonly in February (during 8 of 10 years) and March otherwise (in 2 of 10 years; Baxter *et al.* 1999, p. 183). More recent larval fish sampling exhibited a similar pattern, where peak hatching occurred most commonly in February, but also occasionally in late January or March (Baxter 2021, pers. comm.).

Hatch timing is determined by when fish spawn and the temperature at which embryos incubate with incubation time decreasing with increasing water temperatures (see Figure 2.4). At 7° C (44.6° F), embryos hatch in 40 days (Dryfoos 1965, p. 42). Sibley and Brocksmith (1995, p. 38) reported an average

incubation duration of 29 days at water temperatures ranging from 8 to 9.5°C. Similarly, Moulton (1970, p. 50) noted that incubation time averaged 25 days at temperatures ranging between 9.6 and 10.6°C. Hobbs *et al.* (2013, p. 49) incubated eggs at warmer temperatures than any of the studies mentioned above (12 ± 1 °C) and found the shortest mean incubation duration (16 days). More recently, Yanagitsuru *et al.* 2021 found that incubation took an average of 23.7 days at 9°C, 19.3 days at 12°C, and 16.5 days at 15°C.

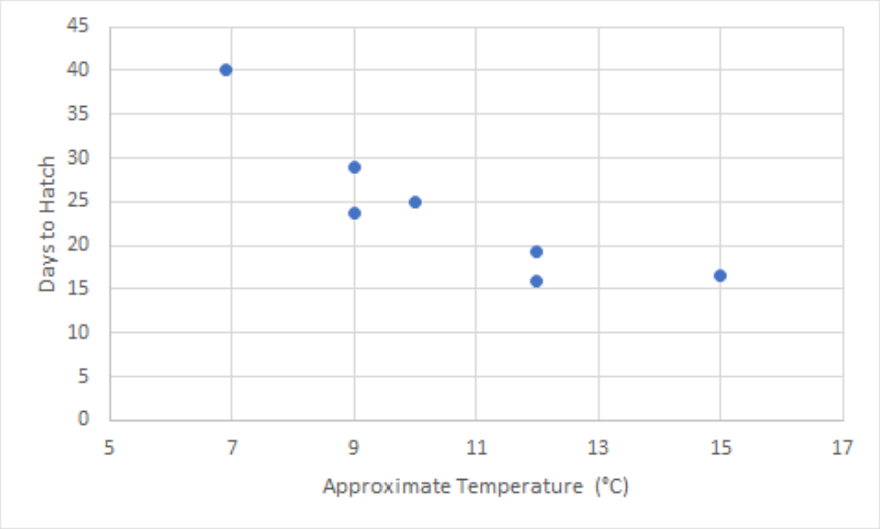

Figure 2.4: Relationship between temperature and days to hatch for longfin smelt embryos (Source: Yanagitsuru *et al.* 2021, Supplementary Table 2).

There are two prevailing theories about how longfin smelt use hydrodynamics to facilitate the transport and retention of their larvae in the low-salinity zone. An older hypothesis suggests that once hatched from spawning areas largely upstream of the low-salinity zone, longfin smelt larvae are predominantly surface-oriented and dispersed widely by river flows and tidal currents, particularly when Delta outflow is high (CDFG 2009a, p. 8). A newer hypothesis is that most eggs are spawned in the low-salinity zone as well as the smaller low-salinity zones of the Bay Area tributaries (e.g., Lewis *et al.* 2019, p. 3), such that the larvae hatch directly into suitable rearing habitats (Grimaldo *et al.* 2020, p. 12). Larval retention is then due to a combination of swimming behaviors (Bennett *et al.* 2002; Kimmerer *et al.* 2014) and vertical and lateral mixing of fresh- and brackish water that has been well-described in the estuary (see Section 2.3). Regardless of how correct or dominant each reproductive conceptual model is, there is good data support for the importance of the low-salinity zone as a critical rearing habitat for the early life stages of longfin smelt (Dege and Brown 2004, Fig. 3, p. 57; Bennett *et al.* 2002, p. 1502; Hobbs *et al*. 2010, Fig. 5 p. 565; Grimaldo *et al.* 2020, Fig. 6, p. 10).

2.4.3. Maturity and Fecundity

Longfin smelt maturation begins in the fall with mature fish observed as late as May of the following year (Tempel and Burns 2021, slide 3). Longfin smelt are sexually dimorphic, where males darken in color and the base of their anal fin hardens and elongates, presumably for sweeping fine sediments

from spawning sites (Wang 1986, pp. 6–10). Most longfin smelt that exhibit onset of maturation are > 90 fork length (FL) (Baxter 2021, pers. comm.), while fecundity increases exponentially as a function of female size, and ranges from about 1,900 eggs in a 73 mm female to over 16,000 in a 132 mm female (CDFG 2009a, Fig. 3, p. 11). Studies of longfin smelt fecundity for the Lake Washington and Harrison Lake populations also yielded similar results, with fecundity tending to be a function of both size and feeding success (Dryfoos 1965, p. 120; Chigbu and Sibley 1994, pp. 7–8). Since hatching is primarily observed annually from January onward, we use January 1 as the anniversary "hatch date" for incrementing age in this SSA. Thus, subadult fish in their first year of life (defined as age-0) will all become age 1 on January 1 and enter their second year of life. And age-1 fish will increment to age 2 on January 1.

2.4.4 Environmental Parameters Influencing Bay-Delta DPS Growth Rates and Length at Age

There is little published information about the growth rates of longfin smelt, but most of the published information available comes from studies on the Bay-Delta DPS. Souza *et al.* (2006, Fig. 1, p. 4) estimated that larval longfin smelt grew at a mean apparent rate between 0.12 and 0.23 mm/day as they reached the juvenile stage. Growth rates of very young larvae (3–5 days post-hatch) have also been studied in the lab (at various temperatures and salinities) for the purpose of identifying ideal conditions for captive rearing (Yanagitsuru *et al.* 2021, entire). In an otolith study, longfin smelt were found to grow slowly up to about 20 days post-hatch, and at a slightly faster rate up to about 120 days of age (Hobbs et al. 2013, Fig. 7, p. 79).

To assess LFS apparent growth, we modified the Lester *et al.* (2004, entire) biphasic growth model to estimate the impacts of factors on somatic growth patterns using a similar model developed by the author (Matthias *et al*. 2016, entire). Our primary objective was to quantify the strength, direction, and potential interactions of abiotic and biotic factors influencing Bay-Delta DPS growth. Our secondary objective was to assess for systematic or long-term changes or patterns in Bay-Delta DPS growth. Our model was designed to assess variation in apparent growth of longfin smelt using a combination of observed environmental conditions (e.g., water temperature, conductivity, Delta outflow, density, and prey availability) and random effects. Details on data used, methods, and application, as well as more detailed results are available in Appendices D and E.

Our growth model results support the conclusion that environmental conditions do influence Bay-Delta growth patterns. The best model included abiotic, biotic, and random effects on the growth increment (see Figures 2.5 and 2.6) and abiotic effects on the length-at-age-0. Abiotic effects on growth were temperature squared, Delta outflow, and a temperature-outflow interaction. Biotic effects represented density using abundance indices and time with associated interactions and prey availability (*Eurytemora Afinnis* and *mysis* shrimp indices). For both abiotic and biotic effects, the main effects and interactions were all significant (except for the mysis index effects during Phase-1 growth) and the effects were different between the two growth phases (Fig. 2.5). The average length of each age class of longfin smelt varies from year to year, but we did not detect systematic trends in length-at-age over time (Fig. 2.6).

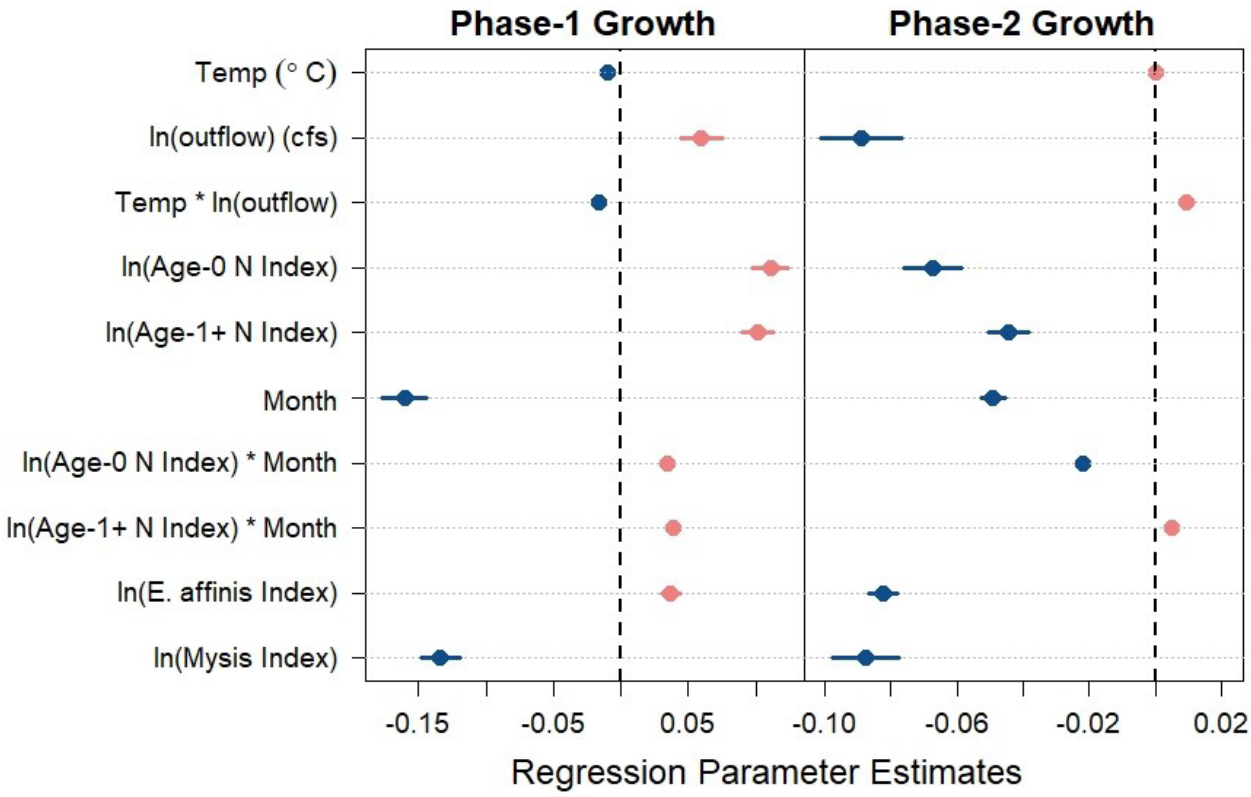

Figure 2.5: Parameter estimates for relationships between environmental variables and growth rates in a biphasic growth model. Colors highlight the direction of relationships: blue indicates a negative relationship, pink indicates a positive relationship, and grey indicates a relationship where the direction may be flat.

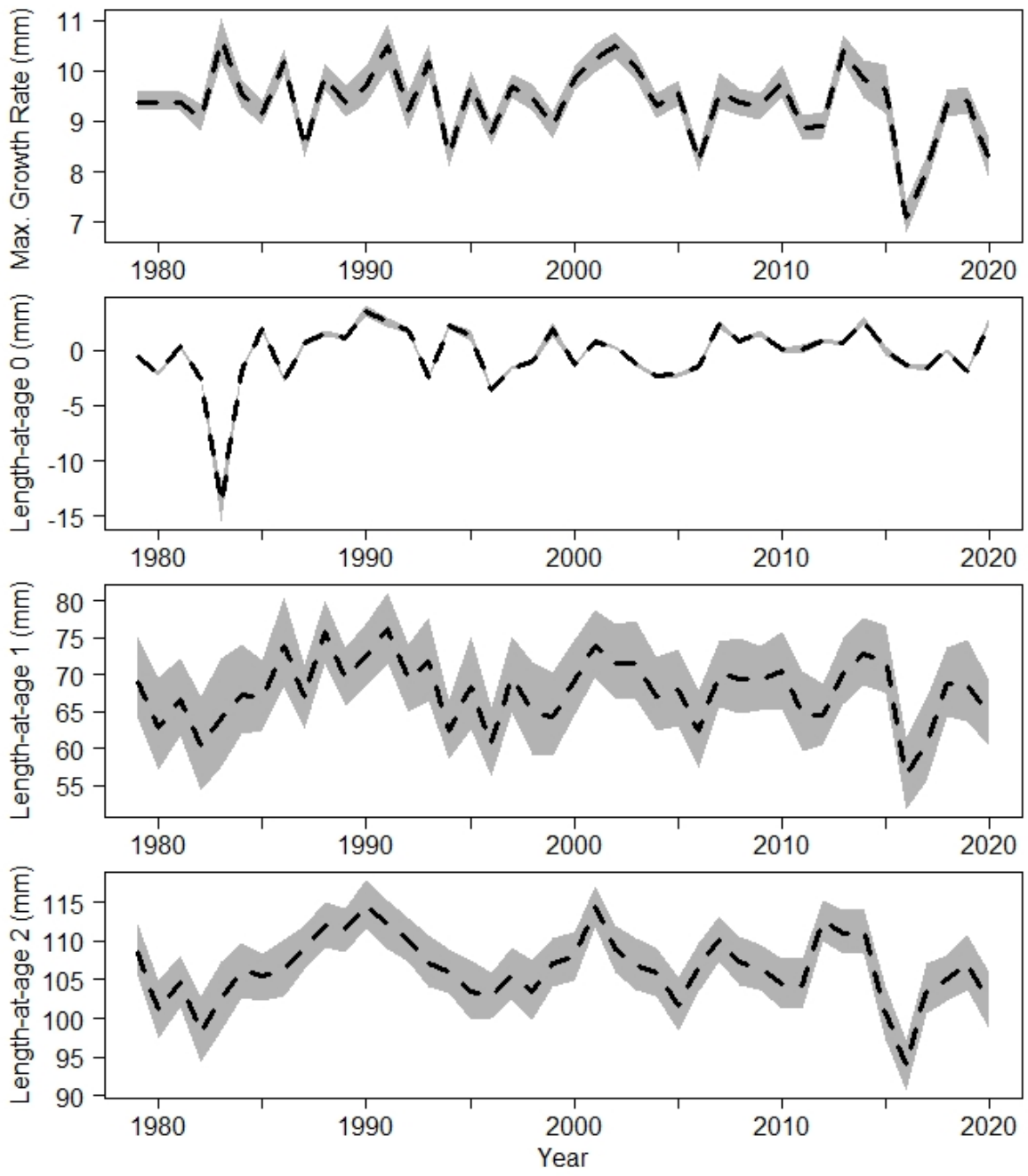

Figure 2.6: Estimated temporal trends in growth patterns from 1979 to 2020. The maximum growth rate (mm; top panel) accounts for variation in the predicted Phase-1 growth and a year-specific random effect predicting the unobserved annual variation in growth patterns. Panels for predicted length-at-age 0, 1, and 2 represent age in years (i.e., 0, 12, and 24 months).

2.4.5. Geographic Distribution and Habitat

Larvae

The spatial distribution of larvae (<20 mm length) within the San Francisco Bay-Delta has not been fully resolved due to lack of adequate coverage by monitoring programs (Grimaldo *et al*. 2017, Fig. 5, p. 1777; 2020, Fig. 6, p. 10). The majority of larvae are affiliated with the estuary's major low-salinity zone generated by the mixing of freshwater outflow from the Delta with the brackish waters of the estuary (see Section 2.3). However, larvae can also be found in tributaries when flows from those tributaries are high enough and temperatures low enough to support egg survival and hatching (Lewis *et al.* 2019, p. 3). The spatial distribution of these larvae reflects the year-to-year variation in the geographic location of the low-salinity zone (Dege and Brown 2004, Fig. 3, p. 57; Grimaldo *et al.* 2020, Fig. 6, p. 10).

Within the low-salinity zone and adjacent waters, larvae have been commonly collected in both littoral (nearshore) and pelagic (offshore) habitats. Upon hatching, the larvae may swim toward the water surface which would facilitate relatively rapid seaward transport (CDFG 2009a, p. 8). However, it is not clear that such a behavior would facilitate retention in the low-salinity zone, especially when Delta outflow is high (Kimmerer *et al*. 2014, Fig. 5, p. 910). Using a 3D hydrodynamic modeling framework, Kimmerer *et al*. (2014, Fig 5, p. 910 and Fig. 6, p. 911) applied the relatively modest swimming capabilities of copepods to show how well simple behaviors could help planktonic animals avoid being washed out to sea and keep them loosely associated within particular salinity ranges. Copepods are considerably smaller than larval fishes, and if they are able to influence their own location in the estuary, it follows that longfin smelt larvae may possess this capacity as well (Bennett *et al.* 2002, p. 1502). The recent findings of larval densities in tidal marsh channels and other edge habitats in densities comparable to offshore waters provides another potential low salinity zone retention mechanism since tidal currents are slower over shallow shoals and associated marsh channels (Bever *et al*. 2016, Fig 8b, p. 15).

Juveniles through Adults

Aggregated survey data have been used to show that juveniles (>20 mm in length) have been detected at one time or another throughout the estuary and into some tributaries to the Delta above tidal influence (Merz *et al.* 2013, Fig. 2, p. 132). However, the spatial distribution of juveniles shows a distinct seaward migration as water temperatures warm in the late spring and early summer (Rosenfield and Baxter 2007, p. 1590; Tobias and Baxter 2022, *in press*).

Juveniles have been collected most frequently from deep water habitats as opposed to shoals (Rosenfield and Baxter 2007, p. 1586). In Lake Washington, age-0 and age-1 longfin smelt favor deep water during daylight and move closer to the surface at night (Quinn *et al.* 2012, p. 342), likely moving in relation to their major source of food, mysid shrimp (Chigbu *et al.* 1998, p. 180). It is possible that the Bay-Delta DPS does so as well, but this has not been evaluated for post-larval fish. Selection for deep

water and a general shift to marine habitat were hypothesized to be behavioral responses to seasonally increasing water temperatures (Tobias and Baxter 2022, *in press*).

Phillis *et al.* (2021, entire) utilized boosted regression trees and concluded that the strongest predictors of juvenile longfin smelt catch in the 20-mm Survey were bottom salinity, Secchi depth, Julian Day, temperature, surface salinity, and the 7-day average position of X2. The same study predicted larval habitat availability during March through July under low and high spawner abundance in dry, moderate, and wet years (see Figure 2.7). These authors also predicted that, in dry years, habitat distributions shifted to Suisun Bay and north San Pablo Bay. Whereas in moderate flow years, their analysis predicted that higher freshwater flows resulted in lower salinity into areas of San Pablo Bay, and habitat suitability was predicted to increase in the South San Francisco Bay. In wet years, they predicted high suitability habitat is available in Suisun Bay, San Pablo Bay, and some of the South San Francisco Bay.

Based on otter trawl survey data, juvenile longfin smelt rapidly adapt to and inhabit increased salinities because about half the juveniles captured by the larval net came from the salinity range 8 to 24 ppt (Baxter *et al.* 1999, pp. 189–190), well seaward of X2. This increase in salinity distribution represents both seasonal increases in upper estuary salinity as outflow declines and downstream movement of some individuals (Baxter *et al.* 1999, p. 191). By their first summer of life, juvenile longfin smelt inhabit salinities up to and including marine water (i.e., 32–33 psu; Baxter *et al.* 1999, p. 191; Rosenfield and Baxter 2007, p. 1590; Kimmerer *et al.* 2009, p. 385).

By May of most years, young-of-the-year longfin smelt begin to reach 40 mm FL (Rosenfield and Baxter, 2007, p. 1581). At this size, and regardless of outflow, these approximately 40 mm young of the year are typically distributed throughout the estuary (Baxter *et al.* 1999, p. 189; Merz *et al.* 2013, pp. 136–139). They are found from low salinity (and occasionally freshwater) on the upstream end of the Bay-Delta DPS' range, to marine conditions on the downstream end. Distributions of older age-0 and age-1 fish have only been described coarsely into densities across shoal (<7m depth) and channel (≥7m depth) habitats. For both age groups, density was almost always higher in the deeper channel habitats, and significantly higher from the first fall through the second spring of life, and between the second fall and second winter of life (Rosenfield and Baxter 2007, p. 1586).

In any given month, Bay Study data indicate that some fraction of the LFS population remain in the Bay, but an unknown fraction may be found in the ocean (Rosenfield and Baxter 2007, p. 1590; Merz *et al.* 2013, p. 142). Longfin smelt have been detected in the nearshore ocean off of San Francisco (Garwood 2017; City of San Francisco and CH2M Hill 1984 and 1985, entire). In addition, Feyrer *et al.* (2015) found a statistical association between the North Pacific Gyre Oscillation (an index of) and age-0 longfin smelt catch in the Bay Study. For this correlation to have any mechanistic basis, longfin smelt would need to be present in the ocean. These observations all support the hypothesis that at least partial anadromy is a life history strategy used by the Bay-Delta DPS, which is consistent with the pattern observed in other populations range-wide (Rosenfield and Baxter, 2007, p. 1590). Recent longfin smelt otolith analyses have supported the conclusion; Lewis *et al.* (2019, p. 63) used isotope ratios in otoliths and indicated that longfin smelt may exhibit at least four unique life history strategies. Another perspective is that the

fish may be displaying a single life history strategy within a continuum, spawning in waters that are fresh to slightly brackish and then consistently transitioning into waters too saline to be discerned using strontium. The important indication is that component life stages of the DPS display variable spatio-temporal distribution as part of its life history strategy.

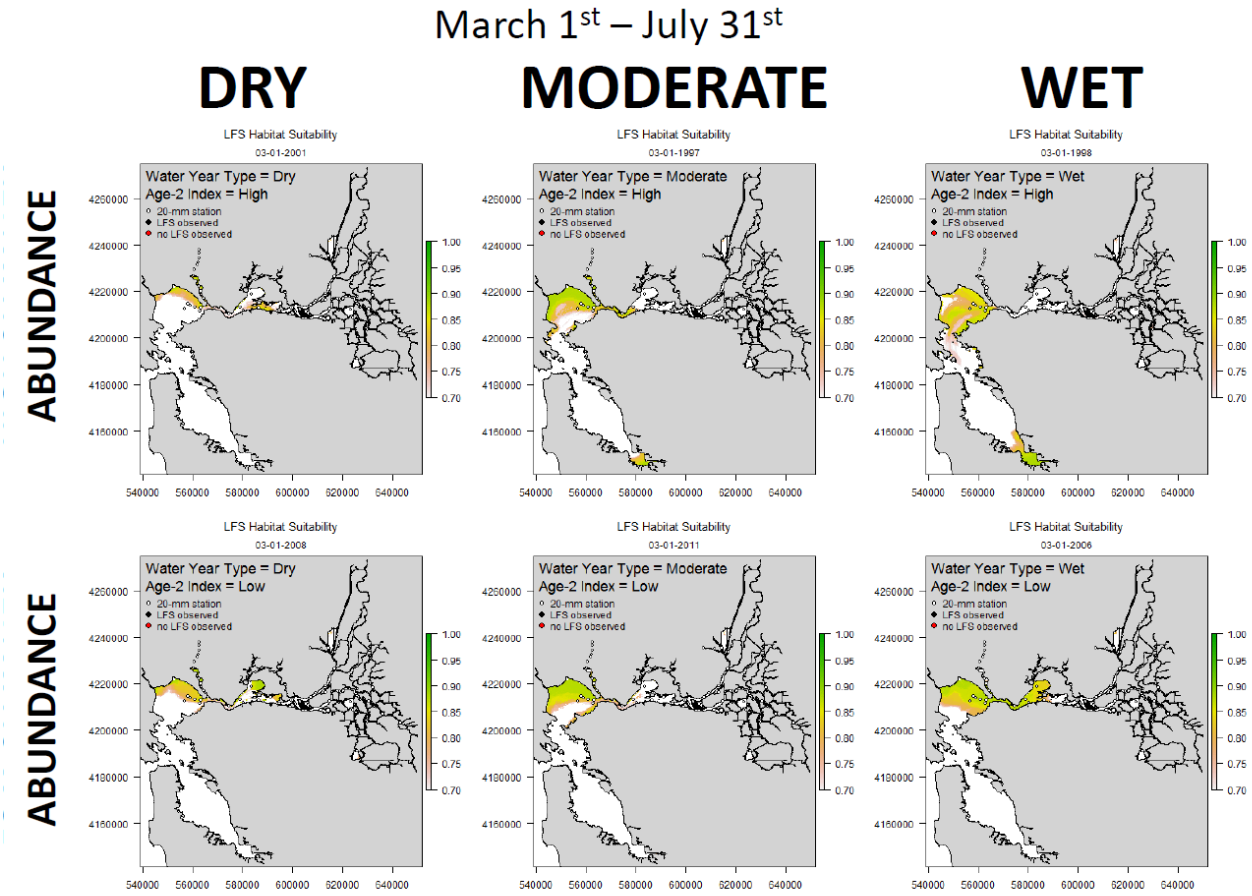

Figure 2.7: Predicted juvenile habitat availability under various scenarios based on boosted regression tree models. Source: Phillis *et al.* 2021, unpublished data

2.5. Diet

Larval longfin smelt select strongly for the calanoid copepod *Eurytemora affinis* as prey; all other prey types combined account for only about 10% of the diet (Barros *et al*. 2022, Fig 6a and 6c, pdf p. 10). When longfin smelt reach about 1 inch in length, the diet switches and is nearly all mysids, a taxonomic group of larger crustaceans commonly called opossum shrimp (Barros *et al.* 2022, Fig 6b, pdf p. 10). This finding of a highly specified diet applies to fresh- and brackish-water habitats throughout the estuary (Barros *et al.* 2022, Fig. 2. pdf p. 2). The currently dominant mysids in the estuary's low-salinity habitats are nonnative species introduced in the 1990s that are smaller than the historically dominant native species, *Neomysis mercedis*, though they are still considerably larger than *E. affinis*. The non-native mysids are also less abundant than *N. mercedis* was in the 1970s and 1980s (Winder and Jassby 2011, Fig 9, p. 685). Both of longfin smelt's primary prey taxa had historical peaks in abundance in the

estuary's largest low-salinity zone generated by outflow from the Delta (Kimmerer 2002a, Fig. 2, p. 45). This meant these peak abundances of prey were spatially associated with similar peaks of larval and small juvenile longfin smelt. The abundance of young longfin smelt's primary prey taxa and their historical relationships to X2 variation were disrupted by food web changes associated with the overbite clam (*Potamocorbula amurensis*) (see Table 2.1). Longfin smelt must switch prey again when they occupy mesohaline to marine habitats as brackish water prey become unavailable. However, what taxa constitute their marine prey has not been evaluated.

Table 2.1. Changes to abundance and X2 relationships for *Eurytemora affinis* and *Neomysis mercedis* following the invasion of the San Francisco Estuary by overbite clam (OC), *Potamocorbula amurensis*. Summarized from Kimmerer (2002a, Fig. 7, p. 47). Note that Kimmerer also evaluated the trends for E. affinis for June-October, but by this time of year longfin smelt have outgrown copepod-sized prey (Barros *et al.* 2022, Fig 6b, p. 10).

Season analyzed	Prey taxon	Pre-OC relationship to X2	Post-OC relationship to X2
March-May	*E. affinis*	No significant relationship	Lower mean density; significant inverse relationship (higher abundance when X2 moves seaward in response to high Delta outflow)
June-October	*N. mercedis*	Significant inverse relationship (higher abundance when X2 moves seaward in response to high Delta outflow)	Lower mean density; significant positive relationship (higher abundance when X2 moves landward in response to low Delta outflow)

2.6. Environmental Requirements of the Distinct Population Segment

This section summarizes the key known ecological requirements for the survival and reproduction of longfin smelt at the individual level at each life stage.

2.6.1 Temperature Range

Longfin smelt larvae appear to be adapted to cool water conditions. An experiment testing embryo hatching success at 9°, 12°, and 15°C found hatching success generally decreased as temperature increased, but so did variation in hatching success (Yanagitsuru *et al.* 2021, Fig 1, p. 5). Embryos also tended to hatch at smaller size as experimental temperature treatments increased (Yanagitsuru *et al.* 2021, Fig 2a, p. 6). Yolk-sac larvae (notochord length 5–7 mm) in the 15°C treatment grew more slowly than larvae in the 9° and 12°C treatments (Yanagitsuru *et al.* 2021, Fig 3a, p. 7). Collectively these results indicate that temperatures approaching and exceeding 15°C impair larval viability, and hence this benchmark may be ecologically significant. It is logical to presume that the Bay-Delta DPS, inhabiting as it does the most southern portion of the species range, has historically been (and is) at the uppermost temperature tolerance range of the species.

Field surveys have detected peak yolk-sac larval (4–9 mm total length) numbers in water temperatures between 8° and 12° C, corresponding to the early rearing months (Grimaldo *et al.* 2017, p. 8). At later larval stages, longfin smelt are still likely restricted to water temperatures below 20°C. Jeffries *et al.* 2016 (p. 1709) found that larger larvae (standard length 15–19 mm, 40 days post-hatch) exhibit cellular stress at 20°C, suggesting that this may be nearing the upper limit of their extended temperature tolerance. In general, age-1 fish inhabit lower temperature water than age-0 fish, although both age classes inhabit 16°–18°C water in summer and fall (Baxter, 2009, fig 8., p 191). Adults are thought to be limited by water temperature >22°C during the summer, and likely spend the majority of this time in cooler Bay habitats and the open ocean. As no standardized field surveys currently exist beyond the Golden Gate Bridge, the oceanic distribution and habitat use of longfin smelt remains largely unknown.

After returning from the ocean, and subsequently maturing in the estuary, the fish return to spawn where water quality conditions are favorable for egg survival. These conditions vary in location depending on delta outflow and the location of the LSZ, as well as flows from Bay Area tributaries. Although spawning can start once water temperatures drop below 16° C (60.8° F) (CDFG 2009a, p. 11), other information suggests temperatures of 13° C and maybe lower are more ideal (Baxter 2016, pers. comm.; Tempel and Burns 2021, slide 12).

2.6.2 Salinity tolerance

In laboratory tests evaluating salinity tolerance, yolk-sac larvae (notochord length 5–6 mm) survived the longest and grew the largest at 5 and 10 ppt (Yanagitsuru *et al.* 2022, in review). Yolk-sac larvae were also able to maintain water balance equally between 0.4 and 10 ppt, but were unable to survive at 32 ppt, which is the equivalent to marine salinity. On the other hand, yolk-sac larvae experienced stalled yolk resorption in freshwater.

In field surveys, peak yolk-sac larval (4–9 mm total length) densities have been found at 2–4 ppt (Grimaldo *et al.* 2017, p. 8), which is also concordant with the early life salinities that produce highest survival to later life stages (Hobbs *et al.* 2010, p. 564). Longfin smelt lab studies, however, did not test larval tolerance to 2–4 ppt salinity. CDFW's 20-mm Surveys have also shown peak larval (mean length of 20.2 mm) distribution near X2 (Dege and Brown 2004, p. 57–58), although larvae have been detected in salinities as high as 12 ppt, likely the result of tidal dispersion of larvae around a core habitat.

2.6.3 Turbidity

The role of turbidity in providing simultaneous feeding and predator avoidance advantages for larval fishes has been well established (Utne-Palm 2002, p. 115; Pangle *et al.* 2012, pp. 10–11). The small size of most fish larvae means that the distances over which they react to prey are very short (e.g., a scale of millimeters). This implies relatively few sediment and algal particles that tend to dominate aquatic turbidity interfere with prey detection. A helpful analogy provided by Utne-Palm (2002, p. 115) is that turbidity in aquatic environments works like fog does in terrestrial environments; at short distances, it has little effect on our ability to see, but at longer distances, it can increasingly obscure objects from sight. Further, the sediment and algal particles often backlight relatively translucent zooplankton, helping larval fishes see these prey more easily (Utne-Palm 2002, p. 119). In contrast, larger fishes that may prey on fish larvae have longer search and reactive distances so more sediment and algal particles are in between these larger fish and their potential prey (Utne-Palm 2002, pp. 122–123). This can visually confound efforts by larger animals that hunt primarily using eyesight to see potential prey, making it more difficult for them to forage effectively.

We assume that these turbidity mechanisms that apply broadly to larval fishes also apply to longfin smelt in the San Francisco Estuary. In laboratory turbidity tests, larvae had higher survival at 40 NTU[1] and grew larger at 20 NTU and 40 NTU as opposed to 10 NTU (Yanagitsuru 2020, pers. comm.). In addition, larvae under the 10 NTU treatment group did not successfully transition from eating rotifers to the larger *Artemia*. Taken together, these recent laboratory experiments combined with the field results described above provide an assessment of early-life habitat needs.

2.6.4 Dietary

As reviewed in Section 2.5, during the time that longfin smelt larvae and small juveniles are feeding in low-salinity habitats, they appear to focus on only two prey taxa. Larvae less than about 2.5 cm (1 in) in length appear to primarily use the copepod *Eurytemora affinis* as prey so it is logical to assume it is a dietary need. The same is true for larvae and small juveniles over about 2.5 cm in length which appear to require mysids as prey. Longfin smelt adults that had returned to Suisun Marsh have shown a strong dietary preference for mysids while relying on copepods and amphipods when mysids are scarce (Burdi 2022, pers. comm.; CDFW unpub Diet Study Data; Feyrer *et al.* 2003, p. 281).

[1] NTU stands for Nephelometric Turbidity Units, i.e. the unit used to measure the turbidity of a fluid or the presence of suspended particles in water. The higher the concentration of suspended solids in the water is, the higher the turbidity and corresponding NTU value is.

Both prey taxa have declined and their relationships with X2 were changed by the overbite clam's impact on the estuarine food web (see Table 2.1). *E. affinis* did not have a significant interannual association with X2 until after the overbite clam began rearranging the food web. It has been assumed that this loss of larval prey could have contributed to the decline of longfin smelt as well as other POD species (Sommer et al. 2007, p. 274). If that were a correct hypothesis, a decline in recruits per spawner would be expected starting in the late 1980s. However, that change was not observed in either of the two studies that have evaluated it (Maunder *et al*. 2015, p. 107; Nobriga and Rosenfield 2016, pp. 54–55). Thus, it does not appear that declining abundance of *E. affinis* has generated a change in early life stage survival large enough to be discerned with available data.

The situation is the opposite for mysids which had higher abundance in wet versus dry years before the overbite clam, but not after (see Table 2.1). This indicates that, prior to the overbite clam invasion, a prey abundance mechanism for juveniles was difficult to statistically distinguish from other recruitment mechanisms associated with years of high Delta outflow. If mysid abundance was important to longfin smelt recruitment, then the expectation following the overbite clam invasion would be a substantial decline, even after accounting for the influence of outflow (or X2). This was observed (Kimmerer 2002a, Fig. 5, p. 46 and Fig. 8, p. 48; Thomson *et al.* 2010, Fig. 6b, p. 1442), which lends support to a food limitation hypothesis. However, if the decline of *E. affinis* cannot be linked to longfin smelt decline, then the only other meaningful early life prey is mysids. Interestingly, several studies that have attempted to link time series of mysid abundance with time series of longfin smelt abundance or survival have not been able to do so. Mysid abundance was not able to predict Fall Midwater Trawl (FMWT) catches of longfin smelt with the strength of statistical inference desired by one study (Thomson *et al.* 2010, Fig. 6c, p. 1442).

The presence versus absence of overbite clam in the estuary was not retained in the longfin smelt model described by Mac Nally *et al.* (2010, Fig. 3, p. 1425) meaning that there was not a consistent change in longfin smelt abundance before and after the overbite clam invasion that couldn't be better explained by other covariates. Further, this model predicted longfin smelt had a top-down (predatory) influence on mysid abundance, rather than a bottom-up influence of food limitation. Similarly, the mysid covariate tested by Maunder *et al*. (2015, Table 2, p. 108) was not retained in any of these authors' alternative life cycle model constructs (Table 3, p. 108).

Chapter 3 – Current Condition

For the Bay-Delta DPS to maintain viability, a significant portion of its population must be resilient to the variable environmental conditions. In this chapter, we start with describing the stressors that the species has historically faced to date, and how the species has responded to these stressors over time. We then show the estimates of species relative abundance based on long-term monitoring program data to document the current condition of the species. Then, we present the results of our quantitative modeling estimating probability of extinction on the current trajectory, and close with a discussion of the 3R's relative to the ecological viability of the DPS.

3.1. Stressors

Here we discuss the most probable stressors and environmental variables that have likely led to the Bay-Delta DPS's current condition, which include the following: habitat loss and degradation via reduced freshwater flow, food web effects from reduced flows and invasive species, increasing temperatures. Additionally, we discuss other potential stressors that are less certain to be influencing abundance patterns or are thought to be influencing population dynamics to a lesser degree. These include: conversion of tidal marsh and environmental contaminants; and more so historically than presently, entrainment via water diversions. Based on our knowledge of the life history of the Bay-Delta DPS, we assess how changes in the system may have affected recruitment and subsequent survival among life stages, resulting in the observed decline in abundance through time, which is presented following this treatment of historical and extant stressors.

3.1.1. Reduced freshwater flow

A significant stressor to the Bay-Delta longfin smelt is reduced flows and alteration of the natural hydrograph—reduction in the magnitude and duration of freshwater flows into and through the Delta and to a lesser extent from the various Bay Area tributaries. In the Bay-Delta, the natural hydrologic cycles of drought and flood would yield a different outflow regime (i.e., "unimpaired flow") if upstream dams and diversions were not in existence, as water project management has decreased springtime flows resulting from upstream storage, and increased summer inflows that are subsequently diverted for urban and agricultural beneficial uses (Kimmerer 2004, p. 15).

Demand for water supplies and flood protection have substantially increased over time. In response, local, State and Federal agencies have built dams and canals, and captured water in reservoirs, to increase water storage during the wet season and convey water to farms and cities during the dry season, resulting in one of the largest man-made water systems in the world (Nichols *et al.* 1986, p. 569). Operation of this system has thus altered the timing, magnitude, and duration of freshwater flows into the Bay-Delta (Andrews *et al.* 2017, p. 72; Gross *et al.* 2018, p. 8). Storage in the upper watershed of peak runoff, and release of the captured water for irrigation and urban needs during subsequent low flow periods, resulted in a broader, flatter hydrograph with less seasonal variability (Kimmerer 2004, p. 15).

In addition to the system of dams and canals built throughout the Sacramento and San Joaquin River basins, the Bay-Delta is unique in having the largest water diversion system on the west coast. The State Water Project (SWP) and Central Valley Project (CVP) each operate water export facilities in the south Delta (Kimmerer and Nobriga 2008, p. 2). Project operation is dependent upon upstream water supply and export area demands, both of which are strongly affected by the interannual variability in precipitation within the broader hydrologic basin draining the Sacramento and upper San Joaquin Valleys. From 1956 to the 1990s, water exports increased, rising from approximately five percent of the Delta inflow to approximately 30 percent of the Delta inflow (Cloern and Jassby 2012, p. 7). By 2012, an estimated 39 percent of the estuary's unimpaired flow in total was either consumed upstream or diverted from the estuary (Cloern and Jassby 2012, p. 8).

Although alterations in the Delta and California's water diversions/storage have dated back to the latter 1800s, the most substantial parts of California's water infrastructure were constructed during the 1940s-1970s (see Section 2.3). It is noted that water year type classifications should not necessarily be conflated with realized estuarine hydrological conditions, as water operations modify these parameters based on supply considerations and extant regulatory requirements. For example, Reis *et al.* (2019, Table 5, p. 12) quantified a statistically-significant reduction in the frequency of realized delta outflow as a proportion of unimpaired flow reaching the Bay. Hutton *et al*. (2017, p. 2500) confirmed statistically-significant decreases in outflow during four months (February, April, May, and November), and increases in July and August—with follow-up analysis indicating primary attribution for these changes associated with the State and Federal water projects (Hutton *et al.* 2017b, Table 3, p. 2523). Further, the magnitude of impairment has changed over time (Hutton *et al.* 2017a, Fig. 4, pp. 2507–2508; Reis *et al*. 2019, Fig. 3, p. 12). It is probable that the magnitude (along with frequency) of realized delta outflow conditions are critical to this underlying relationship between flow variables, ecological conditions, and historical abundance trends, but only more detailed analyses and modeling will help characterize this risk quantitatively *and* mechanistically.

Numerous studies have shown the positive correlation between longfin smelt juvenile abundance and freshwater flow (Stevens and Miller 1983, pp. 431–432; Jassby *et al.* 1995, p. 285; Sommer *et al.* 2007, p. 274; Thomson *et al.* 2010, pp. 1439–1440; Kimmerer 2002a, p. 47; Rosenfield and Baxter 2007, p. 1585; Kimmerer *et al.* 2009, p. 381; Mac Nally *et al.* 2010, p. 1422; Maunder *et al.* 2015, p. 108; Nobriga and Rosenfield 2016, p. 53). Longfin smelt indices have exhibited a persistent correlation with freshwater flow. The survival of longfin smelt through their early life-stages is lower during dry conditions and higher during wet conditions--the evidence for this is that longfin smelt abundance indices nearly always decline sharply during dry periods then rebound when wet weather returns (Mahardja *et al.* 2021, pp. 9–10). In addition, recent multiple and consecutive dry conditions or prolonged drought have been and are expected to continue as significant pinch points putting downward pressure on the Bay-Delta DPS' trajectory, and the population may no longer possess the resilience to be able to recover from a string of consecutive dry years, or years in which water operations are unfavorable during important intervals within their lifestage. Prolonged drought conditions have already occurred and the trend in frequency and duration has increased (Swain *et al*.

2018, pp. 427–433). These drought conditions have exacerbated the impact of reduced flows from human activities.

Biologically speaking, one of the most important aspects of the various estuarine circulation mechanisms is that they can help animals avoid being transported seaward even though the net flow averaged over the entire water column is flowing toward the ocean. The same mixing currents that can aggregate sinking particles can assist in aggregating motile plankton. However, swimming organisms like young longfin smelt (Bennett *et al*. 2002, p. 1502) and their prey (Kimmerer *et al.* 2002, Fig. 9, p. 365; 2014, Fig. 6, p. 911) combine changes in their vertical and lateral position with these variable mixing currents to help maintain themselves in spatial association with particular salinity ranges and other habitat attributes.

Changes in Delta outflow affect both the location and the function of the low-salinity zone. When Delta outflow is low, X2 encroaches into the legal Delta (i.e., east of Chipps Island; Jassby *et al.* 1995, Fig. 2a, p. 274). When this occurs in the winter and spring, it affects where longfin smelt spawn and their larvae and young juveniles rear. Upstream of X2, surface and bottom salinities are always about the same (Jassby *et al.* 1995, Fig. 2c, p. 274). This means that, upstream of X2, there is little if any stratification of the water column and therefore the behaviors that planktonic organisms employ to stay associated with particular salinity ranges become ineffective. As a result, landward (upstream) of X2, these animals are less likely to avoid movement with net flows because the net flow direction is uniform across the water column. This can be beneficial if they occupy water in which the net flow direction is seaward (toward the low-salinity zone), but detrimental if they occupy water in which the net flow direction is moving toward the CVP and SWP water diversions in the southern Delta (Kimmerer 2008, Fig. 16, p. 23). In contrast, fish and invertebrates that are strongly affiliated with in-water structures and vegetation, as well as benthic fish and invertebrates, can resist the net flows in the Delta. However, these are not behaviors that have been attributed to the early life stages of longfin smelt (Bennett *et al.* 2002, Fig. 4, p. 1502; Grimaldo *et al.* 2020, Fig. 6, p. 10).

In terms of flow changes within the legal Delta, the CVP and SWP have a more outsized influence on hydrodynamics than non-project diverters (Hutton *et al.* 2019, Fig. 7, p. 11). Water exports from the Delta increased from the 1950s into the late 1980s (Cloern and Jassby 2012, Fig 7a, p. 7; Service 2019, Fig 5.7). Thereafter, the increasing trend began to level off, but the year-to-year variability increased. The export of water from the southern Delta tends to draw a 'net' flow of water from north to south (Kimmerer and Nobriga 2008, Fig. 7, p. 12). This flow is referred to as 'net' because it expresses a tidally-filtered flow, meaning that the tidal flows that routinely cycle negative (toward the SWP and CVP diversions) and positive (seaward) over hourly time scales have been mathematically removed to characterize the portion influenced by exports as net flow direction. Nonetheless, the transport of water toward the SWP and CVP diversions is fundamentally an instantaneous to tidal time-scale process.
The CVP pumping plant diverts water from Old River during all phases of the tide. In contrast, the SWP includes Clifton Court Forebay (CCF) in front of its diversions. The CCF is a gated, regulating reservoir that helps manage the highly variable water levels in Old River for the CVP pumps and local irrigators. During flood tides, the CCF intake gates are opened to allow the tide (and gravity) to bring water into the forebay. The water that is being exported at the CVP, and the water flowing into CCF, are backfilled by the tide and gravity flow of water from elsewhere in the Delta. Over time scales of weeks to months, this backfilling, which is the hydraulic mechanism for the net flow, dominates the transport of river water in the Delta (Kimmerer and Nobriga 2008, Fig 3, p. 10).

It has long been recognized that abundance indices for age-0 longfin smelt tend to increase in wet years that have followed dry years (Stevens and Miller 1983, Table 8, p. 433; Jassby *et al.* 1995, Fig. 5, p. 280; Rosenfield and Baxter 2007, Table 3, p. 1585); but longfin smelt abundance indices have also declined over time in a range of water year types (Thomson *et al.* 2010, Fig. 6, p. 1442). Freshwater flows entering the estuary change a wide variety of physical, chemical and biological parameters that can influence the distribution and abundance of aquatic species (see Section 2.3). Thus, it is unlikely that a single mechanism associated with or co-varying with wet and dry years is responsible for generating observed patterns in longfin smelt recruitment. Recent analyses that have attempted to consider the influence of wet and dry years in the context of longfin smelt's life cycle have found evidence that the freshwater flow-, or flow-associated mechanisms, influence the number of juvenile recruits produced per spawner (Maunder *et al*. 2015, pp. 105–106; Nobriga and Rosenfield 2016, Fig. 2, p. 53).

Population dynamics of longfin smelt surviving a sufficient duration into the juvenile life stage to begin migrating seaward do not appear to be influenced by freshwater flow variation (Nobriga and Rosenfield 2016, p. 55). These two pieces of evidence imply that the reproductive success of the adult spawners, the survival of eggs and early life stages, or both of these factors, are the endpoints being affected by the freshwater flow- or flow-associated mechanisms. Figure 3.1 shows hypothesized, staggered, but overlapping, timing of flow- or flow-associated mechanisms that might have an important quantitative influence on longfin smelt spawning success, on egg survival, or survival from the larval to the juvenile life stage. Each of these mechanisms is known to covary with flow, or to have done so historically (citations provided below). It is not the existence of these mechanisms, but their *quantitative influence* on the viable egg production and survival of longfin smelt's early life stages that remains a clear science priority in support of longfin smelt conservation.

While the overall pattern relating freshwater flows to abundance indices for the Bay-Delta DPS is widely accepted, the mechanisms driving this correlation are not fully quantified or resolved. Following are the enumerated summaries of mechanistic drivers of Bay-Delta DPS abundance dynamics as related to freshwater flow, or flow-associated physical or biological parameters.

Mechanism 1, spawning locations: High flows during the spawning season likely led to more total spawning effort seaward of the legal Delta (Grimaldo *et al*. 2020, Fig. 6, p. 10) and higher spawning success in Bay Area tributaries (Lewis *et al*. 2019, p. 3). If egg survival tends to be higher seaward of the Delta, then variation in spawning locations may be a recruitment mechanism that covaries with freshwater flow. This is speculation that warrants focused research efforts to better inform longfin smelt conservation.

Mechanism 2, spawning season duration: The duration of the longfin smelt spawning season each year is fundamentally driven by climatic influences on the estuary's water temperatures. Water temperature is greatly influenced by freshwater inflow and ambient air temperatures (Vroom *et al*. 2017, pp. 9918–9920). Wet weather increases tributary outflows from Bay Area streams where overlying air temperatures remain cool longer into the season than is typical in the Delta. This might lead to longer spawning seasons in these smaller systems. Wet weather also increases Delta

outflow, which likely leads to more total spawning effort seaward of the legal Delta (Grimaldo *et al.* 2020, Fig. 6, p. 10). If elevated outflow is maintained into the spring, one expected result would be successful spawning opportunities not available in warmer, lower outflow years when the low-salinity zone is encroaching on the Delta and overlying air temperatures during May typically begin to exceed Bay Area air temperatures (Conomos *et al*. 1985, Fig. 4, p. 5).

Mechanism 3, low-salinity zone location and retention for larvae and young juveniles: The hydrodynamic phenomena reviewed in section 2.3 may create bioenergetically-favorable transport and retention opportunities for larval and juvenile longfin smelt. For instance, the Delta does not have as much shoal habitat as seaward parts of the estuary. When outflow is high enough to place the low-salinity zone over larger shoal and marsh habitats, the lower water velocities and estuarine mixing currents may enhance opportunities for early life stage longfin smelt to maintain position and find food in higher quality habitat (Hobbs *et al.* 2006, p. 916; Grimaldo *et al.* 2017, p. 7).

Mechanism 4, entrainment of larvae and young juveniles: High flows during the spawning season likely lead to more total spawning effort seaward of the legal Delta (Grimaldo *et al.* 2020, Fig. 6, p. 10). This leads to smaller fractions of larvae vulnerable to entrainment in exported water. Higher net flows out of the Delta also better facilitate the seaward transport of larvae that are spawned in the Delta and lessen their risk of entrainment in water diversions (Kimmerer and Nobriga 2008, Fig 7, p. 12; Rosenfield 2010, Fig. 9, p. 40; Grimaldo *et al.* 2009, Table 2, p. 1261).

Mechanism 5, prey availability for larvae (*Eurytemora affinis*): If food limits the survival of longfin smelt during their larval stage, it would logically be associated with declines in *E. affinis*—the predominant component of larval longfin smelt diet (Barros *et al*. 2022, Fig. 6a). The influence of Delta outflow on *E. affinis* production has changed over time, due in large part to the strong influence of overbite clam grazing (Table 2.1). The abundance of *E. affinis* has declined over time (Winder and Jassby 2011, Fig. 6, p. 682), but as of 2011, longfin smelt recruits per spawner had not (Nobriga and Rosenfield 2016, Fig. 2, p. 53). This dissociation of trends makes it unlikely that the decline of *E. affinis* had a major quantitative impact on the survival of larval longfin smelt (Nobriga and Rosenfield 2016, pp. 54–55), but a comparable analysis for the last decade is lacking.

Mechanism 6, prey availability for young juveniles (mysids): If food limits the survival of longfin smelt exceeding about an inch in length, it would logically be associated with mysids—the predominant component of the diet at this lifestage (Barros *et al*. 2022, Fig 6b, pdf p. 10). If mysid abundance was important to longfin smelt recruitment, then the expectation following the overbite clam invasion would be a substantial decline, even after accounting for the influence of outflow (or X2). This is what was observed (Kimmerer 2002a, Fig. 5, p. 46 and Fig. 8, p. 48; Thomson *et al*. 2010, Fig. 6b, p. 1442), which lends support to a juvenile longfin smelt food limitation hypothesis. We recognize that direct statistical support for a bottom-up longfin smelt-mysid link has not been reported in several recent statistical evaluations (Mac Nally *et al*. 2010, Fig. 3, p. 1425; Thomson *et al*. 2010, Fig. 6c, p. 1442; Maunder *et al.* 2015, Tables 2-3, p. 108). However, longfin smelt may continue to rely on mysids as prey until they leave the estuary, and

the survival of these older fish may have declined over time (Nobriga and Rosenfield 2016, Table 5, p. 54). Therefore, it remains possible that changes in mysid abundance have been an important contributor to the observed decline. This is speculation that warrants focused research efforts to better inform longfin smelt conservation.

Mechanism 7, prey delivery from the Yolo Bypass: As outflow from the Delta increases, the proportion of the total flow entering from the Yolo Bypass increases as well (Kimmerer 2004, Fig. 5, p. 16). As the bypass drains, its relatively shallow depth, long residence times, and warmer temperatures can help deliver phytoplankton and invertebrates into the Delta (Sommer *et al*. 2004, Fig. 3 p. 254). However, in the wetter years when Yolo Bypass floods and drains, many, if not most, longfin smelt are rearing in fairly distant locations. Therefore, it is uncertain whether these winter-spring floodplain food subsidies are substantial contributions to larval longfin smelt at the population scale.

Mechanism 8, turbidity of the low-salinity zone: The potential importance of turbidity as a moderator of feeding success and predation risk for young longfin smelt was reviewed in section 2.6.3. Turbidity has declined in the estuary for a combination of reasons. However, the high winds that accompany wet weather can resuspend sediment and increase low-salinity zone turbidity, especially when the low-salinity zone is flowing back and forth over major shoal areas like Suisun Bay (Bever *et al*. 2018, Fig. 11, p. 1957). Further, high winter-spring flows deliver new sediment and particulate matter that can increase turbidity (Kimmerer 2004, Fig. 27, p. 41; Cloern and Jassby 2012, Fig. 10, p. 10).

In summary, during high outflow years, longfin smelt are believed to benefit from a suite of mechanisms that can extend the spawning season and increase the cumulative survival of the early life stages. Conversely, during low outflow years, fewer of these benefits are accrued and survival is reduced. For these reasons, the interannual variation in Delta outflow and to lesser extent, flows in Bay Area tributaries (which can also be represented by correlates like X2) mechanistically represent a primary population need from December through May or June each year.

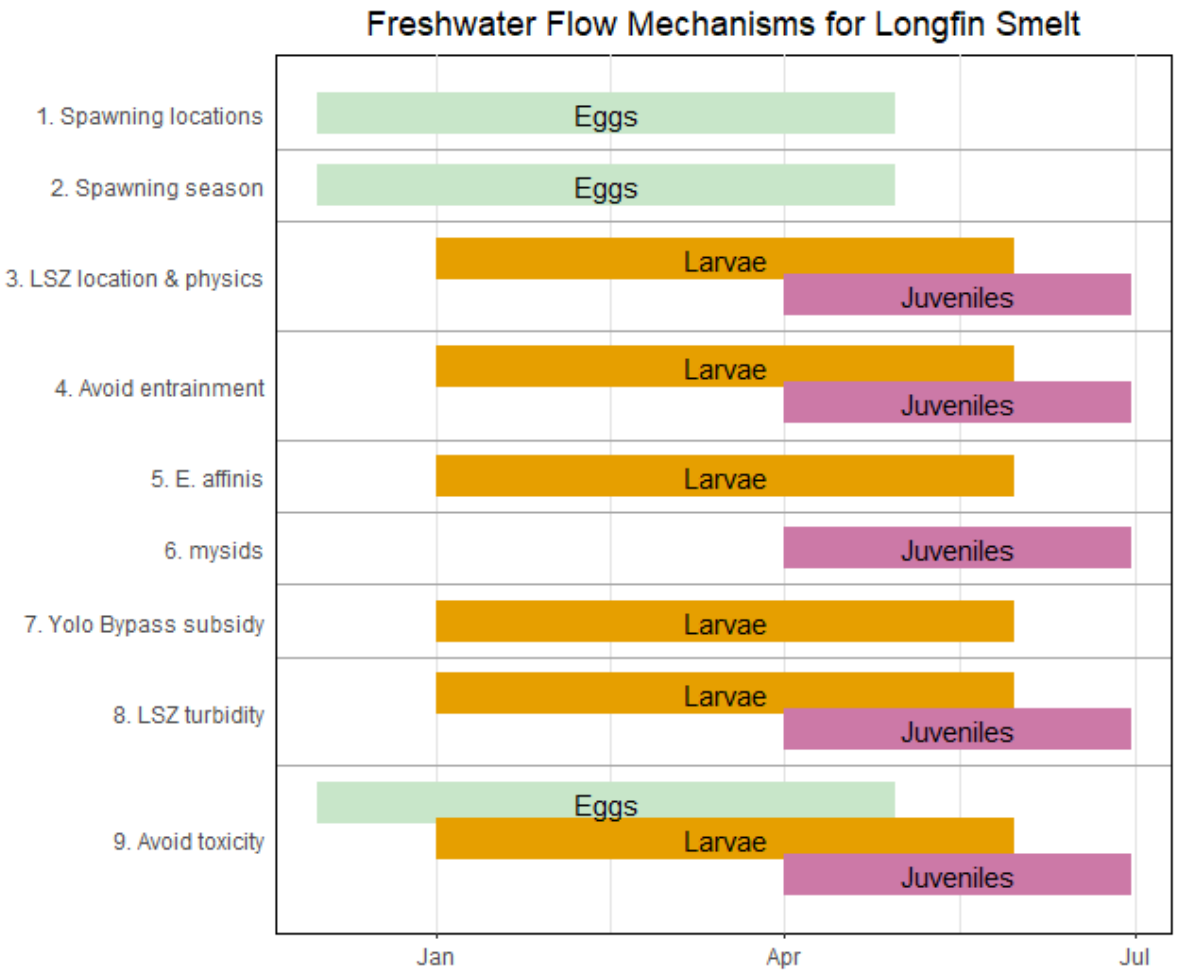

Figure 3.1: Conceptual timeline representing the multiple potential mechanisms by which interannual variation in Delta outflow may mechanistically contribute to recruitment of Age-0 longfin smelt. The life stage durations are approximate in that they start and end on the first and last day of particular months. The reader should recognize that exact stage durations will vary from year to year.

The extended durations of elevated freshwater flow out of the Delta and other estuary tributaries during wetter water years increases the number of beneficial environmental conditions that spawning longfin smelt and their progeny experience. Contrasting this to the pattern in dry years, as X2 and, by extension, the low-salinity zone, moves upstream, longfin smelt migrate farther upstream to reach their spawning habitats (CDFG 2009a, p. 17). Spawning further upstream in the Bay-Delta makes longfin smelt more susceptible to entrainment at the State and Federal water diversions in the south Delta, particularly during late-winter and early spring when larvae are present (Rosenfield 2010, p 13). Studies of hydrodynamics and fish entrainment have found that predicted losses increased with reverse flows in the southern Delta, which are a function of export rates and Delta inflows (Grimaldo *et al.* 2009, p. 1266; Rosenfield 2010, p. 13). In addition, as X2 moves upstream (landward) in the estuary, likely consequences are less spawning habitat available, weakening or absent gravitational circulation (which may have energetic, physiological, and predator avoidance consequences for young longfin smelt) and

decreased water turbidity (which also has survival implications for young longfin smelt based on their role as both predator and prey) (Kimmerer 2002b, p. 1279).

Finally, as the spawning range of the species is significantly concentrated in the west Delta and Suisun Bay during dry years instead of the entire San Francisco Estuary, the Bay-Delta DPS is especially vulnerable to local catastrophic events. For example, if a large oil spill occurred in the Delta during a dry year, the entire spawning class and its progeny could be wiped out. But during wet years where spawning can occur in San Pablo Bay, the South San Francisco Bay, and their tributaries (during exceptionally wet years), a large oil spill in the Delta may not affect spawning occurring in San Pablo Bay and the South San Francisco Bay. Since 1971, large petroleum spills that have demonstrable impacts in the San Francisco Estuary have occurred approximately once every 8 years (CDFW 2021b).

3.1.2. Food limitation

The available information indicates that the Bay-Delta DPS rely on a relatively small number of crustacean meso- and macrozooplankton taxa. Longfin smelt larvae have diets dominated by a copepod, *Eurytemora affinis,* that is common in the low-salinity zone during the spring (CDFW, unpublished data; see Figure 3.2A) indicates that *Limnoithona traspina* are more dominant in January and February larval diets, while other inverts are important at times in the Napa River and San Pablo Bay (Bouley and Kimmerer 2006, p. 221). Like most carnivorous fishes, as longfin smelt larvae increase in body size and mouth gape, they begin taking larger prey that provide more calories per unit of effort expended catching them (i.e., optimal foraging theory). The two most common prey taxa of these larger longfin smelt are epibenthic mysids and amphipods (Burdi 2022, pers. comm.; CDFW unpub Diet Study Data). The copepod *Eurytemora affinis* was also at one time an important prey item for a now much depleted mysid species, *Neomysis mercedis* (Knutson and Orsi 1983, p. 478).

The *Eurytemora affinis* population has been in decline since the 1970s, but beginning in the late 1980s, the zooplankton community started undergoing about a decade of rapid change in species composition, trophic structure, and utility for fish production (Winder and Jassby 2011, pp. 683–685; Kratina *et al.* 2014, p. 1070; Brown *et al.* 2016a, p. 8). As these food web changes were beginning to take place, the production of longfin smelt per unit of outflow or X2 began to decline (Kimmerer 2002a, p. 47; Thomson *et al.* 2010, p. 1442c); coincidental with the invasion of the estuary by the overbite clam (*Potamocorbula amurensis*) (Carlton *et al.* 1990, pp. 81 and Figure 3) and with extended drought in the Central Valley (Rosenfield and Baxter 2007, p. 1589). The filter feeding overbite clam's rapid establishment and growth in the estuary is thought to have diverted resources from the primary food sources of the Bay-Delta longfin smelt (Carlton *et al*. 1990, pp. 90–91; Feyrer *et al*. 2003, pp. 284–286; Rosenfield and Baxter 2007, p. 1589). This decline in the abundance indices was sharp and substantial (generally recognized as a "step decline"). The decline of longfin smelt's historical prey has not been accompanied by a large change in prey use (Feyrer *et al.* 2003, p. 285; Barros *et al.* 2019, p. 15). This suggests that longfin smelt had formed strong predator-prey interactions with their primary prey, a hypothesis supported by empirical data (Mac Nally *et al.* 2010, p. 1426).

As described under Life History, approximately 90% of juvenile and, when they return to the estuary, adult longfin smelt diets are comprised of predominantly mysids and, to a lesser extent, amphipods (Burdi 2022, pers. comm.; CDFW unpub Diet Study Data). *Neomysis mercedis*, which was once a dominant contributor to the low-salinity zone food web, has dropped in numbers by over tenfold and accounted for <4% of total zooplankton biomass after 1994 (Winder and Jassby 2011, p. 684). In addition to lower abundance, CDFW's Zooplankton Study has shown that the average individual sizes of mysids in the San Francisco Estuary have decreased over time (Hennessey 2011, unpublished data), with a species composition shift towards *Hyperacanthomysis longirostris*, an invasive species that reaches maturity at a smaller mass than *Neomysis* (Hennessy 2011, entire). Despite these changes, longfin smelt are one of the few species that continue to rely heavily on *Neomysis* and other mysids as their primary prey (see Figure 3.2B). As longfin smelt exhibit very little variation in prey use, they are considered more susceptible to food web changes than some other fishes (Feyrer *et al.* 2003, p. 281).

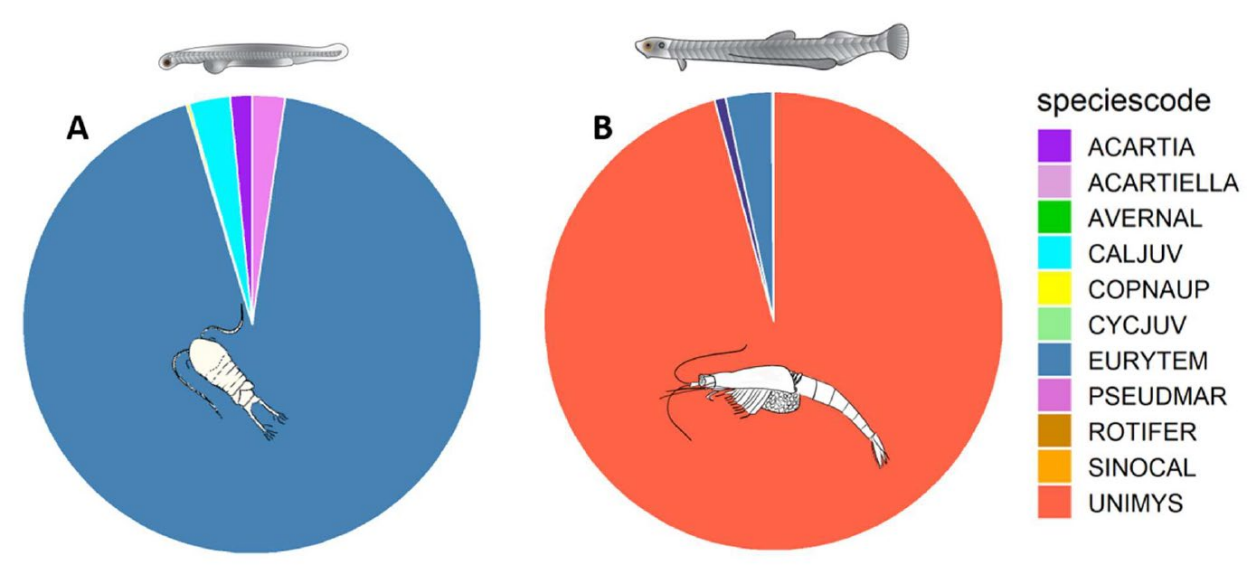

Figure 3.2: Proportion of diet biomass for all longfin smelt broken up between A) larval (<25mm TL) and B) juvenile fish (>25mm TL). Copepod and mysid art by Arthur Barros. Larval and juvenile fish art by Adi Khen. Source: Barros *et al.* 2019, p. 17.

The general decline in diatom phytoplankton and zooplankton is likely affecting juvenile and adult longfin smelt by decreasing food supply for historically important prey species, such as *Neomysis mercedis* (Kimmerer and Orsi 1996, pp. 418–419; Feyrer *et al.* 2003 p. 281). In addition to phytoplankton suppression, laboratory and field experiments have shown that overbite clams feed directly on the nauplii of common calanoid copepods (Kimmerer *et al.* 1994, p. 87), which are the primary prey source for larval longfin smelt.

The Pelagic Organism Decline (POD)

Around 2002–2004, abundance indices for multiple species declined in what was known at the time as the Pelagic Organism Decline or POD. The POD referred to a coincident drop in the FMWT catches of four species (delta smelt, longfin smelt, striped bass, and threadfin shad) (Sommer *et al.* 2007, p. 273), and the event is generally recognized as another step decline. The coincident declines of multiple species suggested a possible common cause, but a mechanism for decline that applied to all four fish was not forthcoming (Mac Nally *et al.* 2010, p. 1426; Thomson *et al.* 2010, pp. 1442–1443). Latour (2016, Fig. 7, p. 244 and p. 245) later hypothesized that changes to fish catchability due to increasing estuary water clarity might be an explanation for the POD.

Fish population dynamics theory is important to interpreting analyses of longfin smelt data from the literature because most of the trend analyses cited above have ignored it. The Bay-Delta DPS has plausibly been declining for over 50 years and that decline is presently at circa 3–4 orders of magnitude below initial observations. The FMWT index is the most commonly used metric of longfin smelt recruitment in the scientific literature. It is generally an index of age-0 fish but the adult longfin smelt population is also declining (Rosenfield and Baxter 2007, Table 3, p. 1585; Nobriga and Rosenfield 2016, Table 2, p. 49, which in turn is limiting how many eggs can be produced. The reason the longfin smelt population keeps appearing to have a 'step decline' or 'change in intercept' of its outflow relationship is at least in part because analyses that do not account for the declining abundances of the parental generations are based on an improper population model that ignores the influence of adult egg supply on how many recruits can be produced (see Figure 3.3).

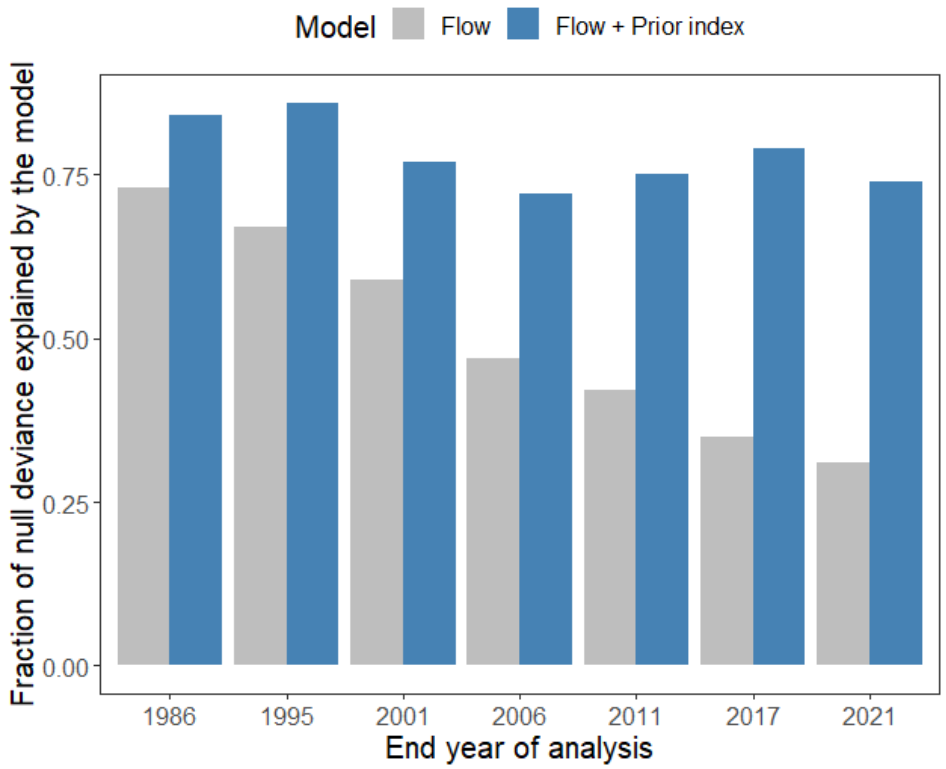

Figure 3.3. Summary of linear regression models predicting the longfin smelt Fall Midwater Trawl (FMWT) indices over time, 1967 through the year listed along the x-axis, i.e., moving from left to right along the x-axis, the length of the data time series is increasing. The gray bars show the fraction of null deviance (akin to an r-squared) explained by generalized linear models of log (Delta outflow) averaged for February-June versus log (FMWT index). The ability of this model to explain trends in the indices has declined substantially over time (see also Tamburello *et al.* 2018). The blue bars depict the explanatory power of models that also include the FMWT index from two years prior as a predictor of the current year index (following Mac Nally *et al*. 2010). This latter model is at least coarsely accounting for the potential of declining adult abundance to limit egg supply which in turn limits how many juveniles can be produced. The predictive capability of this model formulation has not trended downward like the flow-only models have.

3.1.3. Temperature

As described in the Life History and Biology section, longfin smelt are most abundantly detected within a narrow temperature range relative to the range that occurs in the upper estuary. Subadult longfin smelt habitation in the San Francisco Estuary is limited to when water temperatures are below 22°C (Baxter *et al.* 2010, p. 68), and, based on field surveys of ripe and post-spawning females (Wang *et al.* 1986, p. 9; Tempel and Burns 2021, slide 12), successful spawning may require water temperatures below 14°C, while larvae and young juveniles show a preference for temperatures below 12°C and 20°C, respectively, for successful rearing--particularly in food-limiting environments like the San Francisco Estuary, where bioenergetic metabolic demands for caloric intake increase with increasing water temperatures. As the southern-most population, the Bay-Delta DPS likely already experiences the warmest temperatures in the full species range. Water temperature in the Delta commonly exceeds 22°C during the summer (Vroom *et al.* 2017, p. 9904; data from CDEC, CENCOOS, and USGS), and has been predicted to exceed

this threshold for longer periods due to climate change, which would limit habitat occupancy across affected areas, and stress life-stages with limited adaptive motility (i.e., in early spring for young juveniles). It remains unknown to what extent the ocean acts as a thermal refugium for the DPS; however, recent otolith data has shown that adults do exhibit anadromy that had been hypothesized previously by Rosenfield and Baxter (2007, p. 1590). Bay Study Otter trawl age-0 captures in July exhibited mean salinity conditions of 24 ppt, so some juveniles in July (perhaps sooner) can withstand marine salinities (Baxter, 1999, p. 189). Summaries of City of San Francisco outfalls catches also confirm age-0 and age-1 individuals present in the Gulf of Farallones (CDFG, 2009, page 6). The potential effects of climate change are described in detail under the Future Condition chapter.

3.1.4. Loss of suitable spawning habitat

The only fairly well demonstrated aspect of longfin smelt spawning behavior is that the fish appear to find spawning locations in and near the low-salinity zone (Grimaldo *et al*. 2020, Fig. 6, p. 10) and other smaller low salinity habitats in Bay Area tributaries (Lewis *et al*. 2019, p. 3). Just-hatched longfin smelt larvae have been found in pelagic waters and adjacent shoals and wetland areas (Grimaldo *et al*. 2017, p. 1776; Lewis *et al.* 2019, Fig. 2, p. 3). Thus, what other attributes of spawning habitat selection are important to successful reproduction are unknown and would benefit from additional research in support of longfin smelt conservation.

3.1.5. Predation

There is no research from the San Francisco Estuary available from which to develop a complete list of important predators of longfin smelt or to estimate predation rates on longfin smelt to determine how they have trended over time. There have been two recent predator diet studies spatially limited to the legal Delta that tested for prey using DNA extracted from predator stomachs. Michel *et al.* (2018, p. 9) sampled the San Joaquin River between Head of Old River and Stockton, and they did not detect any longfin smelt in any of four species of predators' stomachs. Brandl *et al.* (2021) collected six species of predators from the North Delta. The predator with the most longfin smelt detections was Sacramento pikeminnow (Brandl *et al.* 2021, Table 4). The only other predator from which longfin smelt DNA was detected was striped bass. No longfin smelt DNA was detected from channel catfish, white catfish, largemouth bass or smallmouth bass. Because of this paucity of data, the following discussion is limited to generalities about the role of predators in fish food webs that are broadly applicable and form the basis of major, widely used modeling tools.

The early life stages of fish are often subject to high rates of predation that play important roles in modulating abundance and amplifying the consequences of food limitation (Ahrens *et al.* 2012, Fig. 2, p. 46, and throughout; Pangle *et al.* 2012, pp. 5–6). Thus, changes in vulnerability to predation of eggs, larvae, and small juvenile longfin smelt are a plausible hypothesis for why survival is higher in wetter years than drier years. If predation rates covary with the freshwater flow influence on longfin smelt recruits produced per spawner, they are likely modulated through several other mechanisms like turbidity, temperature, access to zooplankton prey, or outcomes of differences in wet versus dry year hydrodynamics (Fig. 2.8).

Chronic food limitation and predation risk are often tightly linked in fish food webs (Ahrens *et al*. 2012, pp. 47–48). The reason is that prey organisms do their best to limit potential contact with predators.

One effective way to do this is by limiting foraging times, which are often relatively risky because small fishes have to behave in ways that increase their vulnerability to predators when they are actively foraging, e.g., by leaving shelter habitats or simply moving around more actively in surface waters (Ahrens *et al*. 2012, Fig. 1, p. 43). Thus, when food densities decline, prey fishes have two choices. They can either eat less and grow more slowly or they can increase foraging times to compensate for the lower prey densities. Depending on the context of the ecosystem a fish finds itself in, there are pros and cons to either of these choices. How longfin smelt have behaviorally responded to declining prey density has not been studied and would be valuable information from a conservation perspective.

3.1.6. Contaminants

Due to the extensive range of the Bay-Delta DPS, there is potential for exposure to a variety of contaminants. Potential exposure and effects will likely vary based on location and habitat characteristics, which change drastically from fresh to salt water, as well as differing anthropogenic sources (e.g., agricultural practices, industrial and urban wastewater discharge). The Delta is largely an agricultural area with a multitude of tributaries conveying agricultural and urban discharge. The Suisun Bay watershed consists of a mixture of agriculture, managed duck ponds, urbanization, and industry. The San Francisco Bay is encircled by largely urbanized and industrial land uses, with some significant inputs from agriculture in the San Pablo Bay.

Contaminant sources include discharge from municipal wastewater treatment plants, agricultural outfalls, stormwater runoff, and direct application such as for pest control or anti-fouling agents. The types of contaminants can change throughout the year with changes in agricultural use and pest control efforts and storm loading. “Legacy” contaminants in the Bay–Delta, those from historic loading that persist in the environment, such as organochlorine chemicals from past agricultural use and mercury from past mining activity, can bioconcentrate through the food web, posing additional health risks (Connor *et al*. 2007, pp. 87–88; Marvin-DiPasquale and Cox 2007, p. 2). Human population growth has increased the urban footprint over time but there is still a significant presence of agriculture adjacent to Suisun Bay and the Delta. Regulation has reduced the use of some contaminants, only to be replaced by other more potent alternative water-soluble chemicals such as neonicotinoids, which impact non-target species such as aquatic invertebrates and fish (Buzby *et al*. 2020, pp. 15–21). In addition, there are insufficient data to know the full exposure risk of most constituents (Johnson *et al.* 2010, p. viii). Kuivila and Hladik (2008, p. 14) found that of the 163 pesticides being applied, over half were not being monitored.

The Delta and all regions of the Bay have been listed in the 2018 California Integrated Report (Clean Water Act Section 303(d) List and 305(b) Report) as an impaired water for several contaminant compounds (SWRCB June 2018, Appendix A). This list included: elemental contaminants, or ‘metals’ (mercury and selenium), toxic organics (dioxins, furans, polychlorinated biphenyls), and pesticides (chlordane dieldrin, DDT). Additional emerging contaminants of concern include: newer pesticides, flame retardants, nutrients, naturally occurring toxins, micro-plastics (e.g., from synthetic clothing), and pharmaceuticals and personal care products (Klosterhaus *et al*. 2013, pp. 97–98, Table 1; Sutton *et al*. 2017, entire). The U.S. Geological Survey’s (USGS) on-going analysis of water in the Delta suggest that on average 10 new synthetic organic pesticides chemicals are detected every year (CDPR 2020, dataset).

Moschet *et al.* (2017, p. 1558) have indicated the presence of in excess of 50 chemical compounds from a single, 1L, grab sample.

Contaminants can have a variety of direct and indirect impacts on fish and their supporting food web. Direct effects involve impacts to growth, vitality, immunocompetence and disease condition, behavior, reproductive impairment, mutagenicity and direct acute lethality. It is also possible that indirect effects from certain contaminants may manifest via changes in the estuarine community, that consequently impair growth, survival or reproduction of the consumer species.

To date, there are no data documenting the impact of contaminants to longfin smelt in the SFE. Field-based toxicity is difficult to determine, as impacted fish are not recovered in order to be examined (i.e., fish either die from direct exposure and resulting disease, or are eaten). Risk of exposure and effect, as determined by comparison to other species (e.g. delta smelt and inland silverside) potentially include: direct effects on development, growth and reproduction; impacts resulting from impairments to bioenergetic demands, impaired locomotion, reducing feeding success and leading to increased susceptibility to predation, disease, and entrainment (Brander *et al.* 2012, p. 2854; 2016; Connon *et al.* 2009, p. 12; Hasenbein *et al.* 2014, p. 696; Jeffries *et al.* 2015a, p. 17407; Jeffries *et al.* 2015b, p. 55; Cole *et al.* 2016, p. 219; DeCourten and Brander 2017, p. 2). Fong *et al.* (2016, pp. 20-21) suggested that a weight of evidence approach indicates numerous detected contaminants in the Bay-Delta have detrimentally affected the ecosystem, and these authors concluded that contaminants likely played a significant role in the POD.

3.1.7. Entrainment

When water is diverted from the estuary, the opportunity is created for fish to follow the flow of water and become “entrained” by the hydrodynamic footprint of those diversions. There are several sources of entrainment for longfin smelt. These are discussed here in turn.

In-Delta Agricultural Diversions: Water is diverted at numerous sites throughout the Delta for irrigation of crops, particularly during the summer months (Siegfried *et al.* 2014, Figs. 10–11, p. 11) when most longfin smelt are rearing seaward of the legal Delta. Herren and Kawasaki (2001, p. 347) reported over 2,200 such water diversions within the Delta, but CDFG (2009, p. 25) notes that number may be high because Herren and Kawasaki (2001) did not distinguish intake siphons and pumps from discharge pipes. Given the temporal mismatch between seasonal peaks in water diversions to supply farms in the Delta and use of the Delta waterways by longfin smelt, seasonal irrigation of Delta farms does not seem like a major conservation concern for longfin smelt.

Other Diversions: The Barker Slough pumping plant is located in the north Delta and serves as the inlet to the North Bay Aqueduct, which is a municipal diversion that serves Solano County. This diversion is owned and operated by the California Department of Water Resources (DWR) and has positive barrier fish screens that likely limit entrainment of longfin smelt spawned in the vicinity of the diversion.

Downstream in Suisun Marsh, the Roaring River and Morrow Island Distribution Systems (RRDS and MIDS) are additional DWR facilities that divert water from Montezuma and Goodyear sloughs,

respectively. The water is distributed to waterfowl management wetlands in Suisun Marsh and eventually returned to the marsh channels (minus what evaporates). The RRDS is screened while MIDS is not. Both diversions have been observed to entrain or impinge longfin smelt (CDFG 2009b, p. 41). Longfin smelt catches in Suisun Marsh declined earlier in time than they did in other surveys (Rosenfield and Baxter 2007, p. 1589). These authors recommended to evaluate that observation more carefully. The RRDS and MIDS came online in 1979–1980. A key question is whether longfin smelt decline in Suisun Marsh was already underway due to land and water management practices, or might the distribution systems have affected hydrodynamic conditions in the marsh in a way that increased entrainment of longfin smelt or otherwise inhibited their use of the marsh as a spawning habitat?
Entrainment into several power plants may have been an historically important source of longfin smelt mortality (particularly larvae), but these plants have since been decommissioned.

State and Federal Water Export Facilities: The CVP and SWP each include pumping plants in the south Delta. These pumping plants are used to export water to users throughout much of the State. The operation of these facilities can exert a strong influence on regional hydrodynamics (Kimmerer and Nobriga 2008, Fig. 7, p. 12; Hutton *et al.* 2019, Fig. 7, p.11). That hydrodynamic influence can result in the entrainment of fish, sometimes from considerable distances (e.g., Kimmerer 2008, p. 2, Fig. 1, p. 3). In most years, longfin smelt have been collected ("salvaged") in the fish facilities that are in front of each pumping plant. The salvage of fish is an indicator that individuals are being entrained in exported water.

Historically, the salvage of age-1 and older longfin smelt peaked in January (Grimaldo *et al.* 2009, Fig. 5, p. 1262). These fish likely represented individuals searching for spawning habitats and immature individuals comingling with adults. The salvage of age-0 fish peaked in April-May as larvae reached sizes at which they could be retained on the fish screens of the CVP and SWP fish facilities. In all likelihood, however, some larvae began to be entrained once they started hatching in December or January, but remained undetected until about March, with salvage efficiency increasing in April-May as the fish grew larger.

Age-0 longfin smelt salvage has historically been a function of larval abundance and Old and Middle River (OMR) flow (Grimaldo *et al.* 2009, Table 2, p. 1260). This pattern reflects two things: (1) the fish facilities are sampling devices so like other fishing gear, they can catch more fish when there are more to catch, and (2) OMR flow indexes the 'sampling effort' of the fish facilities by reflecting how much and how quickly water is being moved toward the pumping plants. When net OMR flow is positive, San Joaquin River water is generally moving seaward through the Delta. The more net negative OMR is flowing, the more water in the Delta is moving toward the pumping plants, the more of that water has come from the Sacramento River, and the faster that water is moving south.

OMR is a metric that represents a net direction of water flow, meaning that the tidal flow that moves in the positive and negative directions over hourly to spring-neap time scales has been mathematically removed. Nonetheless, the water transport processes OMR represents are instantaneous to tidal time scale variations in gravity flow of water interacting with river and tidal currents via spatial differences in water surface elevation (Andrews *et al*. 2016, equation 5, p. 6).

Longfin smelt can be entrained in exported water when adults and comingling age-1 individuals enter the south Delta, and as larvae and small juveniles that are either rearing or being tidally dispersed

landward of X2 (CDFW 2020, Fig. 13, p. 53). During periods of high Delta outflow adult longfin smelt and their progeny are much less likely to be entrained in exported water because the low salinity zone is not encroaching on the Delta and more individuals may be cued to spawn in Bay Area tributaries if they are likewise flowing high.

It is possible that past entrainment of larval longfin smelt may have reached levels of concern (e.g., 2002 per CDFW 2020, Fig. 10, p. 47; see Figure 3.4). However, since 2009, the entrainment of longfin smelt has not been substantial enough to affect the species population dynamics. The results of two different analytical approaches to the Smelt Larval Survey (SLS) data suggest that it is not likely population-level entrainment of larvae has exceeded 3% since 2009 (Wim Kimmerer, pers. comm.). One analysis coupled particle tracking modeling with the SLS data set and found an upper 95% credible interval of proportional entrainment was 2.9% in the critically dry winter of 2013 and nearly zero in the wet winter of 2017. A second analysis similar in approach to Kimmerer (2008, entire) analyzed all of the SLS data from 2009-2020. Similarly, this approach also found proportional entrainment was unlikely to have exceeded 3% (range = 0.5% to 2.9%). We interpret these findings to indicate that the OMR management strategies in place since 2009 have been an effective conservation strategy for longfin smelt.

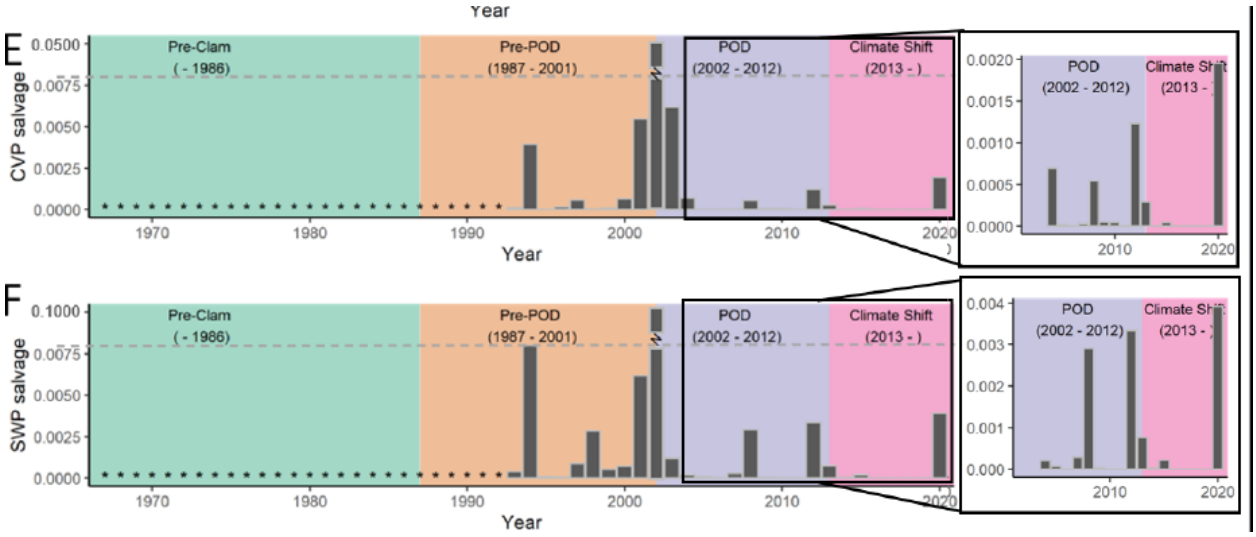

Figure 3.4: Longfin smelt salvage numbers at the SWP and CVP facilities, before and since OMR management by CDFW.

3.2. Current DPS Survey Indices

In the previous section, we detailed the stressors acting on the species. Here we summarize abundance indices showing the DPS' decline over recorded time to its current condition as a result of these stressors. These data begin with simple plots of relative abundance over time, but also include more sophisticated population modeling and viability metrics (summarized herein, and fully documented in a series of technical appendices).

3.2.1 Species relative abundance

Collectively, available survey data indicate a marked, and significant decline for the SF Bay-Delta DPS of longfin smelt throughout the estuary, and across all life stages. To show how the species' status over time to its current condition, we first utilize field survey data from three established surveys--the 20-mm Survey, Bay Study, and FMWT. As described earlier, each of these surveys routinely catches longfin smelt. SLS, although designed for longfin smelt, is not used here as it was designed to assess entrainment risk and not relative abundance, and it has a much shorter survey history (2009-present). Further information about specific surveys: purpose, timing, and geographic coverage are enumerated in Appendix B, following.

The 20-mm Survey (https://wildlife.ca.gov/Conservation/Delta/20mm-Survey) has been conducted since 1995. The CDFW does not produce an index of longfin smelt abundance from the 20-mm Survey, so we adapted the methods for the delta smelt index for longfin smelt. The code and method used to produce the 20-mm index values can be found in Appendix B. As noted in Appendix B, its sampling grid does not include San Pablo Bay, Central San Francisco Bay, or the South San Francisco Bay, and as such the survey underestimates relative abundance in wet years. However, the 20-mm Survey encompasses a significant portion of the distributions of larval and small juvenile longfin smelt, including nearly the entire range during dry years. Since 2000, 16 of 21 years have been classified by DWR as Critical, Dry, or Below-Normal (https://cdec.water.ca.gov/reportapp/javareports?name=WSIHIST). During that period, the trend in longfin smelt catches from the 20-mm Survey has been generally downward (see Figure 3.5).

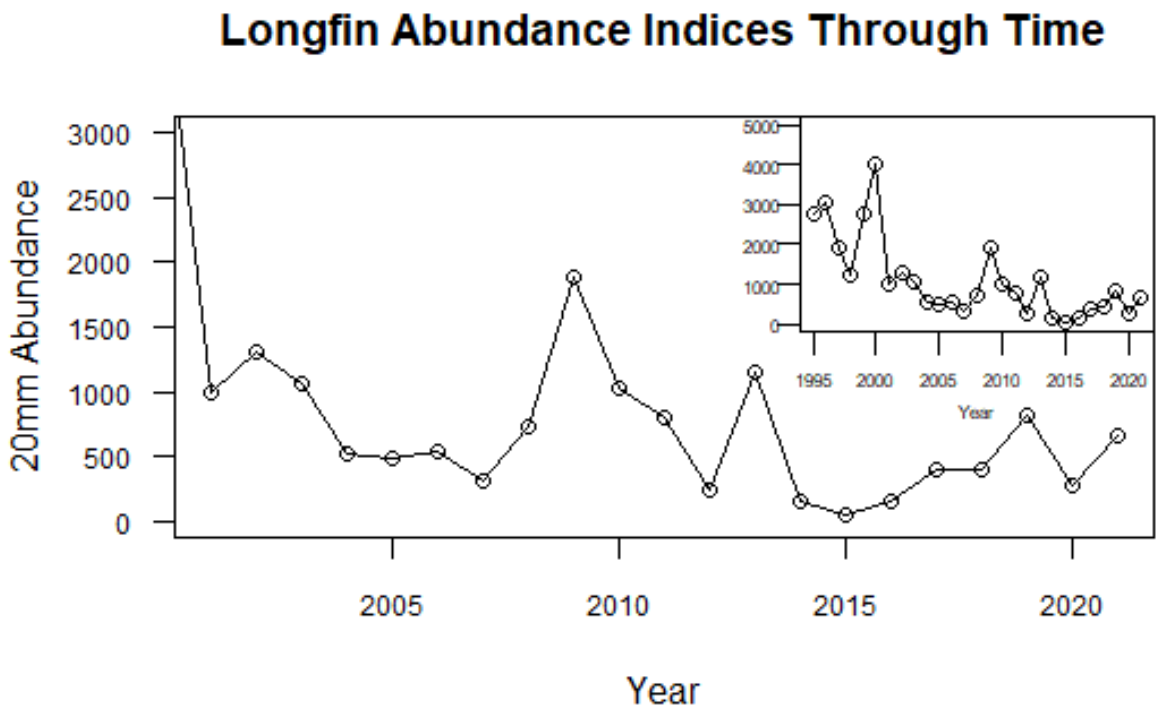

Figure 3.5: Longfin smelt abundance indices from the CDFW 20-mm Survey, 2000–2018 (Inset displays time series since 1995). Source: CDFW 2021a

The FMWT, which captures both juvenile and adult longfin smelt, has the longest history of any survey that is considered effective for the Bay-Delta DPS and has been used to determine the status of the species since the late 1970s (Stevens and Miller 1983, pp. 431–432). Since that time, its peak (unitless) index value recorded was approximately 63,000 in 1982, although the highest ever index value reported was over 80,000 in its first year of completion (1967). The FMWT abundance index for longfin smelt has not exceeded 10,000 since 1983, has not exceeded 1,000 since 2006, fell below 100 for the first time in 2007, and has registered values less than 100 eight more times since then (see Figure 3.6). The 2021 FMWT index for longfin smelt was 323, which was the highest since 2011 (https://www.dfg.ca.gov/delta/data/fmwt/indices.asp).

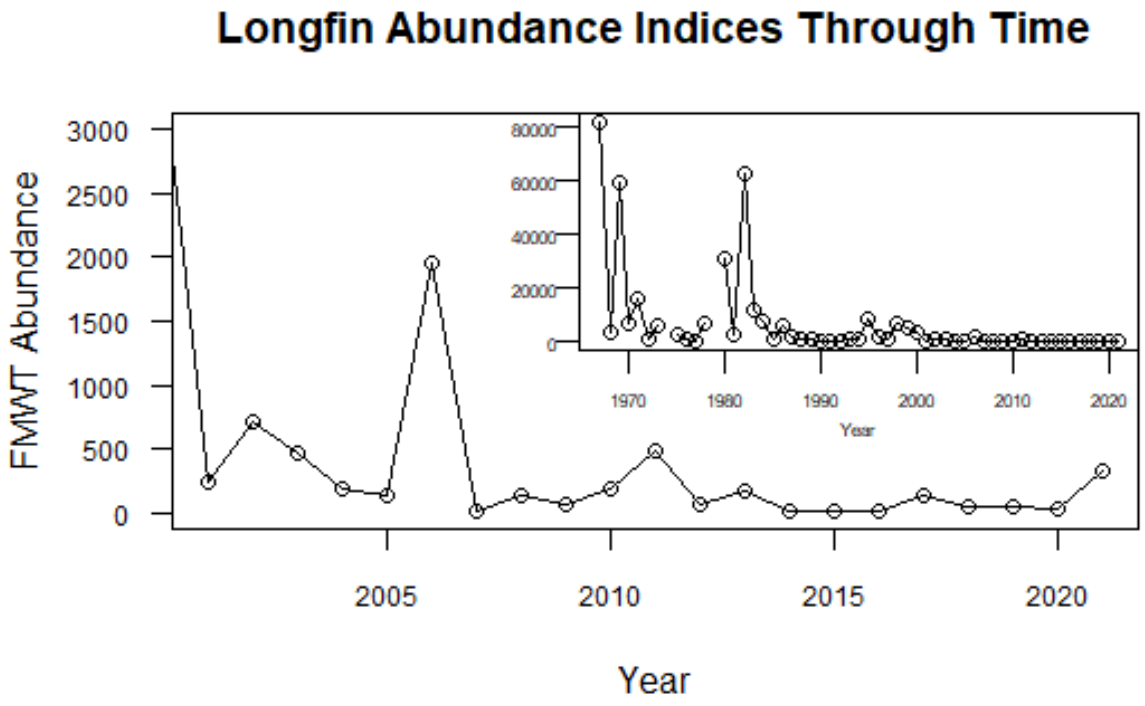

Figure 3.6: Longfin Smelt abundance indices for 2000–2020 from the FMWT (Inset displays time series since 1967). Source: CDFW 2021a

The San Francisco Bay Study (https://wildlife.ca.gov/Conservation/Delta/Bay-Study) samples low-salinity to fully marine waters of the estuary, utilizing both otter (OT) and midwater trawls (MWT); standardized sampling has occurred in most years since 1980. However, sampling was more sporadic in the 1990s and again in several recent years. By deploying two gears, the Bay Study samples near bottom as well as midwater to surface-oriented fishes (Feyrer *et al*. 2015, Fig. 5, p. 3614). Unlike the FMWT, the Bay Study provides separate abundance indices for ages 0, 1, and 2+ longfin smelt. This means there are six Bay Study longfin smelt abundance indices per year; this describes the status of the species at a finer resolution but makes it difficult to summarize the trends concisely. The Bay Study midwater trawl trends are shown in Figure 3.7 and the otter trawl trends in Figure 3.8. The age-0 indices from both surveys suggest abundance peaks occurred in the early 1980s and again in 1995. In most other years, indices for older age classes have been notably lower than age-0 indices. This is expected for the age-1 and age-2+ indices due to the greater cumulative lifetime mortality experienced by the older fish. The Bay Study index values were at or near record lows in 2014 or 2015, which were the last years in the largely continuous time series of Bay Study indices. Reports from 2017 indicated an uptick in age-0 abundance, but still at or near record lows for older age classes.

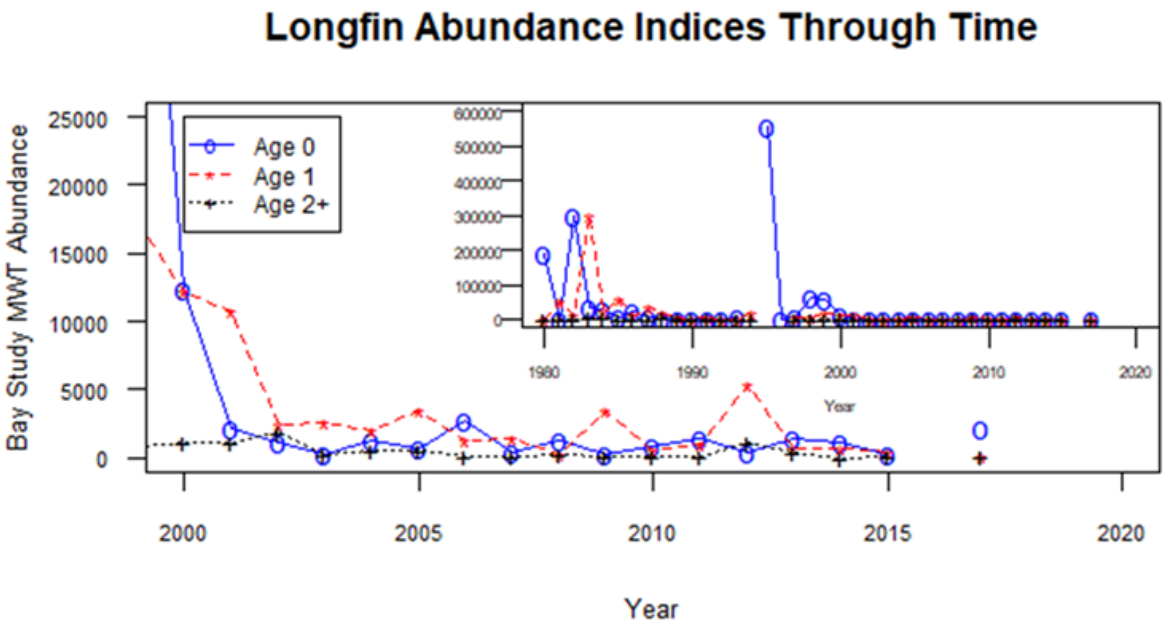

Figure 3.7: Age 0, Age 1, and Age 2+ longfin smelt abundance indices over time from the Bay Study Midwater Trawl, 1999–2017 (Inset displays time series since 1980). Source: CDFW 2021a.

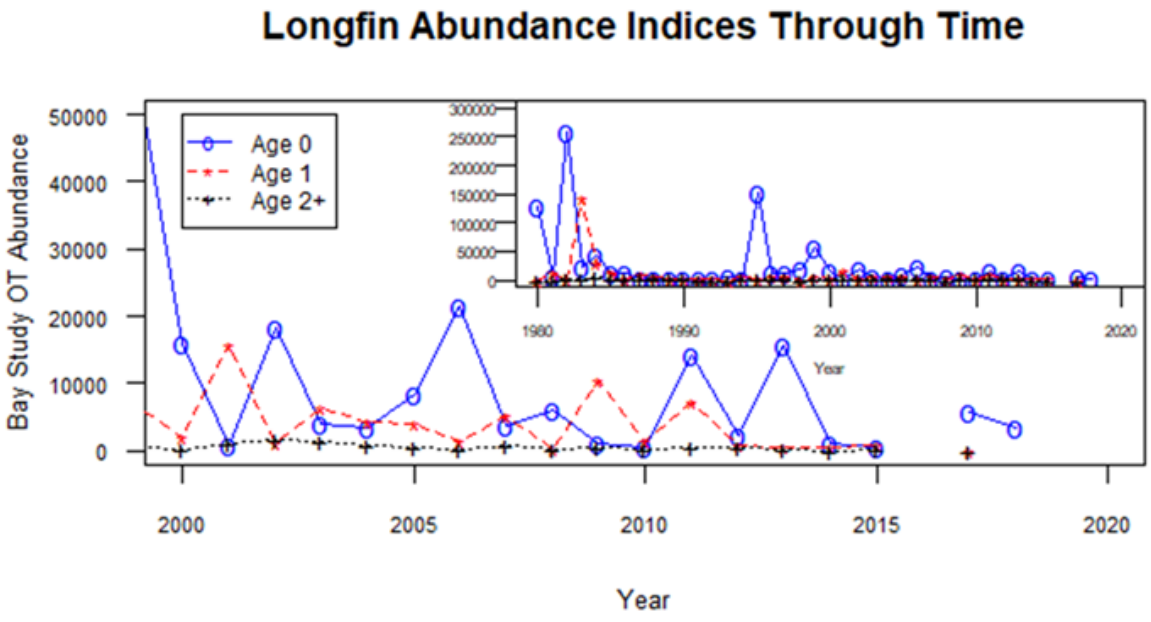

Figure 3.8: Age 0, Age 1, and Age 2+ Longfin Smelt abundance indices over time from the Bay Study Otter Trawl, 1999–2018 (Inset displays time series since 1980). Source: CDFW 2021a

Longfin smelt densities calculated from SLS monitoring data also indicate a decline in abundance. Prior to 2014, larval longfin smelt were generally detected at nearly every SLS sampling station in Suisun Bay,

the confluence of the Sacramento and San Joaquin Rivers, and Northern Delta at densities numbering in the multiple hundreds of individuals per 1,000 m^3 (see Figure 3.9). After 2014, detection frequencies declined and became more variable. Extended dry years compound the negative impacts to longfin smelt as the fish have not shown an ability to quickly recover and reoccupy upstream spawning habitats following drought. Successive years with such unfavorable conditions are likely to continuously suppress longfin smelt abundance which propagates through to the next spawning generation.

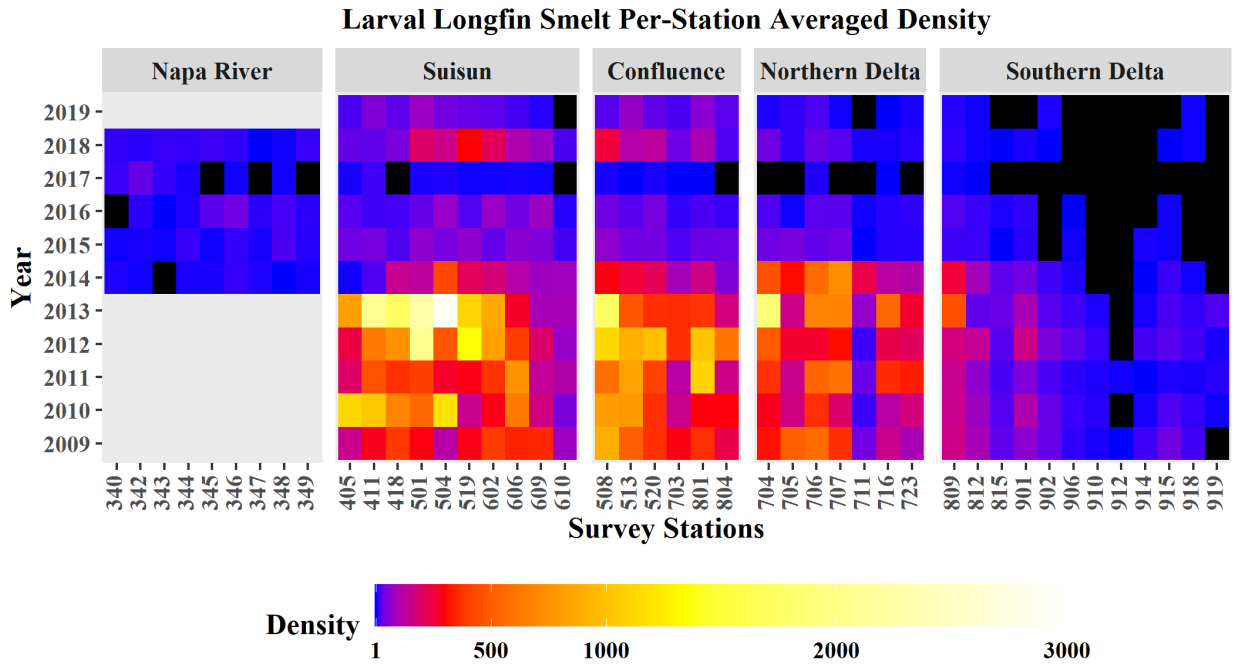

Figure 3.9: Per-station averaged densities for larval longfin smelt across four regions of the Upper Estuary. Densities were averaged at each station for each year of the Smelt Larval Survey. Legend presents average densities per 1,000 m3. Black boxes represent sampling stations that did not detect longfin smelt across all tows for that year. (Eakin 2021, p. 196).

Considering the consistently low abundance indices across all monitoring survey programs and life stages it is apparent that the DPS lacks the ability to recover to the higher abundance numbers seen in the past. All the best available field surveys for documenting long-term abundance trends suggest longfin smelt numbers have substantially declined over time, with current relative abundance reflecting small fractions of the species historical relative abundance. Even considering the small upticks in the most recent survey results, the general trend over time has been lower highs and lower lows in the indices. This supports the conclusion that abundance of all life stages has declined substantially over the course of several decades and that decline has generally continued in recent years. This decline has spanned three to four orders of magnitude in the overall abundance indices over the course of the historical record. In the next section, we summarize these trends numerically as estimates of average annual population growth and consider the consequences of such rates on the long-term viability of the population.

3.2.2. Baseline Scenario and Population Viability Analyses

While descriptive statistics summarizing the historical time series of established (and derived) official relative abundance indices can be informative, they do have limitations (as described herein and in Appendix B) when it comes to inference about population viability, and certainly for ascribing causation relative to potentially important covariates. Therefore, we have performed additional modeling efforts to frame the available information in a context relevant to the purposes of this SSA.

We present a baseline scenario analysis, where we assume that there are no additional changes in the system over time; specifically, this approach assumes that current stressors remain the same and that they have the same magnitude and intensity of impacts on the Bay-Delta DPS into the future. We describe two population viability analyses (PVA; Morris and Doak 2002, Ch. 1 pp. 1–14), which use two different population models to summarize population growth rates and use them to forecast the risk of extinction into the future. These two PVAs, termed count-based and age-structured, use two different model structures: a broad view of the weight of evidence presented by the suite of monitoring surveys and a relatively detailed view of life stage specific vital rates. Details for these modeling approaches are described in Appendix C & Appendix F.

Count-Based PVA

In the first analysis, each abundance index is treated as an independent time series describing the pattern in abundance of longfin smelt. This analysis is done using a count-based PVA framework, which is mathematically and biologically simple as it summarizes the patterns of decline in each of the abundance indices and the impact that has on the probability of quasi-extinction in the future. Quasi-extinction was defined as 1% of the mean of index values since 2008 or lower (≤ 16). Estimates of population growth rates and variability were derived from all available years for each survey. The summaries of the abundance indices and associated count-based PVA represents a quantitative summary of the information that many biologists use to form their intuition about the status of the species.

Values for each of the indices of longfin smelt abundance have decreased substantially over the available time series (Figures 3.5–3.7). Even though this pattern is consistent across each of the indices, it can be difficult to interpret what changes in the indices indicate for population viability because each is constructed differently. When expressed as year over year changes to the indices, we derive estimates of annual population growth rates (lambda) that can be summarized in terms of their central tendency and spread. When population growth rates are less than one, the abundance declines and when population growth rates are greater than one, the abundance grows. Growth rates are multiplicative, so a growth rate of 0.5 indicates that abundance dropped by half, whereas a growth rate of 2 indicates a doubling population.

Mean population growth rates for individual surveys were less than one for most of the abundance index data series, which indicates that population size is declining over time (see Figure 3.10). Only the Bay Study otter trawl index for age-0 longfin smelt produced an estimate greater than one. However, variability was high for all surveys, and confidence limits on each of the estimates included one. This

indicates that even though abundance tends to decline on average, in some years abundance will be stable or increasing.

To summarize the population growth rates from multiple surveys, we performed a meta-analysis on the mean growth rates for each of the surveys. Like most of the individual surveys, the estimated mean population growth value from the meta-analysis was less than one and the error bars included one, but the variability around the mean was much lower. It is noteworthy that for some of the surveys it is not possible to calculate an abundance estimate when zero Longfin Smelt are caught. This has become an issue for some recent years and the inclusion of only index values from years with non-zero catches may bias estimates of mean population growth rates upward.

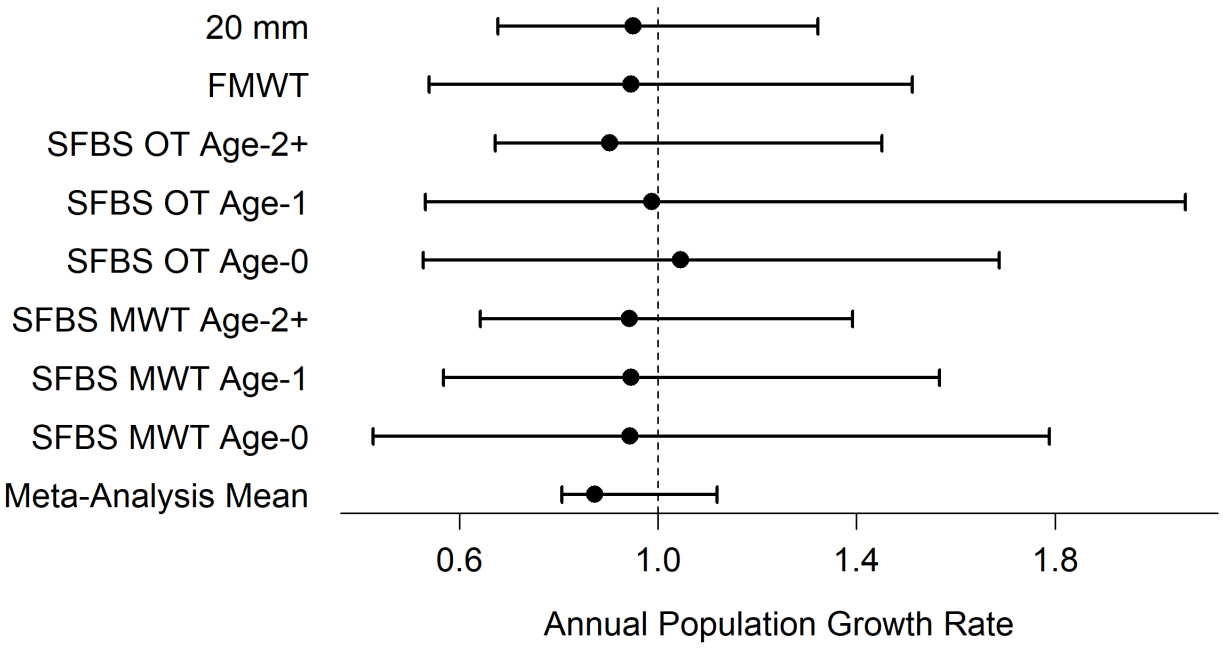

Figure 3.10: Population growth rates (λ) using all available years, based on a count PVA framework, and a mean population growth rate calculated as the mean from a random effects model meta-analysis. Error bars are 95% confidence limits. For individual studies, error bars are derived from the regression method developed by Dennis *et al.* 1991. For the meta-analysis, error bars are derived from the random effects model.

Based on the meta-analysis of mean population growth rates and applying the simplifying assumption that the rate of population growth is constant over time (i.e., applying the historically observed average rate of decline forward through time), we would expect population growth rates to decline an additional 40% over the next 10 years. Confidence limits are 88% decrease to 209% increase, but asymmetry of the confidence limits indicates that decreases are more likely and in fact sampling from the distribution of the estimate we find that abundance decreases more than half of the time (55%). The large variability in

these estimates makes a sustained increase in population size unlikely, as indicated by the probability of quasi-extinction over time. Populations with highly variable growth rates tend to have low viability over time because adding variation tends to make a population grow more slowly over the long term and the population size is more likely to fall below the quasi-extinction threshold than it is for populations with less variable growth rates (Morris and Doak 2002). Without intervention, populations with negative growth rates are expected to go extinct, regardless of the initial population size or the variability in their growth rates. An important question to investigate becomes when extinction is likely to happen because this determines the timeframe for implementing management actions to increase the growth rate.

To illustrate a timeline for extinction risk, we calculated a cumulative distribution function for the time to extinction based on the mean population growth from the meta-analysis, using the mean of the most recent non-missing abundance index values as an initial abundance, and the mean of quasi-extinction thresholds that we calculated for each of the indices. Mean probability of extinction (solid line) and 95% confidence intervals (dashed lines) were calculated using the countCDFxt function from the popbio package (Stubben and Milligan 2007). The starting population size was set to the mean of the most recent non-missing index values (= 1916). Quasi-extinction was defined as 1% of the mean of index values since 2008 or lower (≤ 16). The mean population growth rate exhibits a probability of quasi-extinction exceeding 20% when carried forward for two decades (see Figure 3.11), which was proposed by Lindley *et al*. (2007, Table 1, p. 4) as a criterion ascribing high extinction risk to Central Valley salmonid populations.

The shape of the quasi-extinction curve was influenced by the choice of initial abundance, with lower values producing a steeper slope in the near-term and a higher asymptote in the long-term than was observed for quasi-extinction curves associated with higher initial abundance values. The mean growth rates for each other individual surveys produce similar levels of extinction risk (Appendix C). Predictions for all abundance indices, taken together, show that the probability of quasi-extinction exceeds 20% for all surveys over the next five years and reaches 50% by 2040 (Fig. 3.11). Applying the same assumptions over a longer time horizon (i.e., 2050-2065), the suite of surveys predicts that the probability of extinction for the Bay-Delta DPS under current conditions is roughly 50–80%. Here we present the results of a meta-analysis using values from the official abundance indices associated with various long-term monitoring surveys, but similar results were obtained using annual summaries of catch per tow as an alternative index of abundance for the surveys.

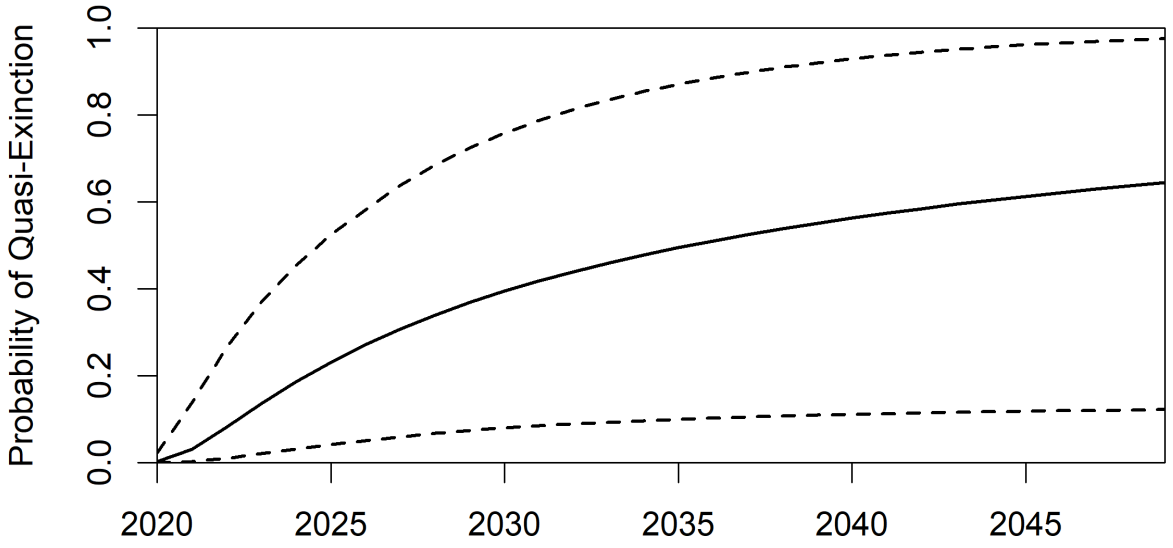

Figure 3.11: Probability of quasi-extinction estimated from a meta-analysis of several surveys that report population indices for Longfin Smelt. Mean probability of extinction (solid line) and 95% confidence intervals (dashed lines) were calculated using the countCDFxt function from the popbio package. The starting population size was set to the mean of the most recent non-missing index values (= 1916). Quasi-extinction was defined as 1% of the mean of index values since 2008 or lower (≤ 16). Estimates of population growth rates and variability were derived from all available years for each survey.

Age-Structured PVA

The second population viability analysis recognizes the need for a model that takes the age structure of the population and density dependence into account. In this analysis, we developed an age-structured state-space population dynamics model and estimated changes in vital rates for the population over time (Appendix F). The population viability analysis that is based on this model explicitly draws on estimates of vital rates (survival and reproduction) that link the age classes. In this model, survival rates from one age class to the next were structured as a proportion, while reproduction rate was structured used the Beverton-Holt equation to represent density dependence. Data on the abundance of the age classes came from Bay Study's abundance indices for both of its sampling gears (midwater trawl and otter trawl). These were incorporated into the model as two observations of each time point.

The age-structured PVA evaluated four age-specific abundance thresholds for quasi-extinction risk: the estimated abundance index associated with the lowest 1st, 5th, 10th, and 15th lower percentiles of the estimated age-specific abundance indices. Specific values associated with each percentile are given in Appendix F, but as a relative index of abundance, the values only have meaning in relation to each other. The population was considered quasi-extinct if the abundance estimate for any age class fell below the specified threshold. Populations. that reach quasi-extinction are considered unable to recover, so if the abundance falls below the quasi-extinction threshold in any year, the population remains "extinct" for all subsequent years in that run of the model.

For each simulation, the initial abundance was drawn from the distribution of estimated age-specific abundance values for 2015, which was the last year of the continuous time series of indices for Bay Study. Vital rates were drawn from the distribution of parameters for all years in the data set (1980–2015). As such, the full historical dataset informed the simulations of future abundance, and the analysis assumes that the future will follow patterns similar to the past. The simulation was run 1000 times and the probability of quasi-extinction is the proportion of times the population reached quasi-extinction at or before the year specified.

The probability of quasi-extinction was sensitive to the choice of quasi-extinction threshold and, as we might expect, setting higher thresholds results in higher probabilities that the population will become extinct (see Figure 3.12). Even with this variability, the model results show a substantial risk of extinction even at low threshold values. For example, using the 10 percent quantile of abundance estimates as the threshold, approximately 60% of simulations reached extinction by 2050. Both the 5 and 10 percent quantile line also meet Lindley *et al*.'s (2007, Table 1, p. 4) criteria for high risk of extinction (20% probability over two decades). The most conservative threshold (1 percent quantile) shown in Fig. 3.12 meets Lindley et al.'s criteria for moderate risk of extinction (>5% over 100 years).

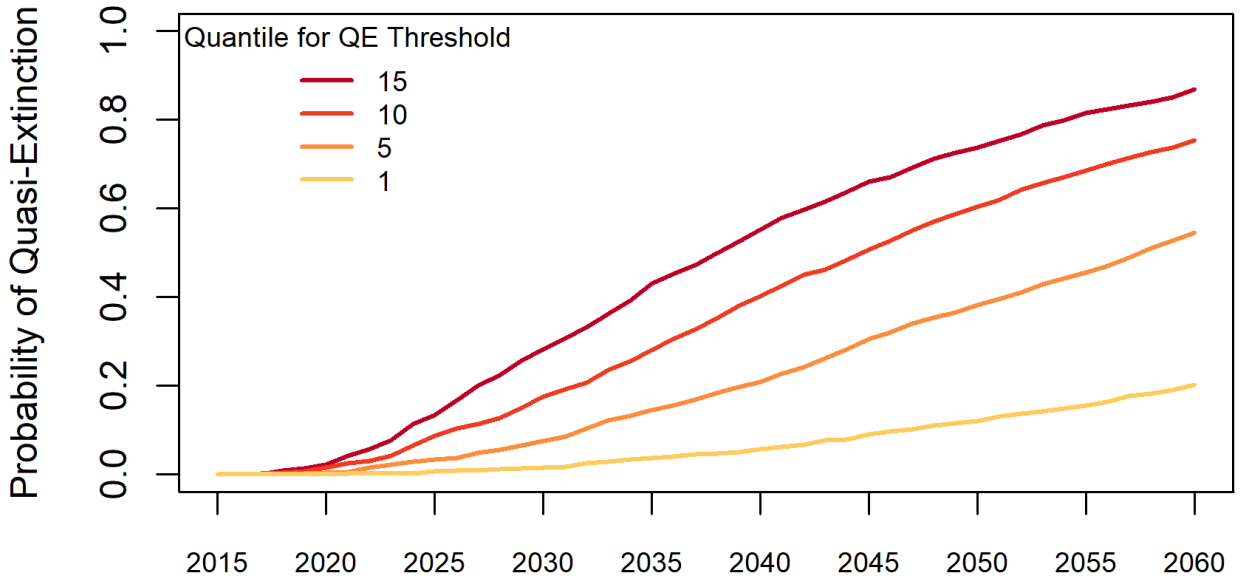

Figure 3.12: Estimated probability of quasi-extinction for four sets of age-specific abundance values, based on the percentiles at the lower end of the distributions of relative abundance estimates. Specific values associated with each percentile are given in Appendix F.

3.3. Summary of the 3 R's

Here, we conclude the current ecological viability by summarizing the species response to these stressors with an assessment of the 3 R's as they apply to the Bay-Delta DPS.

3.3.1. Redundancy

The San Francisco Bay-Delta DPS is a single, genetically-indistinguishable population with basically unidirectional gene flow to northern populations (I.e., a 'source' population), as evidenced by genetic data (Saglam *et al*. 2021, p. 1797). Age structure of the population (more than one age class extant in the system) may yield some buffer against a year with a catastrophic event. However, it is not presently known how many spawning age-classes in any given generation of the Bay-Delta DPS exist. The spawners may: 1) be all or nearly all age-2 or, 2) include meaningful numbers of age-1 and, 3) possibly even age-3 fish. If there is only one spawner age-class in each generation as is the case in Lake Washington, the Bay-Delta DPS has less inherent resilience to poor conditions than if there are multiple spawning age classes. This is one of the most important uncertainties that limits our ability to model the DPS' population dynamics and by extension, evaluate the three Rs. Nonetheless, it is apparent in the trend data that sequential dry years and droughts have strongly contributed to population decline. Inhabiting a hydrologically-connected estuarine system, with a capability of facultative anadromy, the fate of the DPS is reliant upon the ecological condition of the San Francisco Bay-Delta and, to an extent, the DPS' ability to exploit the nearshore Pacific Ocean niche.

3.3.2. Representation

We assess the species representation (adaptive capacity) within the Bay-Delta based on the observed phenotypic plasticity in its life history (to the extent we can infer it from available data) and the current and future conditions within the system that may afford some capacity for behavioral adaptations that enhance growth, survival and reproduction. To the extent that lifestages can tolerate higher salinities (a capacity that increases over developmental time), the species does possess adaptive capability to move seaward, thus seeking cooler thermal refugia and opportunities to sustain its survival, growth, and development until their return to the Delta for spawning. However, like our rationale above, as evidenced by the species relative abundance and the trends observed over time, even with plasticity in its life history, the species has not been able to withstand the cumulative changes to the Bay-Delta ecosystem and has fared poorly amidst the suite of stressors acting upon it. In short, recent and current conditions in the SFE have constrained adaptive options, impaired fitness, and reduced survival. Therefore, we do not anticipate that either genetic or environmental diversity confers sufficient adaptive capacity to the Bay-Delta DPS to overcome the detrimental environmental changes (especially into the anticipated future—see Future Condition chapter, following).

3.3.3. Resilience

Given the biology, life history, and interconnectedness of the San Francisco Estuary that the Bay-Delta DPS inhabits, its lack of population redundancy, and our estimate that it possesses limited inherent adaptive capacity (low representation) within these ecological constraints, the factor most contributing to the Bay-Delta DPS' extinction risk centers on its population resilience (I.e., the interaction of extant stressors on the current standing population). The key stressors impacting the Bay-Delta DPS are inadequate frequency and magnitude of favorable freshwater flow conditions for survival, growth, and reproduction; limited food supplies; and small population size. It is acknowledged that these factors are all ecologically interrelated.

Reduced freshwater flow

The biggest stressor impairing production of longfin smelt is decades of accumulating impairment of freshwater flow caused by the development and redistribution of water supplies in California. Freshwater flow to the estuary, especially as Delta outflow, is the most important species need. This DPS has a long-standing relationship with Delta outflow. With the exception of 2021, abundance indices during Critical, Dry, and Below-normal year types were never higher than the preceding abundance index of the immediately preceding Wet or Above-normal year type. Further, no FMWT index for longfin smelt has ever surpassed the initial 1967 index and in the overbite clam era (1987-present), only one index (1995) has even gotten within ten percent of the 1967 index. Thus, the decline of the Bay-Delta DPS, which is now in its sixth (observed) decade, has led to very low abundance indices.

Loss of food

The invasion of the overbite clam was a catastrophic event as it had an immediate and permanent impact on the pelagic food web in the San Francisco Estuary. The overbite clam both reduces the base primary producers of longfin smelt's food web and competes directly with larval longfin smelt by consuming some of the same prey. The suspected role of food limitation is a lower carrying capacity for longfin smelt, even in wet years. This stronger limit on juvenile fish production has interacted with insufficient frequency of wet years to contribute to persistent species decline. An apparent lack of trophic adaptability provides longfin smelt with little representation to withstand accumulating changes to the food web. This is further evidenced with the species inability to recover from the catastrophic overbite clam invasion.

Small population size

Though not a stressor in itself, small populations are more vulnerable to demographic, stochastic, and allele effects (Foden and Young 2016, p. 40). Based on field survey indices, the abundance of the Bay-Delta DPS has been at, or near, record lows for the past decade. The current small population size thus lowers the species resilience, and limits opportunities for higher recruitment during favorable years. Small populations also have reduced capacity to adapt to environmental changes (representation) due to limited genetic variation (Willi *et al.* 2006, p. 440). Mechanisms for this include: lower fitness owing to

environmental stress (Willi *et al*. 2006, p. 447), inbreeding depression, genetic load, or nongenetic allele effects (Reed 2005, p. 556). However, we lack the information needed to quantitatively assess whether the small population size of the Bay-Delta DPS affects the species representation.

Other Potential (and/or Historical) Stressors

Temperature: Laboratory studies have suggested that longfin smelt are more physiologically sensitive to elevated water temperature than the delta smelt (Jeffries et al. 2016, p. 1714). The 20°C threshold suggested for juvenile longfin smelt is commonly exceeded over large areas of the estuary, particularly the Delta and the lower Sacramento and San Joaquin rivers during the summer months (Vroom et al. 2017, p. 9904; data from CDEC, CENCOOS, and USGS), possibly coaxing the fish to seek cooler oceanic waters. Currently, longfin smelt are able to use facultative anadromy, albeit with a strongly declining population trend in the Bay-Delta—suggesting this strategy may be insufficient to mitigate temperature stress. The Bay-Delta DPS' ability to continue to survive in the Bay-Delta given anticipated warming is discussed in the Future Condition chapter, below.

Entrainment: The best currently available information suggests that if OMR management comparable to what has occurred since 2009 continues, the entrainment of longfin smelt will not have a strong influence on the viability of the Bay-Delta DPS.

Loss of Tidal Marshes: It is unknown how important historical tidal marshes were to longfin smelt, but they currently use a mixture of tidal marsh and open-water habitats. Tidal wetlands and marshes in the San Francisco Estuary were largely converted to other uses by about 1920 and have recently begun to be restored. The loss of tidal marsh habitats may have hampered species productivity, but to date, there are no indications that restoration has been sufficient to stem the decline. Therefore, we cannot conclude whether or not the species has lost resilience due to landscape changes that occurred in the 19th and 20th centuries. The quantitative contributions of restored estuarine marshes to larval growth and rearing remains a potentially important science question in support of longfin smelt conservation.

In Table 3.1, following, we summarize how current drivers are understood to be impacting the Bay-Delta DPS under our evaluation within this SSA.

Table 3.1: Summary of Threats under Current Condition for the San Francisco Bay Delta DPS Longfin Smelt

Stressor/Threat	Life Stage(s)	Mechanism	Magnitude of Threat
Reduced freshwater flow	Larvae and juveniles	Productivity reduction leading to recruitment loss	High Risk
Loss of food	All	Productivity reduction due to food web collapse and increased competition	High Risk
Small Population Size	All	Reduced stock for reproduction, greater vulnerability to stochastic events, Allee effects	High Risk
Temperature Stress (Habitat Constriction)	Adults and late juveniles	Physiological stress: Escape to cooler environments as adults is an option	Constraining?
Increasing temperature	Larvae and younger juveniles	Lethal mortality to early lifestages: Unable to avoid as larvae	Likely Constraining
Predation	Larvae/ juveniles	Higher vulnerability to predation at early life stages	Uncertain
Entrainment	Larval and younger juveniles	Entrainment to the South Delta export facilities and other diversions	No longer considered a substantial stressor with current State protections
Contaminants	All	Direct mortality through reduced fitness or indirect through food web	Uncertain
Tidal habitat loss	Larvae and juveniles	Reduced rearing area lowering growth and recruitment	Uncertain

In summary, the Bay-Delta DPS of longfin smelt is not resilient; more than five decades of declining abundance indices have documented an inability of this fish to sustain itself in the contemporary estuary. The Bay-Delta DPS also has extremely limited redundancy, since it effectively represents a single population inhabiting the San Francisco Bay-Delta and nearshore ocean environment. The representation of the Bay-Delta DPS is thought to be limited as well, reflecting that same declining abundance trend and no discernable and quantifiable compensatory adaptation to historical ecological conditions. Based on our evaluation of the 3 Rs, we conclude the San Francisco Bay-Delta DPS of the longfin smelt is highly vulnerable in its current condition.

Chapter 4 – Future Condition

In the previous chapter, we evaluated the current condition of longfin smelt and described how several stressors have affected the DPS and its habitat. In this chapter we provide information related to the stressors most likely to act on the longfin smelt and its habitat in the future and how those stressors may influence the future condition of the Bay-Delta DPS. It is unlikely that the conditions for the baseline scenario in the count-based PVA presented in Chapter 3 will indefinitely persist owing to known and potential changes anticipated in the future. In order to provide some insight into the future conditions for a particular species, we construct plausible scenarios to assist in articulating how the species needs, threats, and habitat conditions may change in the future.

In the Current Condition chapter, we presented a baseline scenario, where no changes are experienced in the system. In our approach to the species future condition, we present future scenarios of changes in the San Francisco Estuary. We then assess how the species has responded in the past and use that information to help predict the species' response in the future—the most plausible outcomes we can capture in our scenario planning. We finally close with a summary discussion projecting the future ecological scenario the Bay-Delta DPS will most likely face and discussing how that might be anticipated to either increase, decrease, or leave unchanged the risk profile for specific life stages of the Bay-Delta DPS.

4.1. Scenario Planning and its Application

Scenario planning is a comprehensive exercise that involves the development of scenarios to capture a range of plausible future conditions. That development is then followed by an assessment of the potential effects of those scenarios on a given species. Scenarios are not predictions or forecasts of what *will* happen in the future for a species but are projections or explorations into the range of conditions that may exist based on current information (see Figure 4.1). The scenarios are intended to provide the "upper" and "lower" bounds of plausible conditions (see Figure 4.2), outline uncertainties, and provide decision makers with a means for managing risk and maintaining flexibility in current and future decisions.

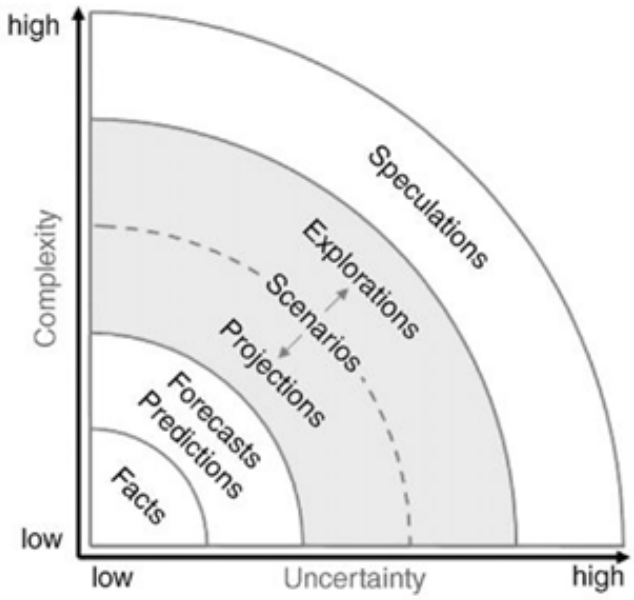

Figure 4.1. The levels of uncertainty and complexity in situations for which scenarios can be useful in considering future possibilities (adapted from Rowland *et al*. 2014). Gray areas represent speculative reasoning that have a higher attendant uncertainty associated with the scenario planning, as these are based upon forecasting that includes its own attendant uncertainty, as well as conceptual risk assessment founded on admittedly imperfect mechanistic understanding of causation (or multifactorial processes and emergent processes that are even more difficult to predict).

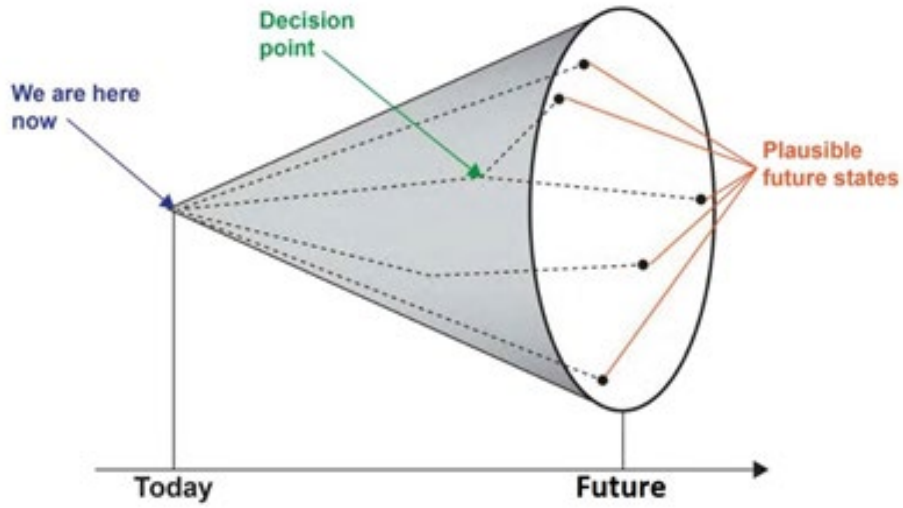

Figure 4.2. Conceptual diagram of the broadening range of plausible alternative futures as one moves farther away from the present and different events and decision points shift trajectories. (Rowland *et al*. 2014 (p. 6) adapted from Timpe and Scheepers 2003, entire). This conical projection is a visual presentation of the SFB DPS longfin smelt "risk profile" we attempted to capture in this chapter of the SSA.

A range of time frames with multiple possible scenarios allows us to create a "risk profile" for the longfin smelt Bay-Delta DPS and its viability into the future. While we do not expect every condition for each scenario to be fully realized, we are using these scenarios as examples of the range of possibility. For each scenario, we describe the stressors that are reasonably anticipated to occur for the DPS and how they may change in the future. We used the best available science to predict trends in future threats facing the Bay-Delta DPS. Data availability varies across the range of the DPS. Where data on future threats or trends were not available, we looked to past threats and their trends, and evaluate if it is reasonable to assume these trends will continue into future and to what degree.

To assess the future viability of the longfin smelt Bay-Delta DPS, we used published information related to the varying conditions of the San Francisco Estuary, including future climate change information and projected increases in water demand, and how these changes may impact how well the estuary can support longfin smelt in the future.

For this SSA, the foreseeable future was assessed out through the year 2050. This period represents our best understanding of the projected future conditions related to climate change and water demands based on anticipated population and agricultural growth. However, we also provide scenarios and data projections through 2100, as they are scientifically available and published, and each of our climate change assessment sections may have its own respective suitable foreseeable future timeframe. As described under the stressors in the Current Condition chapter, reduced freshwater flow, temperature, and invasive species as a source of food limitation have had the largest impact on the DPS, so here we specifically analyze how these threats may change in the foreseeable future.

4.2. Introduction to climate change

Our analysis includes consideration of ongoing and projected changes in climate. The terms "climate" and "climate change" are defined by the Intergovernmental Panel on Climate Change (IPCC). The term "climate" refers to the mean (average) and variability of different types of weather conditions over time, with 30 years being a typical period for such measurements (IPCC 2013a, p. 1450). The term "climate change" thus refers to a change in the mean or variability of one or more measures of climate (for example, temperature or precipitation) that persists for an extended period (IPCC 2013a, p. 1450).

Measurements spanning several decades demonstrate that changes in climate are occurring, and that the rate of change has increased since the 1950s. Examples include warming of the global climate system, substantial increases in precipitation in some regions of the world and decreases in other regions (for these and other examples, see: Solomon et al. 2007, pp. 35–54, 82–85; IPCC 2013b, pp. 3–29; IPCC 2014, pp. 1–32). Specific to the SFE, Bashevkin et al. (2021, p. 2) found a temperature increase averaging 0.017°C per annum, over the last 50 years, with increases most widespread in the late-fall through winter (November to February) and spring (April to June) with warming fastest in the northern regions of the Delta. Climate change models predict increased extremes in winter precipitation frequency and intensity, but these models do not agree on whether the overall impact of these extremes will result in an increase or decrease in annual precipitation (Polade et al. 2017, p. 7).

Scientists use a variety of climate models, which include consideration of natural processes and variability, as well as various scenarios of potential levels and timing of greenhouse gas (GHG) emissions, to evaluate the causes of changes already observed, and to project future changes in temperature and other climate conditions (Meehl *et al*. 2007, entire; Ganguly *et al*. 2009, pp. 11555, 15558; Prinn *et al*. 2011, pp. 527, 529). All combinations of models and emissions scenarios yield similar projections of increases in average global surface temperature (commonly known as global warming), until about 2100 (Wulff *et al.* 2021, entire). Although projections of the magnitude and rate of warming differ after about 2030, the overall trajectory of all the projections is one of increasing global warming through the end of this century. Thus, there is strong scientific support for projections that warming will continue through the 21st century, and that the magnitude and rate of change will be influenced substantially by the extent of GHG emissions (Meehl *et al*. 2007, pp. 760–764, 797–811; Ganguly *et al*. 2009, pp. 15555–15558; Prinn *et al*. 2011, pp. 527, 529; IPCC 2013b, pp. 19–23). See IPCC 2013b (entire), for a summary of other global projections of climate-related changes, such as frequency of heat waves and changes in precipitation.

Global climate projections are informative, and we present the best scientific information available at the time of our analysis. Projected changes in climate and related impacts can vary across and within different regions of the world (IPCC 2013b, pp. 15–16). Therefore, we used "downscaled" projections when they were available and have been developed through appropriate scientific procedures. Downscaled projections provide higher resolution information that is more relevant to the spatial scales used for analyses of a given species (see Glick *et al*. 2011, pp. 58–61, for a discussion of downscaling).

In our climate change analyses, two plausible future scenarios were considered. We selected representative concentration pathways (RCP) 4.5 and 8.5 as the bookends for our analysis. RCPs 4.5 and 8.5 correspond to radiative forcing values in 2100 of 4.5 and 8.5 watts/m^2, which represent scenarios with an effort at abating global GHGs and a business-as-usual scenario, respectively (see van Vuuren *et al.* 2011, pp. 8–10 for RCP model development). Descriptions on how these scenarios were developed and chosen are provided in each of our climate change subsections, and the anticipated effects of each scenario on the risk profile for the longfin smelt DPS are also summarized in each analysis. We used our expert judgment and appropriate analytical approaches to weigh relevant information, including uncertainty, in our consideration of the best scientific information available regarding various aspects of climate change and their most likely impacts on longfin smelt.

4.2.1. San Francisco Bay-Delta Climate Change

There are three climate change drivers that are likely to affect the future condition of the Bay-Delta DPS; warming air temperature, changing precipitation patterns, and sea level rise (see Figure 4.3). Where trends can be reasonably predicted, these drivers of change are expected to have mostly negative impacts on the DPS, both individually and as interactive forces or incentives on the spatial and temporal distribution of longfin smelt and their life history transitions.

Driver	Linkage	Outcome
Warming air temperature	Warmer Bay-Delta water temperature in the fall-winter	• Later Estuary re-entry (?)
	Warmer Bay-Delta water temperature in the spring-early summer	• Compresses spawning season (-) • Compressed estuary rearing (-)
	Less precipitation falling as snow	• Higher winter flow (+) • Lower spring flow (-)
Changing precipitation patterns	More frequent dry years	• Fewer years of strong recruitment (-)
Sea level rise	Higher salinity per unit of freshwater input	• Landward encroachment of the LSZ (-)
	Changes to terrestrial-aquatic ecotones	• Unpredicted habitat changes (?)

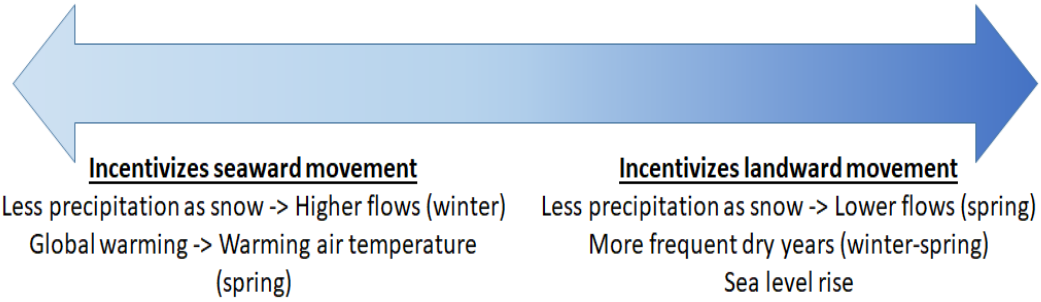

Figure 4.3. Summary of climate change drivers that are affecting and will continue to affect the San Francisco Estuary, the linkages between these drivers and mechanisms affecting longfin smelt, and the anticipated population-dynamic consequences. The direction of impact is shown in parentheses in the outcomes column: (+) = positive effect, (-) = negative effect, and (?) = uncertain direction of effect. The color graded arrow at the bottom depicts interactions among driver-linkages showing how they are expected to interact to create contrasting incentives for where in the estuary longfin smelt will attempt to spawn as adults and where the resulting progeny will rear.

There is greater certainty that sea level will rise leading to greater average saltwater intrusion into the estuary and Delta. The National Academy of Sciences (NAS) projected that sea levels along the California coast south of Cape Mendocino will rise 4–30 cm (2–12 in) by 2030, 12–61 cm (5–24 in) by 2050, and 42–167 cm (16–66 in) by 2100 (NAS 2012, p. 131) compared to year 2000 sea levels. Research indicates that the coastal land area south of Cape Mendocino is sinking at an average rate of about 1 mm (.04 in) per year, although Global Positioning System (GPS)-measured rates vary widely (-3.7–0.6 mm per year) (NAS 2012, p. 93). The NAS committee used output from global ocean models under an IPCC (2007) mid-range greenhouse gas emission scenario (NAS 2012, p. 5). However, carbon dioxide emissions from fossil fuels for the past decade have been at the high end of IPCC scenarios owing to rapid economic growth in developing countries (Le Quéré *et al.* 2009, pp. 831–832).

Climate change could affect longfin smelt due to increases in water temperature. Using projected air temperature global climate models (GCMs), Brown *et al.* 2016b (pp. 5–6) created water temperature projection models spanning 20 areas in Suisun Bay and the Delta through 2100. Although these temperature projections were applied to delta smelt, the spawning window metric included an upper temperature limit of 20°C which is an approximate upper thermal limit for rearing post-larval and juvenile longfin smelt (Jeffries *et al.* 2016, p. 1712). Brown *et al.* (2016b, Fig. 4, p. 13) predicted the delta smelt spawning window would shift earlier in the year. The predictions had substantial spatial and temporal variability, but the general conclusion is that climate warming will affect the estuary faster in the spring as the century progresses. This will increase bioenergetic stress on young longfin smelt and may force them seaward earlier in the year where water temperatures will be cooler. Their capacity to adapt to these changes at the time scale they are projected to occur was questioned by Jeffries *et al.* (2016, p. 1714).

In addition, the spawning window for longfin smelt is earlier than that of delta smelt; longfin smelt typically spawn at temperatures between 7 and 14°C (Wang 2007, p. 38). Thus, their spawning window will likely be shortened as well, resulting in a smaller average annual number of days available for spawning. Laboratory tests have shown that embryotic and larval development is more successful at 9 and 12° C than at higher temperature; temperatures of just 15° C were detrimental for embryo hatching success and larval survival (Yanagitsuru *et al.* 2021, pp. 5–7). Thus, even marginal increases in water temperature could shorten the spawning season and reduce survival of early life stages.

In the following section we provide an in-depth analysis of how climate change may affect the San Francisco Estuary over time, and how the projected changes could in turn impact longfin smelt. We use published datasets that project water temperature increases, shifts in the hydrograph, changes in the frequencies of water year types, and sea level rise specific to the San Francisco Estuary. We then hypothesize how longfin smelt may respond to these projected changes based on the scenario planning exercise.

4.2.2. Temperature trend future condition analysis

To estimate the effect of global warming as it pertains to the effects of rising temperatures on longfin smelt, we use a spatial and temporal approach in Suisun Bay and the Delta, which as described in the species Life History section, are important spawning and rearing habitats for longfin smelt, particularly in low outflow years. Water temperature change projections for San Francisco Bay were not available at time of this writing, so our analysis excludes San Francisco Bay and its tributaries. The embryonic through early juvenile life stages are when longfin smelt are believed to be most vulnerable to warming temperatures because these early life stages do not possess the ability to migrate to the cooler waters of central San Francisco Bay and the coastal ocean.

USGS (Wulff *et al.* 2021, entire) produced regionally downscaled climate change model outputs to forecast water temperatures at fixed locations in the upper San Francisco Estuary, specifically the Sacramento-San Joaquin Delta and Suisun Bay. The downscaled average daily air temperatures from the

climate change scenarios were sub-sampled for the Delta region, and then averaged to produce Delta daily average air temperature for 2010 through 2100. We relate these projected water temperatures to multiple thermal physiological and behavioral thresholds of longfin smelt across life stages to assess future thermal habitat, spawning, and rearing suitability. Our approach is similar to that of Brown *et al.* 2016b (p. 5) for delta smelt, except we reflect how the temperature changes may affect the life history of longfin smelt.

USGS produced water temperatures corresponding to 10 GCMs for RCP 4.5 and 10 GCMs for RCP 8.5. We averaged each of the 10 GCMs to develop ranges and medians for each RCP. The RCP 8.5 scenario represents rapid economic growth with little effort to limit or reduce emissions, reaching atmospheric greenhouse gas (GHG) concentrations exceeding 900 parts per million (ppm) by 2100 (see Figure 4.4). The RCP 4.5 scenario represents a more moderate scenario, with atmospheric GHG concentrations increasing through mid-century, reaching a concentration of 550 ppm, followed by stabilization (van Vuuren *et al.* 2011, p. 17). It should be noted that the State of California Resources Agency focuses on RCP 8.5 for the Delta Climate Change Vulnerability Assessment, as it most closely resembles current emissions trends (Schwalm *et al.* 2020, p. 19657) and presents a more precautionary approach (DSC 2021, p. 3-3). However, other experts have argued that emissions over the past decade may be closer to median scenarios such as the RCP 4.5 (Hausfather and Peters 2020, no pagination). For our rising water temperatures analysis, we define the foreseeable future as 2050, which is also a precautionary approach as both RCPs show similar trends through mid-century. However, we also present scenarios through 2100 as data are available.

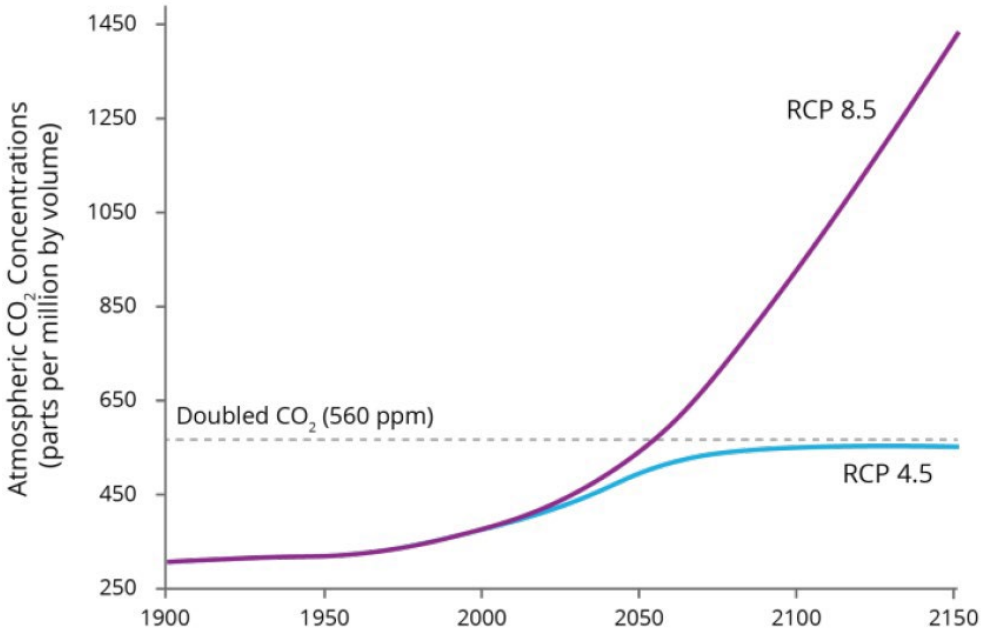

Figure 4.4: Emission of carbon dioxide under the RCP 4.5 and 8.5 scenarios. Source: Modified from van Vuuren *et al.* 2011, p. 17

As described under Life History, subadult and adult longfin smelt rear in central San Francisco Bay and the coastal ocean to escape warming temperatures that occur in much of the estuary during the summer. This movement is likely part of the DPS' adaptive capability and could be facilitated as water temperatures rise toward 20°C in the late spring. Likewise, longfin smelt adults have not been known to return to most of the estuary until temperatures drop below 22°C in the autumn. To project how hospitable habitat in the Delta may change in the future, we project the number of days water temperatures may be above 22°C from a decadal median through 2100. The full dataset is available in Appendix G.

Based on catch data, longfin smelt adults are present under favorable temperature conditions in Suisun Bay and the Delta. For our analysis, we project water temperatures at Martinez, Mallard Island, Decker Island, Jersey Point, and the North Delta in the Sacramento Deepwater Shipping Channel. From the 2010-2020 time period, the annual average number of days above 22°C was 56, 83, 91, 101, and 91 days, respectively. This suggests that longfin smelt are currently unable to inhabit the upper estuary for up to three months each year, which is broadly consistent with survey data.

By our established foreseeable future of 2050, it is projected that the average number of days above 22°C will increase by approximately 30 days for most sites under the RCP 8.5 scenario, with the greatest increase projected at Martinez which is projected to see an extra 36 days with temperatures above 22°C (see Figure 4.5). RCP 4.5 projects increases of 20 additional days in the lower Sacramento and San Joaquin Rivers to 30 additional days in Suisun Bay at Martinez (see Figure 4.6). Both scenarios suggest a shortening of the favorable temperature season for both post-larval/juvenile longfin smelt in the late spring and juvenile/adult longfin smelt in the fall. By 2100, the number of additional days above 22°C is projected to increase by approximately 57–67 days for most sites under the RCP 8.5 scenario, which would result in substantially less time available for longfin smelt to use the estuary in many years.

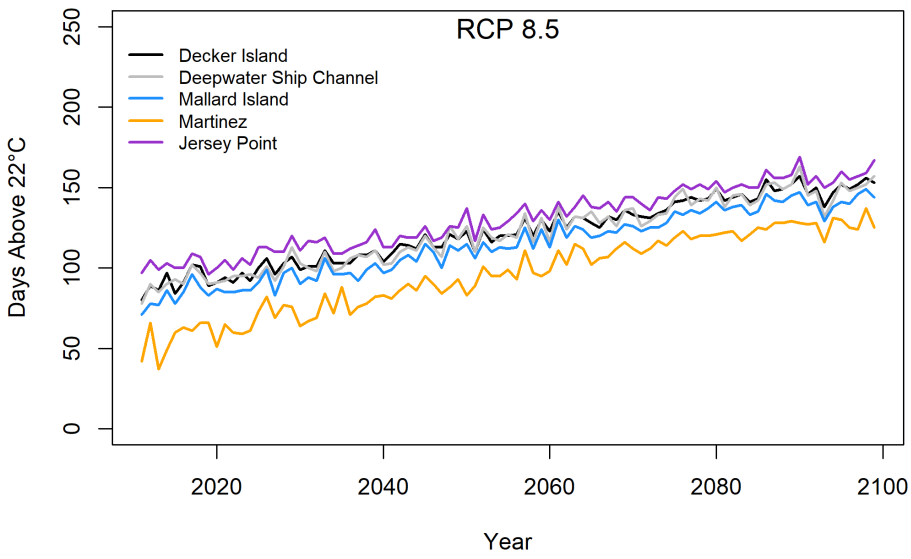

Figure 4.5: Projected number of days above 22°C at five locations under the RCP 8.5 scenario.

As described in the Species Needs and Life History sections, longfin smelt spawning typically begins in December and continues until temperatures approach 14°C. Larval catches from survey data peak at 8°C, and gradually become less frequent at all temperatures warmer than that (Grimaldo et al. 2017, Fig. 6, p. 1778). No longfin smelt of any life stage have been found in water above 22°C (Jeffries et al. 2016, Fig. 2, p. 1709). Here, we use 14°C as a threshold to estimate how the spawning window may change in the future due to rising temperatures, and we use the 22°C threshold to estimate when longfin smelt will seasonally migrate seaward of the Delta. In addition, we use 8–12°C as the favorable conditions temperature zone for larval longfin smelt.

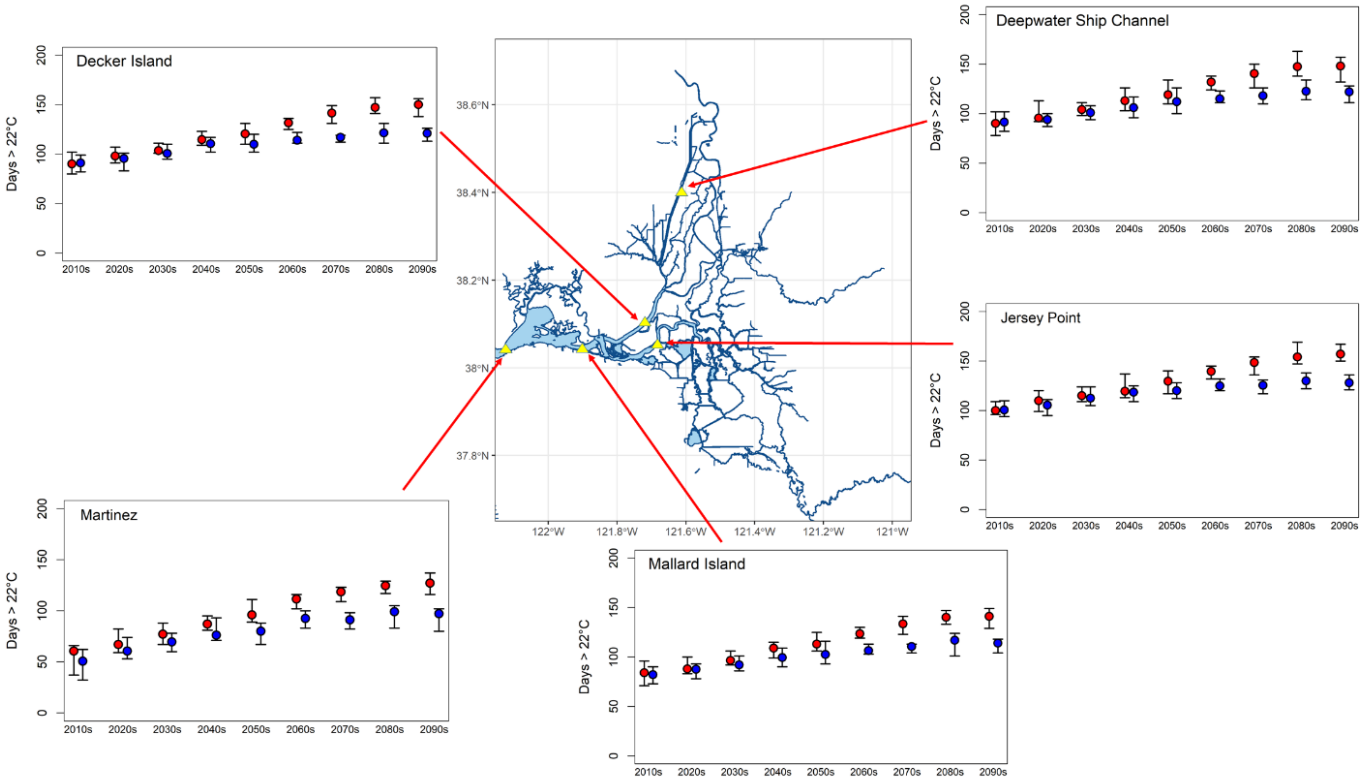

Figure 4.6: Map of the projected number of days above 22°C at five locations under both the RCP 8.5 (red) and RCP 4.5 (blue) scenarios. Lines extend between the minimum and maximum average projections for the 10 GCMs. (Map source: Bashevkin and Barros 2021, entire.)

Taken together, the Delta and Suisun Bay are projected to become less hospitable for adult longfin smelt in the future, with a suitability window that could decrease by more than two months in an average year (this would result in cutting the currently recognized habitability window by more than half). If they can, the young-of-the-year fish would need to make an earlier migration towards the Bay and the ocean. Individuals that are not developed enough to physiologically tolerate marine salinity as temperatures warm toward stressful thresholds will likely suffer higher mortality. Fish that survive their first year of life should be able to more easily come and go from the ocean as needed until they make a final return to spawn and die. We anticipate that adult longfin smelt will return to the estuary later in the fall to

avoid rising temperatures. There is no information available to predict whether this will delay spawning or not, but higher springtime water temperatures will likely truncate spawning opportunities with increasing frequency.

Based on field survey data, there is evidence that juvenile longfin smelt have been leaving the Delta earlier in the summer and returning later during the autumn by 1–2 months, suggesting that they may be spending more time in the coastal ocean than they did historically (Tobias and Baxter *unpublished preprint available at https://www.preprints.org/manuscript/202101.0512/v1*). This delayed return could be part of the species' response and adaptation to a warmer estuary.

In addition, back calculating and estimating hatch times for longfin smelt has suggested that hatching has been occurring earlier in the spawning season (Lewis and Hobbs 2021, unpublished data; Miller 2021, slide 14). Preliminary analysis suggests that outflow, temperature, and salinity may not be drivers of this early hatching behavior (Miller 2021, slides 15–17). But taken together, the spawning window for longfin smelt may have already shortened over recent history, based on field survey data.
To evaluate how the longfin smelt adult spawning window could change due to rising temperatures, we first assessed the environmental conditions where mature females were caught during field surveys. CDFW has been conducting the Longfin Smelt Fecundity Study since 2008 (Tempel and Burns 2021, slide 3), and the data have shown that mature females were collected between November and February. The majority of mature females have been caught at the confluence of the Sacramento and San Joaquin rivers, although detections occur throughout the estuary (see Figure 4.7). The spawning window has been calculated by subtracting an estimated incubation time of 20 days from the last larval (<8 mm) detection by the 20mm Survey. Putting the data together suggests that although the spawning window can vary, recent existing data shows a consistent threshold of <14 °C (see Figure 4.8).

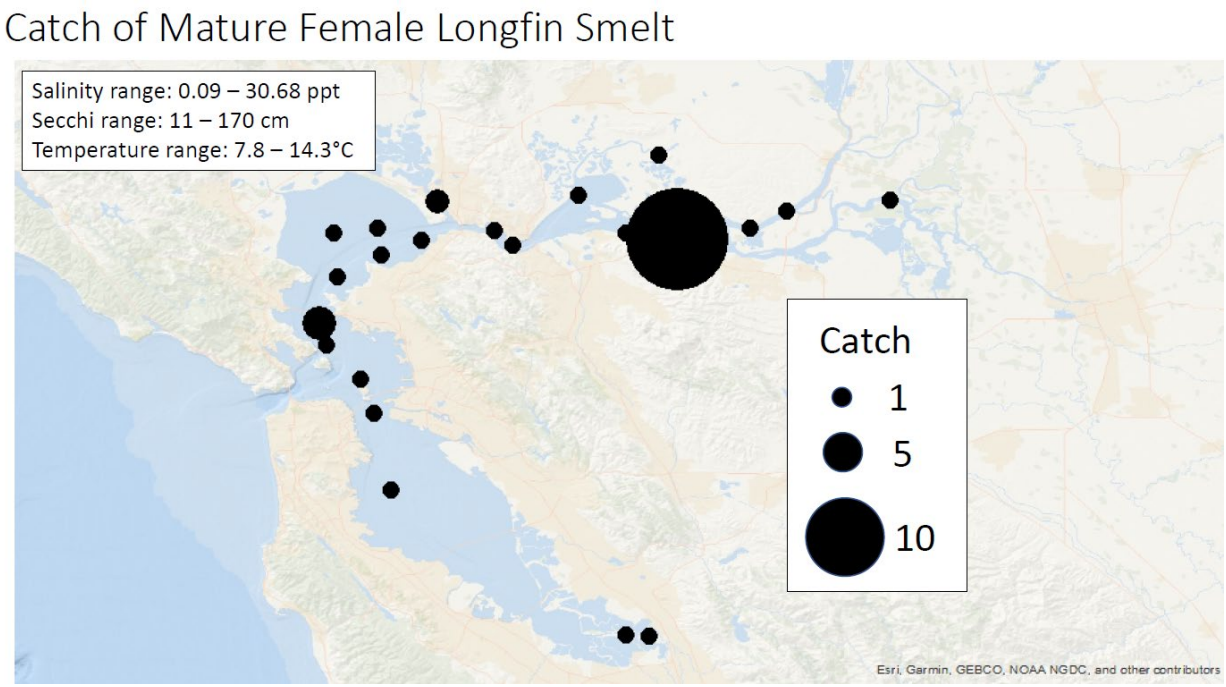

Figure 4.7: Map of mature female longfin smelt catch from DFW's Longfin Smelt Fecundity Study. Source: Tempel and Burns 2021, slide 5

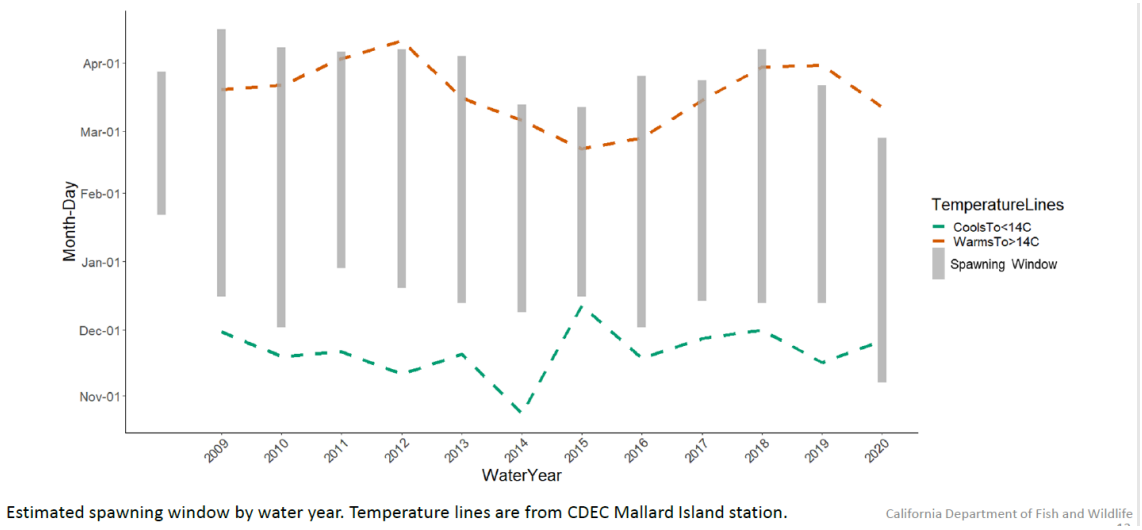

Figure 4.8: The calculated spawning window with temperature lines above (orange dashed lines) and below (green dashed lines) 14 °C. Source: Tempel and Burns 2021, slide 10

Since 2010, the annual average number of days below 14°C has averaged 117–125 days. This suggests a typical spawning season lasting about 4 months. By 2050, under the RPC 8.5 scenario, it is projected that the spawning season in the upper estuary will decrease by 21–24 days (see Figure 4.9). By 2100, the spawning season is predicted to decrease by about 2 months, which would represent a major reduction

in spawning opportunity (see Figure 4.10). The RCP 4.5 scenario projects smaller decreases of 10–11 days by 2050, to 19-24 days by 2100 (see Figure 4.11). Thus, there is high uncertainty about future spawning opportunity for the Bay-Delta DPS of longfin smelt that ranges from unhelpful from a species conservation perspective to potentially catastrophic.

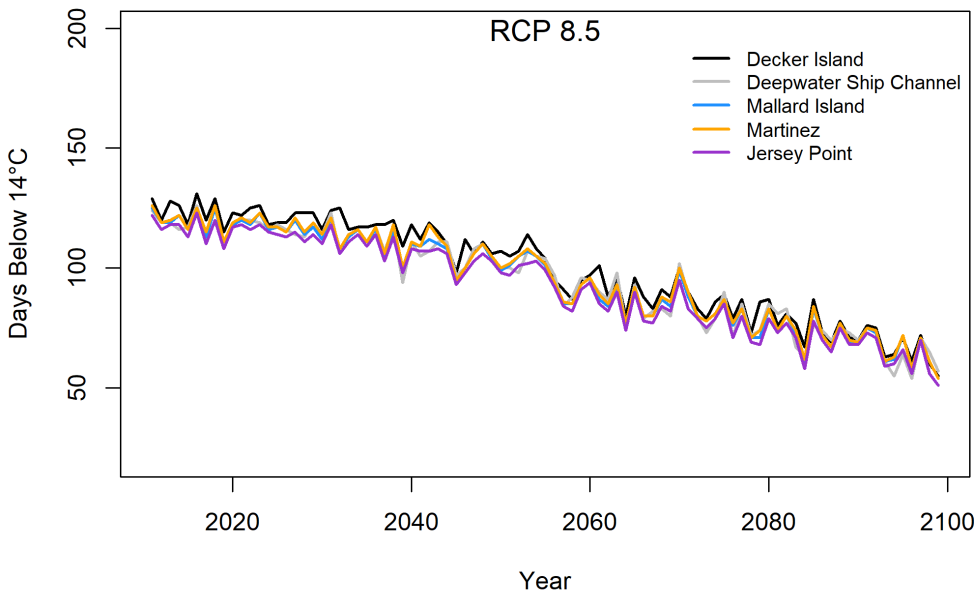

Figure 4.9: Projected total annual days below 14°C at five locations based on the RCP 8.5 scenario.

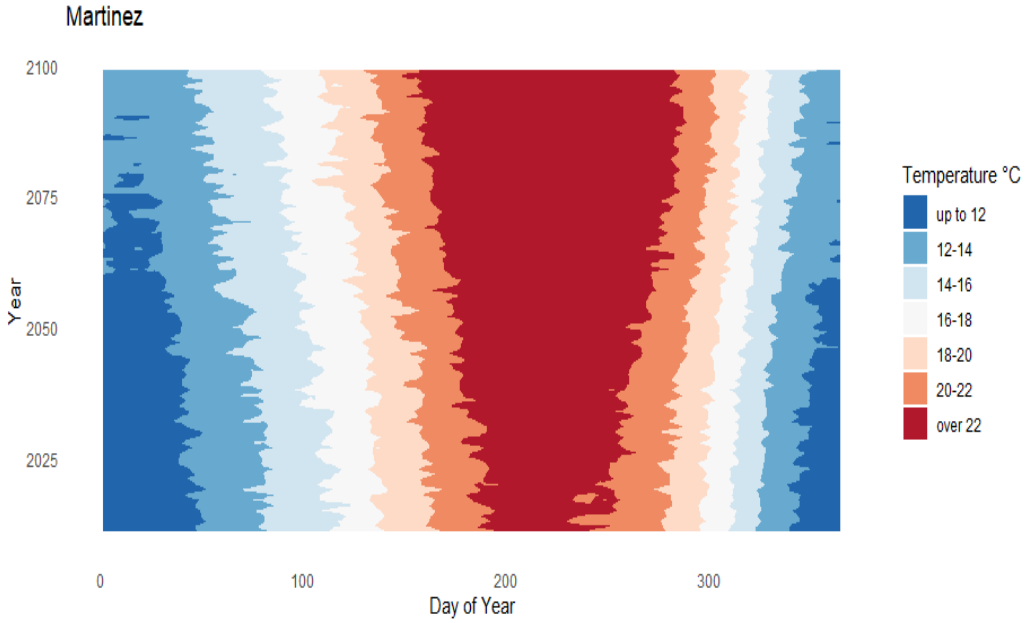

Figure 4.10: Heat map of temperature increases over time at Martinez in Suisun Bay from 2010–2100 under the RCP 8.5 scenario.

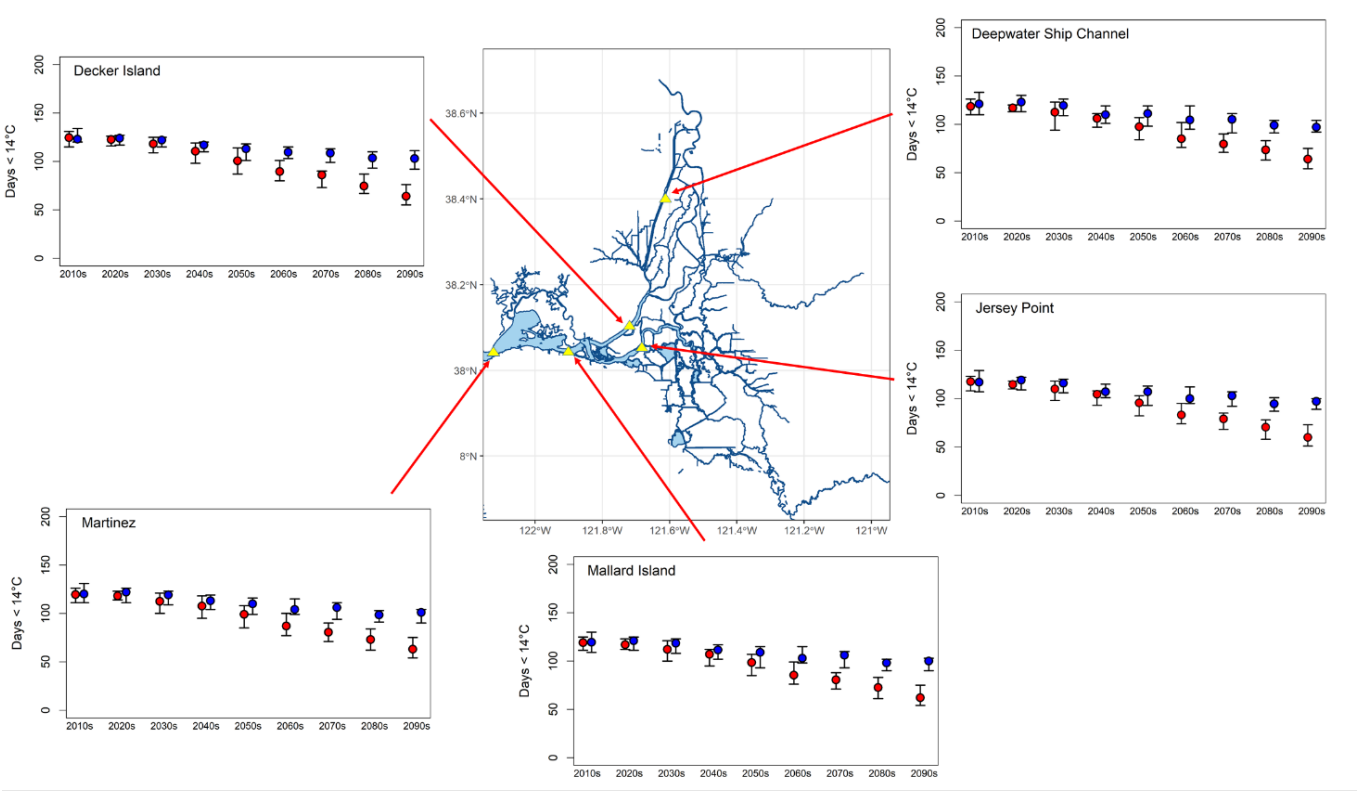

Figure 4.11: Map of the projected number of days below 14°C at five locations under both the RCP 8.5 (red) and RCP 4.5 (blue) outputted scenarios. The red and blue dots represent the mean across all RCP 8.5 an RCP 4.5 projections, respectively. Lines extend between the min and max average projections for all 10 GCMs). Map source: Bashevkin and Barros 2021.

As described under the Species Needs, longfin smelt larvae development success is highly temperature dependent, and the highest probability of success occurs at temperatures of 9–12°C. With extended days and periods outside of this favorable range, it is expected that lower fractions of spawned eggs will hatch into free-swimming larvae, and that yolk-sac larvae may experience slower growth and lower survival (Yanagitsuru et al. 2021, pp. 5–6). Compared to juveniles and adults, longfin smelt embryos and yolk-sac larvae are likely the most vulnerable to rising temperatures as they have the lowest tolerance to elevated temperatures (Baxter *et al.* 2010, p. 68; Jeffries *et al.* 2016, p. 1709; Yanagitsuru *et al.* 2021, pp. 5–6). They also do not yet possess the physiological capability to survive in cooler, higher salinity waters such as those found in the Bay and ocean (Yanagitsuru *et al.* 2022, in review).

In summary, climate change is expected to significantly raise water temperature in the upper estuary. Temperature changes are projected to be most prominent in Suisun Bay, where the number of days above 22°C (upper limit for all post-larval life stage) could more than double, forcing age-0 longfin smelt to trade estuary rearing time for ocean rearing time if they can do so successfully. There is high uncertainty about future spawning opportunity for the Bay-Delta DPS of longfin smelt that ranges from unhelpful from a species conservation perspective to potentially catastrophic. As a cold water species at the southernmost portion of its range, the Bay-Delta DPS is likely already needing to avoid water temperatures above its physiological tolerance during the summer months. Further increases in water

temperatures could mean extended summer-like conditions in which Suisun Bay and the Delta would be inhospitable for the fish. Longfin smelt are already exhibiting a pattern of exiting the Delta earlier in the summer, and this pattern may accelerate as temperatures rise. It is not known if it is a benefit or a risk for longfin smelt to extend ocean residence; historically many individuals stayed in the estuary in the summer. Likely due to rising temperatures, juvenile and subadult longfin smelt appear to be returning to the estuary later in the autumn, and this shift in estuary occupancy could shift further into the late fall or winter as temperatures continue to rise, potentially impacting spawning opportunities, e.g., leading to a constricted spawning temperature window. A shortened spawning window could hamper spawning success and decrease overall fecundity in the population. Lastly, larval longfin smelt may experience increased heat stress with highly uncertain, but potentially catastrophic population consequences.

4.2.3. Flow scenarios future condition analysis

As discussed under the Species Needs section, freshwater flow is the most important known driver of longfin smelt production. As mentioned in the Current Condition chapter, reduced freshwater flow has been a substantial and increasing stressor on the species, likely for many decades. Here we predict how the species may respond to projected further changes of freshwater flow using downscaled global climate models for the Sacramento/San Joaquin watershed. The projections and analyses are based on information published by Knowles *et al.* 2018.

USGS Computational Assessments of Scenarios of Change for the Delta Ecosystem project (CASCaDE2) is an interdisciplinary modeling research effort aimed at projecting responses of the Delta to scenarios of future change. The goals of CASCaDE2 are to provide an improved understanding of, and a new capability to model, the effects of future climate and infrastructure changes on the Delta ecosystem. As part of CASCaDE2, USGS developed an analysis of projections of managed flows in the Sacramento/San Joaquin watershed under future climate change scenarios.

The CASCaDE2 project used outputs from 10 GCMs to produce 20 Coupled Model Intercomparison Project Phase 5 (CMIP5) climate change scenarios. Each GCM was run with 2 scenarios of future GHG concentrations, or representative concentration pathways (RCPs). The two RCPs valuated correspond to radiative forcing values in 2100 of 4.5 and 8.5 W/m2 (RCP 4.5 and RCP 8.5), which represent scenarios with an effort at abating global GHG emissions and a high-end emissions scenario, respectively. These 10 GCMs were selected from a larger ensemble of 31 CMIP5 GCMs as being particularly suitable for California water resources assessments, based on the realism of their simulated climate both globally and in the region of interest. For complete details of the model development, see Knowles et al. (2018 pp. 7634–7638).

The GCM outputs were used to drive models of the Bay-Delta watershed's hydrology and operations. These models produced flow, storage, and meteorological time series reflective of the Sacramento and San Joaquin basins. Water Year (WY) averages were calculated based on trends in basin-averaged precipitation and air temperature. Here, we use WY projections as the primary variable to describe the effect of changing flow conditions on longfin smelt production. We use RCP 4.5 as a more conservative

projection of climate change with stricter global emissions standards, and RCP 8.5 as a high-end emissions scenario. The full dataset is available in **Appendix G**.

An important caveat for Knowles *et al.* (2018) is that the authors assumed no major changes to management infrastructure or strategy due to the difficulty of anticipating the details of such changes. Projecting freshwater demands in a complex water management network like California's is difficult. Another caveat of the data projections noted from Knowles *et al.* (2018) is that estimated demand scenarios were only available for California's level of development (LOD) in 2005 and for 2030. In CASCaDE2, all modeling runs use the 2005 LOD until the beginning of WY2030, after which they use the 2030 LOD. Projections past 2030 may therefore represent an inaccurate estimate of freshwater demand due to uncertainty in overall demand. Urban water demands are projected to increase from around 8 MAF (million-acre-feet) per year in 2030 to 11–13 MAF/year by 2100 (Christian-Smith *et al.* 2012, p. 42), which is roughly a 50% increase due largely to population growth. On the other hand, agricultural water demand is projected to decrease due to changes in cropland (conversion to urbanization), resulting in a decline of approximately 29 MAF/year in 2012 to 27 MAF/year in 2062 (Wilson *et al.* 2016, p. 8), which is a 7.8% decrease.

Averaged across all scenarios, the total Sacramento basin unimpaired runoff is projected to increase by an average of approximately 9.7% over a wide spread of variability by 2099 (Knowles *et al.* 2018, p.7641). Historically from 1980-2009, the mean daily hydrograph of actual impaired Delta inflow displayed rising inflows from mid-December, peaking in February-March, before leveling off in July (see Figure 4.11a). In comparison, the future scenarios project a general tendency leaning towards increased Delta inflow from December-March, followed by a reduction in inflow from April-July (see Figure 4.11b). This is a result of increased projected precipitation falling as rain and reduced snowpack due to rising temperatures that would likely cause higher peak flows in the winter followed by a steep drop off in the spring through mid-summer. Although a similar monthly pattern is seen between the RCP 4.5 and CP 8.5 scenarios, RCP 8.5 projects much higher peak inflows followed by a steeper drop off in April. Historically, approximately 60–65% of unimpaired flow contributions from the Sacramento basin occurred from October 1st to March 31st, but averaged across all scenarios, that percentage is projected to increase to approximately 83%.

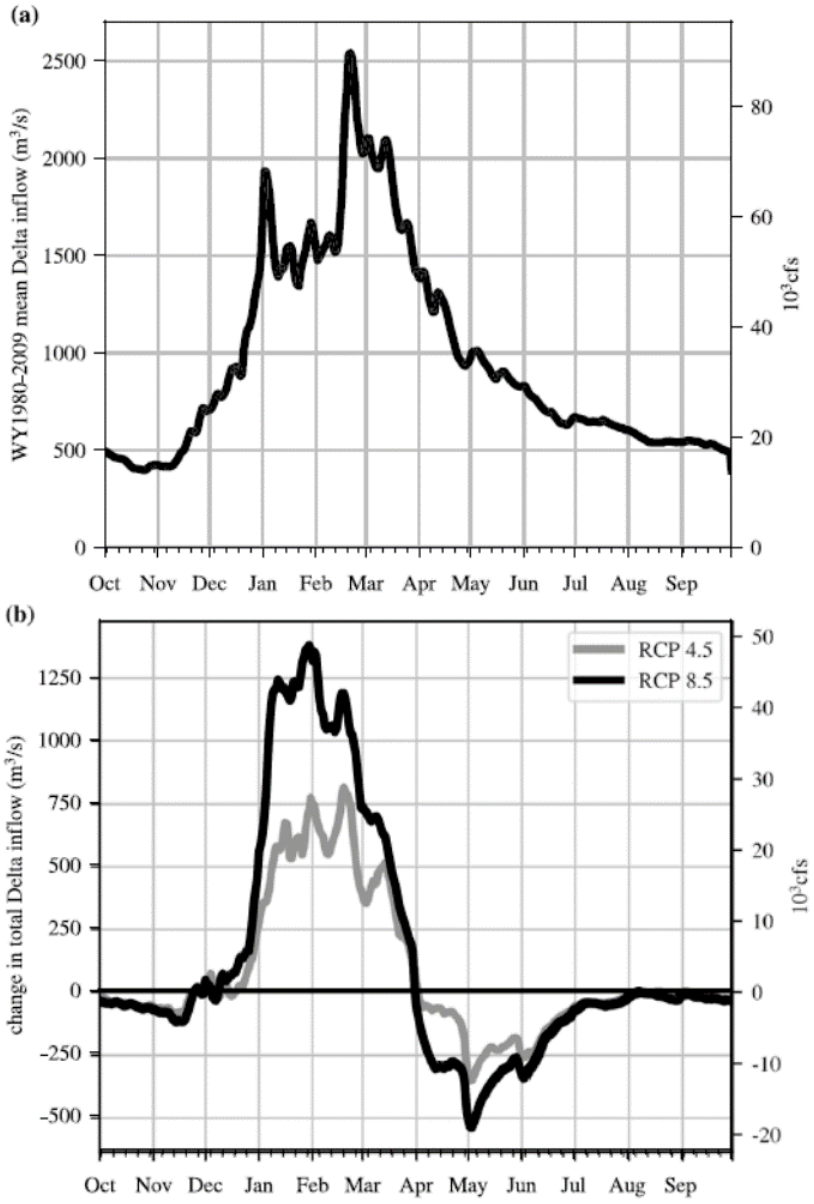

Figure 4.11: (a) The mean annual cycle of Delta inflow for WY1980-2009. The typical WY consists of rising inflow beginning in mid-December, peaking in February-March, before leveling off in July. (b) Difference between WY2070–2099 and the 1980–2009 mean annual cycles of managed total Delta inflow averaged over scenarios of each RCP. Source: Knowles *et al.* 2018, p.7646.

Historically, spring-summer Delta inflow is influenced by snowmelt and reservoir operations, with a gradual decline lasting into the fall until seasonal wet weather returns. Snowmelt runoff has accounted for an average of 40% of annual inflow, as indicated by discharge occurring after April 1st (Knowles and Cayan 2004, p. 320). But with rising temperatures under both scenarios, more snowfall would become rainfall, and the snowpack that does accumulate would melt earlier, potentially resulting in higher frequency extreme flow events during the winter and early spring. By 2099, the total annual snowpack

on April 1 is projected to decline by 89% for the Sacramento Basin and 50% in the San Joaquin Basin compared to 1995 levels (see Figure 4.12). Due mainly to the overall reduced snowpack, projected inflow could face a steep drop during the month of April continuing through the summer (Fig. 4.11). Even in very wet years, this could result in very dry conditions in the late spring and early summer (Knowles *et al.* 2018, p. 7647).

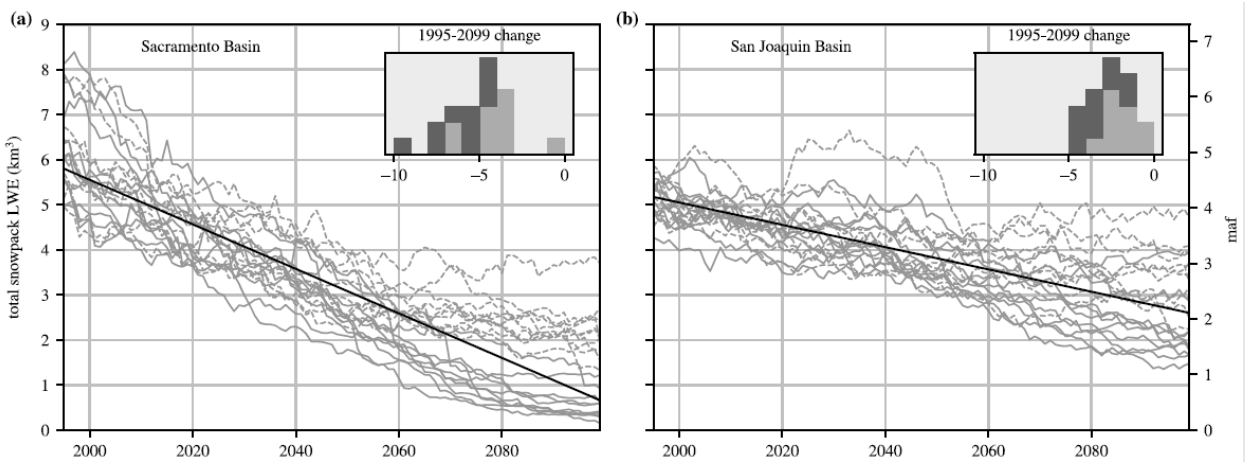

Figure 4.12: Smoothed scenario time series (gray), ensemble regression fit (black), and change histograms (inset) for total April 1st snowpack LWE volume for (a) Sacramento basin and (b) San Joaquin basin. Both panels have a common *y* axis, with units of cubic kilometer. Representative concentration pathway 4.5 scenarios are dashed lines in the plot and light gray in the histograms; representative concentration pathway 8.5 are solid and dark gray. LWE = liquid water equivalent. Source: Knowles *et al.* 2018, p.7641.

As mentioned in the Species Needs section, freshwater flow is a primary driver of longfin smelt productivity, potentially throughout winter and spring (see Fig. 2.8). It is unknown if certain months of freshwater flow are more important than others. In the projected scenarios, the frequency of higher favorable flows during the January-March time periods is anticipated to increase (Fig. 4.11). However, the frequency of favorable flows during the April-June time period is anticipated to decrease. Thus, we anticipate that longfin smelt recruitment would likely be hindered as a result of the lower outflow later in the reproductive and early life rearing season.

The projected annual increases in flow during winter may be beneficial for longfin smelt spawning and egg incubation/larval rearing for as long as water temperatures remain suitable, as it may create more suitable habitat while extending the species range to occupy and utilize during this critical phase in the DPS life history. However, if the water temperatures increase as projected under Wulff *et al.* 2021, then even the annual winter inflow increases may not result in more spawning and larval rearing habitat. On the other hand, the projected lower spring flows could create less suitable conditions for larval rearing in many areas that had been conducive earlier in the season. Longfin smelt larvae have been detected at salinity up to 12 psu (Grimaldo *et al.* 2017, p. 8), though peak catch levels occur between 2–4 psu. If spring outflows decline as projected, larval productivity will likely continue to decline as well due to less

accumulation of recruitment mechanisms as described in section 3.1.1. Thus, on the whole, it is uncertain whether anticipated improvement in winter freshwater flow conditions can compensate for anticipated decline of freshwater flow during spring.

In addition to a changing average seasonal hydrograph, the projected scenarios displayed changes in the frequency of Water Year (WY) types (Knowles *et al.* 2018, data release). Knowles *et al.* 2018 defined the most intensely dry years as falling between the 3rd and 10th percentiles of historical hydrology. Under the RCP 4.5 scenarios, intensely dry years increase in frequency over moving 31-year window projections (see Figure 4.13). For the RCP 8.5 scenarios, all ranges of dry years increased in frequency over the projected century, with the most intensely dry years experiencing the largest relative increase such that the 3rd and 10th percentile projected 3 and 2-fold increases by the end of the century, respectively.

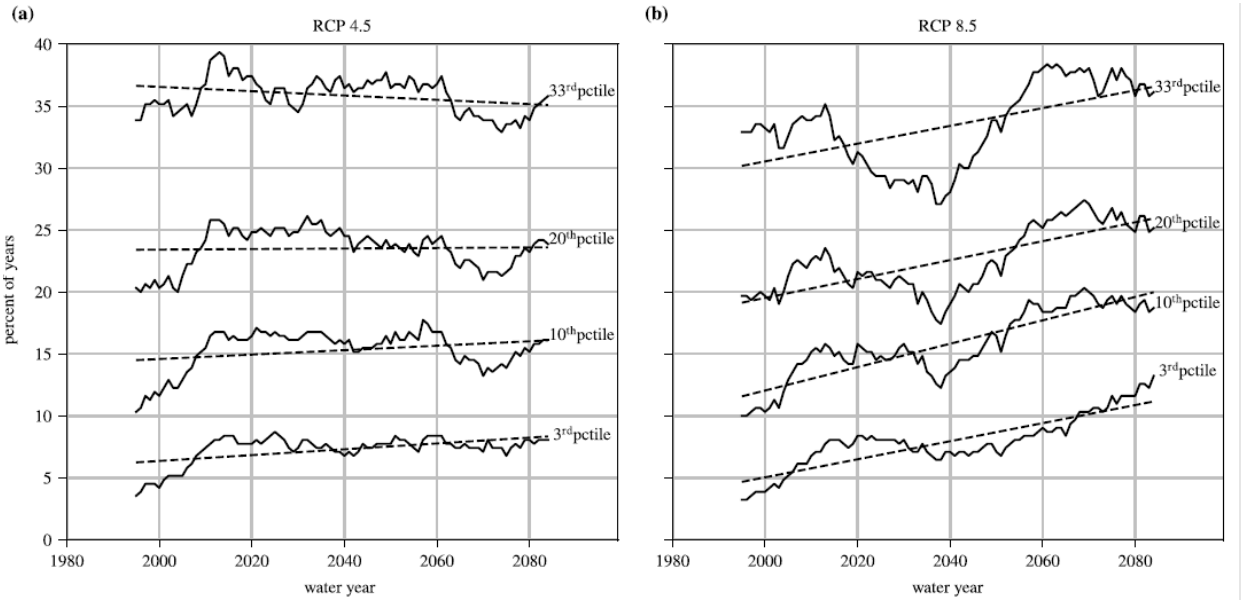

Figure 4.13: The 31-year moving-window percentages of years with projected impaired Sacramento basin WY outflow below global climate model historical-period (WY1980–2009) percentile values, averaged over (a) RCP 4.5 scenarios and (b) RCP 8.5 scenarios. Percentile thresholds are indicated (i.e. the 33rd percentile represent the historical 33% driest years on record, the 20th percentile the 20% driest years on record, etc.). Under the RCP 8.5 scenarios, all ranges of dry years increase in frequency. Under the 4.5 scenarios, only the intensely dry years (10th and 3rd percentile) increase in frequency. Dashed lines are linear fits. RCP = representative concentration pathway; WY = October 1 – September 30 water year. Source: Knowles *et al.* 2018 p. 7646.

As mentioned under the species Current Condition, a primary cause for the longfin smelt decline over time has been the reduction in freshwater flows, which we have concluded in this SSA is the most important species need. As dry years have generally been “bad years” for longfin smelt recruitment, the frequency of dry years and droughts has already taken a substantial toll on longfin smelt such that abundance indices have frequently sunk to new record lows, particularly over the past two decades. The

projected increases in dry year frequency under RCP 8.5 and intense dry year frequency under RCP 4.5 are anticipated to increase the intensity of decline in this already steeply declining DPS.

The 20th Century was a relatively wet one in the past millennium (Cook *et al.* 2009, p. 51–52; Stine 1994, entire), with one of the lowest frequencies of droughts occurring between 1850–1950 (Hughes and Brown 1992, p. 166). Prior to the 21st century, dry and critically dry years occurred approximately 33% of the time. But since 2000, dry and critically dry year frequency has been 43% of years. Based on soil moisture reconstruction, the observed timeframe of 2000–2021 was probably the driest 22-year period on record in at least the past 1,200 years, exceeding even any 22-year period during the last megadrought in the late 1500s (Williams *et al.* 2022, p. 1). In essence, California's complex water infrastructure was likely constructed during a wetter era than what has been typical for the State (Fountain 2015; see Figure 4.14). As the demand for water further increases with population growth (Wilson *et al.* 2016, pp. 7–8), water withdrawals are estimated to be greater than 100% of precipitation by 2050 (Roy *et al.* 2012, p. 2554). And by 2062, water use is projected to increase by 1.8 billion cubic meters over 2015 use rates (Wilson *et al.* 2016, p. 6), so what was considered sufficient water supply in the 20th Century is unlikely to be enough to meet demand for the 21st Century (Stanton and Fitzgerald 2011, pp. 24–28). If the projected increases in frequency of dry years under either the RCP 4.5 and 8.5 scenarios come to pass, longfin smelt productivity is anticipated to keep declining over time as less water and superimposed water demand further exacerbates flow reductions unless alternative ways are found to mitigate for past, present, and future changes to the estuary hydrograph.

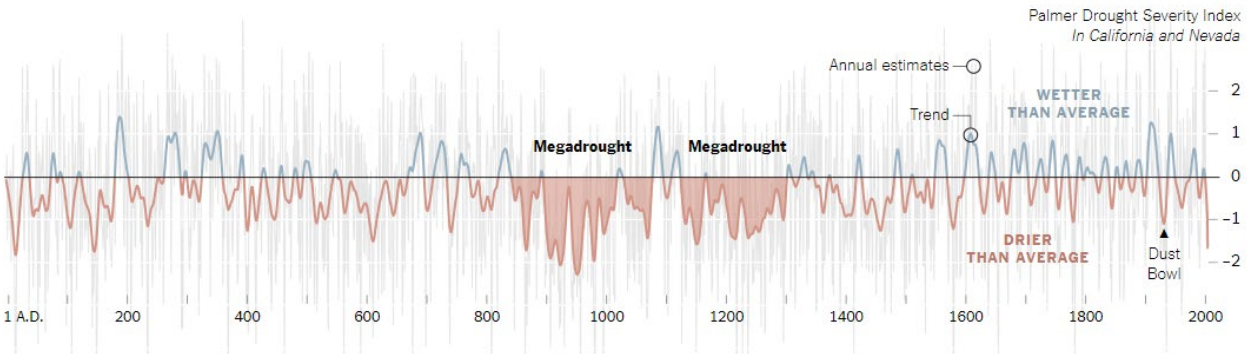

Figure 4.14: Analysis of tree rings suggests that western states have had many droughts of two decades or longer, including two megadroughts lasting longer than 100 years. However, the 20th Century was wetter than average. Source: Fountain 2015.

Longfin smelt's resiliency against droughts in the SFE watershed appears to have decreased over time and the species has always displayed low resistance to drought, defined as the lack of a large-scale decline in occurrence from a wet period to a drought period (Mahardja *et al.* 2021, pp. 6 and 9). Longfin smelt have a predominantly 2-year life span though some experts believe that substantial numbers of individuals may spawn at age 1 and 3. We mentioned above resolving the age distribution of spawners is an important conservation science topic because more spawning age-classes translates into more resilience to brief periods of poor environmental conditions. Nonetheless, consecutive dry years,

which have occurred more frequently over the past 2 decades, limit the effectiveness of this life history strategy. Using the projected scenarios, we estimated the probability that consecutive dry years will occur in the future (see Figure 4.15).

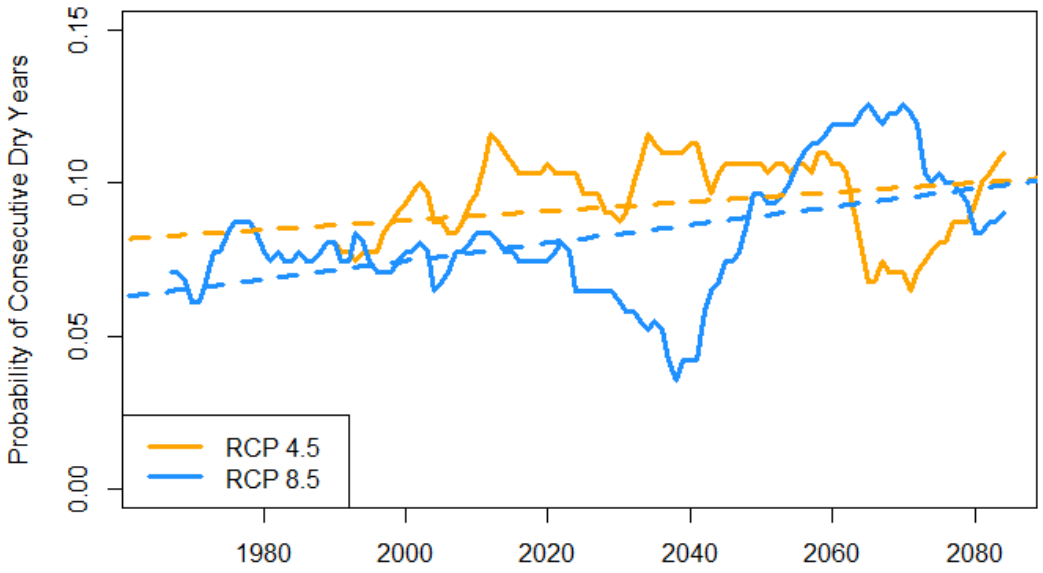

Figure 4.15: The probability of consecutive (2 or more) very dry years within a 31-year moving window (centered on the year indicated on the x-axis) occurring under the RCP 4.5 and RCP 8.5 scenarios. Very dry years are defined as dry and critically dry water year types. Dashed lines represent increasing trends over time (p-values for the slopes of both trend lines were < 0.001).

Droughts and very dry years have become more prevalent over the past two decades, and this trend is likely to increase in the future. Over time, the probability of consecutive dry years significantly increases under both the RCP 4.5 and the RCP 8.5 scenarios. This change is anticipated to steepen the rate of longfin smelt decline unless alternative ways are found to mitigate for past, present, and future changes to the estuary hydrograph.

4.2.4. Sea level rise future condition analysis

Global sea level rise (SLR) is primarily caused by thermal expansion of warming ocean water and melting of land-bound ice as air temperatures increase. Recent research has focused on potential large-scale ice sheet collapse in West Antarctica (where the Ross Ice Shelf is land bound) and Greenland (Mouginot *et al*. 2019), which would rapidly raise ocean levels worldwide (DeConto and Pollard 2016, pp. 5–6; Oppenheimer and Alley 2016, p. 1376). Regional rates of sea level rise are variable, depending on vertical land motion (i.e., uplift and subsidence), winds, and large-scale ocean circulation patterns.

Since its installation in the mid-1850s, the San Francisco tide station, located near the Golden Gate Bridge at the mouth of San Francisco Bay, has recorded an 8-inch increase in local sea levels, with other tide stations in the Bay Area showing comparable rates of sea level rise. Analysis of satellite altimetry data also indicates a recent acceleration of global sea level rise since 2011 (Nerem *et al.* 2018, pp. 2023–

2024). This recent acceleration follows decades of suppressed sea level rise along the west coast of the United States (relative to rates of sea level rise elsewhere in the Pacific Ocean basin), which may be linked to variations in the Pacific Decadal Oscillation (Bromirski *et al.* 2011, pp. 11–12). As with any prediction of the future, it is unclear how long this recent accelerated trend of sea level rise will continue, but it is expected to continue for the foreseeable future (Ruckert *et al.* 2017, Fig. 1, p. 3).

In our sea level rise analysis, we utilize existing data and summaries from the Delta Stewardship Council's Delta Adapts document (DSC 2021), which consists of climate change vulnerability assessments and adaptation plans specific for the Bay-Delta developed in partnership with technical experts, state and local governments, stakeholders, and community representatives. Our analysis focuses on the upper estuary. This focus is helpful in that higher estuary salinity caused by higher sea level, more frequent drought conditions, and higher human water demand (all reviewed above) will compel a larger average fraction of longfin smelt to spawn and rear in and near the Delta. We note that by year 2100 higher end estimates of sea level rise have potential negative implications for tidal marsh restoration efforts throughout the estuary (Buffington *et al.* 2021, Fig. 4, p. 14). Sea level trends in the Delta may be complicated by land subsidence. Decomposition of drained and converted marsh and peat soils within diked Delta islands have caused much of the Delta region to lie below sea level—in some places by as much as 15 to 20 feet (Deverel *et al.* 2020, p. 839). Continued land subsidence may increase the relative rate of locally observed sea level change for the Delta area when comparing water levels to local land elevations.

The State of California Ocean Protection Council (OPC 2018, p. 18) has created sea level rise projections for the San Francisco tide station (Table 4.1). The San Francisco tide station, although not located within the Delta, provides an ocean boundary that is considered representative of regional oceanic sea level conditions that will influence local sea level rise and peak water level response in the Delta. Based on the OPC Guidance, sea levels in the San Francisco Bay-Delta Estuary are likely (66 percent probability) to rise between 0.6 to 1.1 feet by 2050, with an upper range (1-in-200 chance) projection of 1.9 feet. By 2100, sea levels are likely to rise between 1.2 to 3.4 feet, with an upper range projection of 6.9 feet. However, the combination of extreme rates of ice-sheet loss and complex feedback mechanisms could result in accumulated sea level rise of up to 10.2 feet by the end of the century (OPC 2018, p. 25).

Table 4.1: Sea level rise projections for the San Francisco Bay-Delta. Probabilistic projections are based on the Kopp *et al.* 2014 (pp. 388–393) method and shown in feet. Projections are shown for the San Francisco tide station. Source: DSC 2021 p. 51

		Median ***50% probability sea level rise meets or exceeds***	**Likely Range** ***66% probability sea level rise is between***	**1-in-20 chance** ***5% probability sea level rise meets or exceeds***	**1-in-200 chance** ***0.5% probability sea level rise meets or exceeds***	**H++ Scenario** ***Extreme scenario not associated with a probability***
Emission Scenario	**Year**	**N/A**	**Low-risk aversion**	**N/A**	**Medium-high risk aversion**	**Extreme risk aversion**
RCP 8.5	2030	0.4	0.3-0.5	0.6	0.8	1.0
RCP 8.5	2050	0.9	0.6-1.1	1.4	1.9	2.7
RCP 4.5	2070	1.3	0.8-1.7	2.1	3.2	5.2
RCP 8.5	2070	1.4	1.0-1.9	2.3	3.5	5.2
RCP 4.5	2100	1.8	1.2-2.7	3.5	5.8	10.2
RCP 8.5	2100	2.5	1.7-3.4	4.4	6.9	10.2

As with our Delta hydrology analyses, we used RCP 4.5 as the conservative scenario with stricter emissions standards and RCP 8.5 as the "business-as-usual" scenario with fewer global efforts to limit or reduce emissions. However, the State of California has recommended using RCP 8.5 through 2050 because the greenhouse gas emissions worldwide have continued to follow the business-as-usual trajectory (OPC 2018, p. 13). Based on this projection, an increase in sea level of 0.6 to 1.1 feet is likely by 2050, with an upper range estimate of 1.9 feet. Beyond 2050, sea level rise depends partly on emissions over the coming decades and the planet's response to a warmer climate. By 2070, an increase in sea level of 0.8–1.9 feet is likely, with an upper range estimate of 3.5 feet. Under a moderate emissions scenario, an increase in sea level of 1.2 to 2.7 feet is likely by 2100, with an upper range estimate of 5.8 feet. Under a high emissions scenario, an increase in sea level of 1.7 to 3.4 feet is likely, with an upper range estimate of 6.9 feet.

Sea level rise in the San Francisco Bay is likely to affect daily tide and peak storm water levels throughout the Delta (DSC 2021, pp. 5–4). Daily tide levels will respond to sea level rise differently across the Delta and Suisun Marsh, depending on the amount of sea level rise, proximity to the Bay, and local hydrodynamic conditions. In some parts of the Delta, high tide elevations are projected to increase at a faster rate than mean or low tide elevations. This suggests that the tide range in the Delta may also increase as a result of sea level rise. For one foot of sea level rise, this effect is most pronounced in the south Delta, where the tide range is projected to increase by more than 20 percent. The tide range amplification is progressively less in the north Delta (approximately 10 to 15 percent) and central Delta (approximately 5 percent) and negligible in strongly tidally influenced areas such as Suisun Bay, Rio Vista, and the lower Yolo Bypass (DSC 2021, pp. 5–4).

These changes in mean sea level and tidal dynamics will likely affect marsh habitats in the Delta and Suisun Marsh used by longfin smelt. For tidal freshwater and brackish wetlands in the Delta and Suisun Marsh, the Delta Stewardship Council (2021) has defined vulnerability as either the transition from high marsh to low marsh or complete drowning in response to sea level rise. For mid-century (2050) sea level rise scenarios, high marsh tidal wetlands will not be at risk of habitat transitions or drowning under 1 foot of sea level rise (Table 4.2). Under 2 feet of sea level rise, tidal freshwater wetlands in the Delta will be at risk of transitioning to low marsh, but brackish tidal wetlands in Suisun Marsh are predicted to persist and keep pace with sea level rise. If sea level rise, shorter wet seasons, and more frequent drought interact to increase estuarine salinity, tidal wetland ecosystems may be subject to changes in plant community composition that further compromise their ability to keep pace with sea level rise. For late-century (2085) scenarios, tidal wetlands will not be at risk of transitioning to low marsh under two feet of sea level rise but will be at risk of transitioning under 3.5 feet of sea level rise. Under the more extreme end-of-century scenario (6 feet sea level rise by 2100), all tidal wetlands in the Delta and Suisun Marsh are at risk of drowning (becoming subtidal habitats).

Table 4.2: Predicted Habitat Changes of Un-leveed Freshwater and Brackish High/Mid Marsh in the Delta and Suisun Marsh under Different Sea Level Rise Scenarios. Recreated from: DSC 2021, p. 147.

Year	Sea Level Rise	Delta Freshwater Marsh	Suisun Brackish Marsh
2050 (low)	1 foot	High/Mid Marsh Persists	High/Mid Marsh Persists
2050 (high)	2 feet	Conversion to Low Marsh	High/Mid Marsh Persists
2085 (low)	2 feet	High/Mid Marsh Persists	High/Mid Marsh Persists
2085 (high)	3.5 feet	Conversion to Low Marsh	Conversion to Low Marsh
2100	6 feet	Drowned	Drowned

Both the freshwater marshes, Suisun's brackish marshes and bay tributary marshes are important part of young-of-the-year longfin smelt's low-salinity rearing habitat (Grimaldo *et al.* 2017, p. 11; Hobbs *et al.* 2010, p. 565, Lewis et al. 2019, p.63). The same can be true for similar habitats further seaward when low-salinity conditions are available (Fig. 2.4). Field surveys including SLS and the 20mm Survey have historically also detected an abundance of larval and juvenile longfin smelt adjacent to these areas, suggesting that lateral connectivity between marshes and open-water habitats may be an important aspect of nursery habitat for the species. Thus, conversions of freshwater and brackish marshes to low marshes and subtidal habitats may conspire with higher salinity, warmer water temperatures, and a shorter duration wet season to affect habitat suitability for young longfin smelt.

MacWilliams and Gross (2010) evaluated salinity intrusion over one annual hydrologic cycle under five levels of sea level rise between 15 cm and 140 cm based on Delta outflows and operations as they were during 2002. Their model predicted that these increases in sea level would result in an increase in X2 throughout the year (see Figure 4.16), with predicted median increases ranging from 0.7 km for the 15-cm sea level rise scenario to more than 7 km for the 140-cm sea level rise scenario. By 2050, this would likely extend the position of X2 by over 1 km under a moderate scenario, and by nearly 3 km under a more extreme scenario.

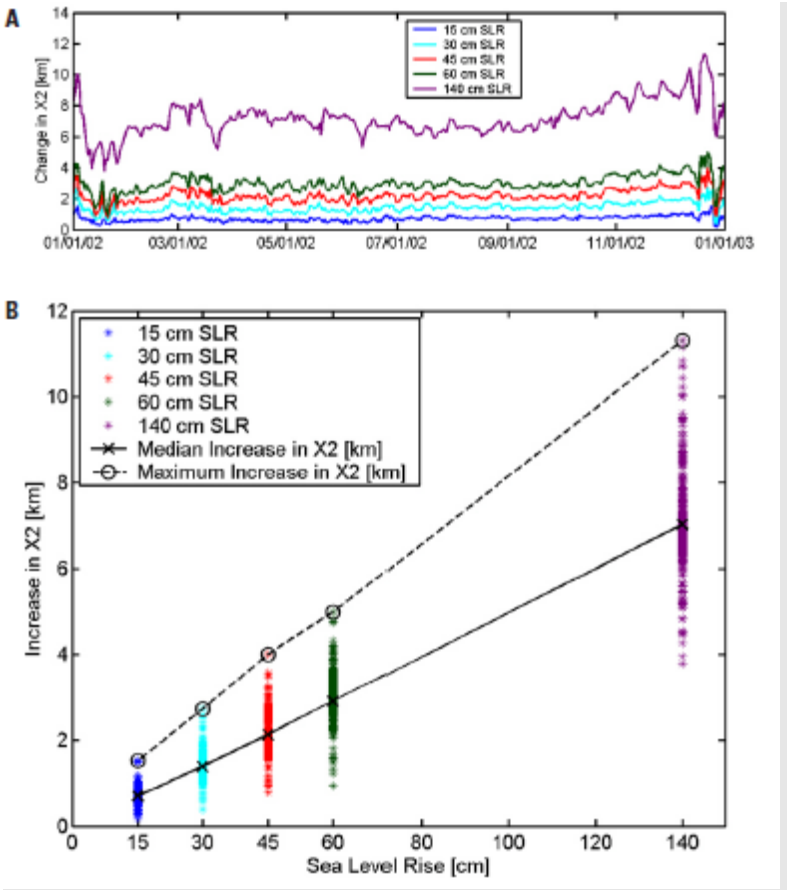

Figure 4.16: (A) Predicted change in X2 relative to Baseline scenario for 15-cm SLR scenario, 30-cm SLR scenario, 45-cm SLR scenario, 60-cm SLR scenario, and 140-cm SLR scenario; (B) Scatter plot of the predicted increase in X2 for each day during 2002 for each of the sea level rise scenarios; solid black line shows the median increase and the dashed black line shows the maximum increase in X2 for each SLR scenario. Modified from Mac Williams and Gross (2010, p. 185).

Chua and Xu (2014) estimated the effect of sea level rise on salinity intrusion, finding that at moderate steady-state flows (300 cubic meters per second), a 1.5-m sea level rise would result in a 10 km increase in X2 relative to present conditions. At higher steady-state flows (2000 cubic meters per second), the effect was less pronounced, with a similar sea level rise producing only a 4 km increase in X2. As it does presently, realized salinity intrusion resulting from sea level rise will vary depending on the natural and human-modulated availability of fresh water to repel it.

These projected changes in X2 could have a significant impact on longfin smelt spawning and rearing (see Figure 4.17). As described in the species Life History section, longfin smelt returning adults are broadly distributed but many aggregate in the LSZ during the spawning season. If the location of X2 increases during the winter due to sea level rise and those average increases are not offset by the anticipated higher average winter flows, spawning habitat could be pushed substantially eastward, potentially resulting in constricted and lower quality spawning habitat. In addition, sea level rise may

compound this effect during the spring when coupled with the projected inflow drop off. The projected eastward shift in X2 may also result in increased entrainment risk (Section 3.1.7). Further, if returning adults have longer spawning migrations, this may require additional energy expenditure or increase predation risk. However, as longfin smelt likely also use tidal currents to move upstream instead of continued directional swimming, it is unknown if extended geographic spawning movements would be a significant added stressor.

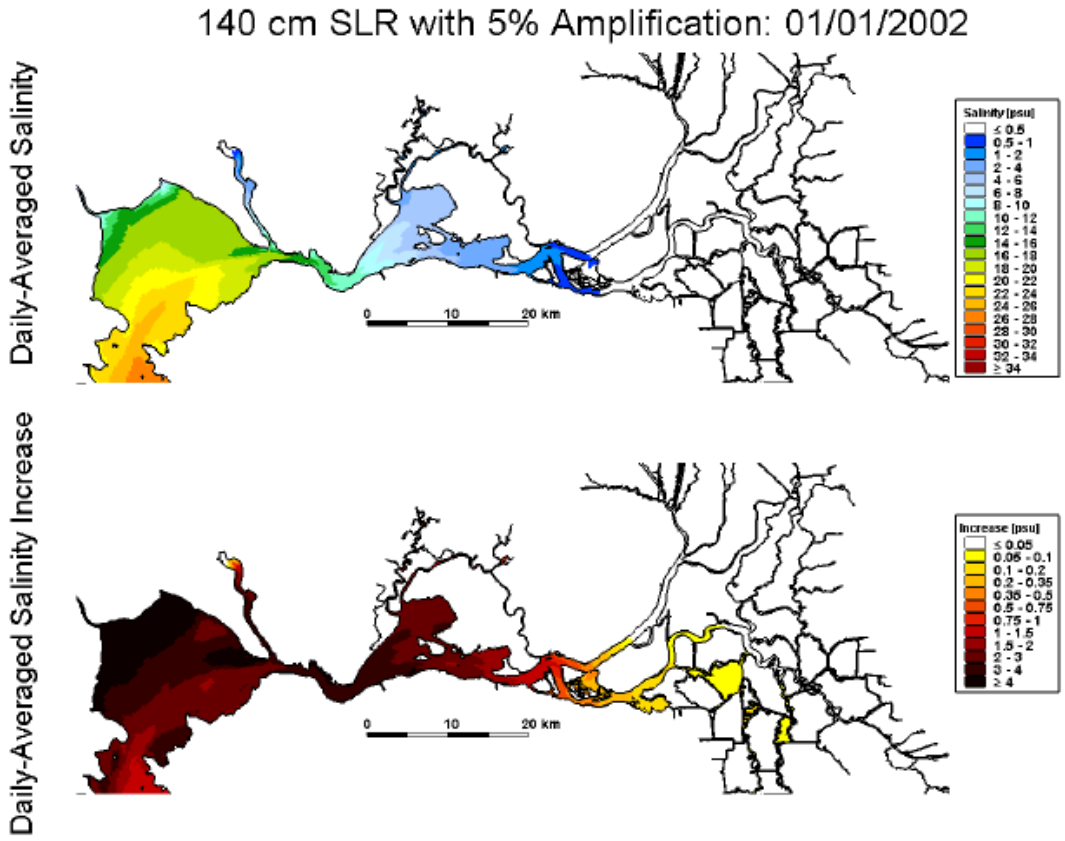

Figure 4.17: Predicted daily- and depth-averaged salinity on January 1, 2002 for the 140 cm SLR with 5% Amplification scenario (top); predicted increase in daily-averaged depth-average salinity on January 1, 2002 relative to the Baseline (0 cm SLR) scenario for the 140 cm SLR with 5% Amplification scenario. Source: MacWilliams and Gross 2010, p. 148.

In summary, the effects of sea level rise on the San Francisco Estuary could result in salt- and freshwater marsh losses and salinity intrusion. Many of the marshes currently used by longfin smelt could be inundated and lost by the end of the century, potentially resulting in lower suitability of remaining open water habitats. The salinity intrusion, if not sufficiently abated by increasing reservoir releases and export reductions (thereby extending already stretched water supplies), would likely shift X2 eastward. The upstream shift in X2 could lengthen the spawning migration of adult longfin smelt, and the salinity increases could render San Pablo Bay and Suisun Bay more frequently inhospitable to larvae, substantially reducing suitable larval rearing habitat.

4.3. Future invasive species

The San Francisco Estuary has historically been one of the most invaded aquatic systems in the world (Cohen and Carlton 1998, p. 556). The rate of invasions increased from an average of one new species established every 55 weeks from 1851 to 1960, to an average of one species every 14 weeks from 1961 to 1995 (Cohen and Carlton 1998, p. 556). In the low-salinity zone, the accelerated invasion rate was linked to drought intensified by water diversion interacting with a ready source of colonizers in the ballast water of international shipping traffic (Winder *et al.* 2011, Fig. 2, p. 4). After the mid-1990s, the invasion rate slowed down likely due in part to new ballast water regulations (Winder *et al*. 2011, p. 7).

The overbite clam, which substantially impacted the food web (see Current Condition), was the most important ecosystem engineer introduced during the period of accelerated biological invasions of the estuary (Brown et al. 2016, pp. 8–9). Cohen and Carlton (1998, pp. 556–557) theorized that the Estuary's favorable transport vectors, depauperate and relatively young biota, and anthropogenic alterations and disturbances made the estuary especially vulnerable to invasions. Here, we consider the effect that existing invasive species will have moving forward. It is likely that additional nonnative species will be introduced to the estuary, but attempting to guess what those species will be, what order they will arrive, and what impacts they could have is far too speculative to be useful here.

There are few biomass-dominant native fish species left in the San Francisco Estuary. Some examples include marine forage fishes like northern anchovy and Pacific herring (Kimmerer 2006, p. 209; Grimaldo *et al.* 2020, p. 3). Another socially important example is Chinook salmon which only remain common due to the considerable subsidy provided by Central Valley fish hatcheries (Sturrock *et al*. 2018, entire). Currently, much of the biomass of the San Francisco Estuary is dominated by species that are not native to it (Matern *et al*. 2002, Fig. 2, p. 804; Nobriga *et al.* 2005, pp. 780–781; Cohen and Bollens 2008, p. 245; Kratina *et al*. 2014, entire). High biomass non-native species include the overbite clam, most of the relatively abundant freshwater and low-salinity epibenthic and planktonic crustaceans, striped bass, various species of gobies, Mississippi silverside, and American and threadfin shad. Nonnative fishes of the family Centrarchidae are also abundant in the legal Delta and its watershed (Mahardja *et al*. 2017, Fig. 2, p. 8).

The biomass dominant planktonic invertebrates of the estuary's low-salinity habitats include several species that invaded after the overbite clam decimated historically abundant taxa, suggesting that its grazing pressure opened niche space that could be filled by novel species that had some kind of life-history workaround to the clam's grazing pressure. The best studied example is the copepod *Pseudodiaptomus forbesi* which is subject to intense grazing pressure in the low-salinity zone (Kimmerer *et al*. 2019, Fig. 6, p. 227). This copepod remains a seasonally dominant species however because its reproductive center is in the Delta upstream of immediate overbite clam grazing pressure (Kimmerer *et al*. 2019, p. 234).

Further downstream, trophic cascades in San Francisco Bay have also been reported to occur as likely effects of changes in community predation pressure on overbite clams (Cloern *et al*. 2007, Fig. 3 and

elsewhere on p. 18563). These limits and oscillations of which species can persist given grazing pressure from overbite clams can be expected to continue into the future. The population-level grazing pressure exerted by overbite clams is tied to seasonally warming temperature (Kimmerer and Thompson 2014, p. 1206). Thus, a warming climate can be expected to result in an increase in the fraction of each year that overbite clam grazing will impact the food web that supports the Bay-Delta DPS of longfin smelt. It is reasonable to expect this will have negative consequences for longfin smelt if it cannot be mitigated.

We detailed elsewhere in this chapter how the future expected condition is a generally warmer and often drier estuary except for predictions of higher average winter flows and flood risks. The nonnative species that dominate the estuary's current fish fauna are for the most part species that are well-adapted to warm water. They are also species that begin their reproductive seasons later than the remnant native fish community (e.g., Meng and Matern 2001, Fig. 7, p. 760; Grimaldo *et al*. 2004, Fig. 6, p. 91). Most of these biomass-dominant nonnative fishes start spawning in the late spring and have reproductive seasons that continue into the summer or fall. This pattern is an indication that current ecological conditions better support a later reproductive season than the ancestral estuary did. Thus, it is logical to expect that generally warmer and drier conditions will further favor the nonnative species life histories and disfavor native species life histories where (e.g., longfin smelt) reproductive timing and early life are related to historical peak freshwater flow seasons. It is important to understand that increasing biomass dominance of warmwater nonnative fishes and higher frequency of poor recruitment years for longfin smelt are a likely outcome of a warmer and drier climate whether or not nonnative species have important direct interactions with longfin smelt (e.g., competition or predation).

4.4. Future DPS Viability Under Our Risk Profile

Climate change is likely to have a substantial impact on the San Francisco Estuary, and thus on longfin smelt. This impact is anticipated to accelerate into the future. As a cooler-water species, the Bay Delta DPS is already experiencing seasonal habitat conditions with water temperatures above its physiological tolerance, which may be exerting downward pressure on the DPS. Both RCP 4.5 and 8.5 global warming scenarios project significant water temperature increases in the Suisun Bay and the Delta, thus potentially rendering certain regions inhospitable for the fish not only during summer, but throughout the year. By 2090, it is projected that there will no longer be any areas below 12°C for larval rearing, which could result in extirpation. In addition, the spawning window, which likely occurs when water temperatures are below 14°C, could be shortened, thus reducing reproductive success.

Climate change is also projected to alter the San Francisco Estuary's hydrology under both the RCP 4.5 and 8.5 scenarios. Warmer winter weather, coupled with increased precipitation in the form of rain, reduces snowpack which will likely result in more extreme flows from January-March, followed by a sharp cut off from April onward. Longfin smelt productivity could benefit from the favorable flows earlier in the season, but the steep drop-off beginning in April could induce dry year-like conditions, thus potentially rendering many of the formerly suitable habitats for larval rearing no longer hospitable. The current impaired April-June flows are already insufficient for longfin smelt productivity, and projected further declines will likely negatively impact the Bay-Delta DPS.

In addition to changes in hydrology, the proportions of WY types are projected to change in the future with a greater frequency of dry years under the RCP 8.5 scenario as well as critically dry years under both RCP 4.5 and 8.5 scenarios. In the past, longfin smelt exhibited poor survival and reproduction during droughts. If patterns in productivity that were observed in recent droughts are an indicator of patterns in future droughts, the projected increased frequency of consecutive dry years and drought under both scenarios would hamper species productivity. Furthermore, the DPS is not expected to exhibit resiliency to bounce back from droughts as they did historically (i.e., prior to the POD and the overbite clam invasion) because of their depleted abundance and food supply. Thus, the projected increased frequency of dry and critically dry years will likely cause further declines in the species productivity and increase the probability of extirpation.

Climate change is also expected to cause considerable sea level rise in the San Francisco Estuary under both the RCP 4.5 and 8.5 scenarios. The resulting sea level rise could lead to more open water and less marsh habitat for longfin smelt rearing. A further consequence of sea level rise is that if salinity intrusion moves the position of X2 eastward, it would reduce spawning and rearing habitat in the Delta. Although salinity intrusion can be mitigated through management actions such as reservoir storage releases, the system would likely continue to be vulnerable during dry years and particularly drought. Further, increased water demand during all year types would functionally further reduce flows in the system. Thus, the projected increased frequency of dry years, coupled with sea level rise under both scenarios, could be catastrophic for the Bay-Delta DPS in light of the relationship between abundance and flow as well as the need to spawn and rear in fresher water environments.

The San Francisco Estuary is one the world's most invaded estuaries, and invasions have increased over time. Invasive species have rarely had a positive impact on the Bay-Delta DPS. The first step decline in abundance was likely caused by the exotic overbite clam, which decimated the food web. Other exotic species have induced additional predation pressure and competition for the population. The San Francisco Estuary will likely experience further invasions in the future, some of which may negatively affect longfin smelt. An invasion into the San Francisco Estuary could also have a similar effect on the already impaired food web.

In Table 4.4, following, we summarize how we anticipate future environmental conditions will impact the risk profile to the Bay-Delta DPS under our scenario planning.

Table 4.4: Future environmental factors and their potential to change the risk profile for the Bay-Delta DPS. Color coding signifies: Red = A significant increase in the magnitude and/or frequency this factor will reduce survival, growth, or reproduction; Yellow = An appreciable increase risk from this driver, and/or a less certain magnitude of influence/mechanism of action; Green = A significant decrease in risk (benefit to the DPS); Gray = An uncertain effect.

Factor	Effect	Potential mechanisms of response(s)	Changes to Magnitude of Risk
Climate Change: SFE warming	Less days <12°C	Larval extirpation in regions = Rearing Habitat Loss	Substantial increase
	Less days <14°C	Constricted spawning window; spawn earlier = Spawning and rearing habitat loss	Moderate increase
	Less days <22°C	Reduced adult habitability; exit the Delta sooner = potential added physiological stress/predation risk, habitat loss(?)	Moderate increase
Climate Change: Altered Annual Hydrograph	Extreme freshwater flow from Jan-March Steep drop off in flow from April-July	Extensive favorable conditions for larvae = spawning and rearing habitat increase	Significant Decrease
		Dry-like conditions reducing productivity = reduced growth and survival	Substantial Increase
Climate Change: Projected WY types or Realized Outflow	Increased frequency of dry years	Reduced productivity = reduced abundance and rebound	Substantial increase
Climate Change: Sea level rise	Loss of tidal marshes, Salinity intrusion	Spawning Habitat Loss	Moderate increase
		Constricted habitat upstream, reduced fitness	Substantial increase
Invasive species	Competition	Reduced food supply	Potentially catastrophic
	Predation	Increased predation stress	Uncertain

Chapter 5 – Conclusion

In our Current Condition evaluation from Chapter 3, we evaluated the status of the Bay-Delta DPS under the framework of the 3 Rs, and indicated we believe that of these, population resilience is the driving consideration for risk evaluation (because redundancy is extremely low, and representation is also believed to be low). We presented abundance index data through time, using multiple available long-term monitoring surveys, and we discussed the extant stressors and how we understand they are limiting the population growth rates. We then evaluated those rates, as indicated through the varied and extensive field-monitoring data, in a simplified, and then a more sophisticated age-structured PVA and were able to quantify the risk profile under a "baseline" scenario which effectively is assuming forward through time, that historical abundance trends and stressors will continue at the same magnitude and frequency.

This Current Condition analysis documented that field survey data indicate that Bay-Delta DPS numbers have declined substantially over time, with abundance indices over the past decade being the lowest on record. We discussed the Bay-Delta DPS resilience in light of historically, and currently extant stressors and their postulated mechanisms of impact. Our meta-analysis based on mean population growth rates and using our baseline scenario (no changes from historically observed conditions or indices moving forward) indicated that the probability of quasi-extinction for the Bay-Delta DPS exceeds 20% for all survey time series over the next five years and reaches 50% by 2040. Applying the same assumptions over a longer time horizon (i.e., 2050–2065), the suite of surveys predicts that the probability of extinction for the Bay-Delta DPS under current conditions is roughly 50-80%. Our age-structured vital rates PVA tested four age-specific abundance thresholds for quasi-extinction risk, and showed a substantial risk of extinction even at low threshold values. For example, using the 10 percent quantile of abundance estimates as the threshold, approximately a 60% of simulations reached extinction by 2050. Both the 5 and 10 percent quantile lines also meet Lindley *et al*.'s (2007, Table 1, p. 4) criteria for high risk of extinction (20% probability over two decades). The most conservative threshold (statistically-conservative, but highest modeled DPS risk tolerance) used in our Age-Structured PVA meets Lindley et al.'s criteria for moderate risk of extinction (>5% over 100 years).

Our Future Condition scenario planning and analyses for the Bay-Delta DPS from Chapter 4, predicted that declines in population-wide abundance will continue into the foreseeable future under both the RCP 4.5 and 8.5 scenarios. We identified substantial increased population stress imposed by climate change through several mechanisms of impact. These projected changes in the San Francisco Estuary resulting from climate change (and the potential for future invaders) are likely to significantly exacerbate the negative influence of numerous stressors on the Bay-Delta DPS' abundance.

Literature Cited

Ahrens, R.N.M, Walters, C.J. and Christensen, V. 2012. Foraging arena theory. Fish and Fisheries 13:41–59.

Andrews, S.W., Gross, E.S. and Hutton, P.H. 2016. A water balance model to estimate flow through the Old and Middle River corridor. San Francisco Estuary and Watershed Science 14(2): *http://dx.doi.org/10.15447/sfews.2016v14iss2art2*

Andrews, S.W., Gross, E.S. and Hutton, P.H. 2017. Modeling salt intrusion in the San Francisco Estuary prior to anthropogenic influence. Continental Shelf Research, 146, pp. 58–81.

Barros, A., Lewis, L., Willmes, M., Parker, C., Bisson, M. and Hobbs, J. 2019. Larval and Juvenile Longfin Smelt Feeding in Restored Tidal Habitats. Final Report for Award F18AC00058 to the U.S. Fish and Wildlife Service.

Barros, A., Hobbs, J.A., Willmes, M., Parker, C.M., Bisson, M., Fangue, N.A., Rypel, A.L. and Lewis, L.S. 2022. Spatial heterogeneity in prey availability, feeding success, and dietary selectivity for the threatened longfin smelt. Estuaries and Coasts: In press, *https://doi.org/10.1007/s12237-021-01024-y*

Bashevkin, S.M. and Barros, A. 2021. deltamapr: Spatial Data for the Bay-Delta. R package version 1.0.0. Available at *https://github.com/InteragencyEcologicalProgram/deltamapr*

Baxter, R. D. 1999. Osmeridae in J. Orsi, editor. Report on the 1980–1995 fish, shrimp and crab sampling in the San Francisco Estuary. Interagency Ecological Program for the Sacramento-San Joaquin Estuary Technical Report 63. Pages 179–216.

Baxter, R. 2016. Personal Communications between Randy Baxter of the California Department of Fish and Game and C. Grant of the USFWS regarding longfin smelt spawning temperatures. May 16, 2016.

Baxter, R. 2016. Longfin Smelt Life History in the San Francisco Estuary. California Department of Fish and Wildlife, presentation, 27 slides.

Baxter, R. 2021. Personal Communications between Randy Baxter of the California Department of Fish and Game and E. Chen of the USFWS regarding longfin smelt catch data analyses. October 5, 2021.

Baxter, R. 2022. Personal Communications between Randy Baxter of the California Department of Fish and Game and E. Chen of the USFWS

Baxter, R., Breuer, R., Brown, L, Conrad, L, Feyrer, F., Fong, S., Gehrts, K., Grimaldo, L., Herbold, B., Hrodey, P., Mueller-Solger, A., Sommer, T. and K. Souza. 2010. Interagency Ecological Program 2010 Pelagic organism decline work plan and synthesis of results through August 2010. Interagency Ecological Program for the San Francisco Estuary. 125 pages.

The Bay Institute. 1998. From the Sierra to the Sea: The Ecological History of the San Francisco Bay-Delta Watershed. Chapter 4: 29 pp.

Beever, E.A., O'Leary, J., Mengelt, C., West, J.M., Julius, S., Green, N., Magness, D., Petes, L., Stein, B., Nicotra, A.B. and Hellmann, J.J. 2016. Improving conservation outcomes with a new paradigm for understanding species' fundamental and realized adaptive capacity. Conservation Letters 9:131–137.

Bennett, W.A., Kimmerer, W.J. and Burau, J.R. 2002. Plasticity in vertical migration by native and exotic estuarine fishes in a dynamic low-salinity zone. Limnology and Oceanography, 47(5), pp. 1496–1507.

Bever, A.J., Mac Williams, M.L. and Fullerton, D.K. 2018. Influence of an observed decadal decline in wind speed on turbidity in the San Francisco Estuary. Estuaries and Coasts 41:1943–1967.

Bever, A.J., Mac Williams, M.L., Herbold, B., Brown, L.R. and Feyrer, F.V. 2016. Linking hydrodynamic complexity to Delta Smelt (*Hypomesus transpacificus*) distribution in the San Francisco Estuary, USA. San Francisco Estuary and Watershed Science, 14(1).

Bouley, P. and Kimmerer, W.J. 2006. Ecology of a highly abundant, introduced cyclopoid copepod in a temperate estuary. Marine Ecology Progress Series, 324, pp. 219–228.

Brander, S.M., He, G., Smalling, K.L., Denison, M.S. and Cherr G.N. 2012. The in vivo estrogenic and in vitro anti-estrogenic activity of permethrin and bifenthrin. Environmental Toxicology and Chemistry 31:2848–2855.

Brandl, S., Schreier, B., Conrad, J.L., May, B. and Baerwald, M. 2021. Enumerating Predation on Chinook Salmon, Delta Smelt and other San Francisco Estuary Fishes using Genetics. North American Journal of Fisheries Management.

Bromirski, P.D., Miller, A.J., Flick, R.E. and Auad, G. 2011. Dynamical suppression of sea level rise along the Pacific coast of North America: Indications for imminent acceleration. Journal of Geophysical Research: Oceans, 116(C7).

Brown, L.R., Kimmerer, W., Conrad, J.L., Lesmeister, S. and Mueller–Solger, A. 2016a. Food Webs of the Delta, Suisun Bay, and Suisun Marsh: An Update on Current Understanding and Possibilities for Management. San Francisco Estuary and Watershed Science, 14(3).

Brown, L.R., Komoroske, L.M., Wagner, R.W., Morgan-King, T., May, J.T., Connon, R.E. and Fangue, N.A. 2016b. Coupled downscaled climate models and ecophysiological metrics forecast habitat compression for an endangered estuarine fish. PloS one, 11(1), p.e0146724.

Brown, L.R. and D. Michniuk. 2007. Littoral Fish Assemblages of the Alien-dominated Sacramento San Joaquin Delta, California, 1980–1983 and 2001–2003 Estuaries and Coasts Vol. 30, No. 1, p. 186–200.

Buffington, K.J., Janousek, C.N., Dugger, B.D., Callaway, J.C., Schile-Beers, L.M., Borgnis Sloane, E. and Thorne, K.M. 2021. Incorporation of uncertainty to improve projections of tidal wetland elevation and carbon accumulation with sea-level rise. Plos one, 16(10), p.e0256707.

Burdi, C. 2022. Personal Communications between C. Burdi of CDFW and E. Chen of the USFWS regarding longfin smelt diet and the CDFW unpub Diet Study data. March 21, 2022.

Buzby, N., D. Lin, and R. Sutton. 2020. Neonicotinoids and Their Degradates in San Francisco Bay Water. San Francisco Estuary Institute (SFEI), Richmond, CA. Contribution #1002. 26 pp.

California Data Exchange Center [CDEC]. 2020. Hydrologic and Climate Data Information Portal. California Department of Water Resources. Accessed 5/18/2022. *https://cdec.water.gov*

[CDFW] California Department of Fish and Wildlife. 2009a. Report to the Fish and Game Commission: A Status Review of the Longfin Smelt (*Spirinchus thaleichthys*) In California.

_____. 2009b. Effects Analysis: State Water Project Effects on Longfin Smelt. Randall D. Baxter, M. Nobriga, S. Slater and R. Fujimura.

_____. 2009c. Longfin Smelt Incidental Take Permit No. 2081-2009-001-03, SWP. 20 pp.

_____. 2020. Effects analysis: State Water Project effects on longfin smelt and delta smelt. *https://wildlife.ca.gov/Search-Results?q=longfin%20smelt#gsc.tab=0&gsc.q=longfin%20smelt&gsc.page=1*

_____. 2021a. Bay-Delta Studies and Surveys. Available online at *https://wildlife.ca.gov/Conservation/Delta*

_____. 2021b. Natural Resources Damage Assessment (NRDA) and Restoration. Available at *https://wildlife.ca.gov/OSPR/NRDA*

[CDPR] California Department of Pesticide Regulation. 2020. Pesticide use data for 2000–2018: Sacramento, California Department of Pesticide Regulation, accessed June 8, 2020.

California Department of Water Resources [DWR]. 2007. Morrow Island Distribution System fish entrainment study. Interim data summary report, Division of Environmental Services, Sacramento, CA.

_____. 2020. Chronological Reconstructed Sacramento and San Joaquin Valley Water Year Hydrologic Classification Indices. Accessed: May 16, 2022. https://cdec.water.ca.gov/reportapp/javareports?name=WSIHIST.

Carlton, J.T., Thompson, J.K., Schemel, L.E. and Nichols, F.H. 1990. Remarkable invasion of San Francisco Bay (California, USA) by the Asian clam *Potamocorbula amurensis*. I. Introduction and dispersal. Marine Ecology Progress Series, pp. 81–94.

Central & Northern California Ocean Observing System [CeNCOOS]. 2022. Ocean and Coastline Data Information Portal. Accessed 5/18/2022. *https://data.cencoos.org*

Chigbu, P. and T.H. Sibley. 1994. Relationship between abundance, growth, egg size and fecundity in a landlocked population of longfin smelt, *Spirinchus thaleichthys*. Journal of Fish Biology. 45:1–15.

Chigbu P., Sibley, T.H., and Beauchamp, D.A. 1998. Abundance and Distribution of *Neomysis mercedis* and a major predator, longfin smelt (*Spirinchus thaleichthys*) in Lake Washington. Hydrobiologia 386: 167–182, 1998.

Christian-Smith, J., Heberger, M. and Allen, L. 2012. Urban water demand in California to 2100: Incorporating climate change. Pacific Institute.

Chua V.P., and Xu M. 2014. Impacts of sea-level rise on estuarine circulation: an idealized estuary and San Francisco Bay. J Mar Sys 139:58–67.

City of San Francisco. 1984. Ocean Outfall Monitoring Program Report: October 1982 to June 1984. Prepared by the Bureau of Water Pollution Control and CH2M Hill. 64 pp.

City of San Francisco. 1985. Ocean Outfall Monitoring Program 1983–1984 Annual Report. Prepared by the Bureau of Water Pollution Control and CH2M Hill. 127 pp.

Cloern, J.E. and Jassby, A.D. 2012. Drivers of change in estuarine-coastal ecosystems: Discoveries from four decades of study in San Francisco Bay. Reviews of Geophysics, 50(4).

Cloern, J.E., Jassby, A.D., Thompson, J.K., and Hieb, K.A. 2007. A cold phase of the East Pacific triggers new phytoplankton blooms in San Francisco Bay. Proceedings of the National Academy of Science 104(47):18561–18565.

Cohen, A.N. and Carlton, J.T. 1998. Accelerating invasion rate in a highly invaded estuary. Science, 279(5350), pp. 555–558.

Cohen, S.E. and Bollens, S.M. 2008. Diet and growth of non-native Mississippi silversides and yellowfin gobies in restored and natural wetlands in the San Francisco Estuary. Marine Ecology Progress Series 368:241–254.

Cole, B.J., Brander, S.M., Jeffries, J.M., Hasenbein, S., He, G., Denison, M.S., Fangue, N.A. and Connon, R.E.. 2016. Changes in *Menidia beryllina* gene expression and in vitro hormone-receptor activation after exposure to estuarine waters near treated wastewater outfalls. Archives of Environmental Contamination and Toxicology 71: 210–223.

Connon R.E., J. Geist, J. Pfeiff, A.V. Loguinov,L.S. D'Abronzo, H. Wintz, C.D. Vulpe, and I. Werner. 2009. Linking mechanistic and behavioral responses to sublethal esfenvalerate exposure in the endangered delta smelt; *Hypomesus transpacificus* (Fam. Osmeridae). BMC Genomics 10:608

Connon R.E., S. Beggel, L.S. D'Abronzo, J.P. Geist, J. Pfeiff, A.V. Loguinov, C.D. Vulpe, and I. Werner. 2011. Linking molecular biomarkers with higher level condition indicators to identify effects of copper exposures on the endangered delta smelt (*Hypomesus transpacificus*). Environ Toxicol Chem 30:290–300.

Connor, M.S., J.A. Davis, J. Leatherbarrow, B.K. Greenfield, A. Gunther, D. Hardin, T. Mumley, J.J. Oram, and C. Werme. 2007. The slow recovery of San Francisco Bay from the legacy of organochlorine pesticides. Environmental Research 105 (2007) 87–100.

Cook, E.R., Seager, R., Heim Jr, R.R., Vose, R.S., Herweijer, C. and Woodhouse, C. 2009. Megadroughts in North America: Placing IPCC projections of hydroclimatic change in a long-term palaeoclimate context. Journal of Quaternary Science, 25(1), pp. 48–61.

DeConto, R.M. and Pollard, D. 2016. Contribution of Antarctica to past and future sea-level rise. Nature, 531(7596), pp. 591–597.

DeCourten, B.M. and Brander, S.M. 2017. Combined effects of increased temperature and endocrine disrupting pollutants on sex determination, survival, and development across generations. Scientific Reports 7:9310.

Dege, M. and L.R. Brown. 2004. Effect of Outflow on Spring and Summertime Distribution and Abundance of Larval and Juvenile Fishes in the Upper San Francisco Estuary. American Fisheries Society Symposium 39 (49–65).

Delta Stewardship Council (DSC). 2021. Delta Adapts: Creating a Climate Resilient Future. Sacramento–San Joaquin Delta Climate Change Vulnerability Assessment. June 2021.

Deverel, S.J., Dore, S. and Schmutte, C. 2020. Solutions for subsidence in the California Delta, USA, an extreme example of organic-soil drainage gone awry. Proceedings of the International Association of Hydrological Sciences, 382, pp. 837–842.

Dryfoos, R. L. 1965. The Life History and Ecology of the Longfin Smelt in Lake Washington. University of Washington, Thesis. Submitted May 20, 1965. pp. 42.

Eakin, M. 2021. Assessing the distribution and abundance of larval Longfin Smelt: What can a larval monitoring program tell us about the distribution of a rare species? California Fish and Wildlife Special CESA Issue:189–202; 2021.

Eschmeyer, W.N. and Herald, E.S. 1983. The Peterson field guide series. A Field guide to Pacific Coast fishes of North America: from the Gulf of Alaska to Baja, California. Houghton Mifflin, Boston. 384 pages.

Feyrer, F., Cloern, J.E., Brown, L.R., Fish, M.A., Hieb, K.A. and Baxter, R.D. 2015. Estuarine fish communities respond to climate variability over both river and ocean basins. Global Change Biology 21:3608–3619.

Feyrer, F. and M.P. Healey. 2003. Fish community structure and environmental correlates in the highly altered southern Sacramento-San Joaquin Delta. Environmental Biology of Fishes, 66(2), pp. 123–132.

Feyrer, F., Herbold, B., Matern, S.A. and Moyle, P.B. 2003. Dietary shifts in a stressed fish assemblage: consequences of a bivalve invasion in the San Francisco Estuary. Environmental Biology of Fishes, 67(3), pp. 277–288.

Foden, W.B. and Young, B.E. 2016. IUCN SSC guidelines for assessing species' vulnerability to climate change. Cambridge, England and Gland, Switzerland: IUCN.

Fong, S., Louie, S., Werner, I., Davis, J. and Connon, R.E. 2016. Contaminant effects on California Bay–Delta species and human health. San Francisco Estuary and Watershed Science, 14(4).

Fountain, H. 2015. In California, a Wet Era May Be Ending. New York Times, published on April 13, 2015. Available at *www.nytimes.com/2015/04/14/science/californias-history-of-drought-repeats.html*

Ganguly, A.R., Steinhaeuser, K., Erickson, D.J., Branstetter, M., Parish, E.S., Singh, N., Drake, J.B. and Buja, L. 2009. Higher trends but larger uncertainty and geographic variability in 21st century temperature and heat waves. Proceedings of the National Academy of Sciences, 106(37), pp. 15555–15559.

Garwood, R.S. 2017. Historic and contemporary distribution of longfin smelt (*Spirinchus thaleichthys*) along the California coast. California Fish and Game 103(3):96–117.

Glick, P., Stein, B.A. and Edelson, N.A., editors. 2011. Scanning the Conservation Horizon: A Guide to Climate Change Vulnerability Assessment. National Wildlife Federation, Washington, D.C. 176 pp.

Grimaldo, L.F., Miller, R.E., Peregrin, C.M., and Hymanson, Z.P. 2004. Spatial and temporal distribution of native and alien ichthyoplankton in three habitat types of the Sacramento-San Joaquin Delta. American Fisheries Society Symposium 39 (81–96).

Grimaldo, L.F., Sommer, T., Van Ark, N., Jones, G., Holland, E., Moyle, P.B., Herbold, B. and Smith, P. 2009. Factors affecting fish entrainment into massive water diversions in a tidal freshwater estuary: can fish losses be managed? North American Journal of Fisheries Management, 29(5), pp. 1253–1270.

Grimaldo, L.F., Feyrer, F., Burns, J. and D. Maniscalco. 2017. Sampling Uncharted Waters: Examining Rearing Habitat of Larval Longfin Smelt *(Spirinchus thaleichthys)* in the Upper San Francisco Estuary. Estuaries and Coasts, pp. 1–14.

Grimaldo, L., Burns, J., Miller, R.E., Kalmbach, A., Smith, A., Hassrick, J. and Brennan, C. 2020. Forage Fish Larvae Distribution and Habitat Use During Contrasting Years of Low and High Freshwater Flow in the San Francisco Estuary. San Francisco Estuary and Watershed Science, 18(3).

Gross, E.S., Hutton, P.H. and Draper, A.J. 2018. A Comparison of Outflow and Salt Intrusion in the Pre-Development and Contemporary San Francisco Estuary. San Francisco Estuary and Watershed Science, 16(3).

Hasenbein, M., Werner, I., Deanovic, L.A., Geist, J., Fritsch, E.B., Javidmehr, A., Foe, C., Fangue, N.A. and Connon R.E. 2014. Transcriptomic profiling permits the identification of pollutant sources and effects in ambient water samples. Science of the Total Environment 468:688–98.

Hausfather, Z. and Peters, G. 2020. Emissions – the 'business as usual' story is misleading. Nature 577, 618–620. *https://doi.org/10.1038/d41586-020-00177-3*

Hay, D. and McCarter, P.B. 2000. Status of the eulachon *Thaleichthys pacificus* in Canada. Canadian Stock Assessment Secretariat.

Hennessy, A. 2011. Double Whammy in the San Francisco Estuary: Smaller mysids and l Estuary: Smaller mysids and less of them. Poster for the IEP annual conference in March 2011.

Herren, J.R. and S. Kawasaki. 2001. Inventory of water diversions in four geographic areas in California's Central Valley. Contributions to the biology of Central Valley salmonids, Volume 2. R.L. Brown, Department of Fish and Game Fish Bulletin. 179: 343–355

Hieb, K., and R. Baxter. 1993. Delta outflow/San Francisco Bay. Pages 101–116 in P. L. Herrgesell, editor. 1991 Annual Report - Interagency Ecological Studies Program for the Sacramento-San Joaquin Estuary, Sacramento, California.

Hobbs, J.A., W.A. Bennett, and J.E. Burton. 2006. Assessing nursery habitat quality form native smelts (Osmeridae) in the low-salinity zone of the San Francisco estuary. Journal of Fish Biology 69: 907–922.

Hobbs, J.A., Lewis, L.S., Ikemiyagi, N., Sommer, T. and R.D. Baxter. 2010. The use of otolith strontium isotopes to identify nursery habitat for a threatened estuarine fish. Environmental Biology Fish 89 (557–569).

Hobbs, J., Lindberg, J., May B. and J. Israel. 2013. Interdisciplinary studies of Delta Smelt and Longfin Smelt in support of IEP's 2010 work plan for the Pelagic Organism Decline (otolith studies, laboratory culture development and genetics). Final Report for U.S. Bureau of Reclamation R10AC20108. 85 pages. DOI: 10.13140/RG.2.1.1635.6961

Hutton, P.H., Rath, J.S. and Roy, S.B. 2017. Freshwater flow to the San Francisco Bay-Delta estuary over nine decades (Part 1): Trend evaluation. Hydrological Processes, 31(14), pp. 2500–2515.

Hutton, P.H., Chen, L., Rath, J.S. and Roy, S.B. 2019. Tidally-averaged flows in the interior Sacramento-San Joaquin River Delta: trends and change attribution. Hydrological Processes 33(2):230–243.

Intergovernmental Panel on Climate Change (IPCC). 2013a. Annex III: Glossary [Planton, S. (ed.)]. *In:* Climate Change 2013: The Physical Science Basis. Contribution of Working Group I to the Fifth Assessment Report of the Intergovernmental Panel on Climate Change [Stocker, T.F., D. Qin, G.-K. Plattner, M. Tignor, S.K. Allen, J. Boschung, A. Nauels, Y. Xia, V. Bex and P.M. Midgley (eds.)]. Cambridge University Press, Cambridge, United Kingdom and New York, NY, USA.

_____. 2013b. Summary for Policymakers. In: Climate Change 2013: The Physical Science Basis. Contribution of Working Group I to the Fifth Assessment Report of the Intergovernmental Panel on Climate Change [Stocker, T.F., D. Qin, G.-K. Plattner, M. Tignor, S.K. Allen, J. Boschung, A. Nauels, Y. Xia, V. Bex and P.M. Midgley (eds.)]. Cambridge University Press, Cambridge, United Kingdom and New York, NY, USA.

_____. 2014. Summary for Policymakers. *In*: Climate Change 2014: Impacts, Adaptation, and Vulnerability. Part A: Global and Sectoral Aspects. Contribution of Working Group II to the Fifth Assessment Report of the Intergovernmental Panel on Climate Change [Field, C.B., V.R. Barros, D.J. Dokken, K.J. Mach, M.D. Mastrandrea, T.E. Bilir, M. Chatterjee, K.L. Ebi, Y.O. Estrada, R.C. Genova, B. Girma, E.S. Kissel, A.N. Levy, S. MacCracken, P.R. Mastrandrea, and L.L. White (eds.)]. Cambridge University Press, Cambridge, United Kingdom and New York, NY, USA, pp. 1–32.

Israel, J.A., and May, B. 2010. Characterization and evaluation of polymorphic microsatellite markers in the anadromous fish *Spirinchus thaleichthys*. Conservation of Genetic Resources 2:227–230.

Jassby, A. D., Kimmerer, W.J., Monismith, S.G., Armor, C., Cloern, J.E., Powell, T.M., Schubel, J.R. and Vendlinski, T.J. 1995. Isohaline position as a habitat indicator for estuarine populations. Ecological Applications 5(1):272–289.

Jassby, A.D., Cloern, J.E. and Cole, B. 2002. Annual Primary Production: Patterns and Mechanisms of Change in a Nutrient-Rich Tidal Ecosystem. Limnology and Oceanography 47. 698–712. 10.4319/lo.2002.47.3.0698.

Jeffries, K.M., Brander, S.M., Britton, M.T., Fangue, N.A. and Connon, R.E. 2015a. Chronic exposures to low and high concentrations of Ibuprofen elicit different gene response patterns in a Euryhaline fish. Environmental Science and Pollution Research 22:17397–413.

Jeffries, K.M., Komoroske, L.M., Truong, J., Werner, I., Hasenbein, M., Hasenbein, S., Fangue, N.A. and Connon R.E. 2015b.The transcriptome-wide effects of exposure to a pyrethroid pesticide on the

critically endangered delta smelt (*Hypomesus transpacificus*). Endangered Species Research 28:43–60.

Jeffries, K.M., Connon, R.E., Davis, B.E., Komoroske, L.M., Britton, M.T., Sommer, T., Todgham, A.E. and Fangue, N.A. 2016. Effects of high temperatures on threatened estuarine fishes during periods of extreme drought. Journal of Experimental Biology, 219(11), pp. 1705–1716.

Johnson, M.L., Werner, I., Teh, S. and Loge, F. 2010. Evaluation of chemical, toxicological, and histopathologic data to determine their role in the pelagic organism decline. Final report to the California State Water Resources Control Board and Central Valley Regional Water Quality Control Board. University of California, Davis.

Kimmerer, W.J., Gartside, E. and Orsi, J.J. 1994. Predation by an introduced clam as the likely cause of substantial declines in zooplankton of San Francisco Bay. Marine ecology progress series, pp. 81–93.

Kimmerer, W.J. 2002a. Effects of freshwater flow on abundance of estuarine organisms: physical effects or trophic linkages? Marine Ecology Progress Series 243:39–55.

Kimmerer, W.J. 2002b. Physical, biological, and management responses to variable freshwater flow into the San Francisco Estuary. Estuaries 25(6B):1275–1290.

Kimmerer, W.J. 2004. Open Water Processes of the San Francisco Estuary: From Physical Forcing to Biological Responses. San Francisco Estuary and Watershed Science. 2 (1) Article 1.

Kimmerer, W.J. 2006. Response of anchovies dampens effects of the invasive bivalve *Corbula amurensis* on the San Francisco Estuary foodweb. Marine Ecology Progress Series 324:207–218.

Kimmerer, W.J. 2008. Losses of Sacramento River Chinook salmon and delta smelt to entrainment in water diversions in the Sacramento-San Joaquin Delta. San Francisco Estuary and Watershed Science 6(2): *https://doi.org/10.15447/sfews.2008v6iss2art2*

Kimmerer, W.J., Gross, E.S. and Mac Williams, M.L. 2009. Is the response of estuarine nekton to freshwater flow in the San Francisco Estuary explained by habitat volume? Estuaries and Coasts 32:375–389.

Kimmerer, W.J., Gross, E.S. and Mac Williams, M.L. 2014. Tidal migration and retention of estuarine zooplankton investigated using a particle-tracking model. Limnology and Oceanography, 59(3), pp. 901–916.

Kimmerer, W.J., Gross, E.S., Slaughter, A.M. and Durand, J.R. 2019. Spatial subsidies and mortality of an estuarine copepod using a box model. Estuaries and Coasts 42:218–236.

Kimmerer, J.W., and M. Nobriga. 2008. Investigating particle transport and fate in the Sacramento-San Joaquin Delta using a particle tracking model. San Francisco Estuary and Watershed Science, Vol. 6, Issue 1 Article 4.

Kimmerer, W.J. and Orsi, J.J. 1996. Changes in the Zooplankton of the San Francisco Bay Estuary Since the Introduction of the Clam *Potamocorbula amerensis*.

Kimmerer, W.J. and Thompson, J.K. 2014. Phytoplankton growth balanced by clam and zooplankton grazing and net transport into the low-salinity zone of the San Francisco Estuary. Estuaries and Coasts, 37(5), pp. 1202–1218.

Klosterhaus, S., R. Grace, M.C. Hamilton, D. Yee. 2013. Method validation and reconnaissance of pharmaceuticals, personal care products and alkylphenols in surface waters, sediments, and mussels in an urban estuary. Environ Int 54: 92–99.

Knowles, N. and Cayan, D.R. 2004. Elevational dependence of projected hydrologic changes in the San Francisco estuary and watershed. Climatic Change, 62(1), pp. 319–336.

Knowles, N., Cronkite-Ratcliff, C., Pierce, D.W., and Cayan, D.R. 2018. Projections of Unimpaired Flows, Storage, and Managed Flows for Climate Change Scenarios in the San Francisco Bay-Delta Watershed, California: U.S. Geological Survey data release, *https://doi.org/10.5066/P9BMMUEV*.

Knowles, N., Cronkite-Ratcliff, C., Pierce, D.W. and Cayan, D.R. 2018. Responses of unimpaired flows, storage, and managed flows to scenarios of climate change in the San Francisco Bay-Delta watershed. Water Resources Research, 54(10), pp. 7631–7650.

Knutson, A.C., Jr., and Orsi, J.J. 1983. Factors regulating abundance and distribution of the shrimp *Neomysis mercedis* in the Sacramento-San Joaquin estuary. Transactions of the American Fisheries Society 112:476–485.

Kopp, R.E., Horton, R.M., Little, C.M., Mitrovica, J.X., Oppenheimer, M., Rasmussen, D.J., Strauss, B.H. and Tebaldi, C. 2014. Probabilistic 21st and 22nd century sea-level projections at a global network of tide-gauge sites. Earth's future, 2(8), pp. 383–406.

Kratina, P., Mac Nally, R., Kimmerer, W.J., Thomson, J.R., and Winder, M. 2014. Human-induced biotic invasions and changes in plankton interaction networks. Journal of Applied Ecology 51:1066–1074.

Kuivila, K.M. and Hladik, M.L. 2008. Understanding the occurrence and transport of current-use pesticide in the San Francisco Estuary Watershed. San Francisco Estuary Watershed Science 6.

Largier, J.L. 1996. Hydrodynamic exchange between San Francisco Bay and the ocean: The role of ocean circulation and stratification. San Francisco Bay: The Ecosystem, pp. 69–104.

Latour, R.J., 2016. Explaining patterns of pelagic fish abundance in the Sacramento-San Joaquin Delta. Estuaries and Coasts 39:233–247.

Lehman, P.W. 2004. The Influence of Climate on Mechanistic Pathways that Affect Lower Food Web Production in Northern San Francisco Bay Estuary. Estuaries 27 (2) pp. 311–324.

Le Quéré, C., Raupach, M.R., Canadell, J.G., Marland, G., Bopp, L., Ciais, P., Conway, T.J., Doney, S.C., Feely, R.A., Foster, P. and Friedlingstein, P. 2009. Trends in the sources and sinks of carbon dioxide. Nature geoscience, 2(12), pp. 831–836.

Lester, N.P., Shuter, B.J. and Abrams, P.A. 2004. Interpreting the von Bertalanffy model of somatic growth in fishes: the cost of reproduction. Proc. R. Soc. Lond. B Biol. Sci. 271, 1625–1631. *https://doi.org/10.1098/rspb.2004.2778*

Lewis, L., Willmes, M., Denney, C., Parker, C., Bisson, M., Barros, A. and Hobbs, J. 2019. Interdisciplinary studies of Longfin Smelt in the San Francisco Bay Estuary. DOI: *10.13140/RG.2.2.12944.33280*

Lewis, L. S., Willmes, M., Barros, A., Crain, P. K. and Hobbs, J. A. 2019. Newly discovered spawning and recruitment of threatened Longfin Smelt in restored and under-explored tidal wetlands. Ecology 101(1), 2020, e02868, 4 pages.

Lewis, L.S., Willmes, M., Barros, A., Crain, P.K. and Hobbs, J.A. 2020. Silicon Valley's Threatened Longfin Smelt: Evidence of Spawning And Recruitment in A Restored Tidal Wetland. The Bulletin of the Ecological Society of America, 101(1), p.e01628. *https ://doi.org/10.1002/bes2.1628*

Lindley, S.T., Schick, R.S., Mora, E., Adams, P.B., Anderson, J.J., Greene, S., Hanson, C., May, B.P., McEwan, D.R., MacFarlane, R.B., Swanson, C. and Williams, J.G. 2007. Framework for assessing viability of threatened and endangered Chinook salmon and steelhead in the Sacramento-San Joaquin basin. San Francisco Estuary and Watershed Science 5(1): *https://doi.org/10.15447/sfews.2007v5iss1art4*

MacNally, R., Thomson, J.R., Kimmerer, W.J., Feyrer, F., Newman, K.B., Sih, A., Bennett, W.A., Brown, L., Fleishman, E., Culberson, S.D. and Castillo, G. 2010. Analysis of pelagic species decline in the upper San Francisco Estuary using multivariate autoregressive modeling. Ecological Applications 20(5):1417–1430.

MacWilliams, M.L. and Gross, E.S. 2010. UnTRIM San Francisco Bay–Delta Model sea level rise scenario modeling report. Delta Conservation Plan. Prepared for Science Applications International Corporation and the California Department of Water Resources. 562 p.

MacWilliams, M.L., Bever, A.J., Gross, E.S., Ketefian, G.S. and Kimmerer, W.J. 2015. Three-dimensional modeling of hydrodynamics and salinity in the San Francisco estuary: An evaluation of model accuracy, X2, and the low–salinity zone. San Francisco Estuary and Watershed Science, 13(1) *https://doi.org/10.15447/sfews.2015v13iss1art2.*

Mahardja, B., Farruggia, M.J., Schreier, B. and Sommer, T. 2017. Evidence of a shift in the littoral fish community of the Sacramento-San Joaquin Delta. PLOS one 12(1): e0170683. *doi:10.1371/journal.pone.0170683*

Mahardja, B., Tobias, V., Khanna, S., Mitchell, L., Lehman, P., Sommer, T., Brown, L., Culberson, S. and Conrad, J.L. 2021. Resistance and resilience of pelagic and littoral fishes to drought in the San Francisco Estuary. Ecological Applications, 31(2).

Mangal, M. and Tier, C. 1993. A simple direct method for finding persistence times of populations and application to conservation problems. Proceedings of the National Academy of Sciences of the USA 90:1083–1086.

Martin, K.L. and Swiderski, D.L. 2001. Beach spawning in fishes: phylogenetic tests of hypotheses. American Zoologist, 41(3), pp. 526–537.

Marvin-DiPasquale, M. and M.H. Cox. 2007. Legacy Mercury in Alviso Slough, South San Francisco Bay, California: Concentration, Speciation and Mobility: Menlo Park, CA , U.S. Geological Survey, Open-File Report number 2007-1240, 98 p.

Matern, S.A. and Brown, L.R. 2005. Invaders eating invaders: exploitation of novel alien prey by the alien shimofuri goby in the San Francisco Estuary, California. Biological Invasions, 7(3), pp. 497–507.

Matern, S.A., Moyle, P.B. and Pierce, L.C. 2002. Native and alien fishes in a California estuarine marsh: twenty-one years of changing assemblages. Transactions of the American Fisheries Society, 131(5), pp. 797–816.

Matthias, B. G., Ahrens, R. N. M., Allen, M. S., Lombardi-Carlson, L. A. and Fitzhugh, G. R. 2016. Comparison of growth models for sequential hermaphrodites by considering multi-phasic growth. Fisheries Research 179:67–75. *https://doi.org/10.1016/j.fishres.2016.02.006*

Maunder, M.N., Deriso, R.B., and Hanson, C.H. 2015. Use of state-space population dynamics models in hypothesis testing: advantages over simple log-linear regressions for modeling survival, illustrated with application to longfin smelt (*Spirinchus thaleichthys*). Fisheries Research 164(2015):102–111.

Merz, J.E., Bergman, P.S., Melgo, J.F. and Hamilton, S. 2013. Longfin smelt: spatial dynamics and ontogeny in the San Francisco Estuary, California. California Fish and Game 99(3):122–148.

McAllister, D.E. 1963. A Revision of the Smelt Family, Osmeridae. National Museum of Canada. Bulletin No. 191. Biological Series No. 71. Department of Northern Affairs and National Resources. Ottawa.

Meehl, G.A., Stocker, T.F., Collins, W.D., Friedlingstein, P., Gaye, A.T., Gregory, J.M., Kitoh, A., Knutti, R., Murphy, J.M., Noda, A., Raper, S.C.B., Watterson, I.G., Weaver, A.J. and Zhao, Z.C. 2007: Global Climate Projections. In: Climate Change 2007: The Physical Science Basis. Contribution of Working Group I to the Fourth Assessment Report of the Intergovernmental Panel on Climate Change [Solomon, S., D. Qin, M. Manning, Z. Chen, M. Marquis, K.B. Averyt, M. Tignor and H.L. Miller (eds.)]. Cambridge University Press, Cambridge, United Kingdom and New York, NY, USA.

Meng, L. and Matern, S. A. 2001. Native and introduced larval fishes of Suisun Marsh, California: the effects of freshwater outflow. Transactions American Fisheries Society 130:750–765.

Merz, J.E., Bergman, P.S., Melgo, J. F. and S. Hamilton. 2013. Longfin smelt: spatial dynamics and ontogeny in the San Francisco Estuary. California Fish and Game 99(3):122–148.

Michel, C.J., Smith, J.M., Demetras, N.J., Huff, D.D. and Hayes, S.A. 2018. Non-native fish predator density and molecular-based diet estimates suggest differing effects of predator species on juvenile salmon in the San Joaquin River, California. San Francisco Estuary and Watershed Science 16(4): *https://doi.org/10.15447/sfews.2018v16iss4art3*

Miller, D.J. and R.N. Lea. 1972. Guide to the Coastal Marine Fishes of California. The Resources Agency. department of Fish and Game. Fish Bulletin 157.

Miller, J. 2021. Longfin Smelt and Long Datasets. USFWS Directorate Fellowship Program final presentation. August 6, 2021.

Monismith, S.G., Kimmerer, W., Burau, J.R. and Stacey, M.T. 2002. Structure and flow-induced variability of the subtidal salinity field in northern San Francisco Bay. Journal of Physical Oceanography 32:3003–3019.

Morris, W.F. and Doak, D.F. 2002. Quantitative Conservation Biology: Theory and Practice of Population Viability Analysis. Sinauer Associates. Sunderland, Massachusetts.

Moschet, C., Lew, B.M., Hasenbein, S., Anumol, T. and Young, T.M. 2017. LC-and GC-QTOF-MS as complementary tools for a Comprehensive Micropollutant Analysis in Aquatic Systems. Environmental Science and Technology 51:1553–1561.

Mouginot, J., Rignot, E., Bjork, A. A., van den Broeke, M., Millan, R., Morlighem, M., Noel, B., Schuechl, B., and Wood, M. 2019. Forty-six years of Greenland Ice Sheet mass balance from 1972–2018. Proceedings of the National Academy of Science 116(19):9239–9244.

Moulton, L. L. 1970. The 1970 longfin smelt spawning run in Lake Washington with notes on egg development and changes in the population since 1964. Master's Thesis. University of Washington, Seattle, Washington. 84 pages.

Moulton, L.L., 1974. Abundance, growth, and spawning of the longfin smelt in Lake Washington. Transactions of the American Fisheries Society, 103(1), pp. 46–52.

Moyle, P.B. 2002. Inland Fishes of California (Revised and Expanded). University of California Press, Ltd. London, England. Pp. 146–150.

Moyle, P.B. 2010. Plantiffs' Notice of Motion and Motion to supplement the Administrative Record. August 9, 2010. Court Proceedings.

Moyle, P. B., and J. A. Israel. 2005. Untested assumptions: effectiveness of screening diversions for the conservation of fish populations. Fisheries 30(5):20–28.

[MTC] Metropolitan Transportation Commission. 2017. Plan Bay Area 2040, final. Adopted July 26, 2017 in collaboration with the Association of Bay Area Governments.

[NAS] National Academy of Sciences. 2012. Sea-Level Rise for the Coasts of California, Oregon, and Washington: Past, Present, and Future. The National Academies Press.

Nerem, R.S., Beckley, B.D., Fasullo, J.T., Hamlington, B.D., Masters, D. and Mitchum, G.T. 2018. Climate-change–driven accelerated sea-level rise detected in the altimeter era. Proceedings of the National Academy of Sciences, 115(9), pp. 2022–2025.

Nguyen, T., Eakin, M. and Hobbs, J. 2021. An exploration of environmental factors associated with Longfin Smelt spawning migration. Presentation for the USFWS Longfin Smelt Workshop, Session 1. August 27, 2021.

Nichols, F.H., J.E. Cloern, S.N. Luoma and Peterson, D.H. 1986. The Modification of an Estuary. Science. Volume 231: 567–573.

Nicotra, A.B., Beever, E.A., Robertson, A.L., Hofmann, G.E. and O'Leary, J. 2015. Assessing the components of adaptive capacity to improve conservation and management efforts under global change. Conservation Biology 29:1268–1278.

Nixon, S.W. 1998. Physical energy inputs and the comparative ecology of lake and marine ecosystem. Limnol. Oceanogr., 33(4, part 2), pp. 1005–1025.

Nobriga, M.L., Feyrer, F., Baxter, R.D. and M. Chotkowski. 2005. Fish community ecology in an altered river delta: spatial patterns in species composition, life history strategies, and biomass. Estuaries, 28(5), pp. 776–785.

Nobriga, M.L., Matica, Z. and Z.P. Hymanson. 2004. Evaluating Entrainment Vulnerability to Agricultural Irrigation Diversions: A Comparison among Open-Water Fishes. American Fisheries Society Symposium 39:281–295.

Nobriga, M.L. and Rosenfield, J.A. 2016. Population dynamics of an estuarine forage fish: disaggregating forces driving long-term decline of Longfin Smelt in California's San Francisco Estuary. Transactions of the American Fisheries Society, 145(1), pp. 44–58.

Nowak, G.M., Tabor, R.A., Warner, E.J., Fresh, K.L. and Quinn, T.P. 2004. Ontogenetic Shifts in Habitat and Diet of Cutthroat Trout in Lake Washington, Washington. North American Journal of Fisheries Management. 24:624–635.

Ocean Protection Council (OPC). 2018. State of California Sea-Level Rise Guidance. 2018 Update. California Natural Resources Agency.

Oppenheimer, M. and Alley, R.B. 2016. How high will the seas rise? Science, 354(6318), pp. 1375–1377.

Oregon Sea Grant. 2008. Aquatic Invasions! A menace to the West. Draft 2010 report and species guide.

Ottersen, G. and Loeng, H. 2000. Covariability in early growth and year-class strength of Barents Sea cod, haddock, and herring: the environmental link. ICES J. Mar. Sci. 57(2): 339–348. doi:10.1006/jmsc.1999.0529.

Pangle, K.L., Malinich, T.D., Bunnell, D.B., DeVries, D.R. and Ludsin, S.A. 2012. Context-dependent planktivory: interacting effects of turbidity and predation risk on adaptive foraging. Ecosphere 3(12):114. *http://dx.doi.org/10.1890/ES12-00224.1*

Peyronnet, A., Friedland, K.D., O'Maoileidigh, N., Manning, M., and Poole, W.R. 2007. Links between patterns of marine growth and survival of Atlantic salmon Salmo salar, L. J. Fish Biol. 71(3): 684–700. doi:10.1111/j.1095-8649.2007.01538.x.

Phillis, C., Fullerton, D., MacWilliams, M., Brandon, J. and Grimaldo, L. 2021. Mapping Longfin Smelt habitat in the San Francisco Estuary using a Boosted Regression Tree model. Presentation for the USFWS Longfin Smelt Workshop, Session 2. September 2, 2021.

Polade, S.D., Gershunov, A., Cayan, D.R., Dettinger, M.D. and Pierce, D.W. 2017. Precipitation in a warming world: Assessing projected hydro-climate changes in California and other Mediterranean climate regions. Scientific reports, 7(1), pp. 1–10.

Presser, T.S. and Ohlendorf, H.M. 1987. Biogeochemical cycling of selenium in the San Joaquin Valley, California, USA. Environmental Management, 11(6), pp. 805–821.

Prinn, R., Paltsev, S., Sokolov, A., Sarofim, M., Reilly, J. and Jacoby, H. 2011. Scenarios with MIT integrated global systems model: significant global warming regardless of different approaches. Climatic Change, 104(3–4), pp. 515–537.

Quinn, T.P., Sergeant, C.J., Beaudreau, A.H. and Beauchamp, D.A. 2012. Spatial and temporal patterns of vertical distribution for three planktivorous fishes in Lake Washington. *Ecology of Freshwater Fish*, 21(3), pp. 337–348.

Radtke, L.D. 1966. State of California: The Resource Agency Department of Fish and Game: Fish Bulletin 136. Ecological Studies of The Sacramento-San Joaquin Delta Part II: Fishes of The Delta. 20 pp.

Raupach, M.R., Marland, G., Ciais, P., Le Quéré, C., Canadell, J.G., Klepper, G. and Field, B. 2007. Global and regional drivers of accelerating CO2 emissions. Proceedings of the National Academy of Sciences of the United States of America. 104: 10288–10293

Redford, K.H., Amato, G., Baillie, J., Beldomenico, P., Bennett, E.L., Clum, N., Cook, R., Fonseca, G., Hedges, S., Launay, F. and Lieberman, S. 2011. What does it mean to successfully conserve a (vertebrate) species? BioScience, 61(1), pp. 39–48.

Reed, D.H. 2005. Relationship between population size and fitness. Conservation biology, 19(2), pp.563–568.

Reis, G.J., Howard, J.K. and Rosenfield, J.A. 2019. Clarifying Effects of Environmental Protections on Freshwater Flows to—and Water Exports from—the San Francisco Bay Estuary. San Francisco Estuary and Watershed Science, 17(1).

Richardson, R.B. and Loomis, J.B. 2004. Adaptive recreation planning and climate change: a contingent visitation approach. Ecological Economics, 50(1–2), pp. 83–99.

Rosenfield, J. A. and Baxter, R. D. 2007. Population dynamics and distribution patterns of longfin smelt in the San Francisco Estuary. Transactions American Fisheries Society 136:1577–1592.

Rosenfield, J.A. 2010. Life History Conceptual Model and Sub-Models. Longfin Smelt, San Francisco Estuary Population. Delta Regional Ecosystem Restoration Implementation Plan [DRERIP].

Rosenfield, J.A. and Lewis, L. 2021. Longfin Smelt Conceptual Model Overview. Presentation for the USFWS Longfin Smelt Workshop, Session 2. September 2, 2021.

Rowland, E.R., Cross, M.S. and Hartmann, H. 2014. Considering Multiple Futures: Scenario Planning to Address Uncertainty in Natural Resource Conservation. Washington, DC: U.S. Fish and Wildlife Service.

Roy, S.B., Chen, L., Girvetz, E.H., Maurer, E.P., Mills, W.B. and Grieb, T.M. 2012. Projecting water withdrawal and supply for future decades in the US under climate change scenarios. Environmental Science & Technology, 46(5), pp. 2545–2556.

Ruckert, K.L., Oddo, P.C., Keller, K. 2017. Impacts of representing sea level rise uncertainty on future flood risks: an example from San Francisco Bay. PLOS one 12(3): *https://doi.org/10.1371/journal.pone.0174666*

Ruhl, C.A., Schoellhamer, D.H., Stumpf, R.P., and Lindsay, C.L. 2001. Combined use of remote sensing and continuous monitoring to analyze the variability of suspended-sediment concentrations in San Francisco Bay, California. Estuarine, Coastal and Shelf Science 53:801–812.

Sağlam, I.K., J.A Hobbs, R. Baxter, L.S. Lewis, A. Benjamin, and A.J. Finger. 2021. Genome-wide analysis reveals regional patterns of drift, structure, and gene flow in longfin smelt (*Spirinchus thaleichthys*) in the northeastern Pacific. Canadian Journal of Fisheries and Aquatic Sciences, v.78 no.12, pp. 1793–1804.

Schwalm, C.R., Glendon, S. and Duffy, P.B. 2020. RCP8. 5 tracks cumulative CO2 emissions. Proceedings of the National Academy of Sciences, 117(33), pp. 19656–19657.

Schoellhamer, D.H. 2000. Influence of salinity, bottom topography, and tides on locations of estuarine turbidity maxima in northern San Francisco Bay. in McAnally, W.H. and Mehta, A.J., ed., Coastal and Estuarine Fine Sediment Transport Processes: Elsevier Science B.V., pp. 343–357.

Shaffer M.L. and B.A. Stein. 2000. Safeguarding our precious heritage. Pages. 301–321. in Stein BA, Kutner LS, Adams JS, eds. Precious Heritage: The Status of Biodiversity in the United States. Oxford (UK): Oxford University Press.

Sibley, T. and R. Brocksmith. 1995. Lower Cedar River Section 205 Longfin Smelt Study, Draft Final Report. Submitted to the U.S. Army Corps of Engineers, Seattle District on December 1, 1995.

Simonsen, M. 1977. The use of discriminate function analysis in the identification of two species of larval smelt, *Spirinchus thaleichthys* and *Hypomesus transpacificus*, in the Sacramento-San Joaquin Estuary, California. MS. University of the Pacific, Stockton, California. 54 pages.

Siegfried, L.J., Fleenor, W.E. and Lund, J.R. 2014. Physically-based modeling of Delta Island Consumptive Use: Fabian Tract and Staten Island, California. San Francisco Estuary and Watershed Science 12(4): *http://dx.doi.org/10.15447/sfews.2014v12iss4art2*

Slater, S.B. 2009. Feeding Patterns of Age-0 Pelagic Fishes in the Upper Estuary. Presentation to the IEP Workshop on June 25, 2009. 54 slides.

Smith, D.R., Allan, N.L., McGowan, C.P., Szymanski, J.A., Oetker, S.R., Bell, H.M. 2018. Development of a species status assessment process for decisions under the U.S. Endangered Species Act. Journal of Fish and Wildlife Management 9:1–19.

Sobczak, W.V., Cloern, J., Jassby, A., Cole, B., Schraga, T. and A. Arnsberg. 2005. Detritus fuels ecosystem metabolism but not metazoan food webs in San Francisco estuary's freshwater Delta. Estuaries, 28(1), pp. 124–137.

Solomon, S., D. Quin, M. Manning, R.B. Alley, T. Bernsten, N.L. Bindoff, Z. Chen, A. Chidthaison, J.M. Gregory, G.C. Hegerl, M. Heimann, B. Hewitson, B.J. Hoskins, F. Joos, J. Jouzel, V. Kattsov, U. Lohmann, T. Matsuno, M. Molina, N. Nicholls, J. Overpeck, G. Raga, V. Ramaswamy, J. Ren, M. Rusticucci, R. Comerville, T.F. Stocker, P. Whetton, R.A. Wood and D. Wratt. 2007. Technical Summary. In: Climate Change 2007: The Physical Science Basis. Contribution of Working Group I to the Fourth Assessment Report of the Intergovernmental Panel on Climate Change [Solomon, S., D. Quin, M. Manning, Z. Chen, M. Marquis, K.B. Averyt, M. Tignor and H.L. Miller (eds.)]. Cambridge University Press, Cambridge, United Kingdom and New York, NY, USA.

Sommer, T., Harrell, B., Nobriga, M., Brown, R., Moyle, P., Kimmerer, W. and Schemel, L. 2001. California's Yolo Bypass: Evidence that flood control can be compatible with fisheries, wetlands, wildlife, and agriculture. Fisheries, 26(8), pp. 6–16.

Sommer, T.R., Harrell, W.C., Mueller-Solger, A., Tom, B. and Kimmerer, W. 2004. Effects of flow variation on channel and floodplain biota and habitats of the Sacramento River, California, USA. Aquatic Conservation: Marine and Freshwater Ecosystems, 14(3), pp. 247–261.

Sommer, T., C. Armor, R. Baxter, R. Breuer, L. Brown, M. Chotkowski, S. Culberson, F. Freyer, M. Gingras, B. Herbold, W. Kimmerer, A. Mueller-Solger, M. Nobriga, K. Souza. 2007. The Collapse of Pelagic Fishes in the Upper San Francisco Estuary. Fisheries 32: 270–277.

Souza, K., K. Hieb, K. Fleming, M. Bryant and R. Baxter. 2006. Apparent growth rates of pelagic fishes and relationship to abundance. Interim Report on Pelagic Organism Decline Investigations. 9 pages.

Stacey, M.T., Burau, J.R., and Monismith, S.G. 2001. Creation of residual flows in a partially stratified estuary. Journal of Geophysical Research 106(C8):17013–17037.

Stanley, S. E., P. B. Moyle, and H. B. Shaffer. 1995. Allozyme analysis of delta smelt, *Hypomesus transpacificus* and longfin smelt, *Spirinchus thaleichthys* in the Sacramento-San Joaquin Estuary, California. Copeia 1995(2):390–396.

Stanton, E.A. and Fitzgerald, E. 2011. California Water Supply and Demand: Technical Report. Stockholm Environment Institute.

Stevens, D.E. 1977. Striped bass (Morone saxatilis) monitoring techniques in the Sacramento-San Joaquin estuary. Pages 91–109 in W. Van Winkle (Ed.), Assessing the effects of power plant-induced mortality on fish populations. Pergamon Press, New York.

Stevens, D.E., and L.W. Miller. 1983. Effects of river flow on abundance of young chinook salmon, American shad, longfin smelt, and delta smelt in the Sacramento-San Joaquin River System. North American Journal of Fisheries Management 3(4):425–437.

Stewart, A.R., Luoma, S.N., Schlekat, C.E., Doblin, M.A., and Hieb, K.A. 2004. Food Web pathway Determines How Selenium Affects Aquatic Ecosystems: A San Francisco Bay Case Study, Environmental Science and Technology, v. 38, no. 17, pp. 4519–4526.

Stillwater Sciences. 2006. Napa River fisheries monitoring program, Final Report 2005. U.S. Army Corps of Engineers, Sacramento, California.

Stine, S., 1994. Extreme and persistent drought in California and Patagonia during mediaeval time. Nature, 369(6481), pp. 546–549.

Stubben, C.J. and Milligan, B.G. 2007. Estimating and Analyzing Demographic Models Using the popbio Package in R. Journal of Statistical Software 22:11.

Sturrock, A.M., Satterthwaite, W.H., Cervantes-Yoshida, K.M., Huber, E.R., Sturrock, H.J.W., Nusslé, H.S., Carlson, S.M. 2018. Eight decades of hatchery salmon releases in the California Central Valley: factors influencing straying and resilience. Fisheries 44(9):433–444.

Sutton, R. M. Sedlak, J. Sun, and D. Lin. 2017. Contaminants of Emerging Concern in San Francisco Bay—A Strategy for Future Investigations 2017 Revision. San Francisco Estuary Institute. Regional Monitoring Program for Water Quality in San Francisco Bay. RMP Contribution #815. 75 pp.

Swain, D.L., D.E. Horton, D. Singh, and N.S. Diffenbaugh. 2016. Trends in atmospheric patterns conducive to seasonal precipitation and temperature extremes in California. Science Advances. April 1, 2016. Vol 2, issue 4. 13 pages.

Swain, D.L., Langenbrunner, B., Neelin, J.D., Hall, A. 2018. Increasing precipitation volatility in twenty-first-century California. Nature Climate Change 8:427–433.

[SWRCB] State Water Resources Control Board [SWRCB]. 2006. Water Quality Control Plan for the San Francisco Bay/Sacramento-San Joaquin Delta Estuary. December 13, 2006.

[SWRCB] 2008. Waste discharge requirements for the City of Stockton Regional Wastewater Control Facility San Joaquin County. October 23, 2008.

[SWRCB] State Water Resources Control Board. 2010. Transmittal of the 2010 Integrated Report [Clean Water Act Section 303(d) and Section 305(b)]. Letter to Alexis Strauss, USEPA, and four CDs of supporting materials, including the staff report, fact sheets, and responsiveness summary, dated October 11, 2010.

[SWRCB] State Water Resources Control Board. 2010b. Development of Flow Criteria for the Sacramento-San Joaquin Delta Ecosystem. Prepared Pursuant to the Sacramento-San Joaquin Delta Reform Act of 2009, dated August 3, 2010.

[SWRCB] State Water Resources Control Board. 2018. Water Quality Control Plan for the San Francisco Bay/Sacramento-San Joaquin Delta Estuary. December 12, 2018.

[SWRCB] State Water Resources Control Board [SWRCB]. 2019. Draft Initial Biological Goals for the Lower San Joaquin River. September 2019.

Tabor, R.A., Footen, B.A., Fresh, K.L., Celedonia, M.T., Mejia, F., Low, D.L. and Park, L. 2007. Smallmouth bass and largemouth bass predation on juvenile Chinook salmon and other salmonids in the Lake Washington basin. North American Journal of Fisheries Management, 27(4), pp. 1174–1188.

Tamburello, N., Connors, B.M., Fullerton, D., Phillis, C.C. 2018. Durability of environment-recruitment relationships in aquatic ecosystems: insights from long-term monitoring in a highly modified estuary and implications for management. Limnology and Oceanography 64(S1):S223–S239.

Tempel, T., Burns, J. 2021. The Longfin Smelt Spawning Window – Is it Clear Enough to See? Presentation for the USFWS Longfin Smelt Workshop, Session 1. August 27, 2021.

Tenera Environmental. 2011. Impingement and Entrainment Monitoring Reports for the Contra Costa and Pittsburg Generating Stations.

Thomson, J.R., W.J. Kimmerer, L.R. Brown, K.B Newman, R. Mac Nally, W.A. Bennett, F. Feyrer and E. Fleishman. 2010. Bayesian change point analysis of abundance trends for pelagic fishes in the upper San Francisco Estuary. Ecological Applications 20 (5). pp. 1431–1448.

Thorp, J.H. and Casper, A.F. 2002. Potential effects on zooplankton from species shifts in planktivorous mussels: a field experiment in the St Lawrence River. Freshwater Biology, 47(1), pp. 107–119.

Tigan, G. 2010. Personal Communications between G. Tigan of the UC Davis Fish Conservation and Culture Laboratory and R. Baxter of the California Department of Fish and Wildlife regarding longfin smelt incubation. February 10, 2010.

Tigan, G. 2015. Personal Communications between G. Tigan of the UC Davis Fish Conservation and Culture Laboratory and R. Baxter of the California Department of Fish and Wildlife regarding longfin smelt yolk-sac development. April 20, 2015.

Timpe, C. and M.J.J. Scheepers. 2003. A look into the Future Scenarios for Distributed Generation in Europe (ECN-C--04-012). Netherlands

Tobias, V. and Baxter, R. 2022. Fewer and Farther between: Changes in the Timing of Longfin Smelt (Spirinchus thaleichthys) Movements in the San Francisco Estuary. Preprints 2021, 2021010512 (doi: 10.20944/preprints202101.0512.v1).

[USBR] U.S. Bureau of Reclamation. 2011. SECURE water act section 9503(c) – Reclamation climate change and water 2011. U.S. Department of the Interior, Denver, CO. 206 pp

[USBR] U.S. Bureau of Reclamation. 2020. Record of Decision: Reinitiation of Consultation on the Coordinated Long-Term Modified Operations of the Central Valley Project and State Water Project. February 19, 2020.

[USFWS] U.S. Fish and Wildlife Service. 2016. USFWS species status assessment framework: an integrated analytical framework for conservation. Version 3.4, dated August 2016.

[USFWS] U.S. Fish and Wildlife Service. 2019. Biological Opinion for the Reinitiation of Consultation on the Coordinated Operations of the Central Valley Project and State Water Project. Service File No. 08FBTD00-2019-F-0164, dated October 21, 2019.

Utne-Palm, A.C. 2002. Visual feeding of fish in a turbid environment: physical and behavioural aspects. Marine and Freshwater Behaviour and Physiology, 35(1–2), pp. 111–128.

Vanderstukken, M., Declerck, S.A., Decaestecker, E. and Muylaert, K. 2014. Long-term allelopathic control of phytoplankton by the submerged macrophyte E lodea nuttallii. Freshwater Biology, 59(5), pp. 930–941.

Van Vuuren, D.P., Edmonds, J., Kainuma, M., Riahi, K., Thomson, A., Hibbard, K., Hurtt, G.C., Kram, T., Krey, V., Lamarque, J.F. and Masui, T. 2011. The representative concentration pathways: an overview. Climatic change, 109(1), pp. 5–31.

Vroom, J., Van der Wegen, M., Martyr-Koller, R.C. and Lucas, L.V. 2017. What determines water temperature dynamics in the San Francisco Bay-Delta system? Water Resources Research, 53(11), pp. 9901–9921.

Wagner, R.W., Stacey, M., Brown, L. and Dettinger, M. 2011. Statistical models of temperature in the Sacramento–San Joaquin Delta under climate-change scenarios and ecological implications. Estuaries and Coast: doi:10.1007/s12237-12010-19369-z.

Wall, G. 1998. Implications of Global Climate Change for Tourism and Recreation in Wetland Areas. Climatic Change 40, 371–389. *https://doi.org/10.1023/A:1005493625658*

Wang, J.C.S. 1986. Fishes of the Sacramento – San Joaquin Estuary and Adjacent Waters, California: A Guide to the Early Life Histories. Technical Report 9 January 1986. Interagency Ecological Study Program For the Sacramento-San Joaquin Estuary. 12 pages plus appendices.

Wang, J. C. S. 2007. Spawning, early life stages and early life histories of the Osmerids found in the Sacramento-San Joaquin Delta of California. U.S. Department of the Interior, Bureau of Reclamation, Mid-Pacific Region, Byron, California. Volume 38. 72 pages plus appendices.

Wells, B.K., Santora, J.A., Schroeder, I.D., Mantua, N., Sydeman, W.J., Huff, D.D. and Field, J.C. 2016. Marine ecosystem perspectives on Chinook salmon recruitment: a synthesis of empirical and modeling studies from a California upwelling system. Marine Ecology Progress Series, 552, pp. 271–284.

Whipple, A.A., Grossinger, R.M., Rankin, D., Stanford, B. and Askevold, R.A. 2012. Sacramento-San Joaquin Delta Historical Ecology Investigation: Exploring Pattern and Process. Prepared for the California Department of Fish and Game and Ecosystem Restoration Program. A Report of SFEI-ASC's Historical Ecology Program, Publication #672, San Francisco Estuary Institute-Aquatic Science Center, Richmond, CA.

Willi, Y., Van Buskirk, J. and Hoffmann, A.A. 2006. Limits to the adaptive potential of small populations. Annu. Rev. Ecol. Evol. Syst., 37, pp. 433–458.

Williams, A.P., Cook, B.I. and Smerdon, J.E. 2022. Rapid intensification of the emerging southwestern North American megadrought in 2020–2021. Nature Climate Change, pp. 1–3.

Wilson, T.S., Sleeter, B.M. and Cameron, D.R. 2016. Future land-use related water demand in California. Environmental Research Letters, 11(5), p.054018.

Winder, M., and Jassby, A.D. 2011. Shifts in zooplankton community structure: implications for food web processes in the upper San Francisco Estuary. Estuaries and Coasts 34:675–690.

Winder, M., Jassby, A.D., Mac Nally, R. 2011. Synergies between climate anomalies and hydrological modifications facilitate estuarine biotic invasions. Ecology Letters 14(8):749–757.

Wulff, M.L., Brown, L.R., Huntsman, B.M., Knowles, N., and Wagner, W. 2021. Data used in projected air and water temperatures for selected regions of the upper San Francisco Estuary and Yolo Bypass under 20 scenarios of climate change, U.S. Geological Survey data release, *https://doi.org/10.5066/P9CXGU44.*

Yanagitsuru, Y.R. 2020. Pers. comm. Presentation to the USFWS on the effect of turbidity on growth, feeding, and survival in Longfin Smelt larvae. Presented on June 11th, 2020.

Yanagitsuru, Y.R., Main, M.A., Lewis, L.S., Hobbs, J.A., Hung, T.C., Connon, R.E. and Fangue, N.A. 2021. Effects of temperature on hatching and growth performance of embryos and yolk-sac larvae of a threatened estuarine fish: Longfin smelt *(Spirinchus thaleichthys).* Aquaculture, 537, p. 736502.

Yanagitsuru, Y.R., Daza, I.Y., Lewis, L.S., Hobbs, J.A., Hung, T., Connon, R.E. and Fangue, N.A. 2022, in review. Effects of salinity on hatching and growth performance of embryos and yolk-sac larvae Longfin Smelt.

Appendix A: Summary of Survey Data Used in this SSA

With the exception of eggs, all longfin smelt life stages are collected by one or more of the current fish-monitoring surveys in the San Francisco Estuary. The following 6 long-term fish monitoring surveys currently capture longfin smelt larvae, juveniles, and adults. We use these surveys to determine trends, relative abundance, and to imply geographic distribution for longfin smelt for all age classes. Each of the surveys targets a specific component of the LFS population, while collectively, the information provides excellent data coverage for habitats utilized by juveniles and adult LFS. These surveys also provide information helpful to determine the changes in abundance and distribution over time.

Smelt Larval Survey (SLS)

The SLS was initiated in 2009 and samples for early-stage longfin smelt larvae biweekly January- March by using a single oblique tow per station in the Delta down to eastern San Pablo Bay. The original purpose of the SLS was to provide density and proximity information for larval longfin smelt in relation to the South Delta export facilities and density information within the species range under conditions of low Delta outflow. The primary limitation of the SLS is that it misses larvae hatching in December and April-May and excludes a significant portion of the larval habitat in San Pablo and the South San Francisco Bay and their tributaries (Grimaldo et al. 2020, Fig. 6, p. 10). However, as required by DFW's 2020 Incidental Take Permit, SLS will now cover the Napa River, and two surveys will now be conducted in December.

20-mm Survey: the 20-mm Survey was initiated in 1995 and samples biweekly from late March to early July using three oblique tows per station from the Delta to eastern San Pablo Bay and the Napa River. The original purpose of this survey was to provide density and proximity information for larval and small juvenile Delta Smelt in relation to the South Delta Export facilities as they neared sizes at which they would be counted in salvage. The 20-mm Survey's extended sampling period overlaps with the spawning and early life rearing of many species of fish, including longfin smelt, which has been one of the most commonly collected species (Mahardja et al. 2017, Table 1, p. 491). Like the SLS, a key limitation of the 20-mm Survey for longfin smelt is that it excludes most waters west of the Napa River (Mahardja et al. 2017, Fig. 1, p. 490). The survey's late-March initiation also means it misses sampling opportunities beginning in February, where some fish may be large enough to be regularly retained by the 20-mm fishing gear. Although, it is not clear if this data would further inform conservation or scientific interpretation in any meaningful way.

Fall Midwater Trawl (FMWT)

The FMWT was initiated in 1967 and has consistently sampled pelagic waters from the Delta into San Pablo Bay monthly from September-December by using 1 oblique tow per station in the water column up to a depth of 40 feet. In some years prior to 2002, the survey extended through March (CDFG 2009, p. 8 and CDFG 2009, Appendix A). Note that the FMWT has more than twice as many stations as other Interagency Ecological Program (IEP) surveys. The survey mostly collects juvenile to small-sized adult

fishes and decapod shrimps (50–150 mm). The original purpose of the FMWT was to determine if age-0 striped bass mortality varied enough from summer to fall to affect adult abundance (Stevens 1977, p. 96). The FMWT does not sample the full range of longfin smelt in the fall, but the time series of the longfin smelt FMWT index tracks those from the more spatially comprehensive Bay Study because longfin smelt return to the upper estuary in the fall and early winter placing enough of them in the FMWT sampling grid to generate a reasonable index (Rosenfield and Baxter 2007, p. 1590). One other potential survey limitation from the perspective of indexing the relative abundance of longfin smelt is they do not fully recruit to the gear until 60–70 mm, a size the average age-0 individual often does not reach until it is transitioning to age-1 (December-February). To the extent that longfin smelt may be using deeper water during the day, this phenomenon would also reduce the capture efficiency of the FMWT.

Bay Study Survey

The Bay Study was initiated in 1980 and samples monthly year-round with 2 tows per station: one with an otter trawl (OT), which samples demersal fishes, crab, and shrimp, and one with a midwater trawl (MWT), which samples pelagic fishes in the water column to approximately 40 feet deep. The Bay Study samples most of the San Francisco Estuary from the western Delta to South San Francisco Bay, and targets juvenile to small-sized adult fishes (20–250 mm). The original purpose of the Bay Study was to provide data to monitor the influence of freshwater outflow on abundance trends and distributional patterns of a suite of fish and invertebrate species (Armor and Herrgesell 1985, p. 211). The limitation of the Bay Study from the perspective of sampling longfin smelt is that juvenile longfin smelt do not fully recruit to OT gear until they are about 40–50 mm and fully to MWT gear until 60–70 mm. Like the FMWT, the Bay Study produces annual indices of relative abundance for longfin smelt. Bay Study data are used to calculate separate indices for OT and MWT for three age classes (age-0, age-1, and age 2+) of longfin smelt for a total of 6 annual abundance indices. The survey's distinction between longfin smelt age classes allows for extensive analysis for species vital rates, life stage transition, and geographical range analyses.

Chipps Island Trawl: Chipps Island Trawl was initiated in 1976 and samples 3–7 days a week using a MWT near the surface to conduct ten 20-minute tows per sampling day and across three trawl lanes (north, central, south) to produce varied catches. The survey used to sample only during spring, but has been sampling year round since 1995. The survey targets juvenile to small adult fishes (40–150 mm), and was originally designed to estimate the percent passage or survival of emigrating juvenile Chinook Salmon. For longfin smelt, Chipps Island Trawl's primary limitation is its sampling location which is restricted to the waters around Chipps Island, and the use of only a surface-towed MWT net meaning it does not sample fish residing lower in the water column. Unlike the surveys above, Chipps Island Trawl makes 10 tows each day and sampling during the winter and spring provides frequent catches of longfin smelt leading up to and during their spawning season.

Suisun Marsh Survey: the Suisun Marsh Survey was initiated in 1980 and samples monthly year-round using a single OT tow at each sampling location within the sloughs of Suisun Marsh. The survey targets

juvenile and small adult fish (25–250 mm), and was originally intended to track trends in distribution and abundance of shrimp and fish communities within the marsh complex. From the perspective of sampling longfin smelt, the primary limitation of Suisun Marsh Survey is its location that is restricted to the marsh.

None of the above listed field surveys sample the local coastal waters believed to provide habitat for some age-1 longfin smelt during July-September (Rosenfield and Baxter 2007). The CDFW Longfin Smelt Science Program is currently discussing the expansion and addition of field surveys to help improve monitoring of the Bay-Delta DPS. This program is intended to both promote science which analyzes assumptions and hypotheses used in the incidental take permit, while also addressing important, longstanding questions related to the ecology of the species. Since FMWT and Bay Study are thought to sample sufficient extent of the range for the DPS for the covered time periods, they produce representative annual abundance indices for tracking abundance trends over time. In addition, we use data from the SLS and 20-mm Survey to estimate the abundance, trends, and distribution of larval and small juvenile Longfin Smelt.

Appendix B: Count-Based Population Viability Analysis Using Indices of Abundance for the Bay-Delta DPS Longfin Smelt

Technical Note 1:
Count-Based Population Viability Analysis Using Indices of Abundance for Longfin Smelt

Version 3.1 – May 17, 2022

Vanessa D. Tobias, USFWS

Introduction

Many monitoring programs collect data that is used to assess population status and trends in abundance for species of management concern. From these, a time series of abundance indices can be used to calculate population growth rates and to forecast the risk of extinction into the future through the application of a population viability analysis (PVA). Different methods for conducting PVAs exist for different kinds of available data. A count-based PVA is classically applied to census data (counts of an entire population), but it is not necessary to count the entire population. A count-based PVA can also be applied to index values, where a population index represents some portion of the total population as long as the proportion of the population that is observed remains relatively constant over time (Morris and Doak 2002).

The San Francisco Estuary is one of the most highly studied and monitored ecosystems in the world. The Interagency Ecological Program (IEP) conducts a suite of fish monitoring surveys in the San Francisco Estuary, some of which have been collecting data for over 50 years. These long-term monitoring datasets create an opportunity to investigate trends in abundance and to estimate the probability of long-term viability of species that are of management concern. Several of the IEP long-term monitoring surveys provide indices of Longfin Smelt abundance in the San Francisco Estuary. Some of these indices are calculated and published annually (e.g., the FMWT abundance index), but others were calculated for this analysis (e.g., the 20-mm Survey). An index of abundance need not be a formal index at all; a summary of catch per unit effort (CPUE) can also be thought of as a population index.

The analysis in this technical note applies a count-based PVA to the IEP's data for Longfin Smelt in order to summarize the information contained in the monitoring data. Applying the PVA method to several datasets that index the abundance of Longfin Smelt captures the landscape of available information and may be used to make decisions about the status of the species or about management actions. It also presents a way to synthesize the evidence of the direction and magnitude of change in LFS abundances from indices calculated using various methods and that exist on varying scales.

Methods

Data

Several long-term monitoring surveys produce abundance indices for Longfin Smelt in San Francisco Bay and the Sacramento San Joaquin Delta. I used abundance indices from the Fall Midwater Trawl (FMWT;

1 index; CDFW), San Francisco Bay Study (SBFBS; 6 indices; CDFW), and the 20-mm Survey (1 index; CDFW) to estimate apparent annual population growth rates for various life stages of Longfin Smelt. Although the Bay Study produces six different abundance indices (3 life stages and two gear types), these estimates of population growth rates are not independent. I present all indices here to provide context for a future discussion about which index, or indices, might be most informative for future monitoring.

The 20-mm Survey does not produce an index of Longfin Smelt abundance, so I adapted the methods used for the Delta Smelt index to create a 20-mm survey abundance index for Longfin Smelt. I calculated CPUE for index stations (Longfin Smelt catch per 10,000 m^3 of water), and then log transformed the CPUE values, using the usual 20-mm method ($\log_{10}(CPUE + 1)$). I calculated the mean of the log-CPUE values for each month within a year and then back-transformed the mean values to put them back on the unlogged density scale. The 20-mm survey index for Delta Smelt bases the selection of surveys on the size of Delta Smelt. For this survey, I used the maximum density value as the index of abundance rather than a mean of specific months. I did this partially for simplicity and partially because using the maximum value reduces the impact of any issues with changing timing of Longfin Smelt presence in the 20-mm survey sampling area. The code that calculates the 20-mm index values is available on request.

Population Growth Rate Calculations

Annual population growth rates (lambdas) were estimated using the linear regression methods outlined in Morris and Doak (2002) which follow methods developed by Dennis et al. (1991). These estimates are based on a simple unstructured population dynamics time series, where a single estimate of population size (or the size of a segment of the population) is produced annually. These models assume no density dependence. I used program R (R Core Team 2019) to fit the linear regressions to estimate $\mu = \log(\lambda)$ and its associated variance.

Meta-analysis for Mean Population Growth Rate

I conducted a meta-analysis using the mean and variance of population growth rates from the individual surveys as independent measurements of population trajectory and variability. A meta-analysis calculates a pooled estimate of the mean growth rate from results of separate studies. I used the metamean function from the meta package in R (Balduzzi et al. 2019).

Selection of Quasi-Extinction Thresholds

This analysis uses distinct values for the quasi-extinction thresholds for each of the surveys because the scale of the abundance indices differs across surveys. The following procedure was developed as an attempt to account for the different magnitudes of index values across the surveys. First, I calculated the mean value of all available index values for each survey over 2009–2018. I then multiplied that mean value by 0.01 to represent a value of a major decline in abundance from the recent average. The major decline value was then rounded to zero decimal places to create an integer value. I also set the minimum value to 1 *a priori*, but none of the calculated threshold values was less than 1. Final quasi-extinction threshold values are reported in Table 2.

Probability of Extinction over Time

I used the function extCDF (package popbio; Stubben and Milligan 2007) to estimate the cumulative density function (CDF) for the probability of extinction using the results of the regression analysis. This function requires inputs of four values: mean and variance of the population growth rate, the current population size, and a quasi-extinction threshold. Mean and variance of the population growth rate as well as the quasi-extinction thresholds were set as described above. The last value, current population size, was set to the most recent index value that was available (Table 1).

To calculate the cumulative probability of extinction over time for the population growth rate derived form the meta-analysis, additional values had to be chosen for the quasi-extinction threshold and the starting population size. I used the mean of the quasi-extinction thresholds and the initial populations sizes for the surveys, respectively. Realizing that these choices could affect the results of the PVA based on the meta-analysis, I also ran the simulation with several additional values and graphed the results to illustrate the potential effect of these choices.

Results

Values for the indices of Longfin Smelt abundance have decreased substantially over the time series (Table 1). This pattern is consistent across all of the indices, even though each index is on a different scale.

Mean population growth rates were less than one for most of the abundance indices, which indicates that population size is declining over time (Figure 1). Only the SFBS otter trawl index for age-1 Longfin Smelt produced an estimate greater than one. However, variability was high for all surveys and confidence limits on all estimates included one. This indicates that even though it is most likely that population size is declining, given the amount and variability in the data that the surveys produce, we cannot exclude the possibility that mean growth rates are stable or increasing. The mean from the meta-analysis was -0.0513 (CI:-0.2155; 0.1128).

Most surveys indicate that there have been substantial reductions in population size. Based on the mean lambda values, and the assumption that lambda is constant over time, declines over 10 years amount to between roughly 43% and 76% of the population. One exception is the SFBS age-1 otter trawl, where the mean lambda value indicates a roughly 57% increase in population size over 10 years. The large variability in these estimates makes a consistent increase in population size unlikely, as indicated by the probability of quasi-extinction over time. Predictions for all abundance indices, taken together, show that the probability of quasi-extinction exceeds 20% for all surveys over the next five years and reaches 50% by 2040 (Figure 3.13). Applying the same assumptions over a longer time horizon (i.e., 2050–2065), the suite of surveys predicts that the probability of extinction for the Bay-Delta DPS under current conditions is roughly 50–80%.

The range of extinction probabilities observed when quasi-extinction values were varied was roughly 20% to 60% by 2050 (Figure 4). The choice of quasi-extinction threshold places the results near the middle of the range of possible ranges of extinction timing. Varying the initial abundance could make the

extinction probabilities higher, and the values that were tested here reached as high as 80% (Figure 5). The values in Figure 3 were near the lower part of the range of extinction probabilities (high abundance). There appeared to be an asymptote at the lower end of the range, with the CDFs overlapping for high abundance values.

Discussion

Long-term monitoring records generally agree that the population of Longfin Smelt in the SFE has declined dramatically over time and that quasi-extinction is likely in the foreseeable future. The index values for recent years are lower than they have ever been and estimates of annual population growth indicate a declining population as well. Longfin Smelt abundance has undergone several step declines since monitoring began (Thomson et al. 2010) as a result of changes in environmental conditions such as the introduction of invasive clams in the mid-1980s (Alpine and Cloern 1992) and the pelagic organism decline (Sommer et al. 2007).

There is considerable variability in the estimated population growth rates, which reflects the fact that in some years Longfin Smelt population estimates increase dramatically, and in some years they decrease. Populations with highly variable growth rates tend to have lower levels of population viability over time because the inherent variability tends to make a population grow more slowly over the long term and the population size is more likely to fall below the quasi-extinction threshold than it is for populations with less variable growth rates (Morris and Doak 2002). Without intervention, populations with negative growth rates are expected to go extinct, regardless of the initial population size or the variability in their growth rates. The main question to investigate becomes when extinction is likely to happen, because this determines the timeframe for implementing management actions to increase the growth rate.

The meta-analysis indicates that on average, the surveys are tracking a decrease in Longfin Smelt abundance over time. The variability around the mean is dampened, compared to the individual surveys, but the confidence bands still include zero. This reflects the variability in the population growth rate over time--even though the surveys generally agree that the population is declining, the years with large growth rates contribute to the observed variation.

It is useful to interpret the rates of population decline and probability of extinction in the context of benchmarks for assessing conservation status. The IUCN Redlist Criteria provide guidance on classifying species of concern, based on thresholds that were developed by expert consensus (IUCN 2016). These standards have been used to provide context for interpreting PVA results for declining species in the United States (e.g., for Monarch Butterflies in Semmens et al. 2016).

For Longfin Smelt, when mean population growth rates are used to calculate reductions in population size over ten years, some long-term monitoring survey datasets classify the Longfin Smelt population as vulnerable and others as endangered (Redlist Criteria A2: vulnerable ≥ 30% decline over 10 years; endangered ≥ 50% decline over 10 years). For all datasets, even when mean estimates of population growth are positive (e.g., SFBS Otter Trawl Age-1), quasi-extinction estimates for Longfin Smelt would classify the population as endangered based on IUCN thresholds because the probability of quasi-extinction exceeds 20% over 20 years (IUCN Criteria E: Quantitative Analysis). The mean population

growth rate exhibits a probability of quasi-extinction exceeding 20% when carried forward for two decades (Figure 3.13), which was proposed by Lindley *et al*. (2007, Table 1, p. 4) as a criterion ascribing high extinction risk to Central Valley salmonid populations.

Cumulative density functions for the probability of extinction contain additional information that puts estimates of population growth and point estimates of extinction probability into a longer-term context. The shape of the curve can be part of the discussion as well. For Longfin Smelt, most of the increase in cumulative probability of extinction occurs in the next two decades, but there may be time to make changes before Longfin Smelt become undetectable by long-term monitoring surveys. In a case like that of Longfin Smelt, where population size is small, but the risk of extinction is relatively small for the immediate future, conservation and management efforts should focus on achieving long-term viability by taking steps to increase the population growth rate for the species (Morris and Doak 2002). Further investigations and summaries of existing knowledge will provide information on what these steps should be.

The selected quasi-extinction thresholds were chosen to represent values that are much lower than recent averages and to be tailored to the magnitudes of individual indices, but they were not informed by considerations of when management actions could still be effective for managing population sizes. As a result, they may be too low for management actions to successfully help the DPS to recover. Before this analysis can be informative to management practices, quasi-extinction thresholds should be examined carefully with management actions in mind.

Next steps

This technical note is part of an on-going effort to describe trends in the abundance of Longfin Smelt in the San Francisco Estuary and to investigate factors that drive those changes. Additional work is planned, and this document will be updated as refinements are made to the data, analysis, and presentation.

This analysis relies on a simplified version of the population dynamics for Longfin Smelt. In particular, it does not account for age structure in the population or potential density dependence, which has been suggested by Nobriga and Rosenfield (2016). Future work will address these issues through more sophisticated population models, which may include matrix models or a life cycle model.

The abundance indices used here are relative indices of abundance, which means that although they are assumed to track changes in the population, they do not have a direct correspondence to absolute population size. Because of this, they are not the best data source for an analysis of population viability and the results of this analysis may be more applicable to evaluating the surveys themselves than the abundance of Longfin Smelt directly. Future work will address this by leveraging on-going efforts to calculate absolute abundance for Longfin Smelt.

References

Alpine, A.E., and J.E. Cloern. 1992. Trophic interactions and direct physical effects control phytoplankton biomass and production in an estuary. Limnology and Oceanography 37: 946–955.

Balduzzi S, Rücker G, Schwarzer G (2019), How to perform a meta-analysis with R: a practical tutorial, Evidence-Based Mental Health; 22: 153–160.

California Department of Fish and Wildlife (CDFW). 2018. Fall Midwater Trawl (FMWT) Data. https://www.dfg.ca.gov/delta/projects.asp?ProjectID=FMWT

California Department of Fish and Wildlife (CDFW). 2016. San Francisco Bay Study (SFBS) Data. https://wildlife.ca.gov/Conservation/Delta/Bay-Study

California Department of Fish and Wildlife (CDFW). 2019. 20-mm Survey Data. https://wildlife.ca.gov/Conservation/Delta/20mm-Survey

Dennis, B., Munholland, P.L., and Scott, J.M. 1991. Estimation of growth and extinction parameters for endangered species. Ecological Monographs 61: 115–143.

IUCN Standards and Petitions Committee. 2019. Guidelines for Using the IUCN Red List Categories and Criteria. Version 14. Prepared by the Standards and Petitions Committee. Downloadable from http://www.iucnredlist.org/documents/RedListGuidelines.pdf.

Lindley, S.T., Schick, R.S., Mora, E., Adams, P.B., Anderson, J.J., Greene, S., Hanson, C., May, B.P., McEwan, D.R., MacFarlane, R.B., Swanson, C., Williams, J.G., 2007. Framework for assessing viability of threatened and endangered Chinook salmon and steelhead in the Sacramento-San Joaquin basin. San Francisco Estuary and Watershed Science 5(1): https://doi.org/10.15447/sfews.2007v5iss1art4

Mace, G.M., N.J. Collar, K.J. Gaston, C. Hilton-Taylor, H.R. Akcakaya, N. Leader-Williams, E.J. Milner-Gulland, and S.N. Steward. 2008. Quantification of Extinction Risk: IUCN's System for Classifying Threatened Species. Conservation Biology 22(6): 1424–1442, DOI: 10.1111/j.1523-1739.2008.01044.x

Morris, W.F. and Doak, D.F. 2002. Quantitative Conservation Biology: Theory and Practice of Population Viability Analysis. Sinauer Associates. Sunderland, Massachusetts.

Nobriga, M.L., and Rosenfield, J.A. 2016. Population dynamics of an estuarine forage fish: disaggregating forces driving long-term decline of Longfin Smelt in California's San Francisco Estuary. Transactions of the American Fisheries Society 145:1, 44–58, DOI: 10.1080/00028487.2015.1100136

R Core Team. 2019. R: A language and environment for statistical computing. R Foundation for Statistical Computing, Vienna, Austria. URL https://www.R-project.org/.

Semmens, B.X., Semmens, D.J., Thogmartin, W.E., Widerholt, R., Lopez-Hoffman, L., Diffendorfer, J.E., Pleasants, J.M., Oberhauser, K.S., Taylor, O.R. 2016. Quasi-extinction risk and population targets for the

easter, migratory population of monarch butterflies (Danaus plexippus). Scientific Reports 6: 23265. DOI: 10.1038/srep23265

Sommer, T., Armor, C., Baxter, R., Breuer, R., Brown, L., Chotkowski, M., Culberson, S., Feyrer, F., Gingras, M., Herbold, B., Kimmerer, W., Mueller-Solger, A., Nobriga, M., and Souza, K. 2007. The collapse of pelagic fishes in the upper San Francisco Estuary. Fisheries Research 32(6):270–277. DOI: https://doi.org/10.1577/1548-8446(2007)32[270:TCOPFI]2.0.CO;2

Stubben, C.J. and Milligan, B.G. 2007. Estimating and Analyzing Demographic Models Using the popbio Package in R. Journal of Statistical Software 22:11.

Thomson, J.R., Kimmerer, W.J., Brown, L.R., Newman, K.B., MacNally, R., Bennett, W.A., Feyrer, F., and Fleishman, E. 2010. Bayesian change point analysis of abundance trends for pelagic fishes in the upper San Francisco Estuary. Ecological Applications 20(5): 1431–1448.

Tables

Table 1: Abundance index data from Bay Study Midwater Trawl (BSMT), Bay Study Otter Trawl (BSOT), Fall Midwater Trawl (FMWT), and 20-mm surveys that were used in the population viability analysis.

Year	BSMT Age-0	BSMT Age-1	BSMT Age-2	BSOT Age-0	BSOT Age-1	BSOT Age-2	FMWT	20-mm
1967	NA	NA	NA	NA	NA	NA	81737.0	NA
1968	NA	NA	NA	NA	NA	NA	3279.0	NA
1969	NA	NA	NA	NA	NA	NA	59350.0	NA
1970	NA	NA	NA	NA	NA	NA	6515.0	NA
1971	NA	NA	NA	NA	NA	NA	15903.0	NA
1972	NA	NA	NA	NA	NA	NA	760.0	NA
1973	NA	NA	NA	NA	NA	NA	5896.0	NA
1974	NA	NA	NA	NA	NA	NA	NA	NA
1975	NA	NA	NA	NA	NA	NA	2819.0	NA
1976	NA	NA	NA	NA	NA	NA	658.0	NA
1977	NA	NA	NA	NA	NA	NA	210.0	NA
1978	NA	NA	NA	NA	NA	NA	6619.0	NA
1979	NA	NA	NA	NA	NA	NA	NA	NA
1980	190790.1	1385.9	2572.0	128320.8	141.6	106.0	31184.0	NA
1981	1958.6	51371.8	644.4	4139.0	11836.6	121.6	2202.0	NA
1982	299068.9	9785.5	2306.9	257965.5	3069.6	1004.8	62905.0	NA
1983	33650.8	296253.0	2865.2	23859.5	142861.2	917.2	11864.0	NA
1984	29218.2	25462.8	4081.8	44329.0	29399.2	5766.6	7408.0	NA
1985	2894.6	58525.3	2693.5	11786.9	12626.3	1185.0	992.0	NA
1986	24908.3	12523.6	2479.2	12069.6	2784.1	287.9	6160.0	NA
1987	2872.3	33470.8	2286.5	1983.6	7173.7	1284.1	1520.0	NA
1988	1724.0	18360.0	4920.9	1093.9	4322.6	2220.2	791.0	NA
1989	1136.7	6594.5	1514.1	970.6	2178.8	368.7	456.0	NA
1990	744.5	2776.2	1058.4	680.6	385.7	316.6	243.0	NA
1991	131.1	3851.7	540.7	244.9	473.8	160.5	134.0	NA
1992	369.9	1133.9	86.0	620.2	447.5	218.3	76.0	NA
1993	5085.7	810.8	22.4	7006.0	53.3	0.0	798.0	NA
1994	NA	16515.5	349.0	2847.2	4206.9	479.1	545.0	NA
1995	555398.1	NA	NA	152973.0	791.0	503.9	8205.0	2779.7
1996	666.3	NA	NA	11045.5	4152.9	247.9	1346.0	3055.9
1997	4585.3	6862.8	1788.8	10691.6	3705.8	1075.3	690.0	1915.3
1998	62852.8	6240.4	1120.2	20605.1	196.7	89.0	6654.0	1214.5
1999	59040.3	17545.6	895.0	57979.8	6827.4	600.4	5243.0	2767.3
2000	12325.8	12132.1	1168.2	16079.2	1841.5	240.4	3437.0	NA
2001	2107.4	10706.9	1154.1	812.0	15507.1	1162.9	247.0	18.1
2002	1172.6	2471.5	1899.7	18132.4	1069.8	1604.3	707.0	1305.1

Year	BSMT Age-0	BSMT Age-1	BSMT Age-2	BSOT Age-0	BSOT Age-1	BSOT Age-2	FMWT	20-mm
2003	230.4	2557.6	185.6	4006.9	6338.8	1291.7	467.0	1064.0
2004	1307.1	2030.2	485.5	3529.1	4322.9	885.9	191.0	527.5
2005	617.3	3487.4	544.7	8459.1	4074.4	593.3	129.0	482.1
2006	2779.8	1341.9	91.1	21516.8	1378.6	284.7	1949.0	533.7
2007	441.3	1350.9	78.9	3636.5	5155.9	814.9	13.0	307.8
2008	1207.3	217.6	229.6	6154.8	343.4	177.5	139.0	737.6
2009	322.6	3485.1	75.2	970.8	10317.0	469.5	65.0	1883.1
2010	867.1	598.9	114.4	628.3	1373.2	279.8	191.0	1025.1
2011	1404.5	950.4	106.2	14261.5	7134.5	503.3	477.0	1010.4
2012	397.5	5353.0	1105.6	2170.2	839.9	359.9	61.0	106.1
2013	1445.0	647.0	324.0	15545.0	574.0	277.0	164.0	1156.8
2014	1193.7	615.5	0.0	1228.4	518.7	63.1	16.0	154.9
2015	230.8	402.9	43.6	536.2	692.6	195.7	4.0	54.7
2016	NA	NA	NA	NA	NA	NA	7.0	167.1
2017	NA	NA	NA	NA	NA	NA	141.0	NA
2018	NA	NA	NA	NA	NA	NA	52.0	NA
2019	NA	NA	NA	16196	1042	146	44.0	810.1
2020	837	NA	NA	12109	NA	NA	28.0	272.3
2021	NA	NA	NA	NA	NA	NA	323.0	662.2

Table 2: Values corresponding to the mean and confidence limits presented in Figure 1 and the values used to produce Figure 2. These values include all years for which index values were calculated.

Survey	Lambda Mean	Lambda Lower CL	Lambda Upper CL	Quasi-Extinction Threshold	Current Abundance Value
SFBS MWT Age-0	0.87308	0.427157	1.784517	10	837
SFBS MWT Age-1	0.943477	0.564922	1.575702	15	161
SFBS MWT Age-2	0.945429	0.639525	1.397656	2	49
SFBS OT Age-0	0.942693	0.516553	1.720385	66	12109
SFBS OT Age-1	1.046333	0.512464	2.136369	25	1042
SFBS OT Age-2	0.987457	0.66608	1.463895	3	146
FMWT	0.902601	0.53455	1.524064	1	323
20-mm	0.946321	0.661538	1.3537	6	662.2174

Figures

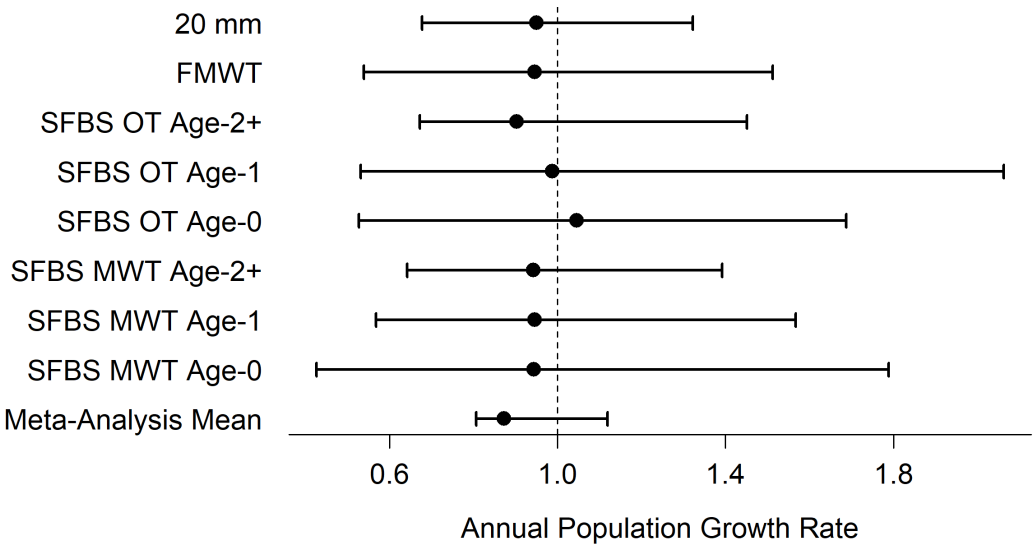

Figure 1: Mean population growth rates from several monitoring programs and a meta analysis of the mean. Calculations were made using all available years for each survey, based on a count PVA framework. Error bars are 95% confidence limits derived from the regression method developed by Dennis et al. 1991.

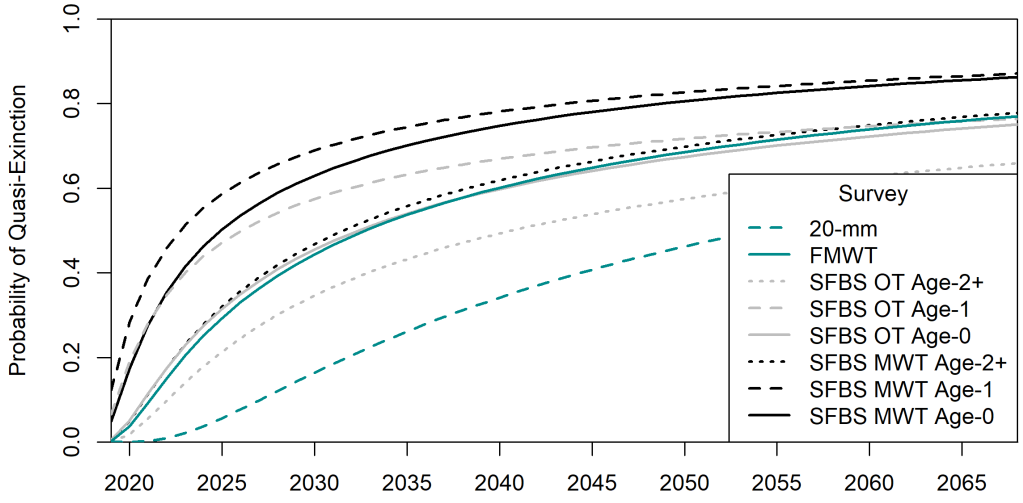

Figure 2: Probability of quasi-extinction for several surveys that report population indices for Longfin Smelt. Quasi-extinction was defined as an index value of one or lower. Estimates of population growth rates and variability were derived from all available years for each survey.

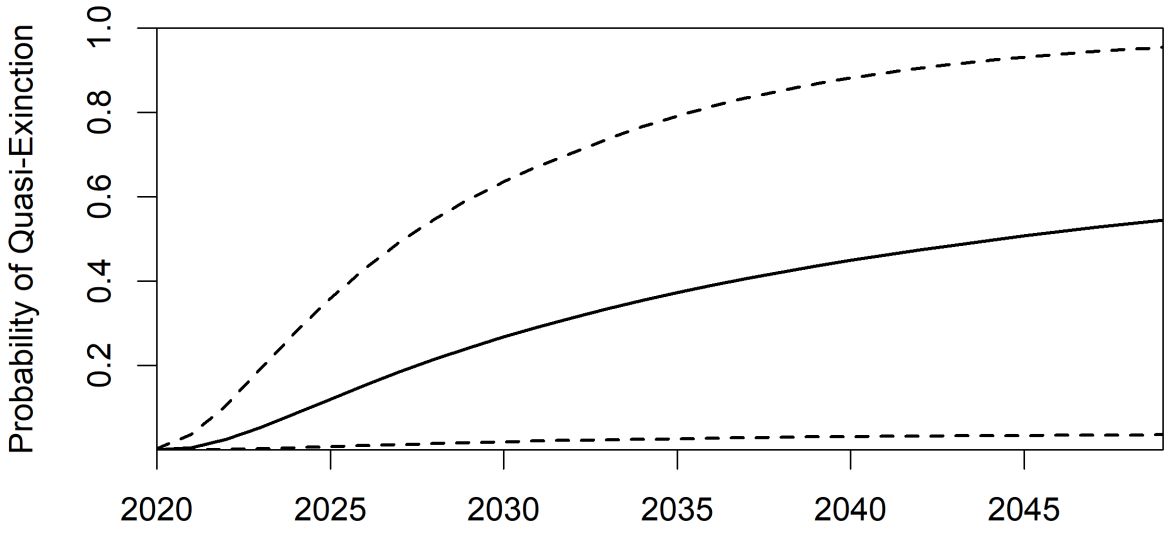

Figure 3: Probability of quasi-extinction, as calculated from the values in the meta-analysis.

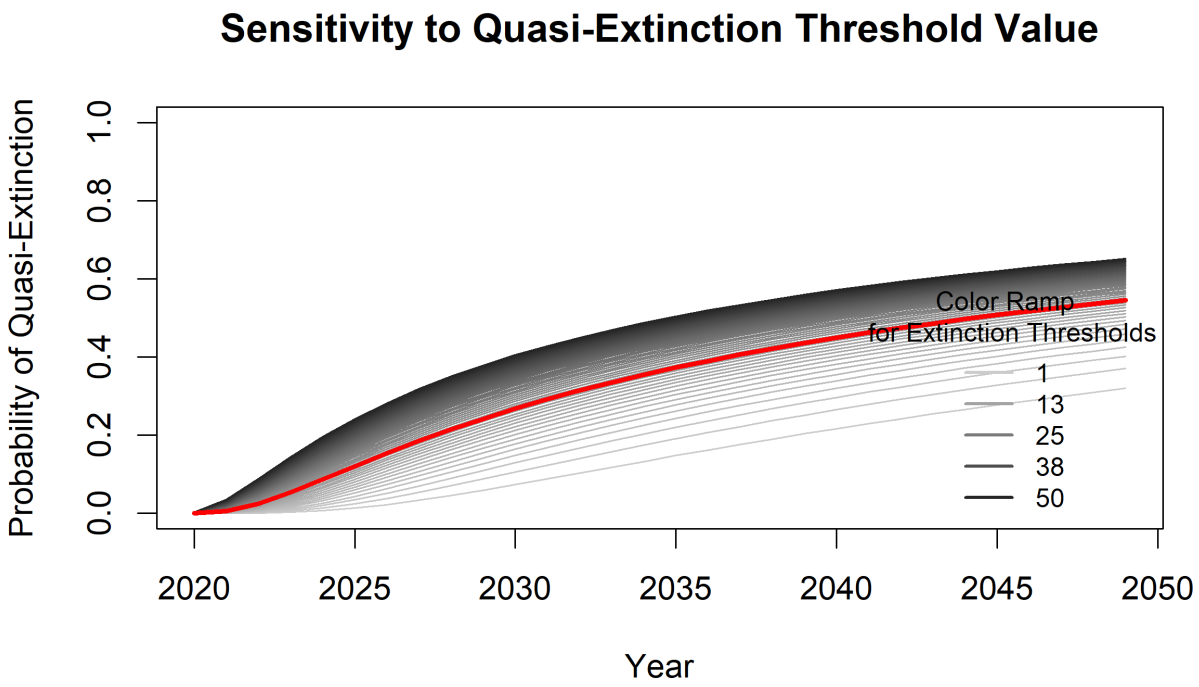

Figure 4: Sensitivity of the probability of quasi-extinction to the choice of quasi-extinction threshold. Grayscale lines represent a range of choices. The red line indicates the choice made to produce Figure 3.

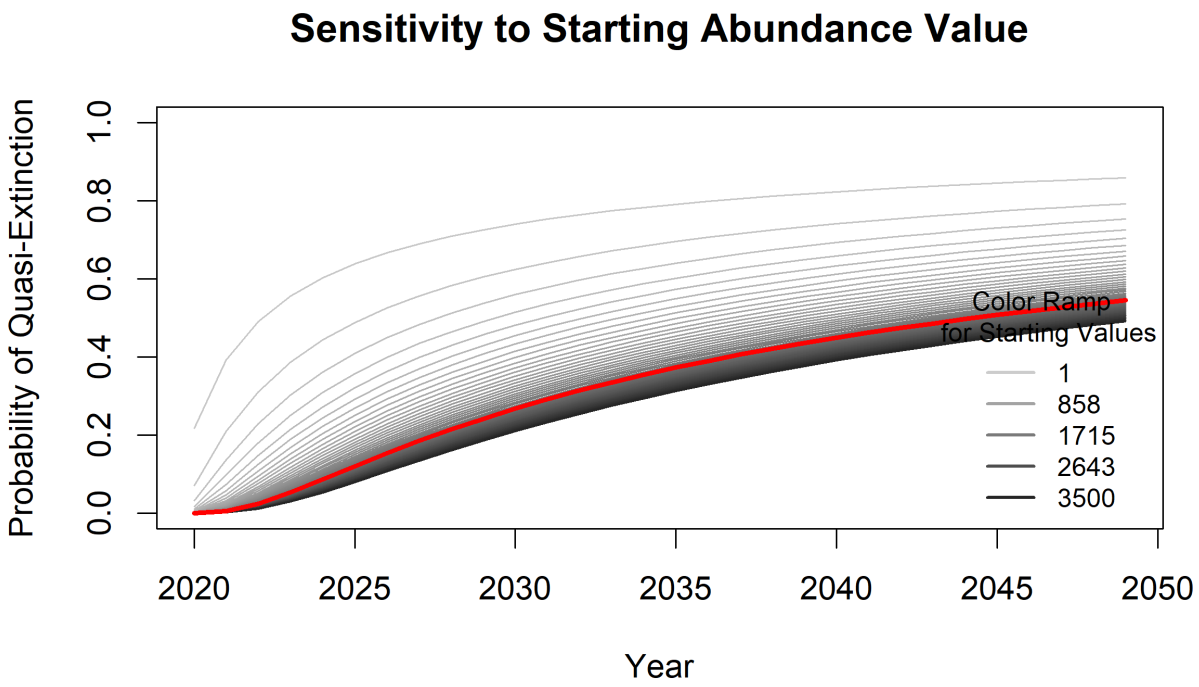

Figure 5: Sensitivity of the probability of quasi-extinction to the choice of starting abundance value. Grayscale lines represent a range of choices. The red line indicates the choice made to produce Figure 3.

Appendix C: Separating Year Classes of Longfin Smelt by Patterns in Length at Date Data

Longfin Smelt Technical Note 2:
Separating Year Classes of Longfin Smelt by Patterns in Length at Date Data

Version 1.2.0 – May 17, 2022
Vanessa D. Tobias, USFWS

Introduction

Longfin Smelt (*Spirinchus thaleichthys*) can live for several years; most are thought to spawn and die at age-2, but some fish live to age-3 (Dryfoos 1965, Moulton 1974, Moyle 1976). Early estimates of maximum size were about 150 mm TL (Miller and Lea 1972), but larger Longfin Smelt have been observed in the San Francisco Estuary. The smallest Longfin Smelt recorded in the San Francisco Estuary are about 5 mm. It is necessary to estimate the ages of fish that are caught in monitoring surveys so that it is possible to calculate age-specific abundance indices and track population dynamics.

Scientists commonly use size to estimate ages for fish. Existing criteria for separating Longfin Smelt into age classes using information about the length of the fish and the month in which it was caught were developed using catches from 1980–1989 (Baxter 1999). These length criteria are used here for calculating the abundance index values for the San Francisco Bay Study. However, the use of static length cutoff values for determining age at specific dates would be problematic if growth rates vary annually or by cohort.

Here I use patterns in the length frequency distributions to reclassify each cohort. The methods are conceptually similar to those described by Baxter (1999), but using data from additional years and surveys allowed me to estimate cutoff values for each month and year combination rather than a single, static set of cutoff values.

Methods

Length Data

Several of the Interagency Ecological Program long-term monitoring surveys collect Longfin Smelt and record their forklengths. I compiled these data and used patterns in observed forklength frequencies in each calendar month to identify age classes. The surveys used in this technical note were: San Francisco Bay Study's (SFBS) long-running otter trawl and midwater trawl, the SFBS larval surveys which occurred in the 1980s, the 20-mm survey, Fall Midwater Trawl (FMWT), Enhanced Delta Smelt Monitoring program's 20-mm and Kodiak surveys, and the Smelt Larval Survey (SLS). Data used in this technical note were limited to the years 1980 through 2020 because these were the years for which the most monitoring studies were active. Details on survey methods can be found in Honey et al. 2004, but some relevant details are described below.

The long-running SFBS survey collects data throughout the year at locations ranging from South San Francisco Bay to the Sacramento-San Joaquin Delta (the Delta). It has the broadest geographic range of the surveys. The SFBS collects fish using two gears: an otter trawl that samples the bottom of the water

column and a midwater trawl that takes an oblique sample throughout the water column. The SFBS truncates length data; it does not record fish less than 40mm. The 20-mm study provides data on smaller fish in the spring. The SFBS larval survey sampled for a shorter run of years (1980–1989) and it used a 505 µ mesh plankton net to sample larval fish. The data used in this technical note are only those fish that were identified as Longfin Smelt. It does not use any unidentified Osmerids, although these do exist in the dataset.

The FMWT uses a net that is similar to the SFBS midwater trawl gear. Geographically, the FWMT covers eastern San Pablo Bay to the Delta and as the name suggests, it generally samples in September through December. EDSM was designed to follow the life cycle of Delta Smelt, but it regularly catches Longfin Smelt as well. It began in 2016. EDSM uses a Kodiak net for most of the year, except during the spring when it uses a 20 mm net. It uses a geographically stratified sampling design to collect data from eastern San Pablo Bay to the Delta, although the sampling frame changes seasonally to accomplish the goals of estimating abundance and distribution of Delta Smelt. The Smelt Larval Survey began in 2005 and its geographic coverage includes Carquinez Strait through the Delta, and sometimes the Napa River. The SLS uses 505 µ mesh plankton nets, similar to the SFBS larval survey.

Existing Length at Date Cutoffs

The SFBS program uses length at date charts to help distinguish between age classes of Longfin Smelt for calculating age-specific abundance indices (Table 1). These are the cutoff values that were developed by Baxter (1999) using data from 1980-1989. Baxter (1999) observed that these cutoff values provided good separation of age-0 and age-1 fish but could only approximately separate age-1 fish from age-2 fish because the lengths of these age classes overlapped considerably. He also noted the apparent existence of older age classes in the data. These length at date criteria were used as rough guides for the age classification process described by this technical note to aid in automated labeling of cutoff values for each month.

Analysis

Changes in the fork length distribution of two year-classes of Longfin Smelt can be seen in monthly frequency distributions of fork lengths observed during one calendar year (e.g., 1983; Figure 1). In this example, from January to May, only the year class that hatched in 1982 is visible and the cluster of length measurements shows growth over time. From June through December, the 1983 year class appears as a cluster of shorter fork length measurements. Visually it is fairly easy to differentiate these year classes and follow the patterns in apparent growth over time; however, it is not obvious how to accomplish this task numerically with the data for a long-term dataset. This technical note focuses on the development of a method to automate the separation of year classes using only length and date information. The peaks of the density plots for each month in a year class identify the modal length for that month (Figure 2). This is a visual representation of the expected length for a fish belonging to the identified year class that is caught in that month.

All calculations and analysis were conducted using pr R (version 4.0.4 “Lost Library Book”; R Core Team 2021). I estimated the univariate density of fork lengths for each month in each year using a Gaussian

kernel (stats::density). The bandwidth that I selected (6.5 mm) was based on visual comparisons of plots. This bandwidth provided adequate smoothing to the density plots, while maintaining the ability to visually distinguish groups of fork lengths within a month. I wrote an algorithm that identifies minimums and maximums in the kernel density plots by taking the first derivative of the density function and identifying places where the sign of the slope changes. Minimum values represent cutoffs between size classes, whereas maximums are the centers of the lengths for an age class. Once clusters of lengths were identified, I classify the kernel density minimums by which age classes they separate, based roughly on the length at age criteria developed for the Bay Study. In this way, the SFBS cutoffs inform the identification of the age classes without influencing the selection of the cutoff values themselves.

Not all age classes are apparent in every month and calendar year combination. To fill these in and adjust any very unusual cutoff values, I used a flexible regression technique. This was a hierarchical generalized additive model (HGAM) based on the GI model formulation from Pedersen et al. (2019). This model formulation has a shared global term (G) that creates a similar shape across all the year classes. The individual term (I) allows individual years to deviate from the shared global term, but applies a penalty to years that are very different. This regression method fills in gaps where no information exists for a cohort using information from all years and the pattern for that particular year. The model was fit using the mcgv package (Wood 2011).

After creating the cutoff values, I classify lengths into age-classes using the specific cutoff values that were identified for that combination of month and year. I then rearranged the resulting data to create cohorts. For example, an age-1 fish that was caught in 2010 was part of the cohort of fish that hatched in 2009.

Validation

I used k-fold validation to test the consistency of the classification method (Hastie et al. 2009, Ch. 7, pp. 241–247). I split the dataset into five folds (or partitions). The first fold was held out to be used as a testing dataset and the other four folds were used as training datasets. I repeated the methods described above on each of the four testing datasets to produce four unique sets of length at age cutoff values. I used these cutoff values to classify the lengths in the testing dataset, which produced four sets of age classifications for each length value in the testing dataset. I compared agreement across these age classifications to assess consistency.

Results

Length at Date Cutoffs

Maximum lengths were calculated for each combination of month and year in the dataset. Appendix B shows a subset of the cutoffs. Figure 3 shows an example of a single year class or cohort (fish that hatched in 1982), as stacked kernel density plots for individual months. The year class panel shows the kernel densities for fork lengths of fish that were classified as belonging to the 1982 year-class. This plot highlights the pattern in apparent growth of the year class over potentially three years (months 1–36). Months 13 – 24 correspond to calendar year 1983, i.e., the example calendar year plot. Lines are missing

in the graph for months when no fish that were caught during that month were identified as belonging to the 1982 year-class.

The maximum lengths for age-0 and age-1 fish used by the SFBS are within the range of maximum length at age that was calculated for individual years when the KD method is applied to the length at date data from multiple surveys (Figure 4). There is some variation in the cutoff values for each month using the KD method that isn't captured by using a single value across all years. There is less separation between the three age classes late in the calendar year. Lines for individual years corroborate the SFBS maximum length at age pattern that shows a steeper slope in the first six months of the age-0 year, followed by a flattening of the cutoff curve. The SFBS cutoff values that separate age-0 from age-1 fish early in the year fall in the lower part of the range of the cohort-specific cutoff values for that time of year. For many cohorts, some fish that the SFBS values identify as age-1 would be identified as age-0.

Using the adjusted cutoff values to assign ages to each length measurement allows the cutoff values to borrow information from adjacent months to make more realistic assignments than would be possible using the nadir values identified by the densities of individual months. For example, in the length data form 1997 (Figure 5), using the density from April alone, the mass of lengths greater than about 35 mm might be classified as all age-1 fish. By incorporating information from before and after that month, it becomes apparent that some of those fish should be classified as age-2+ because there are centers of mass in the age-2+ range for the previous three months. This shows how the regression technique borrows information. Without it, we might think that there were no age-2 fish present and that the age-1 fish were unreasonably large during that month. This use of adjacent information is more important for the cutoff between age-1 and age-2+ than for the separation between the age-0 and age-1 classes because of the differences in the degree of separation between the age groups. There is generally more complete separation between the 0 and 1 than between 1 and 2. This also means that the precision of the 0–1 cutoff values is less important for accurate age discrimination than precision in the 1–2+ cutoffs. There is less data for the older ages, though, as abundance is higher for younger fish.

In the length data collected in the SFE, there was generally good visual separation between the lengths of age-0 and age-1 fish (Figure 5). Distinguishing age-1 and older age classes was not always possible without the help of density plots and code to separate the masses of lengths. In Lake Washington studies, distinguishing year classes was not problematic because there was no overlap in sizes of fish belonging to age-0 and age-1 classes (Dryfoos 1965; Chigbu and Sibley 1994).

Validation

The kernel density method and the SFBS age classes placed lengths into the same age classes in 99.4% of cases (Table 2). Most of the discrepancies between the two methods were in discriminating between age-1 and age-2+ fish. In the k-fold validation tests, the age classifications for lengths in the testing data fold were highly consistent across the classifiers that were trained by the data in the four training folds (Table 3).

Discussion

1. This paper updates the existing static length at date cutoff values for Longfin Smelt. Results here are similar to the existing cutoffs, but this method will allow cutoffs to be more responsive to cohort- or year-specific differences in observed growth patterns.
2. This method is a mathematical way to approximate the visually intuitive process of separating age classes using length frequency data.
3. Classification of length data into consistent age classes by algorithms trained on different subsets of the data indicate that the method is robust.
4. Separating age-0 from age-1 fish was easier than separating age-1 from age-2. This is similar to what other studies found.
    a. Chigbu & Sibley 1994: Bimodal distribution of lengths within a year with no overlap used to separate 1989 and 1990 cohorts.
    b. *Dryfoos 1965: "Determination of the age of the longfin smelt was simplified because no overlap in length frequency between year classes occurred." In the Lake Washington freshwater population, and applied to the separation between age-0 and age-1 fish.*
5. From MAST Biology section, to support age class cutoffs: *Little information has been published on the growth of Longfin Smelt in the San Francisco Estuary. Using 20-mm Survey length data for 1995 through 2004 and analyzing for apparent growth, Souza et al. (2006) found that larval through young juvenile Longfin Smelt grew at a mean apparent rate between 0.12 and 0.23 mm/day, and that growth was not related to outflow. These same authors reported that age-0 Longfin Smelt caught by the Fall Midwater Trawl achieved December (age-10 months) mean length that varied between 50 and 70 mm FL. In Lake Washington, Longfin Smelt at age-10 months averaged from 56 to 82 mm FL in the 1960s (converted from SL and Figure 3 in Moulton 1974). Using the Fall Midwater Trawl range of mean lengths at 10 months and assuming a February 7 mean hatch date (i.e., mid-way through the monthly sampling period) and a December 7 mean date of capture results in annual apparent growth rates varying between 0.20 to 0.23 mm/day. This represents relatively slow growth.*
6. Caveats
    a. This analysis does not include any information about fish with known ages. Data from otoliths would be necessary to confirm ages of fish. This analysis implies ages from patterns in length data using expert opinion as a guide.

Potential next steps

1. Length data that have been classified using the method developed in this technical note will be used to investigate patterns in apparent growth of Longfin Smelt in the San Francisco Estuary. (See LFS TN 3 by Bryan Matthias.)
2. Investigate whether cutoff values are stable over time and of how much interannual variation there is. (This question was identified in the comments on the LFS MAST Biology section.)
3. Length distributions might help us investigate hypotheses about different life history strategies. Length distributions have multiple modes in some years, which might lead us to looking at spatial patterns as well.
4. Additional validation may be possible in the future if data become available for fish that were aged using other techniques such as reading otoliths.

5. Try other kernel density functions. Triangular might be good for emphasizing the cutoffs. (This is currently not a priority because the existing method is largely consistent.)
6. Consider investigating whether there are patterns in the non-matching age classifications from the validation procedure. (There are very few of them, though, so that isn't a priority yet.)

References

Baxter, R. D. 1999. Osmeridae. Pages 179–216 *in* J. Orsi, editor. Report on the 1980–1995 fish, shrimp and crab sampling in the San Francisco Estuary. Interagency Ecological Program for the Sacramento-San Joaquin Estuary Technical Report 63

Chigbu, P., and T. H. Sibley. 1994. Relationship between abundance, growth, egg size and fecundity in a landlocked population of longfin smelt, *Spirinchus thaleichthys*. Journal of Fish Biology 45(1994):1–15.

Dryfoos, R. L. 1965. The life history and ecology of the longfin smelt in Lake Washington. Ph.D. Dissertation. University of Washington, Tacoma WA. 229 pages.

Hastie, T., Tibshirani, R., Friedman, J.H. and Friedman, J.H., 2009. The elements of statistical learning: data mining, inference, and prediction (Vol. 2, pp. 1–758). New York: springer.

Honey K, Baxter R, Hymanson Z, Sommer T, Gingras M, Cadrett P. 2004. IEP long-term fish monitoring program element review. Interagency Ecological Program for the San Francisco Bay/Delta Estuary. IEP Technical report no. 78. Sacramento (CA): California Department of Water Resources.

Miller, D.J. and Lea, R.N., 1972. Guide to the coastal marine fishes of California (Vol. 157, pp. 1–249). State of California, Department of Fish and Game.

Moulton, L. L. 1974. Abundance, growth and spawning of the longfin smelt in Lake Washington. Transactions of the American Fisheries Society 103(1):46–52.

Moyle, P. B. 1976. Inland fishes of California. University of California Press, Berkeley, California. 405 pages.

Pedersen, E.J., Miller, D.L., Simpson, G.L. and Ross, N., 2019. Hierarchical generalized additive models in ecology: an introduction with mgcv. *PeerJ*, *7*, p.e6876.

R Core Team. 2021. R: A language and environment for statistical computing. R Foundation for Statistical Computing, Vienna, Austria. URL https://www.R-project.org/.

Souza, K., K. Hieb, K. Fleming, M. Bryant and R. Baxter. 2006. Apparent growth rates of pelagic fishes and relationship to abundance. Interim Report on Pelagic Organism Decline Investigations. 9 pages.

Wood, S.N. 2011. Fast stable restricted maximum likelihood and marginal likelihood estimation of semiparametric generalized linear models. Journal of the Royal Statistical Society (B) 73(1):3–36

Tables

Table 1: Length at age cutoffs used for SFSB data.

Calendar Month	Minimum Length	Age-0 Maximum Length	Age-1 Maximum Length
1	40	40	90
2	40	42	93
3	40	46	96
4	40	52	100
5	40	59	105
6	40	67	108
7	40	71	111
8	40	75	114
9	40	80	117
10	40	83	120
11	40	85	122
12	40	87	124

Table 2: Confusion matrix comparing age class determinations made by the traditional SFBS length at date criteria and the kernel density (KD) method.

		KD Age Classes		
		0	**1**	**2+**
SFBS Age Classes	**0**	215085	139	0
	1	347	32218	482
	2+	0	465	2922

Table 3: Proportion of age classifications on the length values in the testing data fold (fold 1) that match among kernel density-based algorithms trained on four training data folds (folds 2–5).

	2	**3**	**4**	**5**
2	1.000	0.993	0.995	0.994
3	0.993	1.000	0.993	0.993
4	0.995	0.993	1.000	0.995
5	0.994	0.993	0.995	1.000

Figures

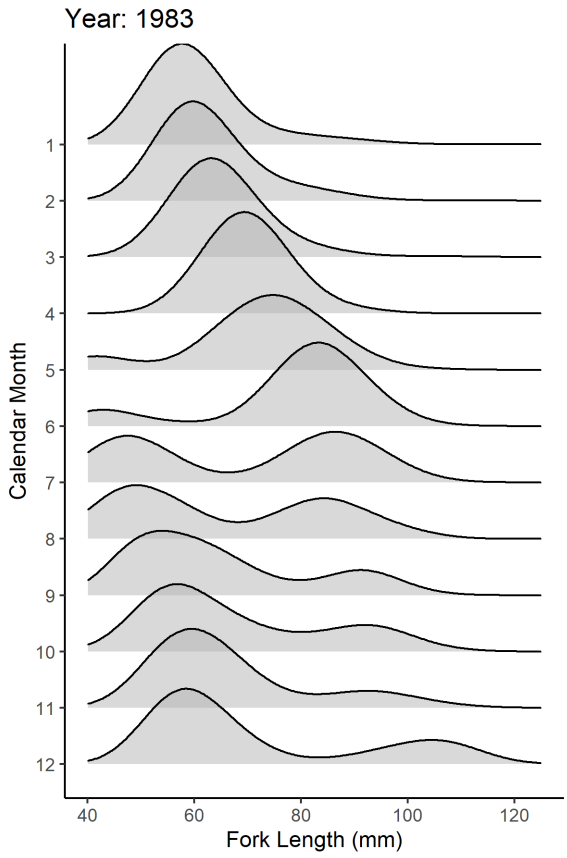

Figure 1: An example of the monthly length distribution of two year classes of Longfin Smelt over one calendar year (1983), as stacked kernel density plots for individual months. The bandwidth for kernel density estimation was 6.5 mm.

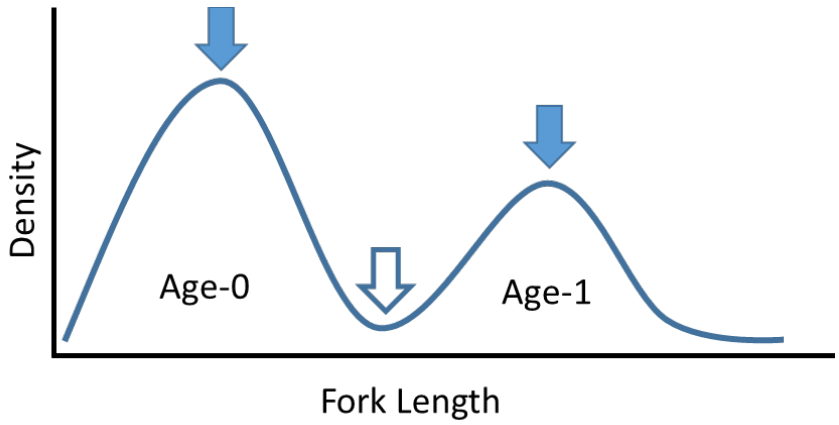

Figure 2: Conceptual diagram of using features of the kernel density plot of fork length to separate year classes of Longfin Smelt that were collected during a calendar month with two age classes present. Filled arrows identify the center of the distributions and the hollow arrow identifies the separation between the two age classes.

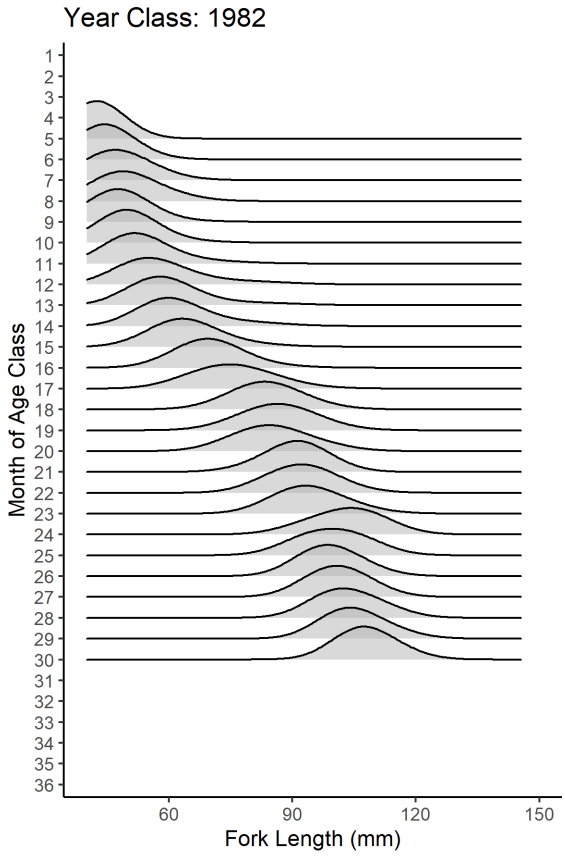

Figure 3: An example of the monthly length distributions of one year class of Longfin Smelt (fish that hatched in 1982) over 36 months, as stacked kernel density plots for individual months. The bandwidth for kernel density estimation was 6.5 mm.

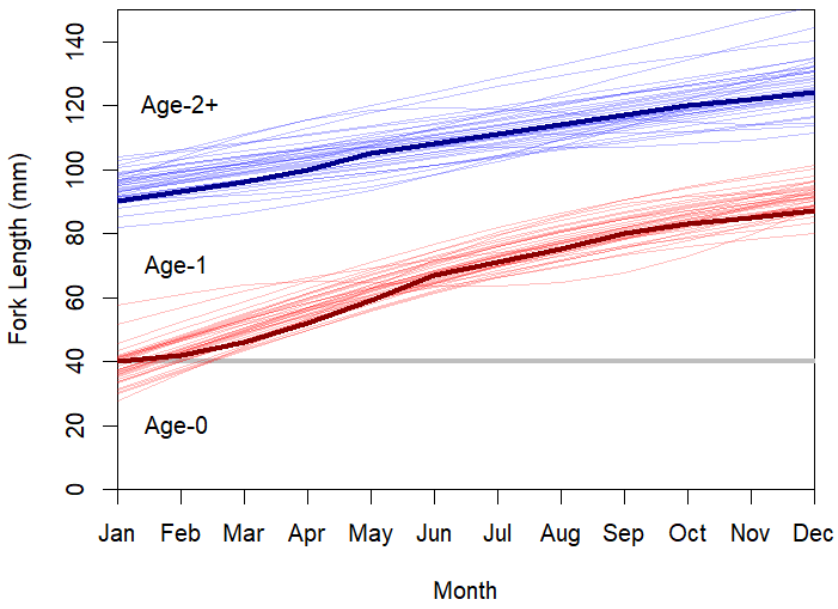

Figure 4: Length at date cutoffs for SFBS (thick lines) and as calculated in this paper (thin lines).

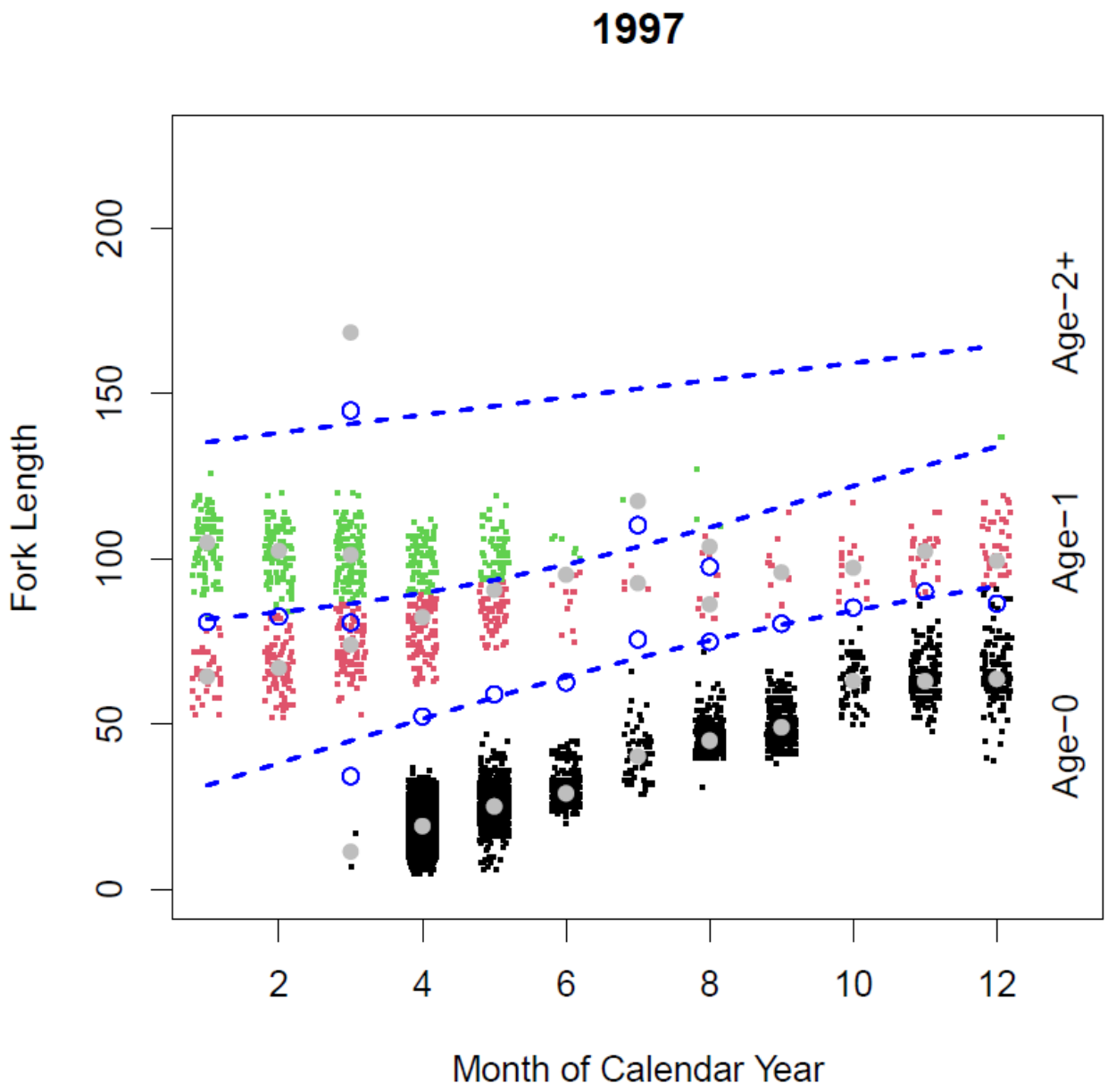

Figure 5: Separation of fork lengths into age classes in a calendar year (1997 as an example).

Appendix D: Assessment of Environmental Factors on Apparent Growth in Bay – Delta DPS Longfin Smelt

Longfin Smelt Technical Note 3:
Assessment of Environmental Factors on Apparent Growth in Longfin Smelt
Version 2.1.0 – May 16, 2022, 2022
Bryan Matthias and Vanessa Tobias, USFWS

Introduction

In fishes, understanding how somatic growth changes over time is important because body size and condition influence population growth rates as determinants of survival, fecundity, and reproductive schedules (Sterns 1992; Charnov 1993; Roff 1993). Fish size is an important factor influencing survival via susceptibility to predation (see Mittelbach and Persson 1998 for review on selectivity of predators) and natural mortality generally decreases as individuals attain larger body sizes (Pauly 1980; Lorenzen 1996, 2000). Thus, conditions supporting faster growth can increase survival, especially during larval and juvenile stages when mortality rates are high. Further, fecundity for many fish species increases proportional to size (i.e., by weight or length, approximately cubed; Beverton and Holt 1957; Ricker 1975; Walters and Martell 2004). For semelparous spawners, larger sizes-at-maturation can result in greater egg production and/or larger eggs (see Johnston 1997 and references within). Either of these effects can influence total reproductive output of a population by increasing the total number of eggs produced and/or offspring survival--numerous studies have identified positive relationships between eggs size and size-at-hatching, better feeding success, faster growth, etc. (see Johnston 1997 and references within). Thus, quantifying changes in somatic growth can serve as an indicator for changes in population growth rates and may be used to better inform management towards subsequent recovery efforts.

Fish populations within many estuaries globally have been declining due to a variety of causes, with overfishing and environmental degradation identified as two major drivers in population declines (reviewed in Whitfield 1999; Lotze et al. 2006; Lotze 2010). Similar to estuaries around the globe, the San Francisco Estuary (SFE) has undergone many changes over the past century and a half (for a more detailed overview of changes see Sommer et al. 2007; Cloern and Jassby 2012) and it has been transformed into a major water transportation hub that provides drinking water for over 25 million people and irrigation water for 750,000 acres of farmland (CDWR 2013). The SFE is the largest estuary on the west coast of North America with a watershed that drains roughly 40% of California's surface (Jassby and Cloern 2000). Due to flow management in the SFE watershed, roughly 39% of the unimpaired runoff is consumed or diverted annually (reaching as high as 65%; Cloern and Jassby 2012). These changes have had major impacts on species that rely on the SFE and its watershed for all or part of their life cycle (e.g., winter and spring-run Chinook *Oncorhynchus tshawytscha*, Steelhead *O. mykiss*, Delta smelt *Hypomesus transpacificus*, and green sturgeon *Acipenser medirostris* are currently federally listed as endangered or threatened in the watershed).

Several long-term monitoring studies have documented declines in SFE productivity in the late 1980s (Kimmerer and Orsi 1996; Kimmerer 2002) and several fish populations crashed in the early 2000s (referred to as the Pelagic Organism Decline [POD]; Sommer et al. 2007). The SFE Distinct Population Segment of Longfin Smelt (*Spirinchus thaleichthys*; hereafter referred to as LFS) was among the POD populations to collapse. In the SFE, LFS was once among the most abundant pelagic fishes (Orsi 1999) and the system historically supported a commercial fishery. There have been several hypotheses put

forward for the LFS population declines and assessing long-term LFS growth patterns may shed light on these hypotheses and identify if changes in growth patterns have contributed to population declines.

Given the importance of somatic growth, the 2020 Longfin Smelt Science Plan (https://water.ca.gov/-/media/DWR-Website/Web-Pages/Programs/State-Water-Project/Files/ITP/ITP-Longfin-Science-Plan_SWP_12232020_-FINAL.pdf) identified factors affecting growth as a science priority to help understand factors affecting population dynamics, improve management tools, and developing informative predictive modeling tools. Here we assess a suite of abiotic (i.e., temperature, outflow, conductivity) and biotic (i.e., abundance, prey availability) factors that may affect LFS apparent growth rates. We acknowledge that other factors may also be important, and these may be addressed in future versions of or extensions of this work. To assess LFS apparent growth, we modified the Lester et al. (2004) biphasic growth model to estimate the impacts of factors on somatic growth patterns based on a similar model developed by the author (Matthias et al. 2016). Our primary objective was to quantify the strength, direction, and potential interactions of abiotic and biotic factors influencing LFS growth. Our secondary objective was to assess systematic or long-term changes or patterns in LFS growth. Quantifying factors that influence growth allows us to investigate growth and its correlates as a potential mechanism for the abundance-outflow relationship (Stevens and Miller 1983; Jassby et al. 1995; Kimmerer 2002). For example, studies have detected changes in the abundance-outflow relationship associated with the establishment of the invasive clam *Potamocorbula amurensis* (Kimmerer 2002) and another attributed to the POD after 2002 (Thomson et al. 2010), but it is unknown if growth patterns changed during these periods.

Methods

Longfin Smelt Length Data

Longfin Smelt length data were obtained and combined from multiple long-term monitoring surveys (Table 1). These surveys spanned from 1981–2020 and contained year-round sampling programs. The San Francisco Bay Study (SFBS), focused on large juveniles and adult fish, had year-round sampling from 1981–2015, covered almost the whole SFE from South San Francisco Bay through the western Delta, and sampled 102,776 fish (mean length of 59 mm and range of 40–197 mm). The 20 mm Survey, designed to capture larval and juvenile fish, sampled from March-August from 1995–2019, covers from eastern San Pablo Bay through the Delta, and has sampled 182,103 fish (mean length of 19 mm and range of 3–183 mm). The Fall Midwater Trawl (FMWT) surveys, designed to capture juvenile and adult fish, mainly surveys from September-January (but has sampled year-round on occasion) from 1981–2017, is similar is spatial coverage to the 20 mm Survey, and has sampled 18,643 fish (mean length of 71 mm and range of 15–185 mm). The Enhanced Delta Smelt Monitoring (EDSM) surveys started recently (2017–2020) using 20 mm nets for targeting the larval stage and Kodiak trawls for juvenile/adults. The EDSM survey is year-round and spatial coverage varies by season (usually Suisun Bay through the north Delta), but switches between the two sampling methods, and has caught 1,297 (mean length of 21 mm and range of 6–43 mm) and 649 (mean length of 73 and range of 30–132 mm) in the 20 mm nets and Kodiak trawls respectively. Finally, the Smelt Larval Survey (SLS) survey captured 5,713 larval and small juveniles (mean length of 8 mm and range of 3–32 mm) from 2005–2007 from January through July and had a

distribution similar to the 20 mm Survey. A total of 311,166 LFS lengths were used in this analysis. A single obvious outlier (length = 282 mm) was removed from the analysis.

Age measurements were not obtained for fish caught during these surveys. Instead, age (in years) was assigned based on length-frequency distributions (see Tobias 2022 for details). Ages were converted to fractional monthly age using the date-at-capture and assuming a birthdate of January 1 each year. Individuals were assigned to cohorts (i.e., all individuals born during the spawning season in a given year), based on their assigned age and capture date.

Abiotic Environmental Data

A suite of variables was used to test for the effects of environmental conditions on LFS growth (Figure 1). These parameters were chosen based on a combination of data availability and expert opinion. Environmental variables related to outflow were obtained from the DayFlow model and averaged over a given month (https://data.ca.gov/dataset/dayflow; daily predictions from 1956–2020). Variables representing temperature (in degrees C) and conductivity (in uS/cm) were obtained from the California Data Exchange Center (CDEC; https://cdec.water.ca.gov/riv_flows.html) at the Martinez (MRZ) long-term automated monitoring station operated by the CA Department of Water Resources Division of Environmental Services. The station is located at 38.03^{o}N, 122.14^{o}W in the Carquinez Straight between San Pablo Bay and Suisun Bay and was chosen for its centralized location that seems representative of general conditions throughout the San Francisco Estuary and availability of a long-term dataset (1983–present). While a single location might not be representative of the exact conditions each fish experience at any given time, the conditions recorded at a centralized location should be correlated with conditions across the SFE and changes in abiotic conditions here (temperature, salinity, conductivity, etc.) should indicate changes across LFS habitat within the SFE (although not necessarily correlated with marine habitats).

Prior to use in the model, environmental data underwent several processing steps. The first step, when possible, was to obtain monthly mean estimates from 1979–2020. Preliminary model fitting using monthly minimum and maximum observed environmental data did not converge properly and were omitted from the analysis. This date range encompasses all age classes for each cohort that were present in the LFS dataset. We then searched for obvious outliers and removed those values (i.e., set to NA; note that this occurred two times with the DayFlow dataset when estimating the monthly minimum values). Finally, negative values for outflow (six instances) were set to 0.01 to allow for logging of minimum outflow in the model (these values were used to calculate the monthly mean discharge, but were changed when processing the minimum observed values and did not impact the analysis because minimum monthly covariates were not analyzed). Due to the nature of these environmental datasets, there were also occurrences of missing values (65–66 instances with temperature and conductivity, with unobserved values prior to 4/1983 and 11/2007–7/2008 accounting for most missing values). We used the monthly geometric mean across all years to fill in missing data points (e.g., a missing temperature in February 1980 was filled in with the geometric mean of February temperatures from all available years). While this does not capture the unobserved variability within a given year, this method allowed us to capture the seasonal trends in temperature and conductivity. Additionally, we calculated mean,

minimum, and maximum temperature and conductivity over the spawning season (Dec 1 – May 31). Finally, we calculated the number of days during the spawning season with 1) Delta outflow over 20,000 cfs and 2) temperatures below 9^{o}C. Because there were years when no days met the above criteria, we added one to these variables to allow for log-transformation (15 of 38 years with temperatures recorded during the spawning season had zero days below 9^{o}C). All parameters were logged (base e) and centered prior to use in the model, unless noted below.

Biotic Environmental Data

We also investigated the impacts of age-0 and age-1+ density on growth (Figure 1). For density, we relied on the SFBS abundance indices using otter and midwater trawls (available from 1980–2018; CDFW 2021). We utilized indices for both age-0 and age-1+ for this analysis to account for differences in early-life and older life stages (Table 2). Unlike other model variables, the abundance indices were on an annual time step (not monthly). Missing age-specific indices from 1977–2020 (17 times for the otter and 23 times for the midwater trawl datasets) and those recorded as zero catch (2 times for the otter and 1 time for the midwater trawl datasets; see Table 2) were filled in using various techniques based on linear regression. Note the difference in date ranges from these surveys ensured that we had abundance indices to cover growth of LFS starting with the 1979 cohort, which required reconstructed abundances for age-2 fish in 1979 (hatched in 1977). All age-zero indices were filled in using predictions from linear regression between the SFBS indices and/or the FMWT index (averaged when possible; the FWMT index was from CDFW 2021). For example, to fill in missing age-0 indices for the SFBS midwater trawl, we utilized a linear regression between the FMWT and SFBS midwater trawl for 1977, 1978, and 2016 and used the average predictions from both the FMWT and SFBS otter trawl for 1994 and 2018. For the 1979 age-0 index, we filled in the missing values using methods outlined below for missing age-1 and age-2 indices. Finally, we used the average observed values from 2000–2018 for age-0 in 2019–2020 to account for differences in recruitment since the 1980s.

Linear regression techniques were also used to fill in missing age-1 and age-2 abundance indices. Briefly, missing values were interpolated using linear regression on log-abundance for a given cohort, based on methods used to estimate mortality in catch curves (e.g., estimating the slope [total mortality rate] for the 2000 cohort using age-0 fish caught in 2000, age-1 fish caught in 2001, and age-2 fish caught in 2002). Because each cohort only had three age-class indices (we excluded values from incomplete cohorts), we used the weighted average slope (estimated as -1.15) calculated from all cohorts using estimates from both otter and midwater trawl where each cohort was given the same weight in the global calculation. This method allowed us to minimize the uncertainty associated with small sample sizes (i.e., number of age-classes). Missing abundance indices were calculated based on the average predictions from forward and/or backward projection where a missing Age-1 index was the average of 1) preceding year log(Age-0 abundance index) minus the weighted average slope and 2) the following year log(Age-2 abundance index) plus the weighted average slope. When multiple abundance indices were missing for a given cohort, observations were filled in using the only available forward/backward projections. Finally, the sum of the Age-1 and Age-2 indices described above were used as the Age-1+ abundance indices for each year. Only abundance indices for Age-0 and Age-1+ abundance from the SFBS otter trawl survey were used in the growth model.

To account for prey availability, we utilized prey density estimated from the zooper R package created by Bashevkin (2020) and estimated the monthly geometric mean of *Eurytemora affinis* and mysid shrimp across all sampling sites within the SFE (NZ028, NZ048, NZ054, NZ060, NZ064, NZ086, NZ0325; Figure 1). Zooplankton sampling at these sites has been regularly conducted since 1972 (see Bashevkin et al. 2022 for details on the zooplankton surveys).

Overview of growth models

The model developed here differs in two important ways from traditional growth models used in fisheries by incorporating 1) multiple growth phases and 2) adding covariates to describe changes in the growth increment. The von Bertalanffy growth model (von Bertalanffy 1938) is the most common model to describe the lifetime growth patterns of fish because it has strong biological and empirical support (Beverton and Holt 1957; Chen et al. 1992; Lester et al. 2004). This model was developed to describe growth patterns of adult fish (e.g., von Bertalanffy 1968) but is often applied to describe lifetime growth patterns of fish. Further, this model is relatively inflexible as it assumes growth in length follows a constant pattern of decreasing incremental growth. Because the von Bertalanffy model is habitually applied to describe lifetime growth patterns, it has been criticized for its inability to represent complex changes occurring over the life of an organism (Day and Taylor 1997; Czarnołe'ski and Kozłowski 1998; Lester et al. 2004). Specifically, criticism has focused on the representation of growth associated with larval and early juvenile stages (Beverton and Holt 1957; Ricker 1975; Walters and Martell 2004) and changes in energy allocation associated with reproduction (Charnov 1993; Charnov et al. 2001; Lester et al. 2004), both of which likely violate the von Bertalanffy model assumptions.

To account for some of these critiques, we utilized the Lester et al. (2004) bi-phasic growth model to describe the underlying growth pattern (i.e., in the absence of inter-annual variation). The Lester et al. (2004) growth model was derived to account for changes in growth patterns associated with maturation. Growth during the first growth phase (i.e., pre-maturation growth) is assumed to be linear and transitions to the von Bertalanffy following maturation during the second growth phase. This model can also be adapted to describe additional growth phases, such as those associated with sex change in sequential hermaphrodites (Matthias et al. 2016) and incorporating early-life growth transitions can be accomplished by utilizing the appropriate data. One of the strengths of this model is the ability to jointly estimate the transition points between the growth phases by utilizing maturity and sex change data (see Matthias et al. 2016; Wilson et al. 2018). If data are available to inform additional transition points, such as early life transitions, it is also possible to incorporate those growth transitions into the model. In the absence of information to inform maturity or other transition points, the model will estimate a growth transition point solely based on length-at-age data and this transition could be independent from maturation (an important critique discussed below).

The second way this model differs from traditional growth models is that we incorporated covariates into the model to estimate the effects of environmental variation on somatic growth, similar to methods outlined by Matthias et al. (2018). Analytical methods commonly used to quantify the impacts of environmental variation on fish growth utilize ANOVA or multiple regression models on growth increments obtained from mark-recapture methods (e.g., Haugen et al. 2007; Vøllestad and Olsen 2008;

Davidson et al. 2010) or back-calculation (e.g., Maceina and Shireman 1982; Maceina et al. 1991). These methods ignore biological processes underlying fish growth often captured by von Bertalanffy and Lester et al. (2004) growth models (see Matthias et al. 2018). Here we apply log-normal regression techniques to describe variation in monthly growth increments resulting from environmental variation within the Lester et al. (2004) model framework (outlined in detail below). For example, individuals growing under ideal conditions will have a larger growth increment than those growing under poor conditions.

Collectively these two differences between our approach and the traditional application of growth models for fish populations allows us to quantify impacts of environmental variation on LFS growth. It should also be noted that we are using data collected via long-term monitoring programs (detailed above). Thus, the data we have available are correlative in nature and the trends we identify will need to be verified using targeted studies. However, this type of analysis has commonly been used to assess temporal variation in growth (e.g., Dorn 1992; Lorenzen 1996; Porch et al. 2002; Shelton et al. 2013; Matthias et al. 2018).

Growth in length

The model developed here was designed to assess variation in apparent growth of LFS using a combination of observed environmental conditions (e.g., water temperature, conductivity, outflow, density, and prey availability) and random effects. We did this by estimating parameters for the Lester et al. (2004) biphasic growth model (equation 1 and Table 3). Traditional formulation of the Lester et al. (2004) growth model was derived using assumptions related to maturation where phase-1 growth was pre-maturation and phase-2 was post-maturation. Histological data were not routinely collected as part of the monitoring surveys and preliminary model runs consistently indicate the estimated age-at-growth transition was not likely associated with maturation (i.e., we estimated a growth transition during the first year of life and Longfin Smelt primarily spawn during their second year of life; CDFG 2009). Therefore, we refer to growth during the initial phase as phase-1 and phase-2 as the second phase to aid clarity. It should also be noted that we do not explicitly account for changes in growth during early life (i.e., post-hatching, post-yolk sac, early juvenile, etc.) and close examination of the predicted length-at-age will be required to determine the ability of this model structure to predict early-life growth. While it is possible to incorporate additional transition points to describe early-life growth, this dramatically increases model complexity, increases the number of parameters to estimate (which may cause convergence issues), and increases the chance of memory allocation issues. Any added complexity to the model will require the use of supercomputers. Equations used in the model can be found in Table 3. The model was run in Template Model Builder (TMB; Kristensen et al. 2016) through Program R (R Core Team 2021).

The Lester et al. (2004) model is a biphasic growth model that separates growth into two growth phases. Phase-1 growth is assumed to be linear and phase-2 growth follows the von Bertalanffy model. An incremental formulation of the Lester et al. (2004) model is

$$L_A = \begin{cases} L_0 & if\ A = 0 \\ L_{A-1} + h & if\ A \leq T_{50} \\ L_{A-1}e^{-k} + L_\infty\left(1 - e^{-k}\right) & if\ A > T_{50} \end{cases} \quad (1)$$

where L_A is the predicted length-at-age A (whole age in months), L_0 is the length-at-age-0, h is the maximum annual growth rate and represents the growth rate in the absence of reproduction, k is the Brody growth coefficient describing how quickly growth approaches L_∞, L_∞ is the average asymptotic size, and T_{50} is the age-at-which 50% of the individuals transition between phase-1 and phase-2 growth. The Lester et al. (2004) model estimates reproductive investment g, which is used to calculate $k = \ln(1 + g/3)$ and $L_\infty = 3hg^{-1}$. If the transition point between the two growth phases (i.e., T_{50}) is linked with the age-at-50% maturity, they can be jointly estimated with a model describing maturation when data are available (see Matthias et al. 2016; 2019 and Wilson et al. 2018). As described above, the exact interpretation of these parameters (specifically h, g and T_{50}) may be confounded if the T_{50} is not associated with maturation and by additional growth transitions for which we are not accounting.

We modified the Lester et al. (2004) growth model described above to account for temporal changes in parameters using a mixed effects framework to describe temporal patterns in growth (Table 3). The model estimates the growth increment from age A to age $A + t$ (where A is whole age in months and $t = 1$ if calculating monthly growth increment or $0 \leq t < 1$ if an individual was captured at age $a = A + t$ months old). Three separate equations were used to describe phase-1, transitioning, and phase-2 growth (equations T1a–T1c respectively; Table 3). The transitioning growth phase (equation T1b; Table 3) was used to account for the possibility that individuals transitioned between growth phases at any time of the year (i.e., $A < T_{50,c} < A + 1$). Equations must be differentiable in TMB, therefore conditional statements cannot be used (e.g., if $A < T_{50}$ then use equation T1a, else use equation T1c). To overcome this constraint, we used logistic equations to represent the transition between growth phases (equations T1d–T1g; Table 3). Under certain conditions, such as with a temporally invariant growth model, equations described in Table 3 will give the same results as the traditional Lester et al. (2004) growth model (equation 1). Within the Lester et al. (2004) model framework, we used both random and fixed effects to assess how unobserved and observed conditions in the San Francisco Estuary influence LFS growth.

We compared two different random effects structures assessing whether growth patterns might have changed over time using cohort- and year-specific effects. These two random effects structures represent different hypotheses on how unobserved conditions influence growth patterns. Holding all fixed effects constant, the cohort-specific growth model assumes all individuals within a cohort have the same underlying growth curve (e.g., h, g, and/or T_{50}), but these growth patterns can change between cohorts. Cohort-specific random effects parameters were phase-1 growth rate h_c and the transition point between pre growth phases $T_{50,c}$, where $\ln(h_c)$ and $\ln(T_{50,c})$ were normally distributed with hyperparameters describing the mean and standard deviation (μ_x and σ_x; equation T1; Table 3). Additional cohort-specific parameters were asymptotic size $L_{\infty,c} = 3h_c g^{-1}$. For this model, the random effects describing year-specific growth effects were set to zero (i.e., $I_y = 0$). The year-specific growth model assumes growth patterns change over time and conditions in calendar year y have similar impacts on all individuals alive at that time (again while holding all fixed effects constant over time). We

modeled a year-specific effect on the growth increment obtained between each time step during a given year I_y (equation T1g; Table 3). The parameter $T_{50,c}$ was modeled as a cohort-specific effect to avoid additional complexity of accounting for changes in maturation patterns over multiple ages and years. This model assumes that L_∞ remains constant over time, but the rate which individuals approach L_∞ changes annually via variation in the growth increment (equation T1g; Table 3). The random effects I_y and $\ln(T_{50,c})$ were normally distributed with hyperparameters describing the mean and standard deviation (μ_x and σ_x; equation T1; Table 3). In the year-specific growth model, the phase-1 growth rate h_c was temporally constant (i.e., $\ln(h_c) = \mu_h$; equation T1; Table 3). Using this framework, if we set both the year- and cohort-specific random effects to the mean (i.e., $I_y = 0$, $\ln(h_c) = \mu_h$, and $\ln(T_{50,c}) = \mu_{T_{50}}$, plus $\gamma_y = \mu_\gamma$ the random effect for length-at-age-0 [described below]), then we have no random effects in the model. To aid convergence, we combined data from multiple cohorts (or years) when data were limited. For instance, with the cohort-specific effects we estimated a single random effect for the first four cohorts and another random effect covering the last three cohorts due to small sample sizes. Similarly, with the year-specific effects, we did not estimate a random year effect on growth for the first three years (i.e., $I_y = 0$ when $1979 \leq y \leq 1981$).

A suite of fixed effects variables was used to describe environmental conditions that may influence growth between age A and $A + 1$ (equations T1–T3; Table 3). We compared the effects of environmental conditions assuming they have equal effects on both phase-1 and phase-2 growth increments (i.e., setting the regression coefficients for phase-1 growth $\beta_x^* = 0$) and unequal effects (i.e., estimating regression coefficients for phase-1 β_x^* and phase-2 β_x growth components; equations T2–T3; Table 3). If $\beta_x^* \neq 0$, this would suggest an ontogenetic shift associated with the growth transition that changes how environmental conditions influence growth patterns. Environmental effects tested were water temperature (not logged; applied as a parabolic relationship where t_{crit}^* and t_{crit} represent the vertex of the parabola for phase-1 and phase-2 growth, respectively; equations T2–T3; Table 3), log(Delta outflow), log(conductivity), and a temperature – log(Delta outflow) (or log(conductivity)) interaction. Delta outflow and conductivity are highly correlated (>80% in log-space) and therefore measuring the similar environmental conditions within the San Francisco Estuary. Thus, they were not used in the same model but were statistically compared using a model comparison framework. To estimate the effects of density dependence and prey availability, we included several interactions between abundance, time, and prey densities. Here we are representing time as numerical month since hatching (assumed to be Jan 1 of a given year) to account for declines in abundance over a given year or, depending on the direction of the interaction, increases in biomass (especially with age-0 fish). Given model complexity and difficulties with convergence, we were only able to test interactions between time * age-0 abundance and time * age-1+ abundance. Attempts to incorporate interactions between abundance and prey densities resulted in convergence and memory allocation issues due to the number of parameters being estimated.

In addition to using mixed effects to describe variation in monthly growth rates, we also used a mixed-effects framework to describe variation in length-at-age-0 $L_{0,y}$ for each year y (i.e., length-at-hatching; equation T4; Table 3). Annual differences in $L_{0,y}$ can represent variation in hatch size and/or variation in hatch date (likely a combination of both, but we are unable to distinguish using these data). If we

assume the distribution of size-at-hatching is relatively consistent across years, then variation in $L_{0,y}$ should primarily be driven by variation in hatch dates. Variation in hatch dates arise from annual differences the timing of spawning and/or lengths of the incubation periods. Therefore, larger values of $L_{0,y}$ should represent earlier mean hatch dates and smaller values (or more negative values) should represent later mean hatch dates because we assumed a hatch date Jan 1 each year. Alternatively, if the hatch dates are constant over time, which is very unlikely, then variation in $L_{0,y}$ would be driven by variation in hatching size. We used a random-intercept regression to describe both random annual variation in $L_{0,y}$ (γ_y, where $\gamma_y \sim N(\mu_\gamma, \sigma_\gamma)$) and assumed linear interactions with environmental covariates (where α_x represent regression coefficients; equation T4; Table 3). Covariates used to estimate $L_{0,y}$ were related to spawning season (Dec 1 – May 31) and included the number of days with Delta outflow over 20,000 cfs (plus one), the number of days under 9ºC (plus one) and mean temperature and conductivity. All environmental covariates predicting the $L_{0,y}$ were logged and centered. Note that we experienced model convergence issues with the random-intercept and therefore only used a single intercept for the model (i.e., $\gamma_y = \gamma_{y=1}$).

The probability of observing a given individual is a function of both the underlying growth pattern, selectivity of the gear used to capture that individual, and spatial overlap of the survey relative to the distribution of the population. If gear selectivity is constant over all sizes, we would expect to observe individuals in proportion to their numeric availability (e.g., mostly small, young fish and few big, old fish). However, due to selectivity we observe fish in proportion to their numeric availability and their availability to the sampling gear. We used a truncated normal distribution to represent minimum size selectivity in the likelihood (equation T5; Table 3) where $N(x)$ is the normal probability density function with mean L_a and standard deviation σ and $\Phi(x)$ is the cumulative distribution function with a left truncation at a specified length $S_{g_i}$for individual i caught with gear g_i. We set g_i as the minimum observed length across all surveys. This is especially important for surveys such as the SFBS, as they only measured individuals above 40 mm in length. For simplicity, we assumed no maximum size selectivity. While we were able to account for some size-selectivity in the model, we were unable to account for spatial selectivity. Due to the migration patterns of LFS, the sampling programs do not cover the entire spatial distribution of the population when LFS move to the Pacific Ocean during summer months. If migration is driven in part by size, then there may be additional size-selectivity that could introduce bias into the model results. To assess this bias and improve the predictive capacity of the model, additional sampling across the entire distribution is needed. Additionally, methods combining otolith increment analysis and back-calculation could also provide valuable insight into potential bias.

Analysis

Following recommendations by Zuur et al. (2009), we planned on using a combined approach of restricted maximum likelihood (REML) estimation to select between different random effects structures (i.e., cohort versus year-specific growth model) and maximum likelihood (MLE) estimation to compare different fixed effects (i.e., assumptions based on how environmental variables effect Phase-1 and Phase-2 growth patterns). However, we ran into convergence issues due to the number of fixed effects parameters being estimated. Therefore, we followed a slightly modified process where (step 1) we

initially fit the different random effects structures (cohort- and year-specific growth models) using REML and compared the models with Akaike Information Criterion (AIC; equations T6 and T7; Table 3; where NLL is the negative log likelihood and p is the number of parameters being estimated). Step 2 assessed if the effects of covariates differed between the growth phases (i.e., if $\beta_x^* = 0$ or $\beta_x^* \neq 0$) with AIC and verifying appropriate model structure using 95% confidence intervals of β_x^* to assess overlap with zero (i.e., assess how many parameters are significantly different from zero). Following this comparison (step 3), we used AIC to assess different representations for environmental conditions (Delta outflow versus conductivity) on both the growth increment and length-at-age-0 L_o. For the final step we compared different fixed effects structures (i.e., a comparison of interactive effects). We ran a suite of models (Table 4) to compare interaction effects, but restricted the number of interactions due to computer memory limitations.

When using the REML framework for model comparison, we are effectively treating all parameters (except those associated with estimating variance) as a random effect. This is beneficial as it allows us to generate unbiased estimates of variance (see Zuur et al. 2009 for more details on this). However, in our case this provides a challenge in comparing different numbers of fixed effects because the number of parameters p used in the AIC calculations does not change (i.e., only parameters associated with variance are counted in the AIC calculation). Therefore, the model comparison framework we used here does not effectively account for the number of parameters estimated within the model. As a result, choosing the most parsimonious model can be challenging if multiple models have close AIC values (i.e., $\Delta\mathrm{AIC} \leq 10$). This does not appear to be an issue in our case, as $\Delta\mathrm{AIC}$ values were consistently large (>250) when comparing models

Results

Initial models run using random effects associated with length-at-age-0 random intercept γ_y and the timing of transition from between the growth phases $T_{50,c}$ were unreliable and had inconsistent model fits. Therefore, we did not pursue models with those random effects further (i.e., we set $\gamma_y = \mu_\gamma$ and $\ln(T_{50,c}) = \mu_{T_{50}}$). It is possible that having consistent larval sampling during the entire hatching period and histology data could help inform these parameters.

Step 1 of our model comparison suggests the year-specific random effects structure (M-2) is better at predicting the observed length-at-age patterns than the cohort-specific growth model (M-1; Table 4). All further model comparisons were made using the year-specific random effect (M-2). For step 2 of our analysis, we compared the assumption that the response to environmental variables was different (M-2) between phase-1 and phase-2 growth versus the same (M-3; Table 4) using both AIC and overlap of Phase-1 regression coefficients β_x^* with zero (using the 95% confidence intervals; not shown). Using both measures the best model was M-2, suggesting the magnitude and (often) direction of the growth response to environmental conditions changes over the lifetime of LFS (Table 4; 5). The third step in our selection procedure compared the effects of Delta outflow (M-2) versus conductivity (M-5) on the growth increment and length-at-age-0. Results suggest the effects of Delta outflow was a better predictor (Table 4). The final step in the model comparison included interactions on both the growth increment and length-at-age-0 (M-6) compared to the best model without interactions (M-2) and

including interactions improved model fits (Table 4). Further assessment of model predictions below focuses on the best model with interactions (M-6).

Holding all effects at their mean and ignoring the random effects (i.e., holding them constant at zero), we predict a mean monthly growth rate during phase-1 (h) of about 8.6 mm (Table 5). This corresponds to a mean asymptotic size of 137 mm ($L_\infty = 3h/g$ where g corresponds to reproductive investment under the Lester et al. (2004) interpretation of the model). The transition between phase-1 and phase-2 growth was predicted at 6.2 months (Table 5). Finally, the length-at-age-0 (holding all effects at their mean) was -0. 3 mm (Table 5).

Prey densities, temperature, Delta outflow, the temperature-outflow interaction were all significant and the effects of these covariates differed between the growth phases (i.e., coefficients did not overlap with zero; Figure 2; Table 5). We predicted a positive relationship between phase-1 growth and the *E. affinis* abundance and a negative relationship between phase-2 and *E. affinis* abundance. We also predicted negative relationships between growth and Mysis abundance for both growth phases. In general, growth increased with temperature, but this relationship had wide confidence bounds for phase-2 growth (although the 95% confidence intervals for β_1 did not overlap zero; Table 5). The critical temperature for phase-1 growth t^*_{crit} was near the upper limit of observed temperatures (23°C; Table 5). For phase-2 growth t_{crit} was extremely negative (-47°C; Table 5), suggesting a linear relationship might have been better than a parabolic relationship. The effects of Delta outflow were opposite for phase-1 (negative) and phase-2 (positive) growth. The interactions between temperature and Delta outflow were also opposite for phase-1 (negative) and phase-2 (positive). For a given temperature during phase-1 growth, we predict growth increasing with outflow until high temperatures (20-22°C), where highest growth was predicted at intermediate temperatures (Figure 2). For phase-2 growth, we predict decreasing growth with increasing Delta outflow across temperatures below 20°C and highest growth at low to intermediate levels of Delta outflow at temperatures above 20°C (Figure 2).

The density and time-related effects (plus interactions) were also significant and the effects differed between the growth phases (Figure 3; Table 5). Phase-1 predicted growth rates were positively related to abundance (both age-0 and age-1+ indices) and negatively related to time. Phase-2 predicted growth rates were negatively related to abundance (both age-0 and age-1+ indices), along with time. For detecting density-dependent effects on growth, look for negative relationships between phase-1 growth and age-0 abundance (positive effect) along with phase-2 growth and age-1+ abundance (negative effect). The effects of age-1+ abundance on phase-1 growth and/or age-0 abundance on phase-2 growth may provide insight into inter-specific effects (e.g., competition if negative relationships) or underlying conditions that may be affecting abundance and growth simultaneously (e.g., positive relationships via unaccounted for effects or interactions). For the interactive effects of abundance and time, it is useful to think about the impacts resulting from declines in abundance over time, given the temporal scale (i.e., a month effect). In general, for phase-1 growth, we predict declines in growth as time since hatching increases (i.e., declining growth over time), but the relative declines in growth are larger at lower abundance indices (Figure 3, but note the transition between the growth phases is around 6.2 months). For phase-2 growth, we see the opposite, where growth generally declines from Jan-Dec, but the relative declines in growth are larger at higher abundance indices (Figure 3).

Environmental covariates for predicting length-at-age-0 $L_{0,y}$ were all significant (i.e., 95% confidence intervals did not overlap zero; Figure 3; Table 5). In general, larger (more positive) values for $L_{0,y}$ suggest earlier mean hatch dates and smaller (more negative) values suggest later hatch dates if size-at-hatching is relatively consistent over time. The number of days during the spawning season (Dec 1 – May 31) with Delta outflow over 20,000 cfs was negatively related to $L_{0,y}$, suggesting that large rain events and/or large reservoir releases over the spawning season led to smaller values of $L_{0,y}$ or later hatch dates (Figure 4; Table 5). We predicted a negative effect of mean water temperature (from Dec 1 – May 31) on length-at-age-0 (Figure 4; Table 5). Assuming $L_{0,y}$ is related to mean spawning time, this suggests that a colder spawning season leads to earlier spawning and/or larger $L_{0,y}$ on Jan-1 than warmer spawning seasons. It is important to note that some of these variables are related and influenced by water management.

Overall, we did not see any major trends in the random year effect I_y on growth or predicted length-at-age-0, 1, or 2 (where age is in years; Figure 5). With I_y, we predicted relatively high growth through the mid-1980s, but this is likely an artifact of sampling design and high reliance on fall surveys (FMWT) and SFBS not measuring individuals <40mm until juvenile sampling increased with the 20mm program in 1995. Predicted length-at-age-0 showed high interannual variation across time and this variation persisted as the cohorts progressed over time. It is important to note that the range in mean length-at-age-0 was only around a 7 mm difference between the lowest and largest predicted values. This variation increased with predicted length-at-age-1, which a range of about 18 mm between age-1 fish in 1982 (58 mm) and 2001 (76 mm). Finally, the range in predicted length-at-age-2 was similar, about 18mm, with the smallest in 1982 (95mm) and largest in 1990 (114mm).

Looking at the general model fits, it appears that the model does a good job predicting the mean length-at-age patterns (Figure 6). There are certain cohorts where the model underestimates the length-at-age of older fish (>10 months of age), but in these instances we had large numbers of small fish caught in the 20mm, SLS, and EDSM 20mm surveys (Figure 6). This pattern could arise from low sample sizes of larger/older fish, size-based mortality patterns (we only observe fish that survived to be caught and have no information on fish that did not survive to be sampled), differences in the distribution of sampling relative to the distribution of the population (e.g., we are not sampling across the entire distribution of the population), and/or many other factors. It is also important to note the selectivity of the SFBS, where only fish >40 mm were measured (easily seen in the 1985 cohort, but present in all other cohorts) and with the SLS study where we see fish recruiting to the gear after hatching (e.g., 2006 cohort; Figure 6). Besides these instances of underestimation at older length-at-age and selectivity, there are no obvious patterns in the residuals (Figure 6).

Discussion

Utilizing a modified biphasic growth model, we identified a suite of biotic and abiotic drivers in LFS apparent growth patterns. Based on model results, we predicted similar magnitudes of abiotic (temperature, Delta outflow), biotic (prey availability), and density-related effects on the monthly growth increments (Figures 2 and 3). This suggests that LFS growth is not driven by a single environmental factor, but rather a mixture of environmental conditions. Although we found high

interannual variability in the predicted length-at-age of LFS, the growth patterns have remained remarkably stable between 1979-2020 considering the declines in SFE productivity and establishment of the invasive clam *P. amurensis* in the late 1980s (Kimmerer and Orsi 1996; Kimmerer 2002), declines in pelagic population sizes in the 2000s (i.e., POD; Sommer et al. 2007), changes to their prey base (Figure 1).

There is very little published information about the growth rates of LFS, but the general patterns in growth predicted here reflect those earlier studies on LFS growth. Using daily otolith increments, LFS display slow growth during early life (larval stage), which increases to about 6 months, then slows again (Hobbs, unpublished). This is depicted with our estimates, with 0.13 mm/day (range 0.07-0.20 mm/day) during the first month compared to 0.23 mm/day (range 0.09-0.35 mm/day) around 6 months and 0.14 mm/day (range 0.08-0.22 mm/day) around 11 months of age. These estimates also fall within the range observed by Souza et al. (2006), who predicted a mean apparent growth rate of 0.12-0.23 mm/day between 1995-2004 using data from the 20mm Survey (data also used in this study). LFS in Lake Washington from the 1960s averaged from 52-77 mm FL at 10-months (Moulton 1974), which is slightly larger than the predicted mean length-at-age-10 months from our model (mean 61 mm with a range of 51-66 mm).

A positive relationship between outflow and LFS abundance has been documented by several studies (Stevens and Miller 1983; Jassby et al. 1995; Kimmerer 2002), but hypotheses remain to be tested about the biological mechanism behind the relationship. For example, higher outflow may create a larger area of low and intermediate salinity habitat where LFS may have a competitive advantage over other estuarine species (Hieb and Baxter 1993, Baxter 1999). This hypothesis would be consistent with a positive outflow-growth relationship and may be a cause for the positive relationship between phase-1 growth and outflow (Figure 2). Another hypothesis is that the relationship between food availability and outflow may drive the apparent relationship between LFS abundance and outflow. For example, the abundance of one preferred prey item, *E. affinis*, has been correlated with the location of X2 in the spring (Kimmerer 2002), which is again consistent with observations for phase-1 growth. In contrast, there was a negative relationship between growth and the water year index using data reported by Souza et al. (2006), which is similar to the predictions between outflow and phase-2 growth (i.e., negative; Figure 2). This suggests that any relationship between outflow and growth may be age (or stage) dependent and/or influenced by other environmental conditions that the fish experience.

The SFE population of LFS occupy habitat near the upper thermal limit of its range. During the initial growth phase (up to 6.2 months) we predicted a positive relationship between temperature and growth, suggesting that LFS growth increases with temperatures, consistent with observations of larval growth from lab studies (Yanagitsuru et al. 2021; here we are classifying larval LFS as being <20mm). However, after transitioning to the secondary growth phase, we predicted a highly variable relationship between growth and temperature. This trend is likely influenced by the distribution of LFS in the SFE because summer water temperatures in many areas of the SFE regularly exceed thermal maxima for LFS and has been found to restrict the distribution of age-1 LFS (Baxter 1999).

The predicted relationships between prey availability and growth indicated that prey densities may be important drivers of early growth during phase-1 (up to ~6 months), but *E. affinis* and Mysis may not be limiting during phase-2 growth. We identified a positive relationship between *E. affinis* densities and

phase-1 growth, suggesting this prey source may be a bottom-up driver of early growth in LFS. This is supported by dietary studies on LFS that show high reliance on *E. affinis* (~90%) until about 25 mm in length, after which they switch to selecting for Mysis (Barros et al. 2022), which is about 4-5 months after hatching. The effects of Mysis on phase-1 growth were opposite of what we would expect, however caution should be used to infer the importance of Mysis during phase-1 growth using these results due to the growth transition around 6-months of age. For phase-2 growth the relationships between both *E. affinis* and Mysis were also opposite of what we would expect. This suggests that bottom-up factors play minor role in influencing growth during phase-2 or, more likely, we did not accurately capture prey availability for phase-2 when large portions of time are spent in ocean.

Density-dependent growth is a key process regulating population growth (Lorenzen and Enberg 2002) and is one of the best-established forms of density-dependence in fishes (Beverton and Holt 1957). With density-dependent growth, we expect a negative relationship between abundance and growth for a given age/phase grouping (i.e., declining phase-1 growth with age-0 abundance or declining phase-2 growth with age-1+ abundance), as predicted for the effects of age-1+ abundance index on phase-2 growth (Figure 3). For phase-1 growth we predicted the opposite, increasing growth with age-0 abundance, suggesting density dependent growth might not be a driving factor in LFS early-life growth. Additional density-dependence may arise via the abundance-time interactions, in which we would expect growth to increase as time-since hatching (Jan-1) increases. This assumes that there is a time-abundance relationship (i.e., mortality) that is relatively consistent over a given year (i.e., abundance in a given year is highest on Jan-1 and declines until Dec-31). If this were the case, we would see a positive effect of time on growth. However, density-dependent growth is also dependent on prey availability, which likely is interacting with abundance. We were unable to account for these interactions due to model complexity and size.

Using otolith increments Hobbs (unpublished), identified a growth transition around 6–7 months, in which the growth rate slowed after this transition. This timing corresponds with our estimated transition between phase-1 and phase-2 growth ($T_{50,c}$) where we are predicting a switch from linear to von Bertalanffy growth around 6.2 months of age. We should note the traditional interpretation of the model assumes this growth transition is associated with maturation and investment into reproduction (Lester et al. 2004). However, previous studies suggest that LFS tend to mature around age-22 months (Dryfoos 1965, Moulton 1974, Hieb and Baxter 1993). Therefore, it is possible that additional data on maturation could help inform the growth transition associated with maturation. The growth transition predicted in our model may be describing an ontogenetic shift occurring during the juvenile growth phase. Juvenile LFS migration from the SFE to the Pacific Ocean is expected to occur in spring or early summer (Rosenfield and Baxter 2007; Tobias and Baxter 2022*, in press*), which should be around 6 months of age. The predicted growth transition may be related changes in growth with seaward migration, could be a sampling artifact due to fish moving out of the sampling area, or could be a combination of both. Further assessment of this change in growth around 6 months of age is necessary.

The LFS dataset used in this model may introduce bias due to migration/spatial selectivity and incomplete sampling of the population during parts of the year (i.e., summer). Juvenile LFS migrate to the Pacific Ocean once water temperatures in the SFE warm from spring into early summer (roughly around 6 months of age assuming a January 1 hatch date) and return to the SFE as temperatures

decrease in the fall and early winter (Rosenfield and Baxter 2007; Jefferies et al. 2016; Tobias and Baxter 2022, *in press*). Some fish that migrate to the Pacific Ocean may remain in marine waters for extended periods (e.g., over the winter), while others return over the fall and winter (reviewed in Chen et al. 2022). Further, LFS are facultatively anadromous within the SFE and some individuals may remain in the SFE over the entire year (Moyle 2002). Given this complex life history, we expect that some of the relationships between growth and environmental factors identified here may be biased using the historical data and future efforts should explore these the magnitude and direction of potential biases. Nevertheless, our predictions of relatively stable LFS growth over time (i.e., predicted lengths-at-age 0, 1, and 2 years) should be robust to bias associated with migration because sampling occurred over the entire year throughout the entire time series and the bias associated with migration should influence all cohorts equally (i.e., we expect the bias to remain stable over all cohorts analyzed). Additionally, there should be minimal spatial sampling bias for comparing predicted length-at-age 0, 1, and 2 (i.e., over winter if we assume a January 1 hatch date) because the timing of the LFS migration patterns in the SFE follow predictable seasonal patterns (Tobias and Baxter 2022, *in press*) and there should be high spatial overlap of the population and sampling distributions over winter months. Ideally, we would be able to sample individuals from across the entire spatial extent of the population and obtaining length samples outside of the SFE would allow us to assess bias in the growth model developed here. Until an expanded sampling program is implemented, it may also be feasible to incorporate and/or compare growth trajectories informed via otolith increment analyses to assess for bias in this growth model associated with migration out of the sampling area.

It has also been suggested that using otolith increment analyses would be a better option to quantify the impacts of environmental conditions on growth and, in some ways, this is a valid argument. Otoliths should provide a better measure of individual growth assuming daily/annual growth increments accurately reflect growth in length. However, there are several major benefits for using the available LFS data. Extracting otoliths is lethal and the methods described here provide a way to measure apparent growth rates using non-lethal means. Further, otoliths from LFS were infrequently collected in the past and using the available data as we have done here may be one of the only ways to quantify changes in growth from the 1980s-present. We should note that ongoing and future efforts using otolith increment analyses are still valuable for quantifying changes in growth patterns. For instance (as mentioned above), otolith increment analyses may still provide an opportunity to assess bias in the growth models developed here. Therefore, future efforts to assess variation in LFS growth should focus on utilizing a hybrid approach that integrates multiple data types to provide robust and unbiased estimates.

Many long-term monitoring programs have been designed to collect information on abundance trends. These programs often collect demographics data (e.g., length, weight, age, maturity, sex, etc.) along with abundance trends that can also be used to monitor changes in population productivity and/or life-history characteristics. We used data from multiple long-term monitoring programs to assess for systematic changes in apparent growth of a population experiencing abundance declines. Results show that apparent growth patterns and predicted length-at-age, while variable, have remained stable from 1979–2020. Given the declining LFS population trajectories in the SFE (see Chen et al. 2022), we recommend continued monitoring of LFS growth patterns as an indicator for changes in population productivity. Additional analytical efforts should be focused on quantifying changes in other life-history characteristics that influence population productivity, such as the maturation schedule (i.e., proportion maturing at a given age), frequency of repeat spawning, and/or mortality. Additionally, changes to the

prey base and SFE productivity may drive changes in egg quality and ultimately larval survival (e.g., thiamine deficiency in Lake Trout *Salvelinus namaycush* and Chinook salmon; Fitzsimons et al. 2009; NOAA 2020). By identifying the drivers of the SFE LFS population decline, we can develop targeted management actions to facilitate population recovery.

References

Barros, A., Hobbs, J.A., Willmes, M., Parker, C.M., Bisson, M., Fangue, N.A., Rypel, A.L., Lewis, L.S. 2022. Spatial heterogeneity in prey availability, feeding success, and dietary selectivity for the threatened longfin smelt. Estuaries and Coasts: In press, https://doi.org/10.1007/s12237-021-01024-y

Bashevkin S.M. 2020. zooper: an R package to download and integrate zooplankton datasets from the Upper San Francisco Estuary. v2.3.1. Zenodo.

Bashevkin, S.M., Hartman, R., Thomas, M., Barros A., Burdi, C.E., Hennessy, A., Tempel, T., and Kayfetz, K. 2022. Five decades (1972–2020) of zooplankton monitoring in the upper San Francisco Estuary. PLOS ONE 17: e0265402. doi:10.1371/journal.pone.0265402

Baxter, R.D. 1999. Osmeridae. Pages 179–216 *in* J. J. Orsi (ed.) Report on the 1980–1995 fish, shrimp and crab sampling in the San Francisco Estuary. Interagency Ecological Program for the Sacramento-San Joaquin Estuary Technical Report 63. 503 pages.

Beverton, R.J.H. and Holt, S.J. 1957. On the dynamics of exploited fish populations. In: Fishery Investigations Series. Ministry of Agriculture, Fisheries and Food, London.

California Department of Fish and Game (CDFG). 2009. Report to the Fish and Game Commission: A status review of the longfin smelt (Spirinchus thaleichthys) in California. 46 pages.

California Department of Fish and Wildlife (CDFW). 2021. Bay-Delta Studies and Surveys. Available online at https://wildlife.ca.gov/Conservation/Delta

California Department of Water Resources (CDWR). 2013. California Water Plan Update 2013. Investing in innovation and infrastructure, Volume 1: the strategic plan. Bulletin 160–13. Sacramento, CA. 2013.

Charnov, E.L. 1993. Life History Invariants: Some Explorations of Symmetry in Evolutionary Ecology. Oxford University Press, Oxford, UK.

Charnov, E.L., Turner, T.F., and Winemiller, K.O. 2001. Reproductive constraints and the evolution of life histories with indeterminate growth. Proc. Natl. Acad. Sci. 98(16): 9460–9464.

Chen, E., Tobias, V., Kakin, M., Hobbs, J., and Roessler, A. 2022. Species Status Assessment for the San Francisco Bay-Delta distinct population segment of the longfin smelt. Editors: S. Detwiler and M. Nobriga.

Cloern, J.E., and Jassby, A.D. 2012. Drivers of change in estuarine-coastal ecosystems: drivers from four decades of studies in San Francisco Bay. Rev. Geophys. 50:1–33.

Czarnołe‘ski, M. and Kozłowski, J. 1998. Do Bertalanffy’s growth curves result from optimal resource allocation? Ecol. Lett. 1, 5–7.

Davidson, R.S., Letcher, B.H., Nislow, K.H. 2010. Drivers of growth variation in juvenile Atlantic Salmon (*Salmo salar*): an elasticity analysis approach. J. Anim. Ecol. 79, 1113–1121.

Day, T., and Taylor, P.D. 1997. Von Bertalanffy's growth equation should not be used to model age and size at maturity. Am. Nat.: 381–393.

Dorn, M.W. 1992. Detecting environmental covariates of Pacific Whiting *Merluccius productus* growth using a growth-increment regression model. Fish. Bull. 90, 260–275.

Dryfoos, R.L. 1965. The life history and ecology of the longfin smelt in Lake Washington. Ph.D. Dissertation. University of Washington, Tacoma WA. 229 pages.

Fitzsimons, J.D., Brown, S.B., Williston, B., Williston, G., Brown, L.R., Moore, K., Honeyfield, D.C., and Tillitt, D.E. 2009. Influence of thiamine deficiency on lake trout larval growth, foraging, and predator avoidance. J. Aquat. Anim. Health. 21:302–14. doi: 10.1577/H08-019.1. PMID: 20218504.

Haugen, T.O., Winfield, I.J., Vollestad, L.A., Fletcher, J.M., Ben James, J., Stenseth, N.C. 2007. Density dependence and density independence in the demography and dispersal of Pike over four decades. Ecol. Monogr. 77, 483–502.

Hieb, K., and Baxter, R. 1993. Delta outflow/San Francisco Bay. Pages 101–116 in P. L. Herrgesell, editor. 1991 Annual Report - Interagency Ecological Studies Program for the Sacramento-San Joaquin Estuary, Sacramento, California.

Hobbs, J.A., Lewis, L.S., Ikemiyagi, N., Sommer, T. and Baxter, R.D. 2010. The use of otolith strontium isotopes (87 Sr/86 Sr) to identify nursery habitat for a threatened estuarine fish. Environmental biology of fishes, 89(3), pp.557–569.

Jassby, A.D. and Cloern, J.E. 2000. Organic matter sources and rehabilitation of the Sacramento-San Joaquin Delta (California, USA). Aquatic Conservation: Marine and Freshwater Ecosystems 10(5):323–352.

Jassby, A.D., Kimmerer, W.J., Monismith, S.G., Armor, C., Cloern, J.E., Powell, T.M., Schubel, J.R., and Vendlinski, T.J. 1995. Isohaline position as a habitat indicator for estuarine populations. Ecological applications, 5(1):272–289.

Jeffries, K.M., Connon, R.E., Davis, B.E., Komoroske, L.M., Britton, M.T., Sommer, T., Todgham, A.E. and Fangue, N.A. 2016. Effects of high temperatures on threatened estuarine fishes during periods of extreme drought. Journal of Experimental Biology, 219(11), pp.1705–1716.

Johnston, T.A. 1997. Within-population variability in egg characteristics of walleye (Stizostedion vitreum) and white sucker (Catostomus commersoni). Can. J. Fish. Aquat. Sci. 54:1006–1014.

Kimmerer, W.J. 2002. Effects of freshwater flow on abundance of estuarine organisms: physical effects or trophic linkages? Marine Ecology Progress Series 243:39–55.

Kimmerer, W.J., and Orsi, J.J. 1996. Changes in the zooplankton of the San Francisco Bay Estuary since the introduction of the clam, Potamocorbula amurensis. San Francisco Bay: the ecosystem. J. T. Hollibaugh. San Francisco, CA, Pacific Division of the American Association for the Advancement of Science: 403–424.

Kristensen, K., Nielsen, A., Berg, C.W., Skaug, H., and Bell, B.M. 2016. TMB: automatic differentiation and Laplace approximation. Journal of Statistical Software, 70(5), 1–21. doi:10.18637/jss.v070.i05

Lester, N.P., Shuter, B.J., Abrams, P.A. 2004. Interpreting the von Bertalanffy model of somatic growth in fishes: the cost of reproduction. Proc. R. Soc. Lond. B Biol. Sci. 271, 1625–1631. https://doi.org/10.1098/rspb.2004.2778

Lorenzen, K. 1996. A simple von Bertalanffy model for density-dependent growth in extensive aquaculture, with an application to Common Carp (*Cyprinus carpio*). Aquaculture 142, 191–205.

Lorenzen, K. and Enberg, K. 2002. Density-dependent growth as a key mechanism in the regulation of fish populations: evidence from among-population comparisons. Proc. R. Soc. Lond. Ser. B: Biol. Sci. 269, 49–54.

Lotze, H.K., Lenihan, H.S., Bourque, B.J., Bradbury, R.H., Cooke, R.G., Kay, M.C., Kidwell, S.M., Kirby, M.X., Peterson, C.H. and Jackson, J.B.C. 2006. Depletion, degradation, and recovery potential of estuaries and coastal seas. Science 312, 1806–1809.

Lotze, H.K. 2010. Historical reconstruction of human-induced changes in U.S. estuaries. Oceanogr. Mar. Biol. Ann. Rev. 48:267–338. doi: 10.1201/EBK1439821169-c5

Maceina, M.J., Bettoli, P.W., Klussmann, W.G., Betsill, R.K., Noble, R.L. 1991. Effect of aquatic macrophyte removal on recruitment and growth of Black Crappies and White Crappies in Lake Conroe, Texas. N. Am. J. Fish. Manage. 11, 556–563.

Maceina, M.J. and Shireman, J.V. 1982. Influence of dense Hydrilla infestation on Black Crappie growth. Proc. Annu. Conf. Southeast Assoc. Fish and Wildl. Agencies 36, 394–402.

Matthias, B.G., Ahrens, R.N.M., Allen, M.S., Tuten, T., Siders, Z.A., & Wilson, K.L. 2018. Understanding the effects of density and environmental variability on the process of fish growth. Fisheries Research 198:209– 219. https://doi.org/10.1016/j.fishres.2017.08.018

Matthias, B.G., Ahrens, R.N.M., Allen, M.S., Lombardi-Carlson, L.A., and Fitzhugh, G.R. 2016. Comparison of growth models for sequential hermaphrodites by considering multi-phasic growth. Fisheries Research 179:67–75. https://doi.org/10.1016/j.fishres.2016.02.006

Mittelback, G.G. and Persson, L. 1998. The ontogeny of piscivory and its ecological consequences. Canadian Journal of Aquatic Sciences 55:1454–1465. https://doi.org/10.1139/f98-041

Moulton, L.L. 1974. Abundance, growth and spawning of the longfin smelt in Lake Washington. Transactions of the American Fisheries Society 103(1):46–52.

Moyle, P.B. 2002. Inland fishes of California (revised and expanded). University of California Press, Ltd. London, England. 146–150.

National Oceanic and Atmospheric Administration (NOAA). 2020. Researchers probe deaths of Central Valley Chinook, with possible ties to ocean changes. https://www.fisheries.noaa.gov/feature-story/researchers-probe-deaths-central-valley-chinook-possible-ties-ocean-changes#:~:text=Scientists%20from%20several%20fish%20and,its%20effect%20is%20not%20clear. Accessed 05/16/2022.

Pauly, D. 1980. On the interrelationships between natural mortality, growth parameters, and mean environmental temperature in 175 fish stocks. ICES J. Mar. Sci. 39, 175–192.

Porch, C.E., Wilson, C.A., and Nieland, D.L. 2002. A new growth model for red drum (*Sciaenops ocellatus*) that accommodates seasonal and ontogenic changes in growth rates. Fish. Bull. 100, 149–152.

R Core Team. 2021. R: A language and environment for statistical computing. R Foundation for Statistical Computing, Vienna, Austria. URL https://www.R-project.org/.

Ricker, W.E. 1975. Computation and Interpretation of Biological Statistics of Fish Populations. Department of the Environment Fisheries and Marine Service, Crown Ottawa, Canada.

Rosenfield, J.A., and Baxter, R.D. 2007. Population dynamics and distribution patterns of longfin smelt in the San Francisco Estuary. Transactions American Fisheries Society 136:1577–1592.

Shelton, A.O., Satterthwaite, W.H., Beakes, M.P., Munch, S.B., Sogard, S.M., and Mangel, M. 2013. Separating intrinsic and environmental contributions to growth and their population consequences. Am. Nat. 181, 799–814.

Sommer, T., Armor, C., Baxter, R., Breuer, R., Brown, L., Chotkowski, M., Culberson, S., Feyrer, F., Gingras, M., Herbold, B., and Kimmerer, W. 2007. The collapse of pelagic fishes in the upper San Francisco Estuary. Fisheries 32(6):270–277.

Souza, K., Hieb, K., Fleming, K., Bryant, M. and Baxter, R. 2006. Apparent growth rates of pelagic fishes and relationship to abundance. Interim Report on Pelagic Organism Decline Investigations. 9 pages.

Stearns, S.C. 1992. The Evolution of Life Histories. Oxford University Press, Oxford, UK.

Stevens, D.E. and Miller, L.W. 1983. Effects of river flow on abundance of young chinook salmon, American shad, longfin smelt, and delta smelt in the Sacramento-San Joaquin River System. North American Journal of Fisheries Management 3(4):425–437.

Thomson, J.R., Kimmerer, W.J., Brown, L.R., Newman, K.B., MacNally, R., Bennett, W.A., Feyrer, F. and Fleishman, E. 2010. Bayesian change point analysis of abundance trends for pelagic fishes in the upper San Francisco Estuary. Ecological Applications 20(5):1431–1448.

Tobias, V.D. 2022. Longfin smelt technical note 2: separating year classes of longfin smelt by patterns in length at date data. Version 2.1.

Tobias, V.D. and Baxter, R. 2022 *In Press*. Fewer and farther between: changes in the timing of longfin smelt (Spirinchus thaleichthys) movement in the San Francisco Estuary. Preprints 2021. 2021010512 doi:10.20944/preprints202101.0512.v1.

Vøllestad, L.A. and Olsen, E.M. 2008. Non-additive effects of density-dependent and density independent factors on Brown Trout vital rates. Oikos 117, 1752–1760.

von Bertalanffy, L. 1968. General system theory: foundations, development, applications. 2nd edition. George Braziller, inc. New York, NY.

von Bertalanffy, L. 1938. A quantitative theory of organic growth (inquiries ongrowth laws. II). Hum. Biol. 10, 181–213.

Walters, C.J., Martell, S.J.D. 2004. Fisheries Ecology and Management. Princeton University Press, Princeton, New Jersey.

Whitfield, A.K. 1999. Ichthyofaunal assemblages in estuaries: a South African case study. Reviews in Fish Biology and Fisheries 9(2):151–186.

Wilson, K.L., Honsey, A.E., Moe, B.J., Venturelli, P. 2018. Growing the biphasic framework: techniques and recommendations for fitting emerging growth models. Methods in Ecology and Evolution 9: 822–833. https://doi.org/10.1111/2041-210X.12931

Yanagitsuru, Y.R., Main, M.A., Lewis, L.S., Hobbs, J.A., Hung, T.C., Connon, R.E. and Fangue, N.A. 2021. Effects of temperature on hatching and growth performance of embryos and yolk-sac larvae of a threatened estuarine fish: Longfin smelt (*Spirinchus thaleichthys*). Aquaculture, 537, p.736502. DOI: https://doi.org/10.1016/j.aquaculture.2021.736502

Zuur, A.F., Ieno, E.N., Walker, N.J., Saveliev, A.A., Smith, G.M. 2009. Mixed effects models and extension in ecology with R. Springer Science + Business Media, LLC. New York, NY.

Tables

Table 1: Sample sizes for each survey used in the Longfin Smelt growth model.

Year	20 mm	EDSM 20 mm	EDSM KT	FMWT	SFBS	SLS	Total
1981	-	-	-	665	3,933	-	4,598
1982	-	-	-	763	31,007	-	31,770
1983	-	-	-	92	14,413	-	15,105
1984	-	-	-	463	4,414	-	4,877
1985	-	-	-	294	2,746	-	3,040
1986	-	-	-	237	2,392	-	2,629
1987	-	-	-	552	1,820	-	2,372
1988	-	-	-	392	1,240	-	1,632
1989	-	-	-	239	429	-	668
1990	-	-	-	152	161	-	313
1991	-	-	-	214	158	-	372
1992	-	-	-	82	95	-	177
1993	-	-	-	636	552	-	1,188
1994	-	-	-	917	328	-	1,245
1995	4,054	-	-	1,940	12,426	-	18,420
1996	17,796	-	-	1,674	1,650	-	21,120
1997	13,533	-	-	603	1,322	-	15,458
1998	7,617	-	-	2,262	4,699	-	14,578
1999	11,160	-	-	1,375	6,655	-	19,190
2000	18,174	-	-	1,449	2,995	-	22,618
2001	10,251	-	-	916	1,140	-	12,307
2002	14,195	-	-	449	1,012	-	15,656
2003	6,180	-	-	316	717	-	7,213
2004	5,494	-	-	129	871	-	6,494
2005	4,197	-	-	65	638	2,104	7,004
2006	3,492	-	-	436	1,191	3,606	8,725
2007	2,603	-	-	10	476	3	3,092
2008	9,022	-	-	87	334	-	9,443
2009	13,577	-	-	51	419	-	14,047
2010	6,698	-	-	83	166	-	6,947
2011	4,923	-	-	292	1,020	-	6,235
2012	3,309	-	-	36	589	-	3,934
2013	12,648	-	-	83	528	-	13,259
2014	1,851	-	-	11	139	-	2,001
2015	451	-	-	3	101	-	555
2016	1,081	-	-	6	-	-	1,087
2017	3,199	283	66	69	-	-	3,617
2018	2,030	61	237	-	-	-	2,328
2019	4,568	34	288	-	-	-	4,890
2020	-	919	43	-	-	-	962

Year	20 mm	EDSM 20 mm	EDSM KT	FMWT	SFBS	SLS	Total
Total	182,103	1,297	634	18,643	102,776	5,713	311,166

Table 2: Indices used to calculate abundance trends in the growth model. Indices were based on Fall Midwater Trawl Catch (FMWT), San Francisco Bay Study (SFBS) midwater trawl (MWT), and SFBS otter trawl (OT). Age-specific indices were available for both SFBS surveys. Values with superscripts were estimated using linear regression techniques (see methods) and values of *a* indicate index was unavailable and *b* indicate the value was recorded as zero. The SFBS OT indices from 1979–2020 were used in the growth model.

Year	FMWT	SFBS MWT Age-0	SFBS MWT Age-1	SFBS MWT Age-2	SFBS OT Age-0	SFBS OT Age-1	SFBS OT Age-2
1977	210	1,238[a]	-	-	3,245[a]	-	-
1978	6,619	21,026[a]	393[a]	-	25,126[a]	1,029[a]	-
1979	-	5,289[a]	7,354[a]	125[a]	737[a]	1,631[a]	326[a]
1980	31,184	190,790	1,386	2,572	128,321	142	106
1981	2,202	1,959	51,372	644	4,139	11,837	122
1982	62,905	299,069	9,785	2,307	257,965	3,070	1,005
1983	11,864	33,651	296,253	2,865	23,860	142,861	917
1984	7,408	29,218	25,463	4,082	44,329	29,399	5,767
1985	992	2,895	58,525	2,693	11,787	12,626	1,185
1986	6,160	24,908	12,524	2,479	12,070	2,784	288
1987	1,520	2,872	33,471	2,287	1,984	7,174	1,284
1988	791	1,724	18,360	4,921	1,094	4,323	2,220
1989	456	1,137	6,595	1,514	971	2,179	369
1990	243	745	2,776	1,058	681	386	317
1991	134	131	3,852	541	245	474	161
1992	76	370	1,134	86	620	448	218
1993	798	5,086	811	22	7,006	53	59[b]
1994	545	1,930[a]	16,515	349	2,847	4,207	479
1995	8,205	555,398	612[a]	1,637[a]	152,973	791	504
1996	1,346	666	31,522[a]	194[a]	11,045	4,153	248
1997	690	4,585	6,863	1,789	10,692	3,706	1,075
1998	6,654	62,853	6,240	1,120	20,605	197	89
1999	5,243	59,040	17,546	895	57,980	6,827	600
2000	3,437	12,326	12,132	1,168	16,079	1,841	240
2001	247	2,107	10,707	1,154	812	15,507	954
2002	707	1,173	2,472	1,900	18,132	1,070	1,604
2003	467	230	2,558	186	4,007	6,339	1,292
2004	191	1,307	2,030	486	3,529	4,323	886
2005	129	617	3,487	545	8,459	4,074	593
2006	1,949	2,780	1,342	91	21,517	1,379	285
2007	13	441	1,351	79	3,636	5,156	815

Year	FMWT	SFBS MWT Age-0	SFBS MWT Age-1	SFBS MWT Age-2	SFBS OT Age-0	SFBS OT Age-1	SFBS OT Age-2
2008	139	1,207	218	230	6,155	343	162
2009	65	323	3,485	75	971	10,317	469
2010	191	867	599	114	628	1,373	280
2011	477	1,404	950	106	14,261	7,134	503
2012	61	398	5,353	1,106	2,170	840	360
2013	164	1,445	647	324	15,545	574	277
2014	16	1,194	615	91[b]	1,228	519	63
2015	4	231	403	44	536	693	196
2016	7	508[a]	106[a]	124[a]	432[a]	127[a]	164[a]
2017	141	2106	161	49	5,844	137[b]	30
2018	52	804[a]	668[a]	51[a]	3,387	1,854[a]	43[a]
2019	-	1,006[a]	255[a]	212[a]	3,939[a]	1,074[a]	588[a]
2020	-	1,006[a]	319[a]	81[a]	3,939[a]	1,249[a]	341[a]

Table 3: Equations used in the longfin smelt growth model (described in methods text).

Description		Equation	Components
(1a)	Growth increment – juvenile	$l_1 = h_c t e^{B^*_{y,m}}$	$L_{\infty,c} = 3h_c g^{-1}$
(1b)	Growth increment – maturing	$l_2 = h_c t e^{B^*_{y,m}}(1-A^*) + \left(L_{\infty,c} - \left(L_{A,y} + h_c t e^{B^*_{y,m}}(1-A^*)\right)\right) * \left(1 - e^{-k(A^*)}\right) e^{B_{y,m}}$	$k = \ln(1 + g/3)$ $A^* = (A + t) - T_{50,c}$ $\ln(T_{50,c}) \sim N(\mu_{T_{50}}, \sigma_{T_{50}})$ Cohort-specific model
(1c)	Growth increment – adult	$l_3 = \left(L_{\infty,c} - L_{A,y}\right)\left(1 - e^{-kt}\right) e^{B_{y,m}}$	$\ln(h_c) \sim N(\mu_h, \sigma_h)$
(1d)	Prob. of growing following juvenile growth phase	$P_1 = (1 - P_2)$	$I_y = 0$
(1e)	Prob. of maturing between ages $A-1$ and A	$P_2 = \left(1 + e^{-(A - T_{50,c})/0.1}\right)^{-1} - P_3$	Year-specific model $\ln(h_c) = \mu_h$
(1f)	Prob. of growing following adult growth phase	$P_3 = \left(1 + e^{-\left((A+t) - T_{50,c}\right)/0.1}\right)^{-1}$	$I_y \sim N(0, \sigma_I)$
(1g)	Pred. length-at-age a for year y	$L_{a,y} = L_{A+t,y} = L_{A,y} + \sum_{j=1}^{3} l_j P_j e^{I_y}$	
(2)	Month-specific effect on adult growth	$B_{y,m} = \beta_1 (x - t_{crt})^2_{1,y,m} + \sum_{j=2}^{n_\beta} \beta_j x_{j,y,m}$	

(3)	Month-specific effect on juvenile growth	$\mathrm{B}^{*}_{y,m} = (\beta_1 + \beta_1^{*})(x - t^{*}_{crt})^2_{1,y,m} + \sum_{j=2}^{n_\beta}(\beta_j + \beta_j^{*})x_{j,y,m}$	
(4)	Length-at-age-0 for year y	$L_{0,y} = \gamma_y + \sum_{j=1}^{n_\alpha}\alpha_j \mathrm{x}_{j,y}$	$\gamma_y \sim N(\mu_\gamma, \sigma_\gamma)$
(5)	Likelihood for each observation i	$L_i = N(L_i \mid L_a, \sigma) * \left(1 - \Phi\left((S_{g_i} - L_a)\sigma^{-1}\right)\right)^{-1}$	
(6)	Total negative log likelihood	$\mathrm{NLL} = -\sum_{i=1}^{n} \ln(L_i)$	
(7)	AIC	$AIC = 2 * \mathrm{NLL} + 2 * p$	

Table 4: Results for model comparison. The x's indicate parameters used in the model estimated separately for phase-1 and phase-2 growth (i.e., assumed the effects on the growth increment may not equal between the growth phases). For model M-3 the ***x***'s (bolded and italicized) shared parameters between phase-1 and phase-2 growth (i.e., assumed the effects on the growth increment were equal between the growth phases).

	Parameter	M-1	M-2	M-3	M-4	M-5	M-6
Random Effect Structure							
	Cohort-specific	x					
	Year-specific		x	***x***	x	x	x
Effects on Growth Increment							
1	Delta Outflow	x	x	***x***		x	x
2	Conductivity				x		
3	Temperature	x	x	***x***	x	x	x
4	Delta Outflow * Temperature						x
5	Age-0 abundance	x	x	***x***	x	x	x
6	Age-1+ abundance	x	x	***x***	x	x	x
7	Time						x
8	Age-0 abundance * Time						x
9	Age-1+ abundance * Time						x
10	*E. affinis* density	x	x	***x***	x	x	x
11	Mysid density	x	x	***x***	x	x	x
Effects on Length-at-age-0 (values calculated over spawning season)							
12	Days over 20,000 cfs	x	x	***x***		x	x
13	Mean Conductivity				x		
14	Mean Temperature	x	x	***x***	x		x
15	Days under 9C					x	
16	Days over 20,000 cfs * Mean Temp.						x
Total Number of Regression Parameters		12	12	6	12	12	20
Delta AIC Value		10,411	3,889	14,847	4,144	5,017	0
Negative Log Likelihood		985,186	981,925	987,404	982,053	982,489	979,981

Table 5: Fixed effect parameter estimates for the longfin growth model with 95% confidence intervals.

Par.	Description	Eq.	Estimate (95% CIs)
σ_I	Standard deviation for year-specific random effect on the growth increment (mean = 0)	T1	0.327 (0.263, 0.408)
σ	Standard deviation around the observed mean length-at-age	T5	6.49 (6.47, 6.51)
h_c	Mean monthly growth increment during phase-1 growth (in mm; constant across all cohorts c)	T1	8.57 (8.44, 8.69)
g	Reproductive investment	T1	0.187 (0.184, 0.190)
γ_y	Intercept for length-at-age-0 ($L_{0,y}$; constant across all years y)	T4	-0.285 (-0.431, -0.138)
$T_{50,c}$	Timing (age in months) of 50% transition between growth phases (constant across all cohorts c)	T1	6.19 (6.18, 6.21)
β_1	Coefficient for temperature on the Phase-2 growth increment	T2, T3	9.0E-5 (4.5E-5, 1.0E-4)
β_2	Coefficient for ln(outflow) on the Phase-2 growth increment	T2, T3	-0.089 (-0.101, -0.077)
β_3	Coefficient for temperature * ln(outflow) interaction on the Phase-2 growth increment	T2, T3	0.009 (0.007, 0.011)
β_4	Coefficient for Age-0 abundance index on the Phase-2 growth increment	T2, T3	-0.067 (-0.076, -0.058)
β_5	Coefficient for Age-1+ abundance index on the Phase-2 growth increment	T2, T3	-0.044 (-0.051, -0.038)
β_6	Coefficient for month on the Phase-2 growth increment	T2, T3	-0.049 (-0.053, -0.045)
β_7	Coefficient for Age-0 abundance index * month interaction on the Phase-2 growth increment	T2, T3	-0.022 (-0.023, -0.021)
β_8	Coefficient for Age-1+ abundance index * month interaction on the Phase-2 growth increment	T2, T3	0.005 (0.004, 0.006)
β_9	Coefficient for *E. affinis* abundance index on the Phase-2 growth increment	T2, T3	-0.082 (-0.087, -0.078)
β_{10}	Coefficient for Mysis abundance index on the Phase-2 growth increment	T2, T3	-0.088 (-0.098, -0.078)
β_1^*	Coefficient for temperature on the Phase-1 growth increment	T3	-0.01 (-0.01, -0.009)
β_2^*	Coefficient for ln(outflow) on the Phase-1 growth increment	T3	0.148 (0.137, 0.16)

Par.	Description	Eq.	Estimate (95% CIs)
β_3^*	Coefficient for temperature * ln(outflow) interaction on the Phase-1 growth increment	T3	-0.026 (-0.029, -0.022)
β_4^*	Coefficient for Age-0 abundance index on the Phase-1 growth increment	T3	0.178 (0.168, 0.188)
β_5^*	Coefficient for Age-1+ abundance index on the Phase-1 growth increment	T3	0.146 (0.136, 0.155)
β_6^*	Coefficient for month on the Phase-1 growth increment	T3	-0.111 (-0.127, -0.096)
β_7^*	Coefficient for Age-0 abundance index * month interaction on the Phase-1 growth increment	T3	0.057 (0.054, 0.06)
β_8^*	Coefficient for Age-1+ abundance index * month interaction on the Phase-1 growth increment	T3	0.034 (0.031, 0.037)
β_9^*	Coefficient for *E. affinis* abundance index on the Phase-1 growth increment	T3	0.119 (0.114, 0.125)
β_{10}^*	Coefficient for Mysis abundance index on the Phase-1 growth increment	T3	-0.046 (-0.057, -0.035)
t_{crt}	Vertex of the Phase-2 temperature-growth relationship (in ^{o}C)	T2	-46.7 (-62.7, -30.8)
t_{crt}^*	Vertex of the Phase-1 temperature-growth relationship (in ^{o}C)	T3	22.8 (22.5, 23.1)
α_1	Coefficient for ln(1 + days over 20,000 cfs) on $L_{0,y}$	T4	-1.69 (-1.86, -1.52)
α_2	Coefficient for ln(conductivity) on $L_{0,y}$	T4	-24.9 (-27.8, -22.1)
α_3	Coefficient for ln(temperature) on $L_{0,y}$	T4	-14.2 (-16.9, -11.6)

Figures

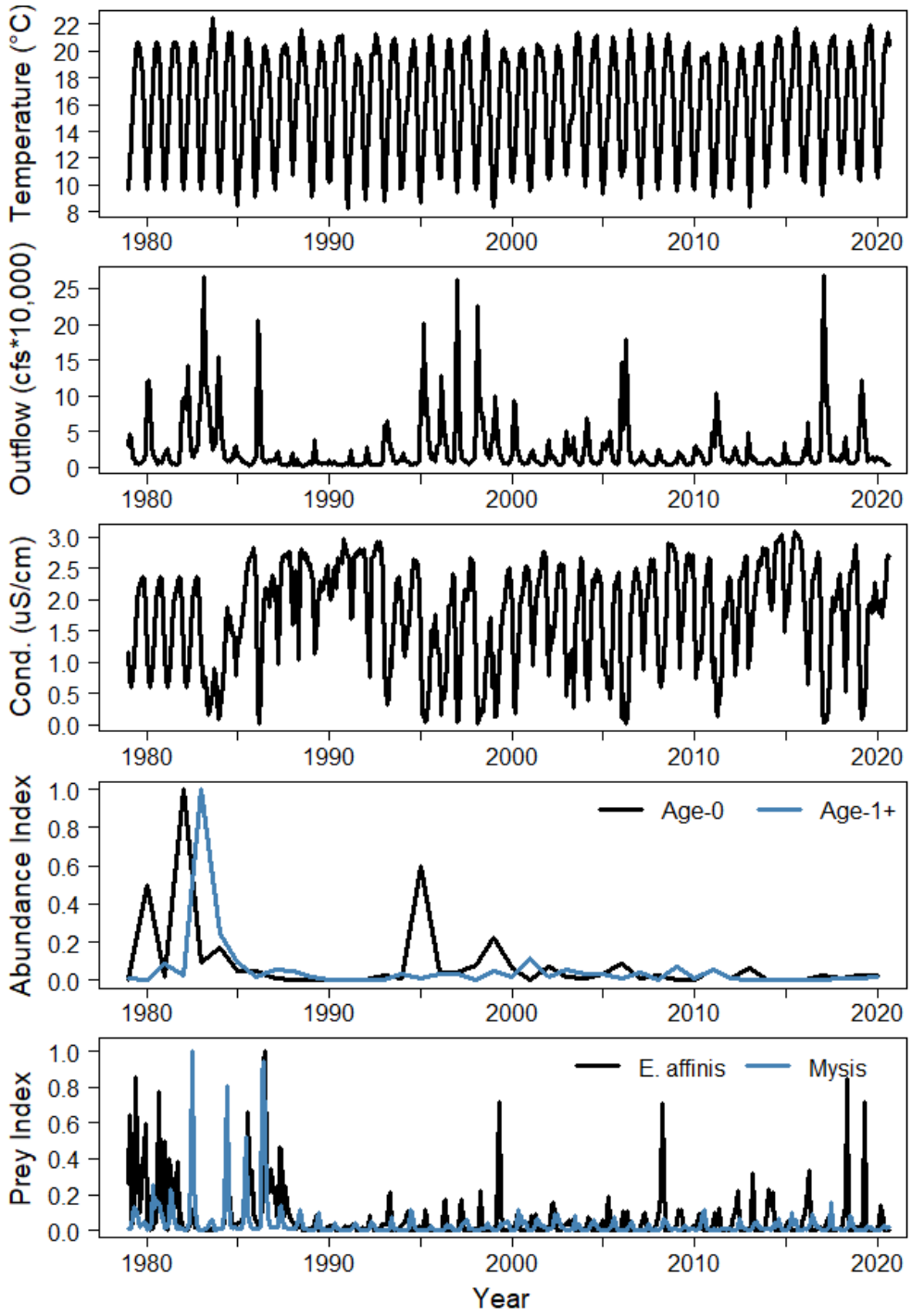

Figure 1: Time series of variables used or tested in the growth model from 1979–2020. Temperature and Conductivity were obtained from the Martinez (MRZ) long-term monitoring station. Delta outflow was obtained from the DayFlow dataset. Longfin Smelt abundance indices were the Age-0 and Age-1+ catch per unit effort (CPUE) trends from the San Francisco Bay Study otter trawl surveys. The Prey indices were the spatially averaged CPUE trends from CDFW zooplankton surveys.

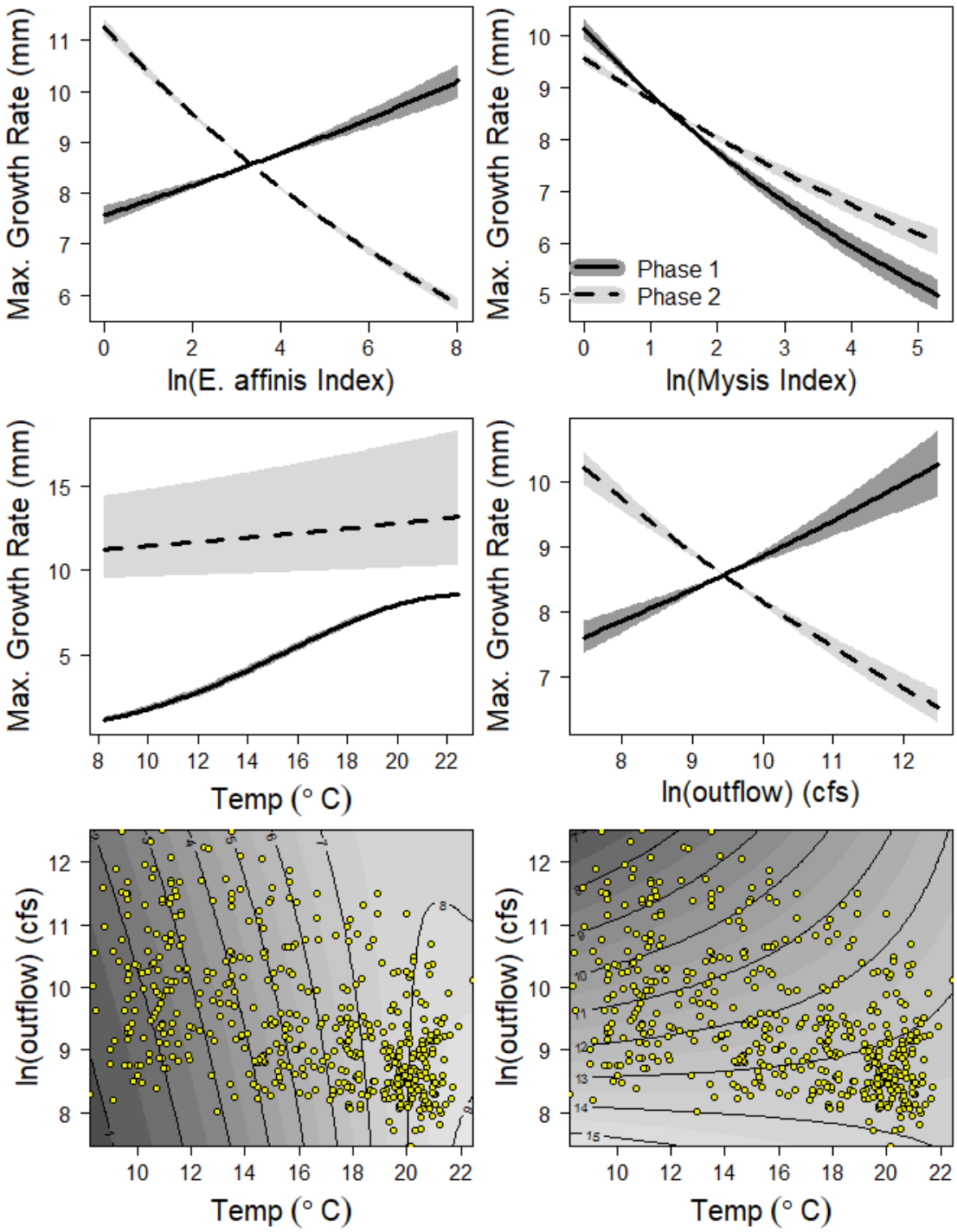

Figure 2: Predicted maximum monthly growth rate (in mm) across prey densities and environmental conditions. Each panel shows the effects across the range of observed environmental conditions while holding all other effects at the mean value. The top and middle rows depict the main effects (solid and dashed lines) and 95% confidence intervals (shaded regions) for Phase-1 and Phase-2 growth. The bottom row depicts the interaction between temperature and ln(Delta outflow) for Phase-1 (left) and Phase-2 growth (right) on maximum monthly growth rate (in mm). Yellow points represent observed temperature-outflow pairs.

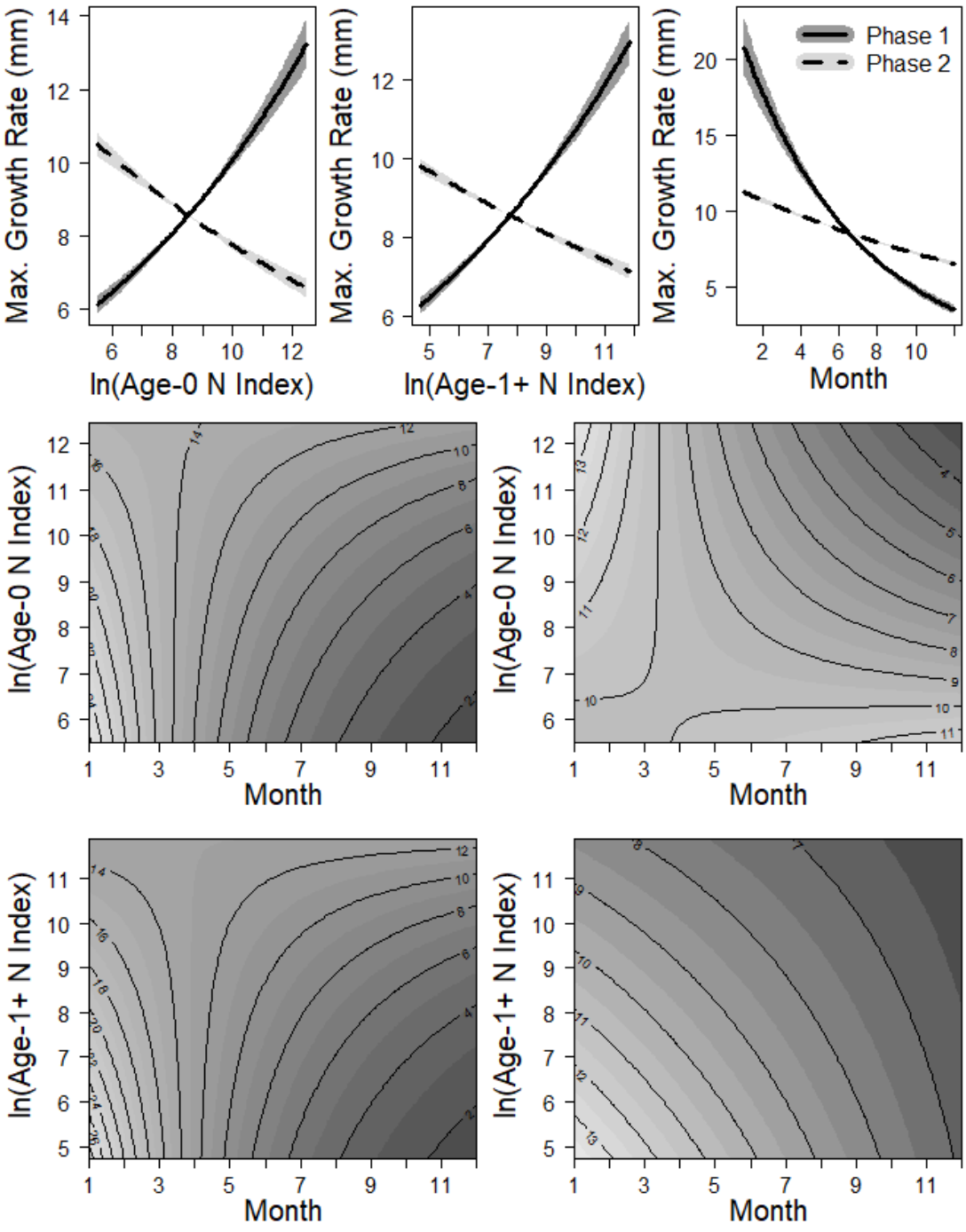

Figure 3: Predicted maximum monthly growth rate (in mm) across density and time. Each panel shows the effects across the range of observed conditions while holding all other effects at the mean value. The top row depicts the main effects (solid and dashed lines) and 95% confidence intervals (shaded regions) for Phase-1 and Phase-2 growth. The middle row depicts the interaction between Age-0 abundance indices and month of calendar year and the bottom row depicts the interaction between Age-1 abundance indices and month of calendar year for Phase-1 (left) and Phase-2 growth (right) on maximum monthly growth rate (in mm).

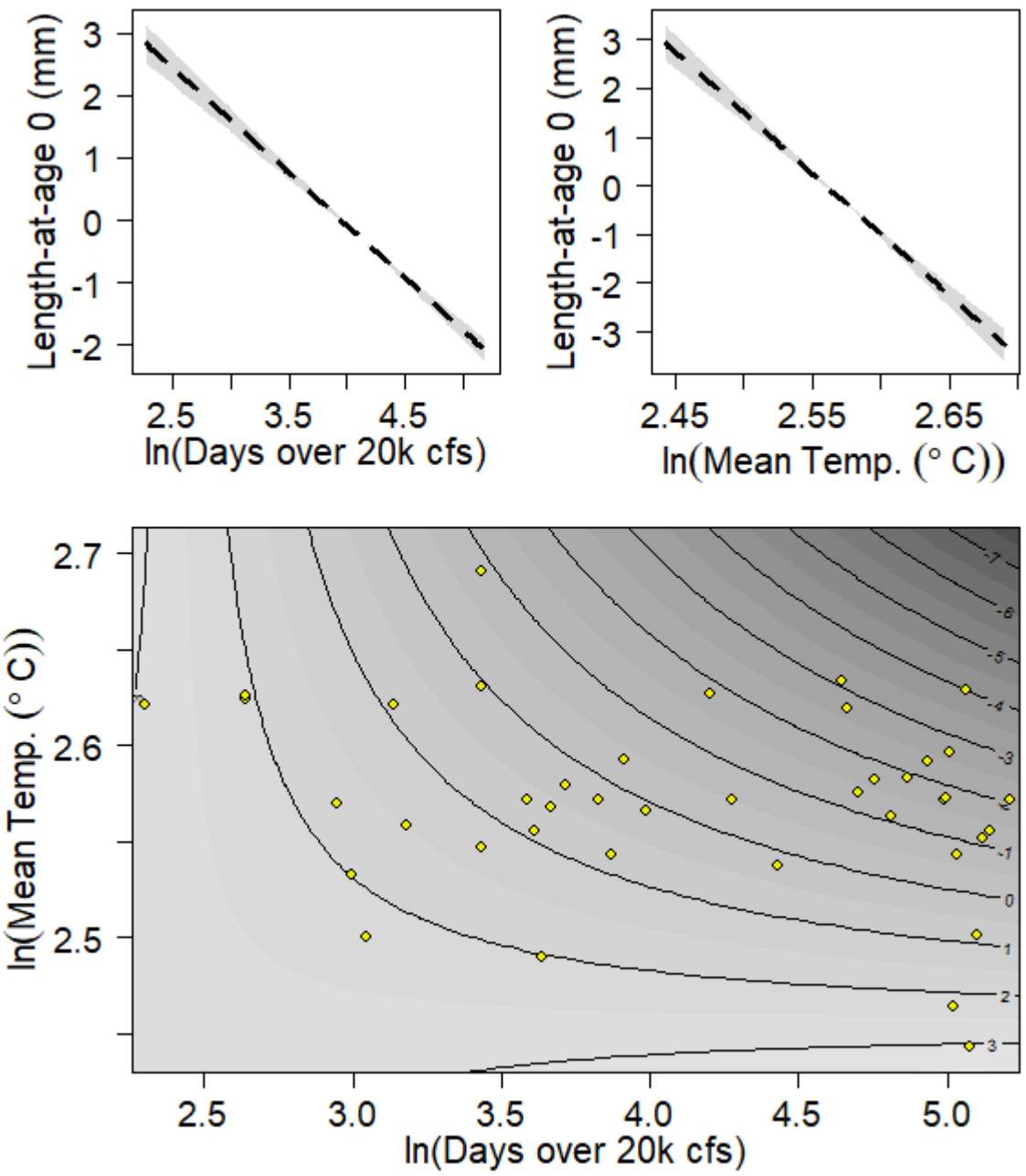

Figure 4: Predicted length-at-age-0 (in mm) across environmental conditions over the spawning season (Dec 1 – May 31). Each panel shows the effects across the range of observed environmental conditions while holding all other effects at the mean observed value. The top row depicts the main effects (dashed lines) and 95% confidence intervals (shaded regions). The bottom panel depicts the interaction between mean spawning temperature and number of days with recorded Delta outflow over 20,000 cfs on predicted length-at-age-0 (in mm).

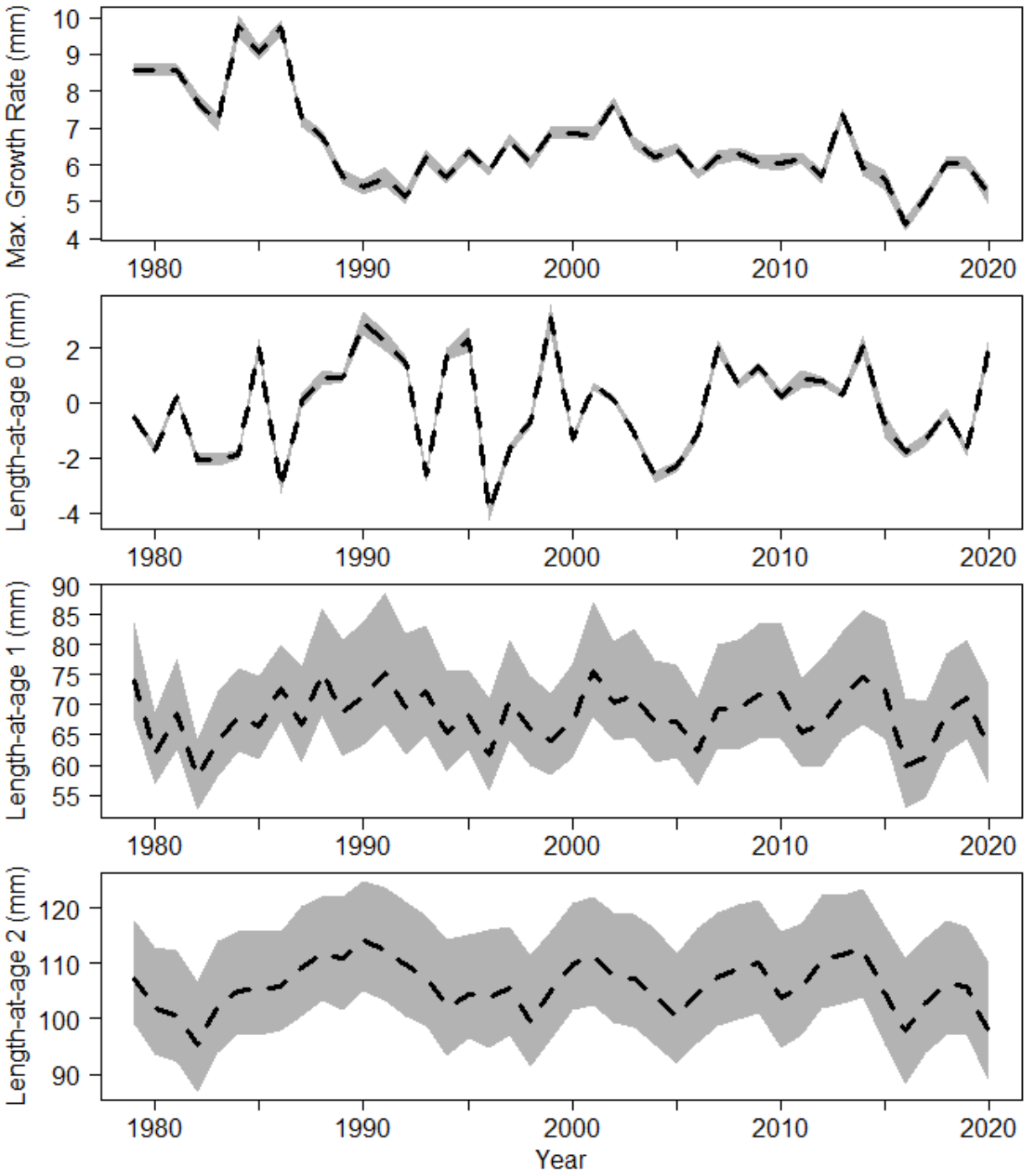

Figure 5: Predicted temporal trends in growth patterns from 1979 to 2020 (dashed lines) with 95% confidence intervals (shaded regions). The maximum growth rate per month (mm; top panel) accounts for variation in predicted non-reproductive growth (*h*; which is temporally constant in the best model) and a year-specific random effect predicting the unobserved annual variation in growth patterns. Panels for predicted length-at-age 0, 1, and 2 represent age in years (i.e., 0, 12, and 24 months).

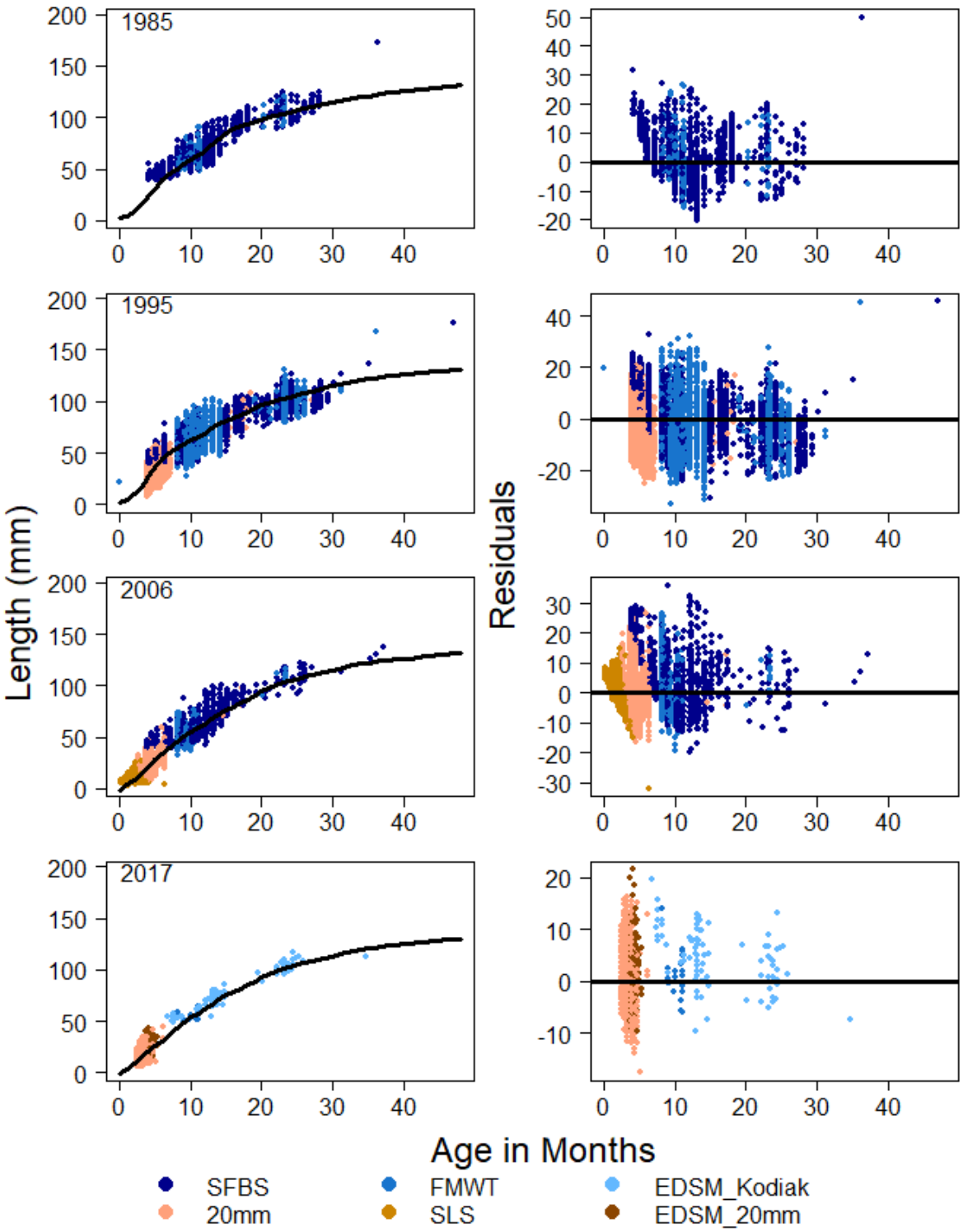

Figure 6: Predicted length-at-age (left side) and residuals (right side) from four representative cohorts depicting model fits. Solid lines represent model predictions and points represent individual length-at-age observations. Blue colors represent sampling programs focused on larger-sized individuals and brown colors represent sampling programs focused on larval individuals.

Appendix E: A State-Space Model for Bay-Delta DPS Population Dynamics

Longfin Smelt Technical Note 4:
A State-Space Model for Longfin Smelt Population Dynamics
Version 3.2.0 – May 20, 2022
Vanessa Tobias, USFWS

Introduction

In an earlier technical note (TN 1; Tobias 2022), I developed a count-based PVA for several long-term monitoring surveys showing that Longfin Smelt populations are likely to fall below quasi-extinction thresholds in the foreseeable future. In TN 1, each abundance index was used as an independent measurement of annual population growth, as measured in a specific LFS life stage. The count-based PVA did not account for the three-year life span of LFS, the population structure, or annual variation in vital rates.

This technical note aims to account for the structure within the LFS life cycle by proposing a matrix model for population growth with three age classes (life stages; Figure 1). The vital rates in the matrix are estimated using a state-space model of population dynamics. Previous research on population dynamics of Longfin Smelt developed models using two life stages or ages of Longfin Smelt. In an extensive model comparison exercise, a state-space model formulation of the Beverton-Holt stock-recruit relationship gave the best explanation for the relationship between juvenile and adult Longfin Smelt abundance values (Maunder 2015). Further research, which used the Ricker model for the stock-recruit function, estimated the effects of environmental factors on juvenile survival and recruits per spawner (Nobriga and Rosenfield 2016). The model for Longfin Smelt population dynamics that I developed for this technical note builds on this previous research to investigate how environmental factors influence the transitions between three age classes.

Methods

Data

Data on relative abundance of Longfin Smelt came from the San Francisco Bay Study's age-specific abundance indices (CDFW 2021). For the environmental covariates, I compiled a dataset of environmental variables on an annual time step from the Department of Water Resources water quality monitoring programs (including temperature and salinity), and the Environmental Monitoring Program's zooplankton data, DayFlow, and ocean upwelling index data from NOAA's monitoring programs.

Data Exploration

I graphed the Bay Study indices on a log scale to visually assess the shapes of the apparent vital rates. This assessment is meant to provide general guidance for the structure of the state-space model.

State Space Model

I fit models for Longfin Smelt population dynamics as state-space models in JAGS (Plummer 2003) via R (package R2jags; Su and Yajima 2015). State-space models are a class of models where there are two

processes: a state process and an observation process. The state process is the underlying pattern or time series that is hidden in the data (i.e., the latent state). The collected data enter the model through the observation process, which assumes that the data points are independent, but noisy observations of the latent state. I used R (version 4.0.4 "Lost Library Book"; R Core Team 2021) to fit all models and make calculations.

There are several advantages of using a state space model for this application. First, the state space model framework allows estimation of observation error and process error, which can improve parameter estimation and variable selection (see Maunder et al. 2015). The ability to describe the relationships in a hierarchical structure allows simultaneous estimation of vital rates and the influence of covariates on those rates. The state-space model framework also offers the ability to include information from multiple gear types into estimating the underlying abundance pattern by including an observation process for each gear type and age class.

The conceptual model for the population dynamics represented in the model is illustrated by Figure 1. I fit an initial model with three states (one for each age class) with two observation processes for each state (one for each of the gear types for each age class) that did not include any environmental covariates. This model served as a baseline for building the relationships and it provided initial estimates of the variability and structure of the vital rates.

The notation for age classes will be as follows: N represents the estimated abundance (latent state) and the subscripts index the age followed by t for time (in years).

Age-0 survival (S_0; age-0 to age-1) and age-1 survival (S_1; age-1 to age-2) were structured as simple ratios using a logit-normal link:

$$\text{logit}(S_{0,t}) = \frac{log(N_{1,\,t+1})}{log(N_{0,\,t})} + \varepsilon_{S0,t}\ ;\ \varepsilon_{S0,\,t} \sim N(\mu_{\text{S0t}},\ \sigma_{\text{S0}t})$$

$$\text{logit}(S_{1,t}) = \frac{log(N_{2,\,t+1})}{log(N_{1,\,t})} + \varepsilon_{S1,t}\ ;\ \varepsilon_{S1,\,t} \sim N(\mu_{\text{S1t}},\ \sigma_{\text{S1}t})$$

Reproduction was structured as a Beverton-Holt equation to represent the relationship between age-2 abundance and age-0 abundance:

$$\log\,(N_{0,t}) = \log\left(\frac{a_t \cdot N_{2,t}}{1+b_t \cdot N_{2,t}}\right) + \varepsilon_{N0};\ \varepsilon_{N0,t} \sim N(\mu_{N0},\ \sigma_{N0,t})$$

where *a* describes density-independent recruitment which is proportional to fecundity, i.e. recruitment when densities are low, and *b* describes the degree of density-dependence. In the code, the model was fit using an alternate parameterization of the Beverton-Holt equation

$$\log(N_{0,t}) = \log\left(\frac{N_{2,t}}{a'_t + b'_t \cdot N_{2,t}}\right) + \varepsilon_{N0}\ ;\ \varepsilon_{N0,t} \sim N(\mu_{N0},\ \sigma_{N0,t})$$

where a'= 1/a and b'=b/a. Note that using the Bay Study abundance indices, the relationship between recruits and spawners comes from the abundance indices from the same year. This is different than the survival relationship, which has a one-year time lag in the relationship. The current version of the model only allows reproduction by age-2 fish (Figure 1). Future model development may include reproduction by a portion of age-1 fish. Each state equation has a separate estimate for the process error, which allows each age class to have its own estimate of variability.

Without environmental covariates, the estimates of certain vital rates were diffuse (especially survival rates), and in the case of the a parameter from the Beverton-Holt equation for reproduction, the model was unable to distinguish between three likely estimates.

Subsequent models included linear models for the effects of environmental covariates on vital rates as a higher level in the hierarchical model structure. These linear models can be thought of as random effects, as the annual estimates of vital rates are treated as random variables in these models. Variables were standardized (centered on the mean and scaled by the standard deviation) prior to inclusion.

There are more environmental variables available for consideration than is prudent to include in a model, so I employed the following variable selection method. The dataset of environmental variables contains several groups of variables that measure the same or similar aspects of the environment (for example, sea surface temperature at two buoys that are near each other and various measurements of outflow volume). I selected variables for consideration such that repeated information was limited--attempting to select one variable to represent each group. Next, I used a stochastic search variable selection method (SSVS) within the model to select informative variables. To do this, I included the chosen variables in the state process with spike and slab priors (O'Hara and Sillanpää 2009) which allow the model to estimate the probability that they should be included (i.e., that their inclusion explains variability). The priors included a random effect for the number of variables that should be included in the model. This random effect had a prior that peaked around 20% with long tails to allow the number of parameters to vary as needed (dbeta(2,8)), although the selection of 20% as the peak was somewhat arbitrary.

The observation portion of the model incorporates data from both of the Bay Study's gear types, with separate estimates of observation error for each combination of gear and age class (six total observation errors). Separate observation errors account for variability in the relationships between the two gear types. I also included a scaling factor that accounts for large-scale differences in observations between the two gear types for each age class. Currently, each age class has a single scaling factor, but future versions of the model may include a time-varying factor to account for the apparent changes in the expected catch ratios between the two gear types over time (Figure 4). Variables can also be included in the observation process to identify factors that influence the observations. I chose not to do this at this stage of model development, but future development may include a structure to account more explicitly for the patterns in the relationships between the gears.

Forecasting Extinction Risk

In addition to understanding the drivers of the observed patterns in abundance for each age class, it is useful to forecast abundance into the future. To do this, I used the state equations from the state-space model as the framework and a random draw of the posterior estimates for the vital rate parameters and the starting abundance. I drew the starting abundances from the estimated age-specific abundances for 2015. I used these random draws to run the autoregressive equations forward to 2060. I repeated the procedure (including draws for starting abundances and vital rates) 1000 times to produce a distribution of abundance values for each age class at each time point.

I incorporated quasi-extinction into the forecasting algorithm by setting minimum values for each age class. If the estimated abundance fell below the threshold for quasi-extinction, the estimate for that age class was set to zero. This propagated through the forecasts such that if any age class met the criteria for quasi-extinction, abundance estimates for each of the age classes would eventually go to zero. There was no obvious or empirical level to set for quasi-extinction in this model, so I ran the simulation with four quantiles at the low end of the abundance estimates for comparison (Table 2). In Technical Note 1 (Tobias 2022), I used 1% of the most recent ten years of the surveys as the threshold for quasi-extinction. One way to address this is to use the historical environmental variables to hindcast abundance. This can then be qualitatively compared to the abundance indices to give an idea for how well the estimates predict the observed patterns in abundance. I graphed the results of hindcasting with various abundance quantiles as quasi-extinction values and included the age-0 abundance indices for reference. I used age-0 because they usually have the highest values of the three age classes and have the widest range of values.

Results

Data Exploration

Rates of survival appear to be adequately described by simple rates, rather than an equation for density dependence (Figure 2 and Figure 3). Patterns in the residuals for those relationships suggest that survival rates are not static and that covariates are necessary to fully understand what drives population dynamics. For example, survival rates tend to be lower in more recent years than predicted by the regression analysis that estimated a single static rate of survival for all years. A simple rate does not appear to adequately describe the shape of the reproduction relationship. For the otter trawl indices, the slope of the regression was not significantly different from zero (Figure 2); although the slope of the regression for midwater trawl was significantly different from zero, the data points clearly deviate from a linear relationship (Figure 3). In the data exploration, I use age-2 fish as a proxy for spawning stock because most spawning is thought to occur at age-2. I recognize that some age-1 fish may also be spawning so the relative abundance of spawners may be higher than is represented here. Also note that the age-2 abundance index includes both male and female fish, so reproduction described here is not directly comparable to female fecundity rates. The sex ratio for adult Longfin Smelt is roughly equal (IEP MAST), so multiplying rates by two would be more similar to estimates of female fecundity.

The relationship between the two timeseries of observations created by the two gear types is somewhat complicated (Figure 4). A simple ratio can describe much of the relationship for the gear-specific

abundance indices for each of the age classes, but residuals for each age class show a distinct pattern over time.

Population Model

The estimated latent states for the relative abundances follow the patterns in the time series of the Bay Study abundance indices (Figure 7). The estimated states are also plausible, in that the highest abundance values are generally for the age-0 class and decline across cohorts.

Using the SSVS procedure, a small number of covariates were selected to explain patterns in each of the vital rates for some of the parameters, but for other parameters several variables appeared to have similar chances for inclusion (Figure 5). The range of inclusion probabilities for covariates varied somewhat across the vital rates. The density dependence portion of the reproduction equation had variables with the strongest evidence for inclusion while the other vital rates all had inclusion probabilities close to 0.2, which was the mean value for the prior distribution that was set for inclusion probabilities.

The time series for each of the vital rates after refitting the model with the selected environmental variables is shown in Figure 6. There are a few patterns that emerge. The mean of the density-independent reproduction parameter (*a*) was steady over time, but the estimates have substantial variability. The degree of density dependence (*b*) appears to increase over the length of the time series but is interrupted by a sharp decline in the mid-1990s. Age-0 survival is high, largely over 0.85, until the early 1990s, after which the mean survival appears to decline. The mean line has several peaks and valleys after the mid-1990s which make the survival estimates appear more chaotic. The biggest valley is around 2008, but smaller dips occur in 1996, 2000, and 2013–2014. Age-1 survival is fairly steady over time, but there are small fluctuations form year to year and valleys are visible in 1993 and 2014.

Forecasting Extinction Risk

The median total abundance (sum of abundance for all age classes) forecasted by the simulations reached a peak within a few years of the starting year and then declined to near zero by the end of the time series (Figure 8). The confidence bands were larger for larger mean values, and they tapered down as mean abundance declined. These simulations can also be visualized as the proportion of simulation runs that fall below a threshold for quasi-extinction. The proportion of simulations that fall below the quasi-extinction threshold increases over time for all of the thresholds, from 1% to 15% of the population estimates (Figure 9). The trajectory for the most conservative threshold (15%) increases steeply for several years before leveling out slightly and reaching a maximum value of approximately 80% in 2060. The trajectory for the riskiest threshold (1%) is less steep and reaches a maximum value of approximately 20% by 2060.

Hindcasting simulations indicated that 20% was too high to be used as a quasi-extinction threshold because simulations uniformly failed to recover from a population crash in 1990, but lower thresholds were able to recover (Figure 10). The 1% threshold appears to be over-confident for population increases in the most recent years. For example, small upticks in the abundance indices in 2006 and

2011 correspond with big increases in estimated abundance with narrow confidence intervals. The 15% threshold appears to strike a reasonable balance.

Discussion

Taken together, these trends create a negative feedback loop with decreasing reproduction and decreasing survival. Throughout model development, although some details varied depending on the model structure or covariates included, the results have always indicated a change in vital rates in the early to mid-1990s. Based on the current model formulation, a change in parameters associated with reproduction occurred at time. The most likely covariates to explain this change are related to hydrology (outflow and inflow), salinity, and food availability. In addition to declining reproduction, declining survival rates over time indicate that the chances that the recruits survive to spawn themselves is also declining. There are several years in the time series when poor conditions converge to negatively affect multiple vital rates simultaneously. For example, 1993 and 2014 saw low survival rates for both age-0 and age-1 Longfin Smelt.

Forecasts of population size using vital rates estimated by the model indicate that it is likely that Longfin Smelt population sizes will dip below recoverable levels within a decade if these recent levels of reproduction and survival continue. Results were similar across a range of quasi-extinction thresholds. I used the estimates of vital rates from all years of the available surveys (i.e., 1980 to 2015). Using all available years rather than just the most recent years may introduce more variability into the forecasted population size than is realistic if there are vital rates that have trends over time and if the earlier part of the time series does not reflect conditions moving forward. In particular, the effect of density dependence (b) and age-0 survival (S_0) may be affected by this choice of years because of the apparent trends in their estimated time series since about 2000 (Figure 6). Adding variability to the vital rates affects the confidence intervals on the predictions, but it also may affect the estimates of population viability over time. Populations with highly variable vital rates tend to have lower levels of population viability over time because adding variation tends to make a population grow more slowly over the long term and the population size is more likely to fall below the quasi-extinction threshold than it is for populations with less variable growth rates (Morris and Doak 2002).

Although these results imply that if future vital rates are similar to those observed in the past there is substantial risk of extinction for Longfin Smelt, they also imply potential mechanisms for recovery. These modeling results suggest that increasing reproductive rates in consecutive years can reset the population to higher levels. Results also suggest that environmental conditions may affect several vital rates simultaneously, which would be reflected in the abundance trajectories for multiple life stages.

Acknowledgements

This modeling effort benefitted from the advice and prior work of many people. The Core Team for the Longfin Smelt Species Status Assessment gave feedback on several iterations of the modeling framework and interpretation of results. The Core Team includes J. Hobbs, M. Eakin, and E. Chen. J. Miller compiled environmental data from several sources. J. Hobbs, K. Hieb, and J. Burns provided abundance index data. B. Matthias gave feedback on model structure and processed environmental data for use on an

annual time step. Code for the Delta Smelt life cycle model by K. Newman, L. Polansky, and L. Mitchell was also a helpful reference for code formulation.

References

California Department of Fish and Wildlife (CDFW). 2021. San Francisco Bay Study (SFBS) Data. https://wildlife.ca.gov/Conservation/Delta/Bay-Study

IEP Mast Report. In progress. An updated conceptual model of Longfin Smelt biology. Interagency Ecological Program, Management, Analysis, and Synthesis Team.

Maunder, M.N., Deriso, R.B. and Hanson, C.H., 2015. Use of state-space population dynamics models in hypothesis testing: advantages over simple log-linear regressions for modeling survival, illustrated with application to longfin smelt (Spirinchus thaleichthys). Fisheries Research, 164, pp.102–111.

Morris, W.F. and Doak, D.F. 2002. Quantitative Conservation Biology: Theory and Practice of Population Viability Analysis. Sinauer Associates. Sunderland, Massachusetts.

Nobriga, M.L. and Rosenfield, J.A., 2016. Population dynamics of an estuarine forage fish: disaggregating forces driving long-term decline of Longfin Smelt in California's San Francisco Estuary. Transactions of the American Fisheries Society, 145(1), pp.44–58.

O'Hara R.B, M.J. Sillanpää., 2009. A review of Bayesian variable selection methods: what, how, and which. Bayesian Analysis 4(1): 85–118. DOI: 10.1214/09-BA403

Plummer, M., 2003. JAGS: A program for analysis of Bayesian graphical models using Gibbs sampling. In Proceedings of the 3rd international workshop on distributed statistical computing (Vol. 124, No. 125.10, pp. 1–10).

R Core Team. 2021. R: A language and environment for statistical computing. R Foundation for Statistical Computing, Vienna, Austria. URL https://www.R-project.org/.

Tobias, V.D. 2022. Longfin Smelt Technical Note 1: Count-Based Population Viability Analysis Using Indices of Abundance for Longfin Smelt (version 2.0).

Yu-Sung Su and Masanao Yajima, (2015). R2jags: Using R to Run 'JAGS'. R package version 0.5–7. https://CRAN.R-project.org/package=R2jags

Tables

Table 4: Environmental variables

Category	**Variable**	**Details**	**Data Source**
Hydrology	Outflow	Median annual outflow	Dayflow dataset
	Inflow	Median annual inflow	Dayflow dataset
Water Quality	Low Temperatures	Count of days < 15° at Martinez (MRZ)	DWR water quality dataset
	High Temperatures	Count of days > 20° at Martinez (MRZ)	DWR water quality dataset
	Salinity	Count of days < 2 PSU at Martinez (MRZ)	DWR water quality dataset
Prey Availability	Copepods	Eurytemora gC/m^3 in Suisun Bay (NZ048) in March	Environmental Monitoring Program dataset
	Mysids	Mysid CPUE in Suisun Bay (NZ048) in November	Environmental Monitoring Program dataset
Ocean Temperature	Upwelling Index	Mean upwelling index in August	NOAA dataset

Table 5: Values for abundance quantiles, some of which were used as quasi-extinction thresholds to calculate risk of quasi-extinction in Figure 9.

Quantile	Age-0	Age-1	Age-2
50%	4185	1616	161
20%	1801	451	61
15%	1600	338	49
10%	1399	245	38
5%	1171	162	26
1%	868	80	13

Figures

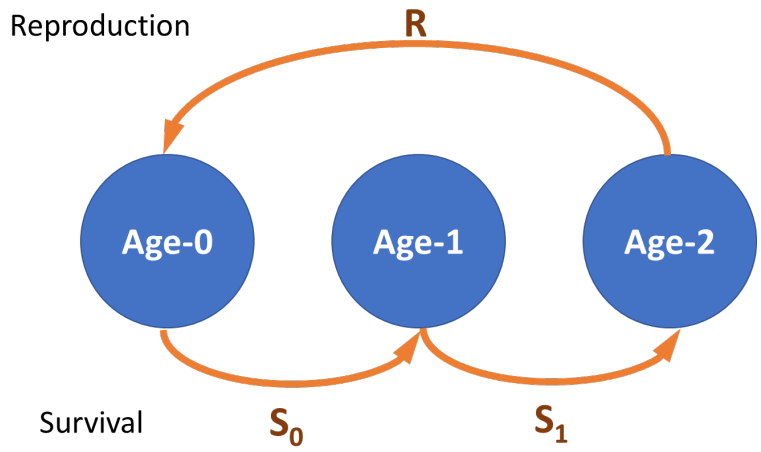

Figure 6: Age-based conceptual model for Longfin Smelt population dynamics.

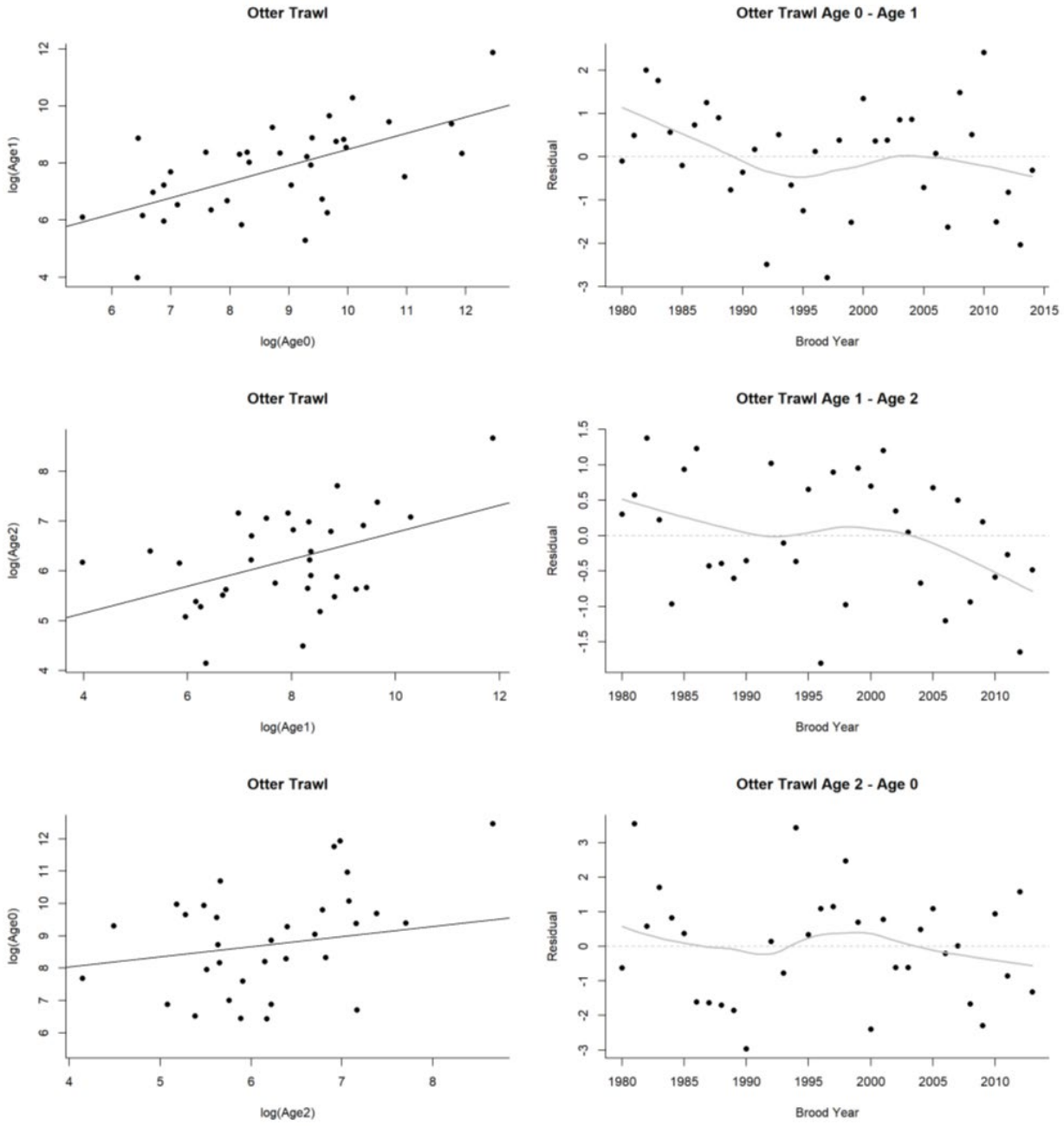

Figure 7: Relationships between otter trawl age class indices on a log scale provide a visual assessment of vital rates. Left column (top to bottom): Age-0 survival, Age-1 survival, and reproduction. Solid lines represent linear regressions. Survival plots have slopes with $p < 0.05$; reproduction plot $p > 0.05$. Right column (top to bottom): residuals for the linear regressions in the left column, plotted over time. Solid lines represent a loess smoother.

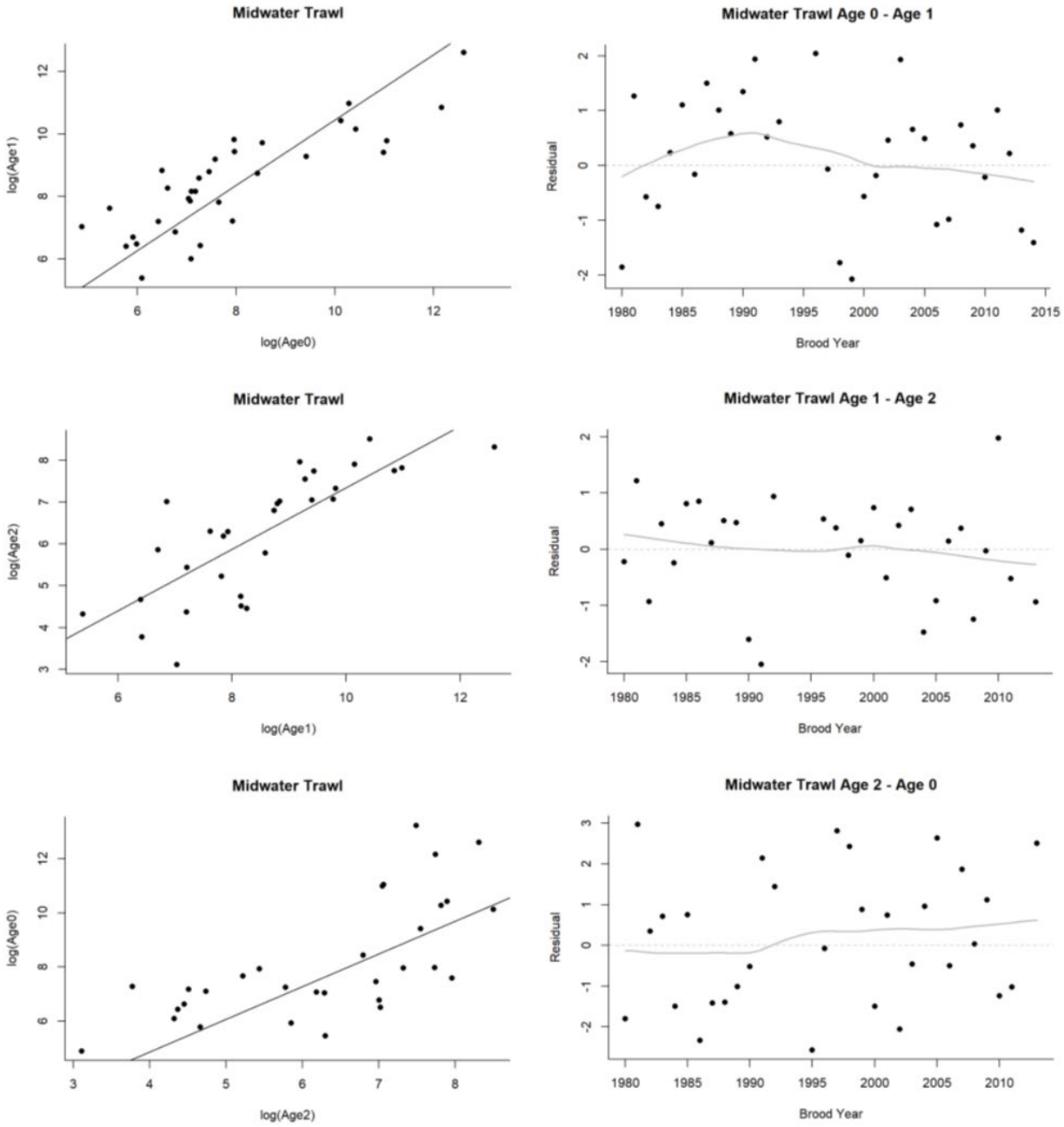

Figure 8: Relationships between midwater trawl age class indices on a log scale provide a visual assessment of vital rates. Left column (top to bottom): Age-0 survival, Age-1 survival, and reproduction. Solid lines represent linear regressions. All plots have slopes with $p < 0.05$. Right column (top to bottom): residuals for the linear regressions in the left column, plotted over time. Solid lines represent a loess smoother.

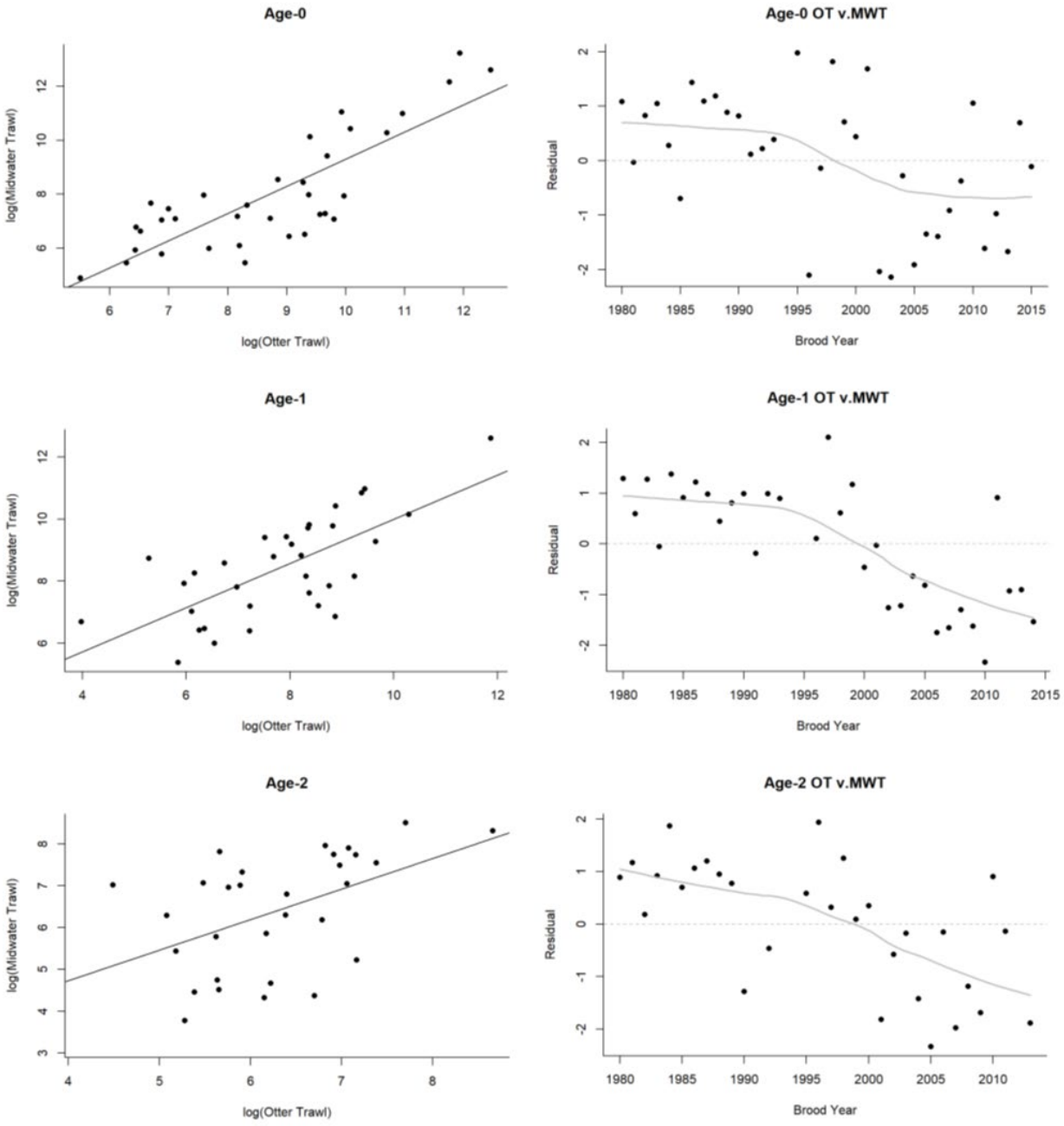

Figure 9: Relationships between abundance indices for the two gear types used by the Bay Study. Left column (top to bottom): data points with a line representing a linear regression between the two gear types for age-0, age-1, and age-2 abundance indices. Slopes for all lines are significantly different than zero ($p < 0.05$). Right column: residuals for the regressions in the left column plotted over time. The solid line represents a loess smoother.

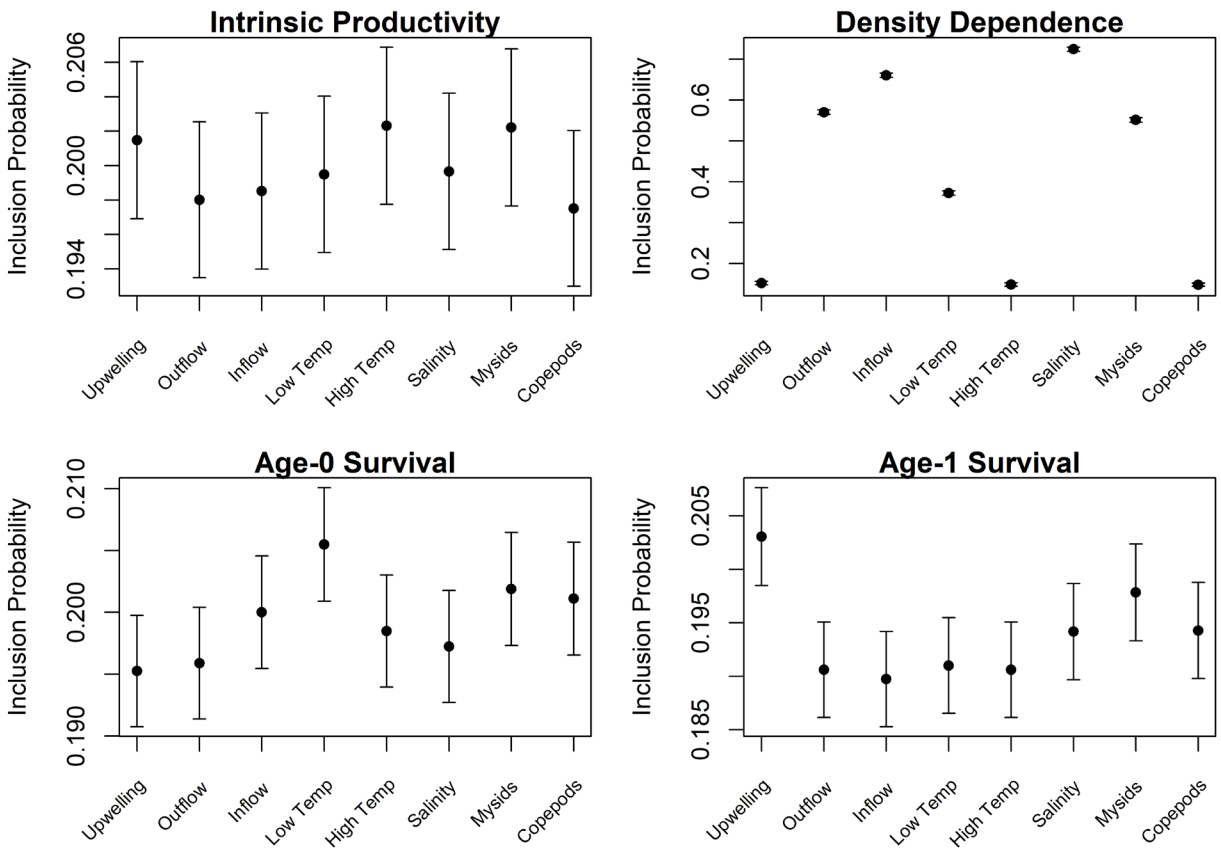

Figure 10: Inclusion probabilities with 95% confidence limits for a set of variables to explain vital patterns in the estimated vital rates. Top row: parameters in the Beverton-Holt equation for reproduction- a is the density independent rate and b estimates density dependence. Bottom row: survival for age-0 and age-1 fish. All environmental variables were standardized. The dashed horizontal line is at 0.2 to indicate a 20% probability of inclusion.

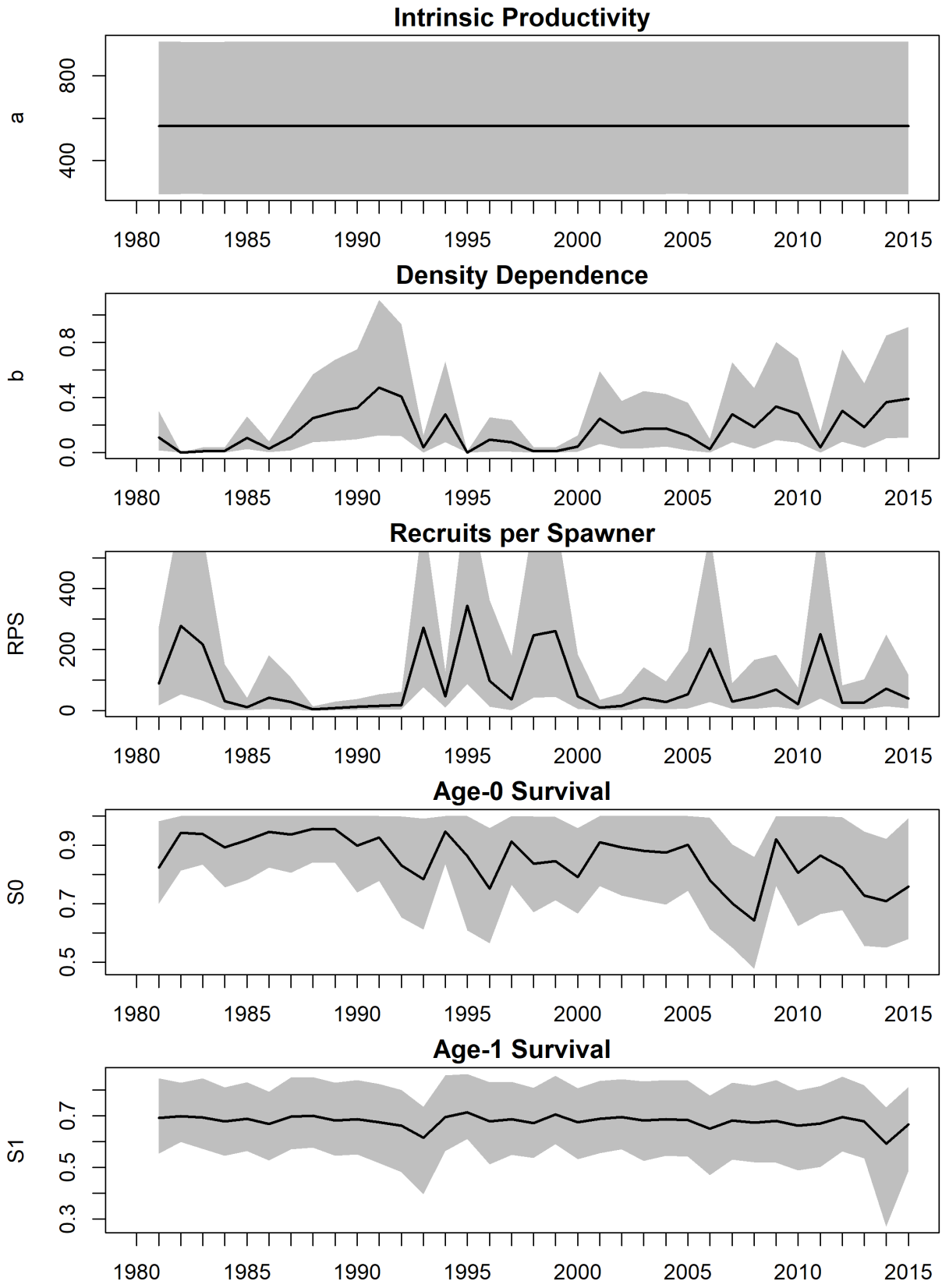

Figure 11: Time series plots for estimated vital rates.

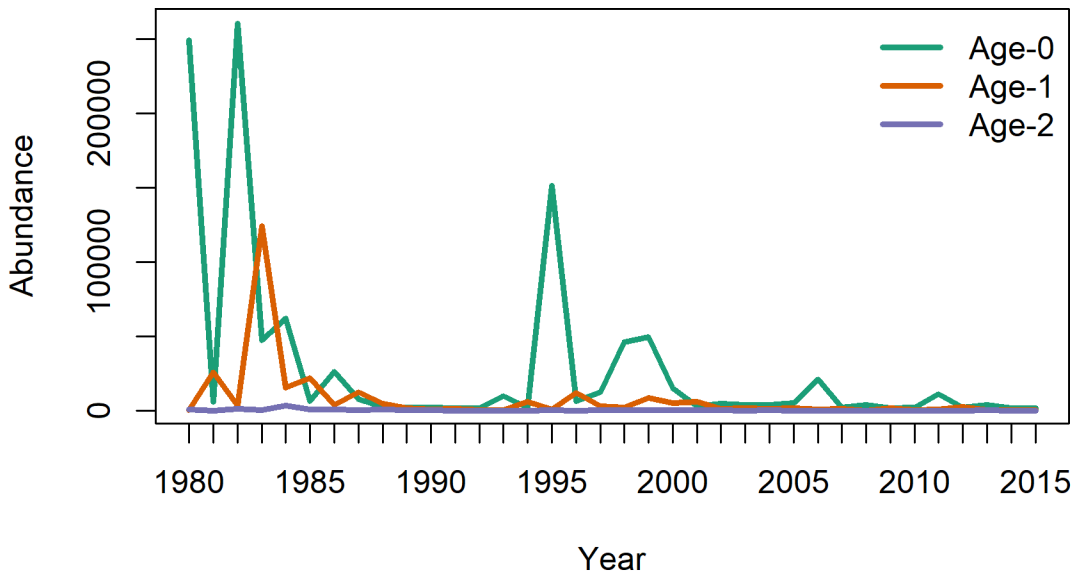

Figure 12: Estimated relative abundance (latent states) for three age classes of Longfin Smelt. Error bars are omitted for readability.

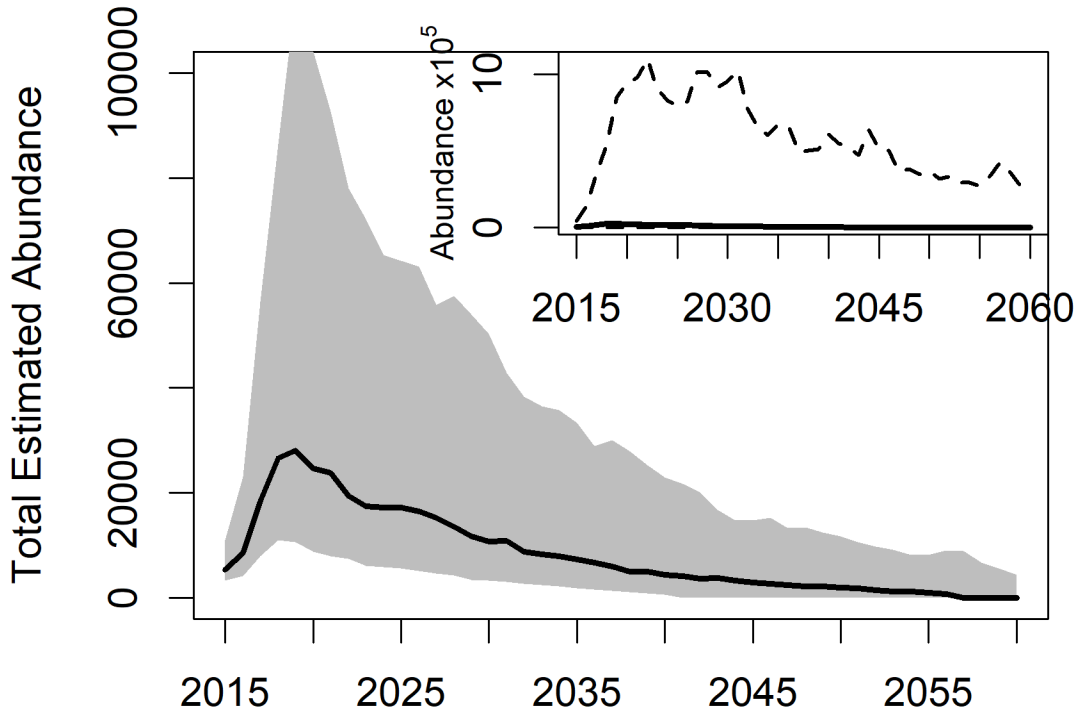

Figure 13: Projected total abundance index values using values randomly sampled from posterior distributions of vital rate parameters from 2005 to 2015, not accounting for the influence of environmental covariates. Black lines in both the main graph and the inset represent the median estimate. The grey envelope in the main plot represents the middle 50% of the estimates around the median. This panel highlights the shape of the estimates over time. The inset shows the median and a dashed line representing the 95% confidence interval. This panel highlights the variability in the estimates.

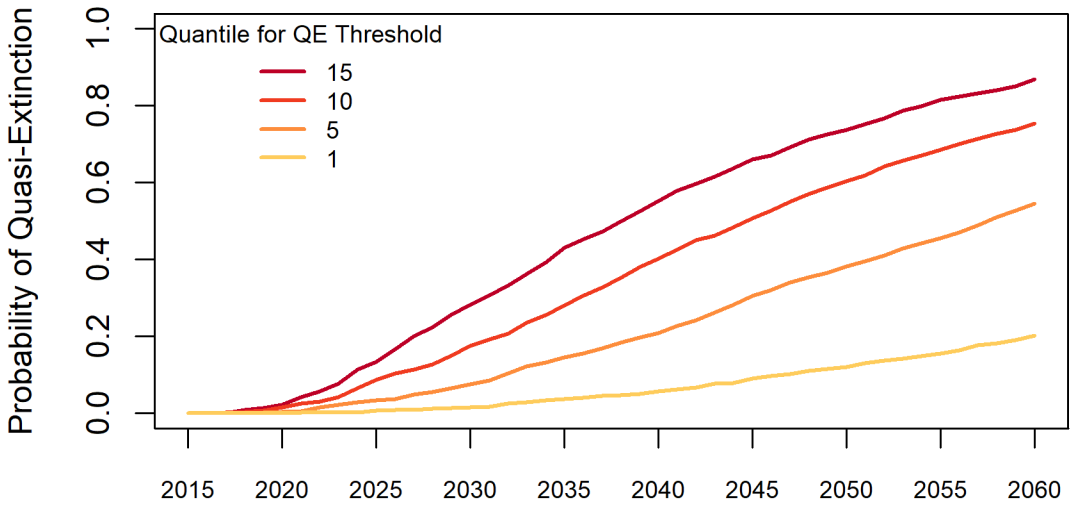

Figure 14: Quasi-extinction probabilities associated with using four different quantiles of population estimates as quasi-extinction values in simulations of abundance index values using values randomly sampled from posterior distributions of vital rate parameters from 2005 to 2015, not accounting for the influence of environmental covariates. Abundance values associated with each quantile are in Table 2.

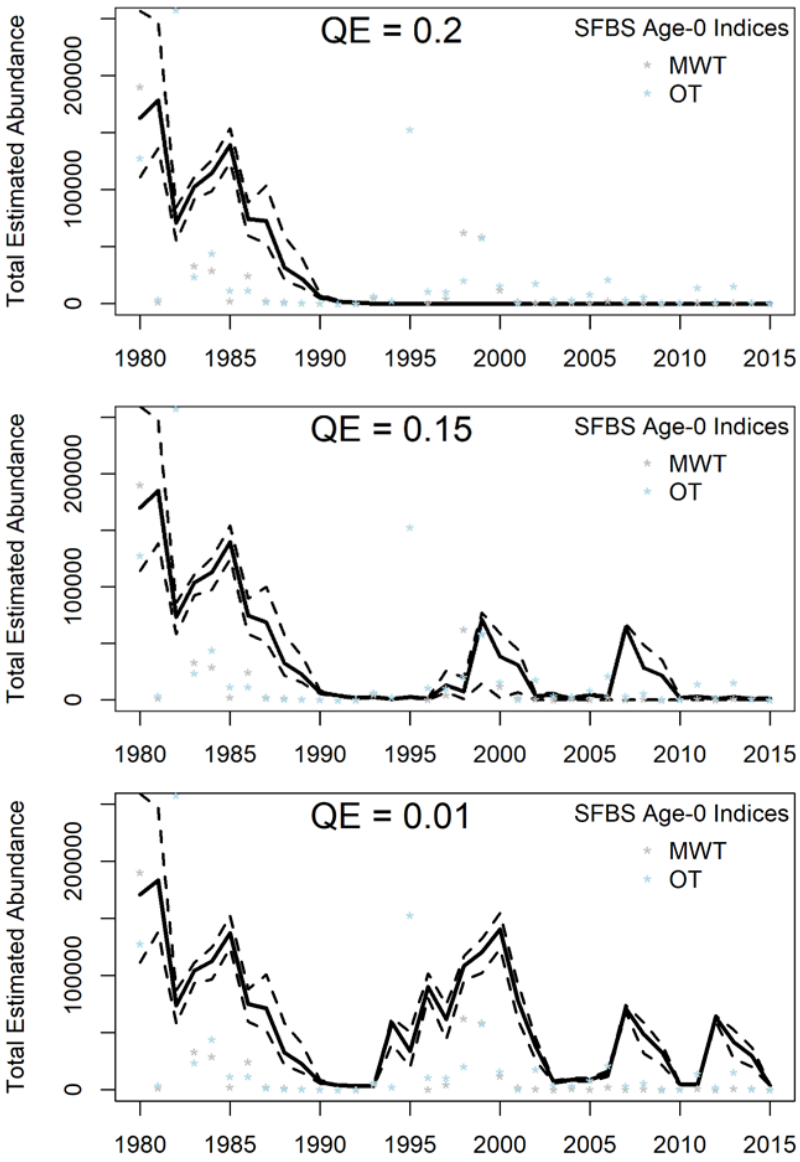

Figure 15: Estimated historical total (all ages) abundance of Longfin Smelt produced by hindcasting with environmental variables for three different abundance values used as quasi-extinction thresholds. The age-specific abundance values associated with the population quantiles are documented in Table 2. Values for the age-0 abundance indices produced by the SFBS are also included on the graphs for reference.